

Design Guide 33  
**Curved  
Member  
Design**



**Smarter. Stronger. Steel.**

American Institute of Steel Construction  
312.670.2400 | [www.aisc.org](http://www.aisc.org)

@Seismicisolation



Design Guide 33

# Curved Member Design

Bo Dowswell, PE, PhD

© AISC 2018

by

American Institute of Steel Construction

*All rights reserved. This book or any part thereof must not be reproduced in any form without the written permission of the publisher.*

*The AISC logo is a registered trademark of AISC.*

The information presented in this publication has been prepared following recognized principles of design and construction. While it is believed to be accurate, this information should not be used or relied upon for any specific application without competent professional examination and verification of its accuracy, suitability and applicability by a licensed engineer or architect. The publication of this information is not a representation or warranty on the part of the American Institute of Steel Construction, its officers, agents, employees or committee members, or of any other person named herein, that this information is suitable for any general or particular use, or of freedom from infringement of any patent or patents. All representations or warranties, express or implied, other than as stated above, are specifically disclaimed. Anyone making use of the information presented in this publication assumes all liability arising from such use.

Caution must be exercised when relying upon standards and guidelines developed by other bodies and incorporated by reference herein since such material may be modified or amended from time to time subsequent to the printing of this edition. The American Institute of Steel Construction bears no responsibility for such material other than to refer to it and incorporate it by reference at the time of the initial publication of this edition.

Printed in the United States of America

@Seismicisolation

# Author

**Bo Dowswell, Ph.D., P.E.**, is a principal of ARC International, Birmingham, AL, and an adjunct professor at the University of Alabama at Birmingham. Dr. Dowswell is a member of the AISC Committee on Specifications, the AISC Committee on Manuals, and the AISC Task Group on Industrial Buildings and Nonbuilding Structures.

# Acknowledgments

The author would like to thank the AISC Bender/Roller Committee members, who provided invaluable insight into the practical aspects of bender/roller operations and technical information on the effects of bending steel members. The members of the review committee and their review comments are gratefully acknowledged:

Craig Archacki  
Craig Barnshaw  
Harry Cole  
Barry Feldman  
Louis Geschwindner  
Scott Goodrich  
David Hornsby  
Benjamin Kaan

Larry Kloiber  
James Neary  
Davis Parsons  
Ken Pecho  
Bill Scott  
William Segui  
Brian Smith  
Cliff Schwinger

Victor Shneur  
Marc Sorenson  
Jennifer Traut-Todaro  
Mike West  
Charles Wood  
Ronald Yeager

# Preface

This Design Guide provides guidance for the design of curved steel beams based on structural principles and adhering to the 2016 AISC *Specification for Structural Steel Buildings* and the 15th Edition AISC *Steel Construction Manual*. Both load and resistance factor design and allowable strength design methods are employed in the design examples.

@Seismic<sup>IV</sup>isolation

# TABLE OF CONTENTS

<b>CHAPTER 1 INTRODUCTION.....</b>	<b>1</b>	<b>CHAPTER 4 FABRICATION AND DETAILING.....</b>	<b>31</b>
1.1 PURPOSE.....	1	4.1 INTRODUCTION .....	31
1.2 CURVED MEMBERS IN COMMERCIAL STRUCTURES .....	1	4.2 GEOMETRY OF CURVED MEMBERS.....	31
1.2.1 Vertically Curved Members.....	1	4.2.1 Circular Geometry .....	31
1.2.2 Horizontally Curved Members .....	1	4.2.2 Parabolic Geometry.....	31
1.2.3 Specialty Bends .....	1	4.3 TOLERANCES .....	32
1.3 CURVED MEMBERS IN INDUSTRIAL STRUCTURES .....	1	4.3.1 Chord Length.....	32
1.3.1 Vertically Curved Members.....	1	4.3.2 Curvature .....	32
1.3.2 Horizontally Curved Members.....	1	4.3.3 Cross-Sectional Dimensions .....	32
1.3.3 Specialty Bends .....	2	4.4 FABRICATION CONSIDERATIONS .....	34
<b>CHAPTER 2 CURVING STEEL MEMBERS.....</b>	<b>9</b>	4.5 DETAILING REQUIREMENTS .....	34
2.1 INTRODUCTION .....	9	4.5.1 Standard Circular Curves.....	35
2.2 BENDING GEOMETRIES.....	9	4.5.2 Off-Axis Curves.....	35
2.2.1 Standard Bends.....	9	4.5.3 Compound and Reverse-Compound Curves .....	35
2.2.2 Off-Axis Bends .....	9	4.5.4 Multi-Axis Curves .....	35
2.2.3 Compound Bends .....	9	4.5.5 Variable-Radius Curves .....	35
2.2.4 Reverse-Compound Bends .....	9	4.5.6 Spiral Curves .....	35
2.2.5 Multi-Axis Bends .....	14	4.5.7 Detailing Examples .....	36
2.2.6 Variable-Radius Bends.....	14	<b>CHAPTER 5 GENERAL DESIGN ISSUES .....</b>	<b>45</b>
2.2.7 Spiral Bends .....	15	5.1 INTRODUCTION .....	45
2.3 BENDING PROCESSES .....	16	5.2 MATERIAL PROPERTIES.....	45
2.3.1 Pyramid Roll Bending .....	17	5.2.1 General Design Considerations .....	45
2.3.2 Incremental Step Bending.....	17	5.2.2 Idealized Material Behavior .....	46
2.3.3 Induction Bending.....	17	5.2.3 Ductility and Toughness.....	46
2.3.4 Rotary Draw Bending .....	22	5.2.4 Unfavorable Conditions .....	48
2.3.5 Other Methods .....	22	5.3 RESIDUAL STRESSES.....	49
<b>CHAPTER 3 DESIGN FOR BENDING.....</b>	<b>25</b>	5.3.1 Theoretical Residual Stresses .....	49
3.1 INTRODUCTION .....	25	5.3.2 Actual Residual Stresses .....	50
3.2 CURVING MECHANICS .....	25	5.3.3 Effect on Structural Performance .....	52
3.3 FRACTURE .....	26	5.4 NONLINEAR FLEXURAL STRESSES.....	53
3.3.1 Constraint.....	26	5.5 STRUCTURAL EFFECTS OF CROSS-SECTIONAL DISTORTION .....	54
3.3.2 Flange-to-Web Fracture.....	26	5.5.1 Rectangular Elements .....	54
3.3.3 Tension Flange Bolt Holes .....	26	5.5.2 Round HSS Ovality .....	55
3.4 CROSS-SECTIONAL DISTORTION.....	27	5.6 CONTRACT DOCUMENTS .....	55
3.4.1 General Guidelines.....	27	<b>CHAPTER 6 VERTICALLY CURVED MEMBERS.....</b>	<b>57</b>
3.4.2 Open Sections .....	28	6.1 INTRODUCTION .....	57
3.4.3 Rectangular HSS .....	28	6.2 ARCH GEOMETRY .....	57
3.4.4 Round HSS .....	30		
3.4.5 Other Shapes .....	30		



# Chapter 1

## Introduction

### 1.1 PURPOSE

In addition to the dramatic aesthetic effect of curved structures, the structural efficiency of arches and other vertically curved members makes them an attractive choice for both architects and engineers. Many commercial and industrial structures rely on horizontally curved members where straight members would be impractical. Although the visual appeal of curved structures is enhanced by their simplicity, the structural behavior of curved members can be much different from their straight counterparts. Despite the widespread use of curved structural steel members, detailed guidance relative to United States design practice is scarce. The purpose of this publication is to provide design guidance and practical information on the fabrication and detailing of curved members. Bender/roller companies who specialize in curving steel members can provide further information on the fabrication of curved members. AISC bender/roller companies are listed at the end of this Design Guide.

### 1.2 CURVED MEMBERS IN COMMERCIAL STRUCTURES

For commercial structures, the primary reason for using curved members is often the aesthetic appeal. Curved members can be fabricated to architecturally exposed structural steel (AESS) standards, making exposed steel an attractive option for these buildings. The additional cost of curving steelwork is often small in relation to the overall cost of the structure (King and Brown, 2001).

#### 1.2.1 Vertically Curved Members

The ability of arches to span long distances provides an opportunity for large open spaces. A similar visual effect can be created with vertically curved roof beams, as shown under construction in Figure 1-1 and for the car dealership in Figure 1-2. The cost of curving the roof beams can be partially offset compared to non-curved construction by the savings in the ridge detail, flashing and apex connections (King and Brown, 2001). The pedestrian bridge in Figure 1-3 utilizes the structural efficiency of an arch while providing exposed structure aesthetics.

#### 1.2.2 Horizontally Curved Members

Although horizontally curved members are less efficient structurally than straight beams, they are often used to carry loads at curved floors and roofs. Curved architecturally exposed beams were used for the recreation center in

Figure 1-4 and the canopy in Figure 1-5. In some cases, such as for transportation and pedestrian bridges, horizontally curved structures are required due to geometrical constraints. Figure 1-6 shows horizontally curved truss segments for a light rail transit system.

#### 1.2.3 Specialty Bends

Specialty bends are often required to form members to the proper geometry. Because parabolic curves are efficient for resisting gravity loads, many arches have a parabolic geometry (Figure 1-3), which requires a variable-radius specialty bend. A variable-radius curve was also used for the event pavilion in Figure 1-7, where the roof members were bent into an elliptical shape. Off-axis bending for the eave strut in Figure 1-8 was required because the center of curvature was not in the same plane as the member principal axis. Figure 1-9 shows a series of canopies that were bent into an S-curve, and Figure 1-10 shows a small-radius spiral staircase. The curved members in Figure 1-11 arch over a pedestrian bridge and serve as structural supports for the guardrail system. The art installation in Figure 1-12 illustrates the capability of bender/rollers to form complex curves with small, varying radii about multiple axes.

### 1.3 CURVED MEMBERS IN INDUSTRIAL STRUCTURES

Industrial buildings and nonbuilding structures are usually designed for functionality rather than aesthetics. Therefore, curved members are typically used out of necessity or because they are more efficient than straight members. For example, horizontally curved monorail beams are required where the monorail track must follow a curved path. Most liquid and bulk storage structures are constructed in a circular shape, which is efficient in resisting pressure from the stored contents. Curved members are used for circumferential roof members and shell stiffeners for these structures.

#### 1.3.1 Vertically Curved Members

Vertically curved members are primarily used as circumferential shell stiffening rings for horizontal vessels, large industrial ducts, and tubular conveyor galleries.

#### 1.3.2 Horizontally Curved Members

Horizontally curved members can be used for monorail beams, chimney grillages, circumferential shell stiffeners, and silo/tank roofs. Although most floor framing around

circular vessels and chimneys is straight (potentially with curved grating openings), curved framing is also an option. Rothman (1980) discussed the design of a 120-ft-diameter, 50-ft-deep circular cofferdam using I-shaped members bent about their strong axis to form the ring walls. This efficient structural system allowed a large workspace that was unimpeded by internal bracing.

### 1.3.3 Specialty Bends

Specialty bends are used primarily for spiral stairs providing access for circular vessels and for monorail beams with compound curves, as shown in Figure 2-6(a). Helical strakes, which are protruding fins that can be connected near the top of slender stacks to suppress vortex-induced vibration, are shown in Figure 2-10.



*Fig. 1-1. Vertically curved roof under construction (courtesy of AISC Bender/Roller Committee).*



*Fig. 1-2. Vertically curved roof for a car dealership (courtesy of AISC Bender/Roller Committee).*



*Fig. 1-3. Arch pedestrian bridge (courtesy of AISC Bender/Roller Committee).*



Fig. 1-4. Horizontally curved roof beams for a recreation center (courtesy of AISC Bender/Roller Committee).



Fig. 1-5. Horizontally curved members for a circular canopy (courtesy of AISC Bender/Roller Committee).



*Fig. 1-6. Horizontally curved trusses (courtesy of AISC Bender/Roller Committee).*



*Fig. 1-7. Elliptically curved roof members (courtesy of AISC Bender/Roller Committee).*



*Fig. 1-8. Curved eave strut (courtesy of AISC Bender/Roller Committee).*



*Fig. 1-9. S-shape canopy members (courtesy of AISC Bender/Roller Committee).*



Fig. 1-10. Spiral staircase (courtesy of AISC Bender/Roller Committee).



Fig. 1-11. Pedestrian bridge (courtesy of AISC Bender/Roller Committee).



Fig. 1-12. Art installation (courtesy of AISC Bender/Roller Committee).

# Chapter 2

## Curving Steel Members

### 2.1 INTRODUCTION

This chapter describes various geometries available for curved members and the methods used to bend these members. Due to the wide variety of bending equipment available, almost any structural shape can be curved, including HSS, hot-rolled open sections, welded built-up members, and multi-sided shapes formed by cold bending. Because each bender/roller has different capabilities, the early communication of bending requirements will allow potential complications to be addressed in the preliminary design stages.

### 2.2 BENDING GEOMETRIES

Members can be curved to create many different geometries. Standard bends are the simplest type, where a member is bent about a principal or geometric axis to form a single-radius curve. Members can also be bent about a non-principal axis or about more than one axis, providing three-dimensional curvature. Bender/roller companies have the capability to provide multiple arcs within a member, as well as parabolic, elliptical and other non-circular bends. Spirals are another common specialty bend. For specialty bends, the cost can be several times that of a standard bend. Because there are practical limits to bending capabilities, which are dependent on the member properties, a bender/roller company should be contacted for recommendations in the conceptual stages of design.

#### 2.2.1 Standard Bends

Standard bends, where a member is bent about a principal or geometric axis to form a single-radius curve, are shown in Figure 2-1. In this case, the member can be bent about the weak axis, known as bending the easy way, or bent about the strong axis, known as bending the hard way. Hard-way and easy-way bending are sometimes called camber and sweep, respectively. However, be aware that these terms are typically also used to describe mill tolerances or a small curvature induced in a beam to partially offset gravity-load deflections. Standard bending orientations for several common structural shapes are shown in Figure 2-2.

#### 2.2.2 Off-Axis Bends

For off-axis bends, also called conical rolling, the member is curved about a non-principal or non-geometric axis

as shown in Figure 2-3. Most off-axis bends are fabricated with a constant rotation relative to the plane of curvature; however, they can also be formed with a variable twist along the member axis. Special tooling is often required to limit distortion and ensure dimensional accuracy. Off-axis bends are used when members are both curved and sloped, and a member axis must be parallel to the curved surface. In commercial structures, this can occur in canopies, arched roofs, and horizontal members in a dome. These members are also used for circumferential stiffeners in industrial cone-shaped plate structures, such as hoppers and stacks.

#### 2.2.3 Compound Bends

A compound curve has two or more arcs in the same plane, joined tangentially without reversal of curvature. The members can be fabricated as a continuous curve or with a straight segment between tangent points as shown in Figures 2-4(a) and 2-4(b), respectively. Compound bends can be formed from a single straight member or by bending two or more straight members into simple curves and splicing them together. Members with compound bends are used to support both vertically and horizontally curved architectural features. In industrial structures, they are typically used for monorail beams.

#### 2.2.4 Reverse-Compound Bends

A reverse-compound curve, also known as an S-curve, has two or more arcs in the same plane joined tangentially with reversal of curvature, as shown in Figure 2-5. Completed I-shaped and HSS members with reverse-compound bends, as shown in Figure 2-6, are used in the same applications as compound bends.

To fabricate these members, the member is removed from the machine after the initial bend is completed, turned over, and placed back into the same machine, or a different machine, to complete the second bend. Due to the difficulty in fitting the member into the machine after the first bend is completed, a straight segment between the tangent points of each curve may be required as shown in Figure 2-5(b). The minimum straight segment length varies with the member geometry and the bending machine; therefore, the bender/roller company should be consulted for specific requirements. S-curves can also be formed by bending two straight members and splicing them together at the tangent point.



(a) Rectangular HSS bent the hard way



(b) Tees



(c) Half-round HSS

Fig. 2-1. Standard bends (courtesy of AISC Bender/Roller Committee).

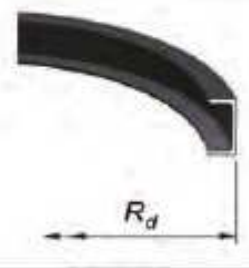
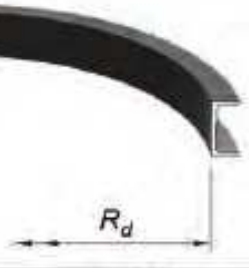
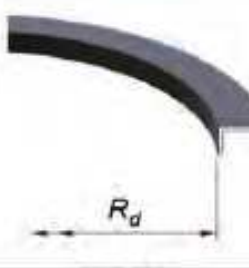
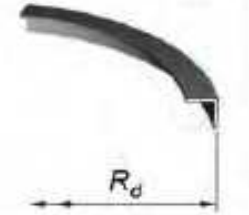
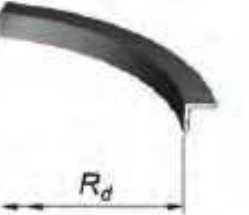
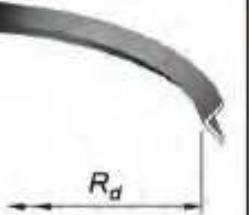
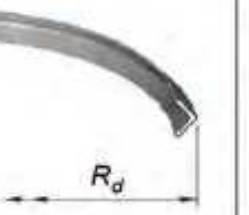
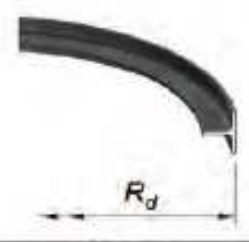
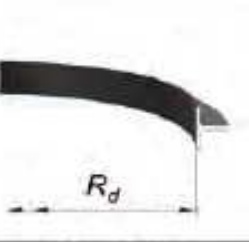
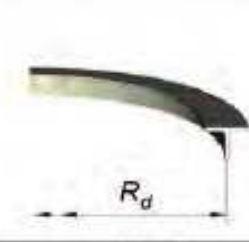
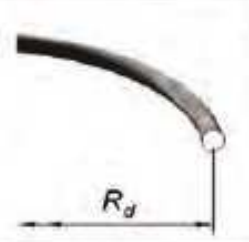
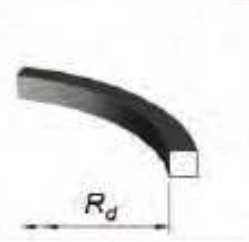
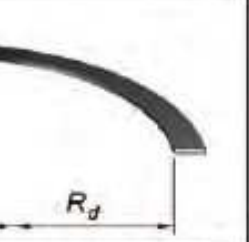
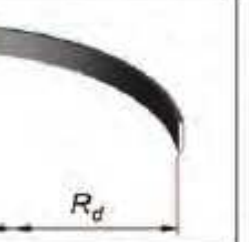
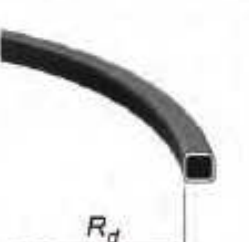
Section	Orientation			
I-Shape				
	Hard Way		Easy Way	
Channel				
	Flanges In		Flanges Out	
	Hard Way			
Angle				
	Leg In		Leg Out	
	Heel In			
Tee				
	Stem In		Stem Out	
	Stem Up			
Bar				
	Round		Square	
	Rectangular-Hard Way			
HSS				
	Round		Square	
	Rectangular-Hard Way			

Fig. 2-2. Bending orientations.

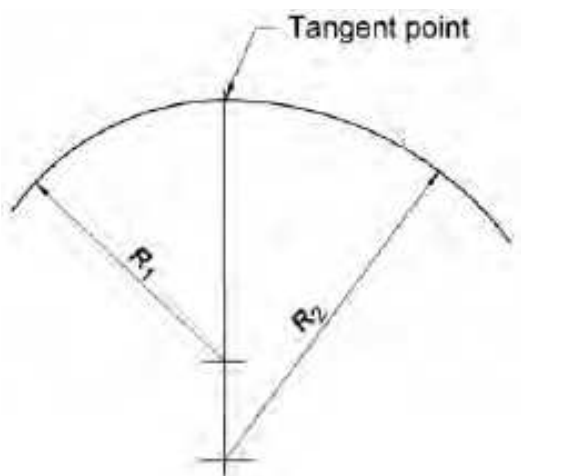


(a) I-shape

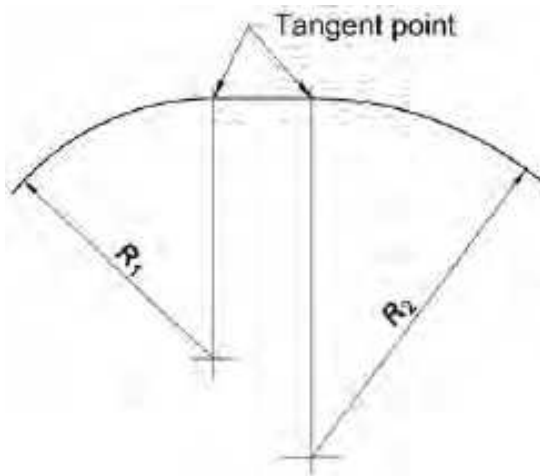


(b) HSS

Fig. 2-3. Off-axis bends (courtesy of AISC Bender/Roller Committee).

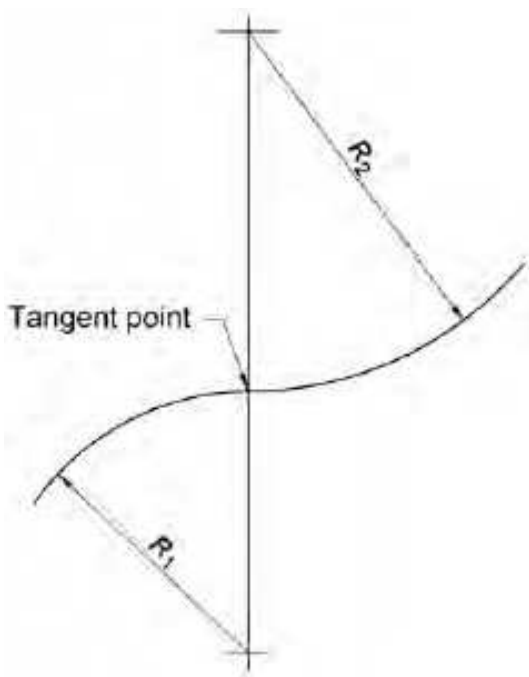


(a) Without straight segment

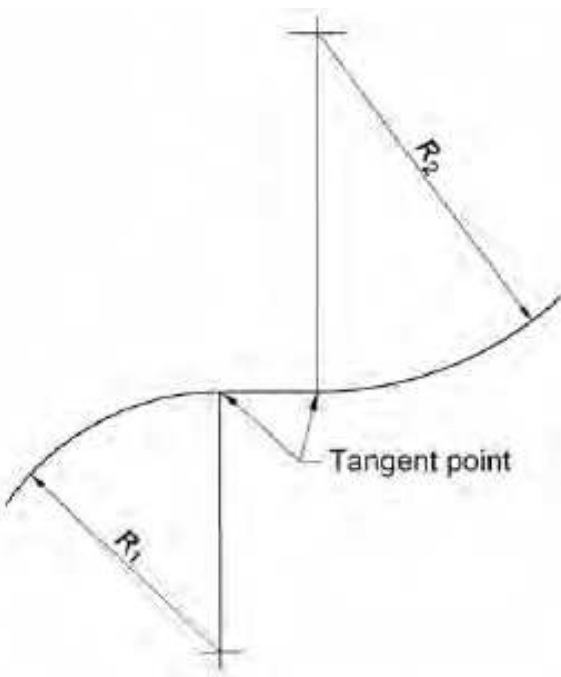


(b) With straight segment

Fig. 2-4. Compound bends.



(a) Without straight segment

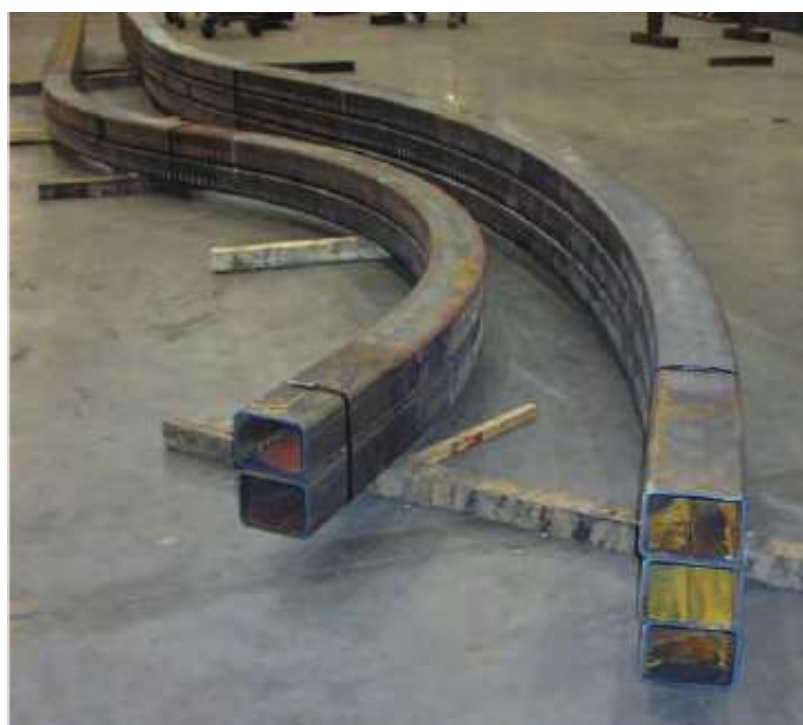


(b) With straight segment

Fig. 2-5. Reverse-compound bends.



(a) I-shape



(b) HSS

Fig. 2-6. Reverse-compound bends (courtesy of AISC Bender/Roller Committee).

### 2.2.5 Multi-Axis Bends

Multi-axis bending, also known as multi-plane bending, is used where curvature is required about more than one axis, as shown in Figure 2-7. The lack of cross-sectional rotation distinguishes multi-axis bends from off-axis bends. Generally, the bender/roller will treat each axis independently, with separate bends for each plane of curvature. Multi-axis bends are used where members are both curved and sloped, and the member axes must remain in the same plane over the entire member length.

### 2.2.6 Variable-Radius Bends

Parabolic, elliptical and other non-circular bends are variable-radius bends, also known as multi-radius bends. The funicular form for a member resisting a uniform gravity load is defined by a parabola; therefore, many arches, such as the one in Figure 2-8(a), are shaped to a parabolic curve. Elliptical bends can be required where a curved plane interfaces with a skewed plane as shown in Figure 2-8(b).



(a) Channel



(b) HSS

Fig. 2-7. Multi-axis bends (courtesy of AISC Bender/Roller Committee).



(a) Parabolic



(b) Elliptical

Fig. 2-8. Multi-radius bends (courtesy of AISC Bender/Roller Committee).

### 2.2.7 Spiral Bends

Using strict definitions, a spiral is a two-dimensional multi-radius curve, and a helix is a three-dimensional curve with an arc in one plane and a constant slope in a perpendicular plane. However, the terms are often used interchangeably in construction. A helix is the curve formed by bending about an axis on the surface of a cylinder or cone while rising at a constant angle. This curving process is often called sloped rolling or pitched rolling. The lack of cross-sectional rotation along the member axis distinguishes spiral bending from off-axis bending.

Normal pyramid rolling machines (see Section 2.3.1) are not capable of helical/spiral bending. Because the member must be fed into the rolls at the rise angle, specialized equipment with wide rolls is required. This specialty bend also requires adequate clear space to properly position the member in the rolls. Fitting a spiral staircase also requires significant shop floor space as shown in Figure 2-9. Rectangular bars bent into a helix are often connected near the top of slender steel stacks to suppress vortex-induced vibrations as shown in Figure 2-10.



(a)



(b)

*Fig. 2-9. Spiral stair stringers (courtesy of AISC Bender/Roller Committee).*



*Fig. 2-10. Helical strakes (courtesy of AISC Bender/Roller Committee).*

## 2.3 BENDING PROCESSES

Curved members can be formed by bending, heat curving, segmenting, or cutting to curve. Bending, which is the most used and generally the most economical curving process, is the primary focus of this document. However, the other methods will be discussed briefly in this section.

### *Heat Curving*

Heat curving is a bending process that relies only on the application of heat in specific patterns to induce curvature. Concentrated heat application causes material expansion. The expanding material is restrained by adjacent cooler areas, causing inelastic deformation of the heated material. The heated area contracts upon cooling, causing a net shrinkage that induces a permanent curvature.

Cross-sectional elements at the inside edge of the finished curve can be heated continuously, but are usually heated at discrete locations along the member length, approximately 2 to 3 ft apart (Thatcher, 1967). Heat is applied in wedge-shaped segments using an oxyfuel torch, and the temperature is monitored using temperature crayons or other equipment. Several heat patterns and restraint conditions are described by Avent and Mukai (1998). Generally, the curvature increases with the temperature and width of the heat pattern; however, the minimum attainable radius is approximately  $150D$ , where  $D$  is the member depth in the plane of curvature (Brockenbrough, 1970b). Due to the many variables involved, accurate prediction of the final curvature is difficult; therefore, the proper curvature is usually obtained using a trial-and-error process. Selection of the shape and location of the heat application points is an art that relies heavily on past experience.

Heat curving is primarily used by fabricators for cambering and curving to very large radii and for repairing damaged members. Large plate girders and other heavy built-up shapes can be fabricated straight, with the final geometry induced by heat curving. This method is labor-intensive; therefore, it is rarely used as the primary curving method when bending is an option. Heat curving can also be used to make small changes in curvature to cold-bent members after the bending process is complete and the member has been removed from the bending machine.

### *Segmenting*

Segmented members are fabricated by splicing several straight members together, typically using miter joints at discrete locations to approximate the geometry of a curved member. This curving method is rarely used due to the segmented appearance, the high fabrication cost, and the local stress concentrations that are inevitable where the member changes directions at the miter joints.

### *Cutting to Curve*

Built-up shapes can be fabricated of two or more elements that are either cut to the final shape or bent to the final shape before assembly. Prior to assembly, cross-sectional elements requiring strong-axis curvature are cut to shape, and elements that are curved in the weak direction are bent to shape. For horizontally curved members, the flanges are cut to the curved shape and fitted to the web, which has been bent to the curved shape. For vertically curved members, the flanges are bent and the web is cut to the required radii. Cambered plate girders can usually be fabricated without pre-bending the flanges because bending under the self-weight of the flange plate is often adequate to bring the flange-to-web interfaces into contact.

This method is often used to camber large plate girders that exceed the capacity of available bending machines; however, the primary advantage may be the out-of-plane dimensional stability of slender webs which can distort when other curving methods are used. When very small-radius bends are required, cutting to curve may be the best option; however, a considerable amount of scrap is often generated. Other disadvantages include the requirement of special jigs for fitting the member and ensuring the proper curvature and the need to recheck the curvature after welding because the weld shrinkage distortion can alter the as-fit curvature (Thatcher, 1967).

### *Bending*

Several methods are available for bending steel members: pyramid roll bending, incremental step bending, induction bending, rotary draw bending, and other processes. Some methods are more common in the steel construction industry, while others are used more in the forming of parts for automobile, piping and other industries. Members of almost any shape can be curved by bending, including rolled open shapes, welded built-up shapes, and closed shapes.

Cold bending, where the member is bent at room temperature, is usually more economical than hot bending or induction bending; however, there are cases where the required geometry cannot be formed by cold bending. The primary advantage of hot bending is that the material yield strength is lower compared to the room temperature value, requiring smaller forces to be exerted by the bending machine.

Each bending method has advantages and disadvantages, and each bender/roller company has developed unique bending methods and often use one-of-a-kind, patented machines. Developing proper bending techniques that ensure accurate and consistent dimensions requires significant judgment and experience. Due to differences in equipment, technique and personnel, the capabilities of each bender/roller vary significantly. For example, one shop may have the capability to bend heavy members the hard way, another shop may

specialize in spiral bends, and another may be able to bend hollow shapes to a tight radius with minimal distortion. It is advantageous to involve a bender/roller early in the design process to provide information on the results that can be expected from each bending process.

When a member is bent to form a permanent curvature, it must be strained beyond its yield point, inevitably causing some level of cross-sectional distortion. The tendency for cross-sectional distortion during the bending process can be controlled using various techniques. HSS wall distortion is often limited by using an internal support mechanism, such as a mandrel, a smaller HSS member, or filling the member with supporting material such as sand. Many bending machines control the distortion of open shapes with specialized rolls and various forms of mechanical restraint. Bender/roller companies may have hundreds of specialized rolls, mandrels, die sets and other tooling to bend various HSS and open shapes with minimal distortion.

### 2.3.1 Pyramid Roll Bending

Pyramid roll bending is a cold-bending method where a member is bent progressively by repeatedly passing it through a set of three adjustable rolls in a pyramid arrangement. Force is applied by opposing rolls as shown in Figure 2-11. The distance between rolls is manipulated before each pass, bending the member into successively smaller radii. This process is repeated until the proper curvature is formed. Pyramid roll bending can be used to provide curvature up to a 360° angle. Figures 2-12(a), 2-12(b) and 2-12(c) show pyramid roll bending of an I-shape bent the hard way, a channel bent the easy way, and a round HSS, respectively.

When curving I-shaped sections, the tension and compression flanges tend to bend locally toward one another. These flange forces induce web compression stresses, potentially causing web buckling distortion. This can be controlled with supplementary rolls providing a restraining tension force on the inner surface of the tension flange on both sides of the web. These supplementary rolls are shown in Figure 2-11 and Figure 2-12(a). In some cases, the web is restrained against buckling by compression rollers on each side of the

web. To provide support during the bending operation, the rolls are contoured to match the cross-sectional shape of the workpiece. Figure 2-13(a) shows rolls contoured for bending round HSS members. Contoured rolls can also be used for other cross-sectional profiles, as shown in Figure 2-13(b). Special rolls can be used to stabilize the cross-sectional elements and reduce distortion in common rolled shapes. Figures 2-14(a), 2-14(b) and 2-14(c) show special rolls for easy-way bending of I-shapes, hard-way bending of bars, and bending of tees, respectively.

### 2.3.2 Incremental Step Bending

Incremental step bending is a cold-bending method that uses hydraulic rams to apply bending forces at several discrete, closely-spaced locations along the member. Cross-sectional elements can be supported mechanically or hydraulically to reduce distortion during the bending operation, resulting in the potential for small-radius bends with minimal distortion. Figure 2-15 shows the incremental step bending process for a rectangular HSS member.

### 2.3.3 Induction Bending

Induction bending is a hot-bending method that utilizes an electric induction coil to heat a narrow band—typically between 2 in. and 6 in.—around the member circumference to between 1,500°F and 1,950°F before it is curved by force. Equal wall thickness around the perimeter of the cross section is necessary for uniform heating throughout the section. As the member moves through an induction heating coil, it can be bent incrementally (similar to incremental step bending), but is usually rotated around a fixed-radius pivot arm as shown in Figure 2-16. When a pivot-arm is used, a hydraulic ram pushes the straight section of the member through the coil at a constant rate (typically 1 to 2 in./min), with the leading end following the arc set by the pivot arm. After passing through the coil, the material adjacent to the heated section is usually sprayed with a coolant (usually water) or cooled with forced air, or the member is sometimes allowed to cool slowly in still air. Figures 2-17(a) and 2-17(b) show the induction bending process for round and rectangular HSS

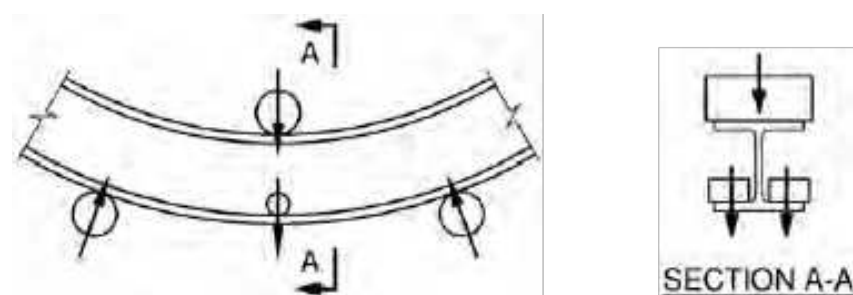


Fig. 2-11. Pyramid roll bending forces.



(a) *I*-shape



(b) *Channel*



(c) *Round HSS*

Fig. 2-12. *Pyramid roll bending (courtesy of AISC Bender/Roller Committee).*



(a) Round HSS



(b) Extrusion

Fig. 2-13. Contoured rolls (courtesy of AISC Bender/Roller Committee).



(a) I-shape



(b) Bar



(c) Tee

Fig. 2-14. Special rolls (courtesy of AISC Bender/Roller Committee).



Fig. 2-15. Incremental step bending of a rectangular HSS (courtesy of AISC Bender/Roller Committee).

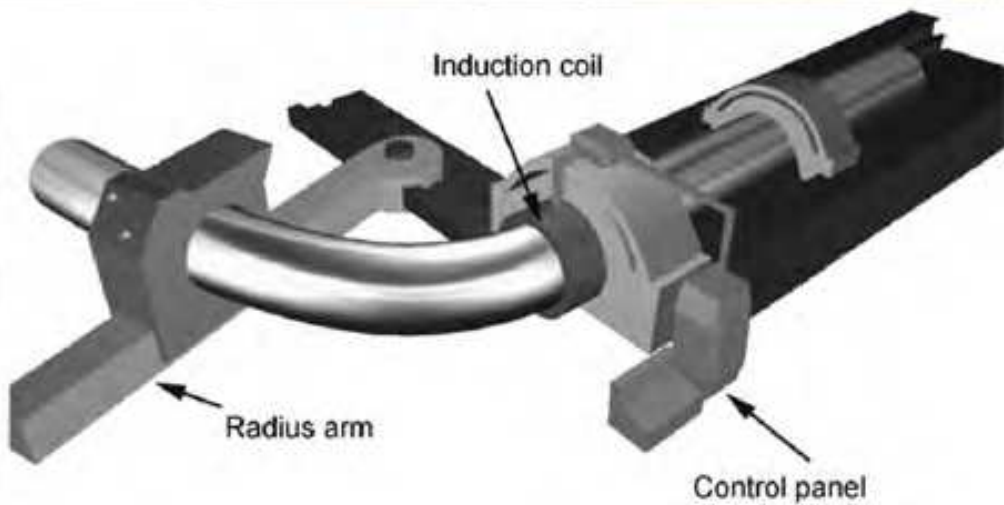


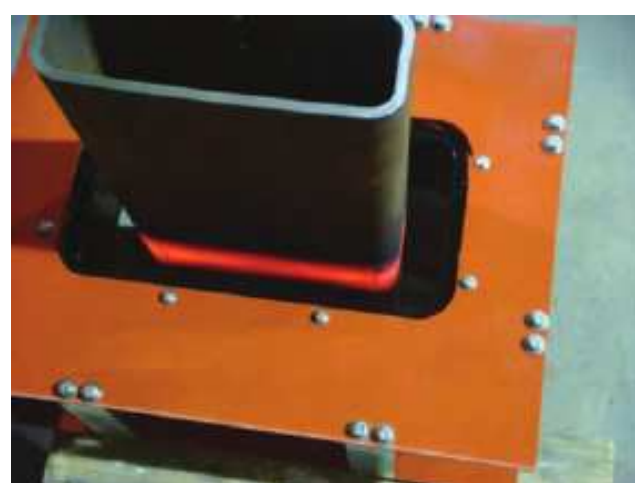
Fig. 2-16. Induction bending machine (King and Brown, 2001).



(a) Round HSS



(b) Rectangular HSS



(c) Heat source and heated band around the perimeter of rectangular HSS member

Fig. 2-17. Induction bending (courtesy of AISC Bender/Roller Committee).

members, respectively. Figure 2-17(c) shows the heat source and the heated band around the perimeter of a rectangular HSS member.

Although induction bending usually costs more than cold bending, there are several advantages that can make it the most appropriate bending method for some structural members. Because the inelastic bending strains are confined to the narrow heat band, small-radius bends are possible with high dimensional accuracy and low cross-sectional distortion. Also, heavy shapes that exceed the capacity of cold-bending machines can often be bent with induction bending machines. Hollow shapes with wall thicknesses up to 6 in. have been successfully bent with induction bending equipment; shapes with 1½- to 2-in.-thick walls are commonly bent.

Induction bending may provide a viable method when the dimensional requirements cannot be met with cold bending. For example, induction bending may be the only method with the capability to bend a multi-sided hollow shape to a small  $R/D$  ratio with limited cross-sectional distortion. Because bending special shapes requires a significant investment in tooling, duplicate member quantities are required to make this method economically feasible.

As will be discussed in Section 5.2.3, the induction-bending process is inherently a form of heat treatment. With proper control of the essential variables (see Section 4.5), material properties can be enhanced by induction bending.

Another potential advantage to induction bending is dimensional stability. A slight change in curvature can occur during lifting/handling, fabrication and erection (see Section 4.4). However, bender/roller experiences indicate that induction-bent members are less susceptible to dimensional changes. This behavior is likely caused by the lower residual stresses compared to those induced during cold bending. (See Section 5.3 for a discussion of residual stresses.)

### 2.3.4 Rotary Draw Bending

Rotary draw bending is a cold bending method where the member is clamped to a rotating bend die and drawn around the bend die as shown in Figure 2-18. The tailing tangent is held against the bend die by a pressure die, and the bend die rotates until the desired geometry is formed. A mandrel is often placed inside the member to restrain cross-sectional distortion during the bending process. Bends can also be formed with special draw-bending equipment where deformations are controlled by tensioning along the member axis.

Rotary draw bending is commonly used to form small-radius bends in smaller-size round, square and rectangular HSS members. Specific tooling is required for each member size, shape and bend radius; therefore, this method is best suited for projects requiring many identical bends. Some bender/roller companies have hundreds of die sets, likely eliminating any initial tooling costs for common geometries. This bending method is primarily used in the machine and parts industry (Weisenberger, 2016) and for piping (Riviezz, 1984). The maximum degree of bend is 180°, but the minimum bend radii of round HSS is approximately 50% smaller than that of other cold-bending methods (Riviezz, 1984).

### 2.3.5 Other Methods

Other methods can be used to bend members, including ram bending, gag pressing and hot bending.

#### Ram Bending

Ram bending is a cold-bending method that uses a hydraulic ram to apply a force near the midspan of two widely spaced supports. The member is moved through the machine so the force can be applied at discrete locations as required to produce the desired curvature. Figure 2-19 shows ram bending of a round HSS member.

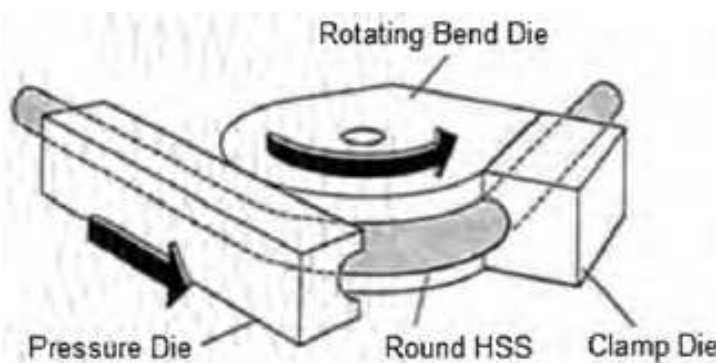


Fig. 2-18. Rotary draw bending (courtesy of AISC Bender/Roller Committee).

### Gag Pressing

Gag pressing, also known as point bending or cold cambering, is a bending method that uses hydraulic rams to simultaneously apply forces at discrete locations along the member to produce large-radius bends. This is the most common method for cambering beams to offset a portion of the service-load deflections; therefore, the hydraulic rams are located approximately at one-third points to produce a curved shape approximating a typical beam deflection curve. The supports for most cambering machines are between 20 and 28 ft apart.

Beams are usually cambered in a custom-built machine at the fabricator's shop; however, members can also be cambered by a bender/roller company. Because beam lines can be used only with straight members, beams are usually cambered after they are cut to the final length and holes are punched or drilled. If the machine capacity is exceeded, heat can be applied to the member to reduce the yield stress. Because many bender/roller companies have specialized, high-capacity equipment, it can be more economical for the fabricator to sublet the cambering of large beams. Further information on cambering beams can be found in *Modern Steel Construction* articles by Criste (2009), Alwood (2006) and Downey (2006), and in an AISC *Engineering Journal* paper by Ricker (1989).

### Hot Bending

Hot bending is any process where curvature is induced by load application at an elevated temperature. Also known as heat-assisted bending, the primary advantage of hot bending is that the material yield strength is lowered from the room temperature value, requiring smaller forces to be exerted by the bending machine. Heat is applied directly to the member by flame, by heating in a furnace, or by induction coil, followed by the application of a bending force. The member can be bent around preset forms, but more often the bending force is applied using one of the previously discussed bending methods. For HSS members, the heat can be applied either externally or internally. For cambering beams by gag pressing, the application of heat is typically used only where the beam strength exceeds the machine capacity. To ensure any changes to the member mechanical properties are insignificant, temperatures are held below the limits in AISC Specification Section M2.1: 1,100°F for ASTM A514/A514M (ASTM, 2016) and ASTM A852/A852M (ASTM, 2007) steel, and 1,200°F for other steels. These temperatures are much lower than those induced during induction bending.



Fig. 2-19. Ram bending of a round HSS (courtesy of AISC Bender/Roller Committee).



# Chapter 3

## Design for Bending

### 3.1 INTRODUCTION

As with straight members, curved members must be designed for proper performance under service conditions. For curved members, another important design consideration is the behavior during the bending operation. This chapter discusses curving mechanics and provides information on reducing the risk of fracture and excessive cross-sectional distortion during bending.

Early in the design process, engineers must determine if the conceptual geometry is attainable with the preliminary member sizes. Inquiries to bender/roller companies requesting the minimum bending radius for a specific member size are common. Guidelines are typically unavailable because curvature limits are dependent on the member's resistance to cross-sectional distortion and fracture, as well as the equipment and techniques used by the bender/roller. Also, any general guidelines are quickly outdated due to continuously evolving bending techniques. This chapter provides current information on bending limits as well as specific examples; however, an accurate minimum radius for a specific condition can be provided only by the bender/roller providing the service.

### 3.2 CURVING MECHANICS

When a member is bent to form a permanent curvature, it must be strained beyond its yield point. To form the final bending radius,  $R$ , the bending operation stretches the material on the outside of the bend and shortens the material on

the inside of the bend, as shown in Figure 3-1(a). The material behavior of the cross-sectional elements is similar to the uniaxial tension stress-strain curve shown in Figure 3-1(b). When flexural stresses exceed the yield point of the material, further strains result in constant stress until the material reaches the strain-hardening range, where the material strength increases nonlinearly. Curving of structural steel members involves bending the member into the inelastic range and often into the strain-hardening range.

For members curved to a very small radius, the simplifying assumptions used to derive the straight-beam equation,  $\sigma = Mc/I$ , are no longer valid. However, for members with relatively large radii typical of curved steel construction, flexural stresses can be calculated using the straight-beam equation (Boresi et al., 1993). This subject is further discussed in Section 5.4. Using straight-beam theory, the maximum flexural strain is  $\epsilon_{max} = y_o/R$ . For members that are symmetric about the axis of curvature, where  $y_o = D/2$ , the maximum strain is:

$$\epsilon_{max} = \frac{D}{2R} \quad (3-1)$$

The maximum flexural strain can be expressed as a multiple of the yield strain (Bjorhovde, 2006):

$$\epsilon_{max} = \alpha \epsilon_y \quad (3-2)$$

where

$D$  = member depth in the plane of curvature, in.

$R$  = radius of curvature of the neutral axis, in.

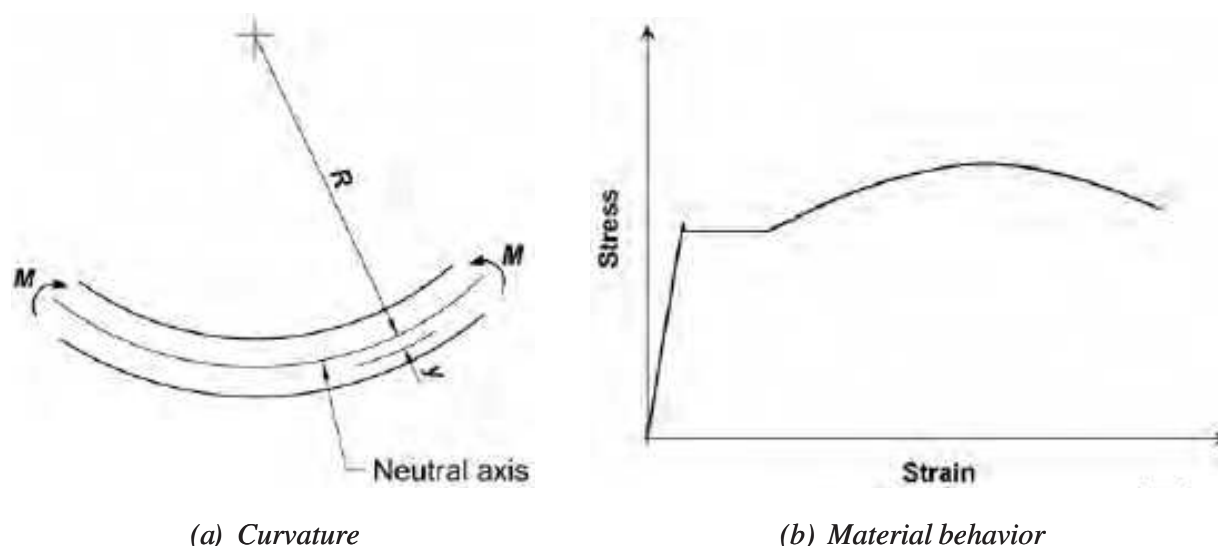


Fig. 3-1. Bending mechanics.

**Table 3-1. Approximate Strain Ratios**

Description	$\alpha$	$R/D^b$ ( $F_y = 36$ ksi)	$R/D^b$ ( $F_y = 50$ ksi)
97% of $M_p$ for W-shape bent the hard way	2.0	—	145
97% of $M_p$ for W-shape bent the easy way	3.5	—	83.1
Strain hardening begins at $\epsilon \approx 1.5\%$ ( $F_y = 50$ ksi)	8.7	—	33.3
Strain hardening begins at $\epsilon \approx 1.5\%$ ( $F_y = 36$ ksi)	12	33.3	—
Conservative limit suggested by Bjorhovde (2006) <sup>a</sup>	12	33.6	24.2
$\epsilon = 3\%$ ( $F_y = 50$ ksi)	17	—	16.7
$\epsilon = 3\%$ ( $F_y = 36$ ksi)	24	16.7	—
$\epsilon = 5\%$ ( $F_y = 50$ ksi)	29	—	10.0
$\epsilon = 5\%$ ( $F_y = 36$ ksi)	40	10.0	—

<sup>a</sup> For  $\alpha > 12$ , it is recommended that advice be sought from an experienced bender/roller (Bjorhovde, 2006).

<sup>b</sup> For members that are symmetric about the axis of curvature.

“—” indicates a non-applicable condition.

$y_o$  = distance from neutral axis to the outermost fiber, perpendicular to the axis of curvature, in.

$\alpha$  = strain ratio

$\epsilon_y = F_y/E$  = yield strain, in./in.

The strain ratio,  $\alpha$ , can be used to predict member behavior during the bending process, and to provide approximate limits on the bending radii. For example, when the member geometry requires  $\alpha > 12$ , additional precautions may be necessary to ensure the quality of the curved member (Bjorhovde, 2006). In this case, bender/roller companies can provide valuable recommendations. For reference,  $\alpha$  values for several common strain magnitudes are listed in Table 3-1.

### 3.3 FRACTURE

During the bending process, the curved member is subjected to inelastic flexural tension strains. Although the strain levels are only a small portion of the elongation capacity of a uniaxially loaded element, stress concentrations and constraint can lead to cracking. Any holes, cuts, copes and welded fittings are sources of stress concentrations.

#### 3.3.1 Constraint

The stress-strain curves in Figure 3-2(a) show the effect of constraint on the ductility of a tension element. The uniaxial curve has considerable ductility as a result of the shear stresses that develop due to unrestrained necking of the material. For elements that are constrained, these shear stresses cannot develop freely; therefore, the ductility decreases. An example is shown in Figure 3-2(b), where the web opening creates a notch, reducing the ductility of the adjacent web tension element.

#### 3.3.2 Flange-to-Web Fracture

In pyramid roll bending, when supplementary rolls are used to control web deformations, as can be seen in Figures 2-11 and 2-12(a), the rolls exert a significant tension force on the web. The required tension force increases with decreasing radius of curvature. In extreme cases, where bending strains are greater than approximately 3%, this can cause a web fracture at the flange-to-web fillet. To reduce the risk of fracture, the machine operator can reduce the tension force; however, this can lead to increased web distortion.

#### 3.3.3 Tension Flange Bolt Holes

Because beam lines can be used only with straight members, the most economical fabrication sequence is to punch or drill the required bolt holes before bending. Any holes fabricated after bending must be manually punched or drilled. When only a small curvature is required, such as for a cambered beam, holes are generally formed before bending. However, for small-radius bends, stress concentrations at tension-flange holes can lead to fracture at the net section during the bending operation. Even if fracture can be avoided, excessive hole elongation can render the member unusable. Because holes create a discrete weak point along the member length, the inelastic behavior concentrates at the holes, potentially forming a sharp bend (kink) with no curvature between holes.

According to the AISC *Specification for Structural Steel Buildings* (AISC, 2016c), hereafter referred to as the AISC *Specification*, Section F13.1, the limit state of tensile rupture is not applicable when  $F_u A_{fn} \geq Y_t F_y A_{fg}$ , where  $Y_t = 1.0$  for  $F_y/F_u \leq 0.8$  and  $Y_t = 1.1$  otherwise. This limit ensures that rotations inducing up to 4% strain can be expected without rupture (Dexter et al., 2002). Swanson (2016) showed that

the AISC *Specification* equations are conservative for calculating the net-section rupture strength; however, the limiting criterion for small-radius bends should likely be based on the tolerable level of hole elongation and kinking of the member during the bending operation. Bender/roller companies can provide specific guidance based on their judgment and experience. Based on the experiments of Arasaratnam (2008) and Douty and McGuire (1965), hole elongation and kinking can be avoided if  $F_u A_{fh} \geq 1.1 F_y A_{fg}$ .

### 3.4 CROSS-SECTIONAL DISTORTION

Distortion, which is a deviation from the original cross-sectional shape, occurs in every bent member to some degree. As discussed in Section 3.2, the bending operation induces inelastic compression stresses in the member that can cause cross-sectional distortion and local buckling, also known as waving or wrinkling. Local buckling can be in the form of a single half-wave or a series of wrinkles along the entire bend length. Distortion can also be caused by localized forces where the rollers or other parts of the bending machine make contact with the member. The potential for distortion is dependent on the bending radius, cross-sectional dimensions of the member, cross-sectional shape of the member, bending axis, bending method/techniques, level of cross-sectional support (mandrel or other support), and the level of initial geometric imperfections.

#### 3.4.1 General Guidelines

For a given member geometry, the level of distortion is dependent on the width-to-thickness ratio of the cross-sectional elements. Members with thicker elements can be bent to smaller radii with less distortion. Because the

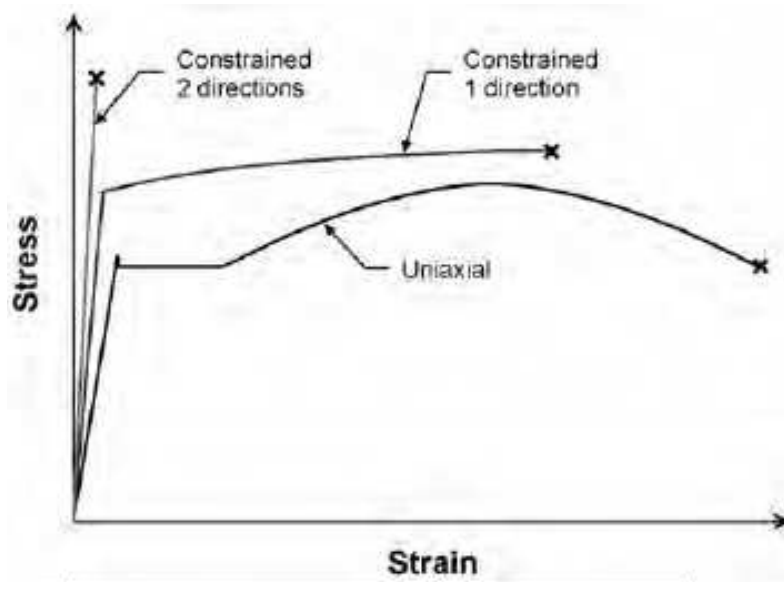
bending operation often requires thicker elements than required for strength under service loads, member selection should consider the trade-off between the tolerable level of distortion, the bending cost, and the cost of thicker cross-sectional elements.

Generally, cross-sectional shapes that are efficient in resisting local buckling also efficiently resist distortion. Round members are more resistant to distortion than members with flat elements, and stiffened flat elements are more efficient than unstiffened elements.

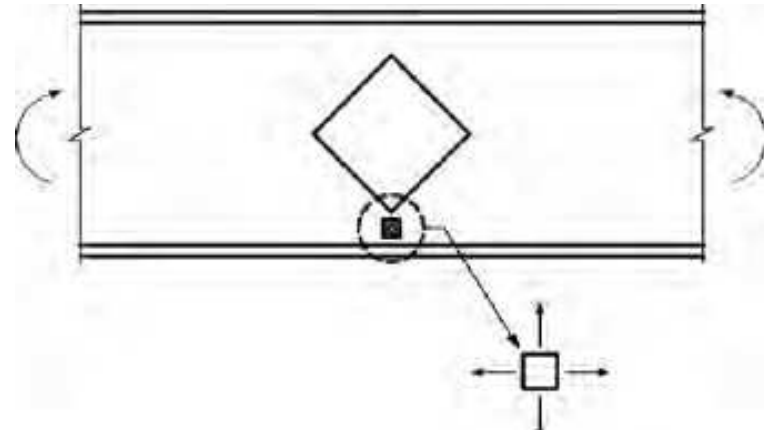
In AISC *Specification* Section B4.1, the limiting width-to-thickness ratios for compact compression elements,  $\lambda_p$ , are sufficient to provide a minimum rotational ductility of 3, which is equal to a strain ratio of  $\alpha = 4$ , before the onset of local buckling (Lukey and Adams, 1969; Yura et al., 1978). Furthermore, compact sections are believed to be sufficient to prevent local buckling before the onset of strain-hardening, which corresponds to  $\alpha = 8.7$  for  $F_y = 50$  ksi and  $\alpha = 12$  for  $F_y = 36$  ksi.

Due to the many variables affecting the distortion level, specific guidelines for the required element thickness are not available. Generally, sections with  $\lambda \leq \lambda_p$  can be expected to perform well for large- and medium-radius bends. For small-radius bends, the highly ductile member requirements in Section D1.1b of the AISC *Seismic Provisions* (AISC, 2016b), where  $\lambda \leq \lambda_{hd}$ , may be required. In extreme cases, the bender/roller company may suggest more stringent width-to-thickness ratios.

Table 3-2 lists several shapes with a range of minimum cold-bending radii that are from a survey of several bender/roller companies. In many cases, the minimum radius was from records of past projects, where members were bent successfully without appreciable distortion. In most cases, a



(a) Stress-strain curves



(b) Constrained tension element

Fig. 3-2. Effect of constraint.

given member can be bent to smaller radii than those listed, at the potential risk of larger distortions. The bending methods used to develop Table 3-2 are pyramid roll bending (including angle rolls and proprietary three-roll curving machines), incremental step bending, and rotary draw bending.  $R/D$  values near the upper range require only standard tooling. Values near the lower range may require web restraint, mandrels, or other non-standard tooling that can increase the cost. In some cases, hot bending and/or induction bending can be used to significantly reduce the  $R/D$  values; however, there is usually a cost increase with these bending methods. Although not clear in some cases, each bending orientation follows a general trend: when the sectional slenderness decreases, the minimum  $R/D$  ratio decreases and the maximum value for  $\alpha$  increases.

### 3.4.2 Open Sections

For open sections, local buckling can occur in one or more cross-sectional elements subjected to compression during the bending operation. Also, when curving I-shaped sections the hard way, radial forces cause the tension and compression flanges to bend locally toward one another. These flange forces induce web compression stresses, potentially causing web buckling distortion. As discussed in Section 2.3.1, many bending machines control the distortion of open shapes with specialized rolls and various forms of mechanical web and/or flange restraints.

### 3.4.3 Rectangular HSS

Square and rectangular HSS members tend to distort as shown in Figure 3-3, with a concave compression flange and outward bowing of the web (Kennedy et al., 1986; Chiew et al., 2016). The primary sources of distortion are sidewall crippling due to high contact forces from the roller, web local buckling caused by the combined shear and flexural stresses,

and flange local buckling due to flexure (Brady, 1978). Web and flange distortion parameters,  $\rho_w$  and  $\rho_f$ , can be expressed with Equations 3-3 and 3-4, respectively (Kennedy, 1988). Another common form of distortion for square and rectangular HSS is where the tension flange width reduces and the compression flange widens, forming a slight keystone shape. HSS wall distortion is often limited by using an internal support mechanism such as a mandrel, a smaller HSS member, or filling the member with supporting material such as sand.

$$\rho_w = \frac{b_1 - B}{B} \quad (3-3)$$

$$\rho_f = \frac{e}{D} \quad (3-4)$$

where

$B$  = member width perpendicular to the plane of curvature, in.

$D$  = member depth in the plane of curvature, in.

$b_1$  = maximum width including sidewall deformation, in.

$e$  = compression flange distortion, in.

All square and rectangular HSS members listed in Part 1 of the *AISC Steel Construction Manual* (AISC, 2017), hereafter referred to as the *AISC Manual*, can be cold bent. The bend radii in Table 3-2 provide some insight into the available bending capabilities. Other examples of members that have been successfully cold bent with minimal distortion are:

- HSS8×8×3/8 bent to a 10-ft radius
- HSS8×8×1/4 bent to a 12-ft radius
- HSS16×8×1/2 bent the easy way to an 11-ft radius
- HSS14×4×3/8 bent 11° off-axis to form a variable radius between 17 ft and 21 ft

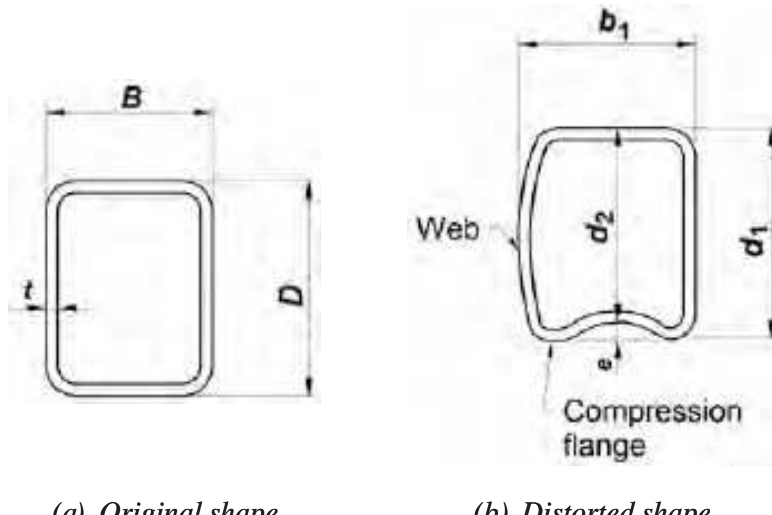


Fig. 3-3. Rectangular HSS distortion.

Table 3-2. General Guidelines for Minimum Cold-Bending Radii

Member	Bending Orientation	Sectional Slenderness ( $F_y = 50$ ksi)	Minimum Bending Radius, $R_d$ (ft)	Minimum $R/D$	Maximum $\alpha$ ( $F_y = 50$ ksi)
<b>Wide Flange (W)</b>					
W12x22	Hard way	Highly ductile	9.5 to 22	9.8 to 21	14 to 30
W12x40	Hard way	Compact	9.5 to 22	10 to 23	13 to 29
W14x90	Hard way	Noncompact	15 to 70	13 to 60	4.8 to 22
W16x26	Hard way	Compact	20 to 38	16 to 29	10 to 18
W18x40	Hard way	Highly ductile	18 to 52	12 to 35	8.3 to 24
W12x22	Easy way	Highly ductile	4.5 to 7.0	13 to 21	14 to 22
W12x40	Easy way	Compact	4.5 to 10	6.7 to 15	19 to 43
W14x90	Easy way	Noncompact	14 to 35	12 to 29	10 to 24
W16x26	Easy way	Compact	4.5 to 10	9.8 to 22	13 to 30
W18x40	Easy way	Highly ductile	10 to 18	20 to 36	8.1 to 15
<b>Tee (WT)</b>					
WT7x21.5	Stem in	Compact	8.0 to 15	14 to 26	17 to 33
WT7x41	Stem in	Compact	8.0 to 14	13 to 23	12 to 21
WT7x21.5	Stem out	Compact	6.0 to 10	10 to 18	15 to 27
WT7x41	Stem out	Highly ductile	5.5 to 6.0	9.2 to 10	28 to 30
<b>Channel (C)</b>					
C12x20.7	Hard way	Highly ductile	11 to 21	10 to 20	14 to 26
C12x20.7	Easy way	Highly ductile	3.0 to 6.0	12 to 24	18 to 36
<b>Round HSS</b>					
HSS8.625x0.500	—	Highly ductile	3.5 to 10	4.9 to 14	21 to 59
HSS8.625x0.322	—	Compact	3.5 to 15	4.9 to 21	14 to 59
HSS8.625x0.188	—	Noncompact	10 to 18	14 to 25	12 to 21
<b>Square HSS</b>					
HSS6x6x $\frac{1}{2}$	—	Highly ductile	3.0 to 7.5	6.5 to 16	18 to 45
HSS6x6x $\frac{1}{4}$	—	Compact	4.5 to 30	9.5 to 61	4.7 to 30
<b>Rectangular HSS</b>					
HSS12x6x $\frac{1}{2}$	Hard way	Highly ductile	9.0 to 12	9.5 to 13	22 to 30
HSS12x6x $\frac{1}{4}$	Hard way	Compact	18 to 85	19 to 86	3.4 to 15
HSS12x6x $\frac{1}{2}$	Easy way	Compact	8.5 to 20	18 to 41	7.1 to 16
<b>Angle (L)</b>					
L4x4x $\frac{5}{8}$	Leg out	Highly ductile	2.5 to 3.0	7.5 to 9.0	15 to 18
L4x4x $\frac{1}{2}$	Leg out	Compact	2.0 to 3.0	6.0 to 9.0	15 to 23
L4x4x $\frac{5}{16}$	Leg out	Compact	2.0 to 4.0	6.0 to 12	12 to 23
L4x4x $\frac{5}{8}$	Leg in	Highly ductile	2.5 to 3.5	7.5 to 11	12 to 18
L4x4x $\frac{1}{2}$	Leg in	Compact	2.5 to 3.5	7.5 to 11	12 to 18
L4x4x $\frac{5}{16}$	Leg in	Compact	3.0 to 5.0	9.0 to 15	9.3 to 15
<p>Note: The minimum radii listed are for general guidance in the conceptual design stages and smaller radii can often be obtained. More accurate information is available from the bender/roller, who can provide project-specific guidance, bending radii for other member sizes, information on complex bends, and the availability of other bending methods.</p>					
<p><math>D</math> = member depth in the plane of curvature, in.</p>					
<p><math>R_d</math> = bending radius for detailing as shown in Figure 2-2, ft</p>					
<p><math>R</math> = centroidal radius of curvature, in.</p>					

Large rectangular built-up box-shaped members can be induction bent. In one case, a 32 in.  $\times$  30 in.  $\times$  1 in. box was formed by welding two bent C-shape plates together. The member was then formed into a parabolic curve using induction bending. Induction bending may also be the best option for some specialty curves. For example, an HSS20 $\times$ 12 $\times$ 5 $\frac{1}{8}$  stair stringer has been induction bent to a spiral shape with a 14-ft plan radius.

#### 3.4.4 Round HSS

Round HSS members tend to ovalize during the bending operation, where the deviation from the theoretical shape forms an oval as shown in Figure 3-4. Ovalization is expressed using the difference between the major and minor axis dimensions after bending according to Equation 3-5. For cold-bent members, the contour of the die or rolls, as shown in Figure 2-13(a), can result in a singly symmetric deformed shape because the inner (compression) half of the cross section is restrained by the roll. Therefore, the inner wall retains an almost circular shape, but the outer (tension) wall tends to deform toward the center of curvature. Distortion can be reduced with an internal support mechanism such as a mandrel, a smaller HSS member, or filling the member with supporting material such as sand.

$$\rho = \frac{D_{\max} - D_{\min}}{D_n} \quad (3-5)$$

where

$D_{\max}$  = maximum outside diameter, in.

$D_{\min}$  = minimum outside diameter, in.

$D_n$  = nominal outside diameter, in.

Local buckles can form at the inner (compression) wall in a single half-wave or a series of wrinkles along the entire bend length. A form of local buckling, known as oil-canning, can cause collapse of the cross section due to the combined effect of ovalization and local buckling in a single half-wave.

All round HSS members listed in the AISC *Manual Part 1* can be cold bent. Rotary draw bending can be used to bend relatively small-diameter HSS to small radii. For example, a 6-in.-diameter HSS member can be rotary draw bent to a 12-in. centerline radius. Large fabricated round hollow sections, 40-in.-diameter and larger, can be induction bent with minimal distortion.

#### 3.4.5 Other Shapes

Many other shapes can be bent, including both open members formed by cold bending and closed multi-sided members formed by cold bending. For large round shapes fabricated from plates and large multi-sided shapes bent to small radii, induction bending may be the only feasible option, especially if distortion is a design factor.

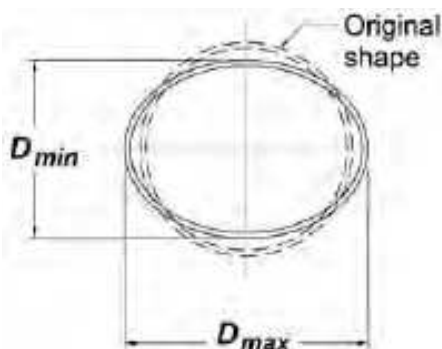


Fig. 3-4. Round HSS ovality.

# Chapter 4

## Fabrication and Detailing

### 4.1 INTRODUCTION

This chapter discusses fabrication and detailing considerations for curved members. Equations for the geometry of both circular and parabolic curves are provided. Detailing requirements for each type of curve are discussed, as well as dimensional tolerances and several other factors affecting the fabrication of curved members.

### 4.2 GEOMETRY OF CURVED MEMBERS

Accurate information on the geometry of curved members must be conveyed to the bender/roller. Typically, overall dimensions are provided on the design drawings, and detail dimensions, calculated by the steel detailer, are shown on the shop drawings. The shop drawings should provide all dimensions required by the bender/roller.

#### 4.2.1 Circular Geometry

It is common practice to designate circular member curvature in terms of the radius. Design drawings typically indicate the radius to either the member centroid or to another convenient location on the cross section, such as the inner or outer surface of the member. For detailing, the reference location for the radius dimension is a point on the cross section that is dependent on the member cross-sectional shape and the bending axis, as shown in Figure 2-2. Figure 4-1 shows the circular geometry and dimensions commonly used in circular curves. The relationship between the  $x$  and  $y$  coordinates is provided by Equation 4-1.

$$y = H - R + \sqrt{R^2 - \left(\frac{L_s}{2} - x\right)^2} \quad (4-1)$$

The arc length or developed length is:

$$L_d = R\theta \quad (4-2)$$

The chord or span is:

$$L_s = 2R\sin\left(\frac{\theta}{2}\right) \quad (4-3)$$

The rise is:

$$H = R\left[1 - \cos\left(\frac{\theta}{2}\right)\right] \quad (4-4)$$

where

$H$  = rise, in.

$L_d$  = arc length (developed length), in.

$L_s$  = chord (span), in.

$R$  = radius, in.

$\theta$  = subtended angle, rad

Circular arch geometry is commonly described using the rise-to-span ratio,  $H/L_s$ , which can be calculated with Equation 4-5.

$$\frac{H}{L_s} = \frac{1 - \cos\left(\frac{\theta}{2}\right)}{2\sin\left(\frac{\theta}{2}\right)} \quad (4-5)$$

If  $H$  and  $L_s$  are known, the radius and subtended angle can be calculated with Equations 4-6 and 4-7, respectively.

$$R = \frac{4H^2 + L_s^2}{8H} \quad (4-6)$$

$$\cos\left(\frac{\theta}{2}\right) = 1 - \frac{8}{4 + \left(\frac{L_s}{H}\right)^2} \quad (4-7)$$

#### 4.2.2 Parabolic Geometry

Because parabolic curves are efficient arch forms, they are often used for long-span structures resisting gravity loads. Design drawings typically indicate the rise and the span

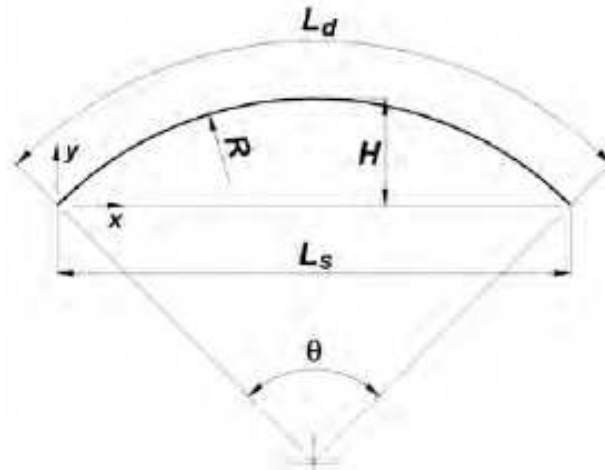


Fig. 4-1. Circular geometry.

dimensions. Figure 4-2 shows a parabolic curve, with the relationship between the  $x$  and  $y$  coordinates provided by Equation 4-8.

$$y = 4H \frac{x}{L_s} \left(1 - \frac{x}{L_s}\right) \quad (4-8)$$

The arc length is:

$$L_d = \frac{L_s}{2} \left[ \sqrt{1 + \left(\frac{4H}{L_s}\right)^2} + \frac{L_s}{4H} \sinh^{-1} \left(\frac{4H}{L_s}\right) \right] \quad (4-9a)$$

When  $0 < H/L_s \leq 1$ , the arc length can be estimated with Equation 4-9b.

$$L_d = L_s \left[ 1 + \frac{8}{3} \left(\frac{H}{L_s}\right)^2 + \frac{32}{5} \left(\frac{H}{L_s}\right)^4 \right] \quad (4-9b)$$

### 4.3 TOLERANCES

Length and curvature tolerances for bent members in the *AISC Code of Standard Practice for Steel Buildings* (AISC, 2016a), hereafter referred to as the *AISC Code of Standard Practice*, are similar to those for straight members. Tolerances that are not addressed in the *AISC Code of Standard Practice* should be mutually agreed upon by the contractor and the owner. At any stage of design, bender/roller companies can provide valuable input for practical tolerance limits. Members that must meet architecturally exposed structural steel (AESS) requirements should be designated in the contract documents. In most cases, bending and fabrication to AECC standards will increase the cost; therefore, AECC should be specified only where appropriate.

#### 4.3.1 Chord Length

The permissible tolerances for chord length are defined in *AISC Code of Standard Practice* Sections 6.4.1 and 6.4.2(b). For curved structural members, the variation in the detailed chord length for members that frame to other structural steel elements is:

- (a) For members that are equal to or less than 30 ft in length, the variation shall be equal to or less than  $\frac{1}{16}$  in.

- (b) For members that are greater than 30 ft in length, the variation shall be equal to or less than  $\frac{1}{8}$  in.

#### 4.3.2 Curvature

The permissible tolerances for curvature, which are the same for both AECC and non-AECC members, are defined in the *AISC Code of Standard Practice* Sections 6.4.2 and 10.4.4. For curved structural members, whether composed of a single standard structural shape or built-up, the permitted as-fabricated variation from the theoretical curvature is equal to the standard camber (in the strong direction) and sweep (in the weak direction) tolerances permitted for straight members in the applicable ASTM standard. If an applicable ASTM standard does not exist, the maximum variation in curvature is  $\frac{1}{8}$  in. times one-fifth of the total arc length in feet for members 10 ft or greater in length. For members less than 10 ft in length, the permissible variation in curvature is  $\pm\frac{1}{8}$  in. Sharp kinks or sharp bends are cause for rejection.

The variation in curvature can be inside or outside of the theoretical arc and is measured at the middle ordinate. The middle ordinate is the rise dimension,  $H$ , in Figures 4-1 and 4-2. The location of the theoretical arc is defined by the contract drawings and may be dimensioned either at the work line, the member's inner surface, or the member's outer surface.

#### 4.3.3 Cross-Sectional Dimensions

As discussed in Section 3.4, cross-sectional distortion occurs in every bent member to some degree. For small-radius bends, the distortion can be visible; therefore, it is important to establish and specify an acceptable level of distortion prior to bending. Distortion tolerances should be based on the potential effect on structural performance and any aesthetic requirements for AECC members. Generally, AECC requirements are more stringent than strength requirements. In most cases, reasonable cross-sectional distortions can be tolerated without a reduction in local buckling strength.

Cross-sectional tolerances specified in ASTM A6, ASTM A53 and ASTM A500 (ASTM, 2016) are mill tolerances. Because any initial geometric imperfections are amplified during the bending process, it may be impractical to expect post-bending imperfections to meet the ASTM requirements. Permissible distortion tolerances should be discussed with the bender/roller in the design stages of the project.

#### AECC Members

*AISC Code of Standard Practice* Section 10.1.1 defines five categories of AECC:

AECC 1: Basic elements.

AECC 2: Feature elements viewed at a distance greater than 20 ft (6 m).

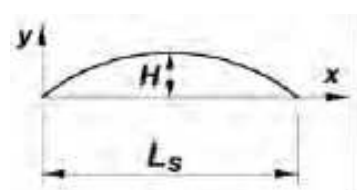


Fig. 4-2. Parabolic geometry.

AESS 3: Feature elements viewed at a distance less than 20 ft (6 m).

AESS 4: Showcase elements with special surface and edge treatment beyond fabrication.

AESS C: Custom elements with characteristics described in the contract documents.

Because the acceptable distortion decreases with increasing category, the bending cost generally increases. Any minimal distortion, especially for large-radius bends, is likely to be acceptable for AESS 1 and 2 without further work. For AESS 3 or 4, distortion can often be corrected by applying filler and sanding to the proper finish before painting; however, proper matching between the sanded filler and blasted steel surfaces can be difficult.

#### Open Sections

The implied out-of-flatness tolerance for rectangular elements in AISC *Specification* (AISC, 2016c) Section B4 is  $(\delta_o)_{max} = 0.264t$ , where  $t$  is the element thickness (Dowswell, 2010). For elements with  $\delta_o > 0.264t$ , Section 5.5.1 provides a method to evaluate any reduction in local buckling strength caused by excessive distortion. For AESS, distortion of flat elements in open shapes must be visibly acceptable to the architect at a distance compatible with the AESS category under any selected lighting condition (AISC, 2003).

#### Rectangular HSS

The permissible cross-sectional variation for ASTM A500 square and rectangular HSS members larger than 5 1/2 in. is 1% of the largest outside flat dimension. This tolerance includes depth/width tolerances and allowances for convexity/concavity of the wall, but does not include distortion caused by the bending operation. Post-bending tolerances of 1% to 2% are common for wall distortions calculated with Equations 3-3 and 3-4 (Kennedy, 1988; CIDECT, 1998). These tolerances are often expressed as a single value independent of the HSS dimension, with common values of 1/8 in. and 3/16 in. For cases where the HSS forms a keystone shape, if

tolerances are not specified in the contract documents, maximum deformations of approximately  $\pm 5\%$  of the HSS width can be expected. For AESS, the suggested tolerance for all distortion types is  $\pm 1/2$  in. applied to the nominal width and depth (AISC, 2003).

#### Round HSS

Round HSS members tend to ovalize during the bending operation (Figure 3-4). Ovalization is expressed as a percentage of the difference between the major and minor axis dimensions after bending according to Equation 3-5. Forming tolerances for round, straight members in ASTM A500 and A53 are much smaller than can be achieved after bending. For curved segments in piping systems, ASME B31.1 (ASME, 2016) specifies a maximum ovalization tolerance of 8%, which is easily achievable for most geometries common to steel structures.

A more stringent tolerance may be required in some cases. For example, when a curved segment connects to another straight or curved segment with circumferential butt welds, the ovality tolerance and orientation should ensure proper HSS wall alignment for the weld joint. A tolerance of 5% is achievable by cold bending in most cases, especially for members with less than approximately a 14-in. diameter, but small-radius bends with more stringent tolerances (less than 5%) may require induction bending. In some cases, especially at the tangent point of multi-axis bends, mating walls may need to be brought into alignment by applying force and/or heat. Alternatively, bolted flange connections or other connections that will accommodate larger tolerances can be used.

Local buckling wrinkles can also form in areas of high compression stress. Although not generally specified for structural members, a common piping tolerance limits the depth of wrinkles on the inside of the bend, measured from crest to trough, to a maximum of 1.5% of the nominal pipe size.

AESS ovality tolerances must be selected based on aesthetics. From Figure 4-3, which shows ovalization values of

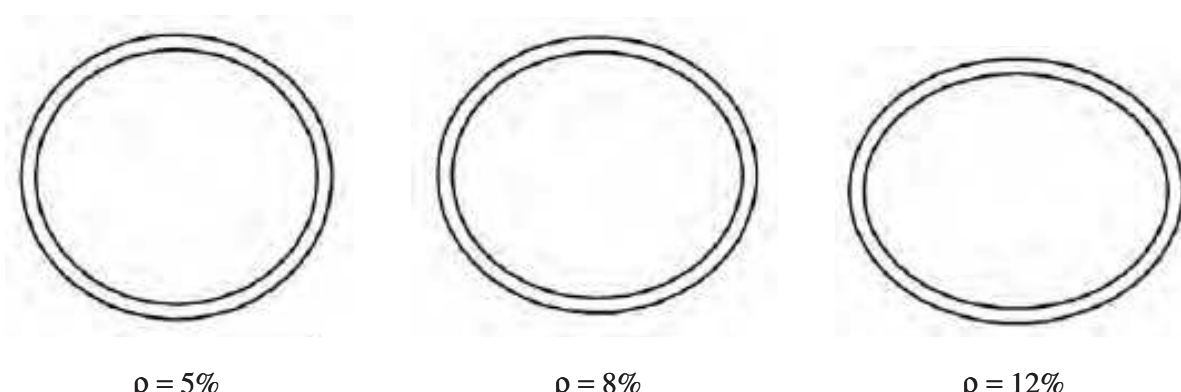


Fig. 4-3. Round HSS ovality.

5%, 8% and 12%, it appears that the commonly accepted 5% tolerance is likely to produce imperceptible ovalization distortions. In many cases, the 8% tolerance may be acceptable as well.

#### 4.4 FABRICATION CONSIDERATIONS

The bending operation is usually performed by a specialty bender/roller company as a subcontractor to the fabricator. However, there are several considerations for curved members that must be addressed by the fabricator. For optimal results, the fabricator should work closely with the bender/roller. Although not ideal, when a standard bend is required quickly, benders can often set up the equipment and bend a member the same day it is received. Specialty bends and bends requiring nonstandard tooling may require significantly more lead time. The cost of bending a member varies with the bender/roller, depending on the bending method and techniques used. The cost usually increases as the tolerable level of distortion decreases. For curvatures typical in building construction, it is likely that the radius can be achieved economically with minimal distortion.

All required tolerances must be conveyed to the bender/roller. The fabricator is also responsible for informing the bender/roller when processing must meet AEES requirements. In many cases, the more restrictive AEES tolerances and surface condition requirements will increase the bending and fabrication cost; therefore, AEES should be specified only where it is required.

When ordering curved members, the fabricator should recognize that the bending process requires an additional straight length at each end of the arc. Known as the grip length, or the lead and tail dimensions, this straight segment can be trimmed after bending. The required grip length is different for each bender/roller, bending method and bending machine. Generally, an additional length between 1 ft and 7 ft is required at each end. A conservative estimate of the member length can be calculated by adding  $8D$  ( $4D$  at each end) to the arc length, where  $D$  is the member depth in the plane of curvature. Bender/roller companies can provide more accurate values for each specific case.

Splices are often required to limit member lengths for handling, shipping or galvanizing. Any limitations caused by the bending machine or the bender/roller shop layout must also be considered in the selection of splice locations. Preferably, any shop-welded splices should be welded after the bending operation has been completed. This allows more efficient handling and positioning in the bending machine, ensures some adjustability at the splice after bending, and eliminates potential inelastic deformation of the splice weld metal. For induction-bent members, any pre-bend welds are subjected to the heating/cooling cycle discussed in Section 2.3.3; therefore, the post-bend material properties of the

weld and heat affected zone may need to be verified with a bending procedure qualification test.

HSS members that are manufactured by cold bending and welding along a longitudinal seam may require special attention during the bending process. To reduce the potential for weld rupture, the longitudinal weld seam should be located on the inside of the bend (Taylor, 2001) or near the neutral axis (Smith and King, 2002; TPA, 1998). Also, the location of weld seams relative to the plane of curvature may be an aesthetic consideration for AEES members.

Often, the cross-sectional element thickness required for strength is less than that required to limit distortion during the bending operation. Although the member sizes shown on the contract drawings should consider the requirements for bending the member, before material is ordered the bender/roller should be consulted regarding the cross-sectional element thicknesses required to limit distortion. For AEES members, distortion should be minimized, and this information should be provided to the bender/roller along with any additional tolerances. Any initial cross-sectional geometric imperfections are amplified during the bending process; therefore, any members ordered for bending should be within the ASTM cross-sectional tolerances.

If the fabricator uses heat curving or hot bending to provide curvature, the temperature limits in AISC *Specification* Section M2.1 must be followed. This will ensure the virgin mechanical properties (strength, ductility and toughness) are retained.

A slight change in curvature can occur during lifting/handling, fabrication and erection. Because these losses are unpredictable, dimensional inspections should be performed at the bender/roller shop. Any potential change of curvature can often be limited by using proper techniques for shipping, lifting/handling and erection (Feldman, 2008; AISC, 2003).

As with straight members, steps should be taken to minimize warping and distortion during galvanizing of curved members. Distortion of curved members will likely be similar to that of the corresponding straight member. The risk of distortion can be minimized by using symmetrical cross sections and sections with uniform (or almost equal) cross-sectional element thicknesses (ASTM, 2013). Several successful cases have been reported, including the galvanizing of unsymmetrical angle cross sections that were formed by press-brake bending and subsequently curved into a circular ring (Wendt, 2010).

#### 4.5 DETAILING REQUIREMENTS

General detailing requirements for curved members are similar to straight members; the detailer should provide all dimensions, locations and sizes required to procure, fabricate, ship and erect the member. For standard two-dimensional curves, a view in the plane of curvature is

required. Specialty bends, described in Section 2.2, require further information to properly specify the geometry. The detailer should be aware of the additional member length required for bending, which is discussed in Section 4.4. It will be beneficial to the fabricator and to the bender/roller if the tolerances and any AESS requirements are provided on the shop drawings. See King (2005) for further detailing requirements for curved members.

#### 4.5.1 Standard Circular Curves

For circular members, it is standard practice to designate member curvature in terms of the radius. For each member and bend orientation, the reference location for the radius dimension is shown in Figure 2-2. Detail dimensions are used primarily in fabrication, but additional dimensions necessary for the purposes of checking and inspection are also appropriate. For each circular segment, all dimensions in Figure 4-1 are required. The arc length is necessary to determine the member length. Arc lengths are typically dimensioned with a reference radius, for example: Arc = 30'-0 @ 50'-0 rad. The radius and subtended angle are required for bending the member. The chord and rise are required for checking the member dimensions and for determining the overall size of the member, which can be critical for shipping, surface preparation, heat treating and galvanizing. For members with a straight segment at the end of a circular segment, the tangent point should be located and the length of the straight segment must be dimensioned.

#### 4.5.2 Off-Axis Curves

Off-axis curves require the same dimensions in the plane of curvature as circular curves. In addition to a view in the plane of curvature, a cross-sectional view is necessary to show the member axis rotation relative to the plane of curvature.

#### 4.5.3 Compound and Reverse-Compound Curves

For compound and reverse-compound curves, each curved segment must be dimensioned separately with all dimensions required for standard circular curves. Any straight segments between tangent points must be dimensioned.

#### 4.5.4 Multi-Axis Curves

For multi-axis curves, a separate view is required for each plane of curvature, with each curved segment dimensioned separately providing all dimensions required for standard circular curves. Any straight segments between tangent points must be dimensioned. Due to the potential difficulties in providing three-dimensional geometry on paper, bender/roller companies may prefer to work from the detailer's three-dimensional model.

#### 4.5.5 Variable-Radius Curves

Variable-radius curves require a detailed layout of the member, as shown in Figure 4-4, with  $x$  and  $y$  coordinates for several discrete points along the member length. The frequency of the coordinate points is dependent on the radius variation at that location and the accuracy required. As a general guideline, these coordinates can be specified in 12-in. increments, minimum. With the typical accuracy of curving these members, smaller increments are not justified (Feldman, 2008). However, providing more increments than required will allow the bender/roller the option to use all dimensions or determine that fewer points can be used (King, 2005).

#### 4.5.6 Spiral Curves

Spiral curves must have a plan view showing the radius of curvature and all other dimensions required for standard circular curves. A developed elevation view should be provided designating the true slope (i.e., pitch or bevel) of the member

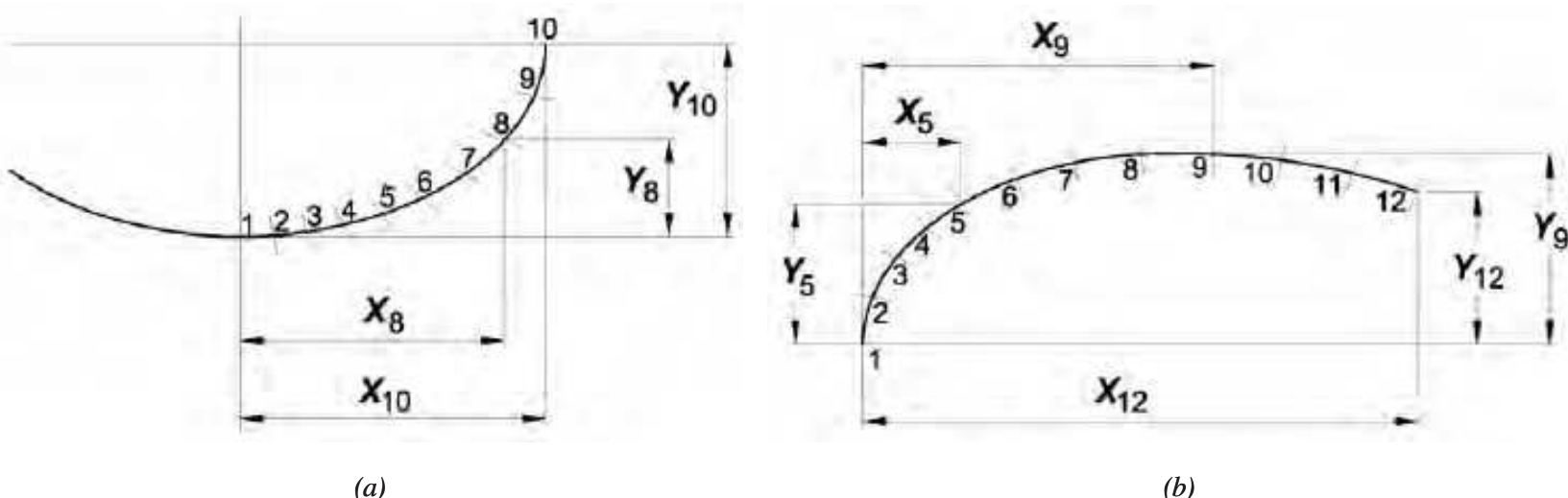


Fig. 4-4. Variable-radius curves.

with the direction of curvature clearly shown. The developed view of spiral stair stringers should be dimensioned as for a straight stair, including dimensions for the height (rise) and the developed horizontal length (run).

#### 4.5.7 Detailing Examples

Figure 4-5(a) shows an example of the detail dimensions required for a horizontally curved beam. The plan view is used to show the curve dimensions, and an elevation view is necessary to properly dimension the copes and the beam end connections. The curb plate is detailed separately in Figure 4-5(b). The plate is fabricated using the cut-to-curve method described in Section 2.3, with the horizontal plate cut to the final shape and the vertical plate curved to shape by cold bending. Due to the large width-to-thickness ratio of the horizontal plate, it would be difficult to curve by bending without significant distortion.

Figure 4-6 shows a truss with a vertically curved bottom chord. Each work point is located along the developed chord arc length as well as in both the vertical and horizontal

directions. The required panel-point geometry is provided by dimensioning parallel and perpendicular to the axis of curvature. Bottom chord end connections are dimensioned parallel and perpendicular to both the axis of curvature of the chord and the axis of the supporting member.

An example erection drawing for a spiral stair is shown in Figure 4-7. Figures 4-8 through 4-13 show a partial set of details. The lower segment from the first floor up to the landing is shown in Figure 4-8. The inner and outer stringers for the lower segment are detailed in Figures 4-9 and 4-10, respectively. Because the outer stringer has a longer arc length (developed length) than the inner stringer, the true slope (i.e., pitch or bevel) of the outer stringer is less than for the inner stringer. The plan view of the landing is shown in Figure 4-11 and the upper stair segment, from the landing up to the second floor, is shown in Figure 4-12. The top of the stair is flared with short stringer segments curved to very small radii as detailed in Figure 4-13. These short segments may be best fabricated using the cut-to-curve method.

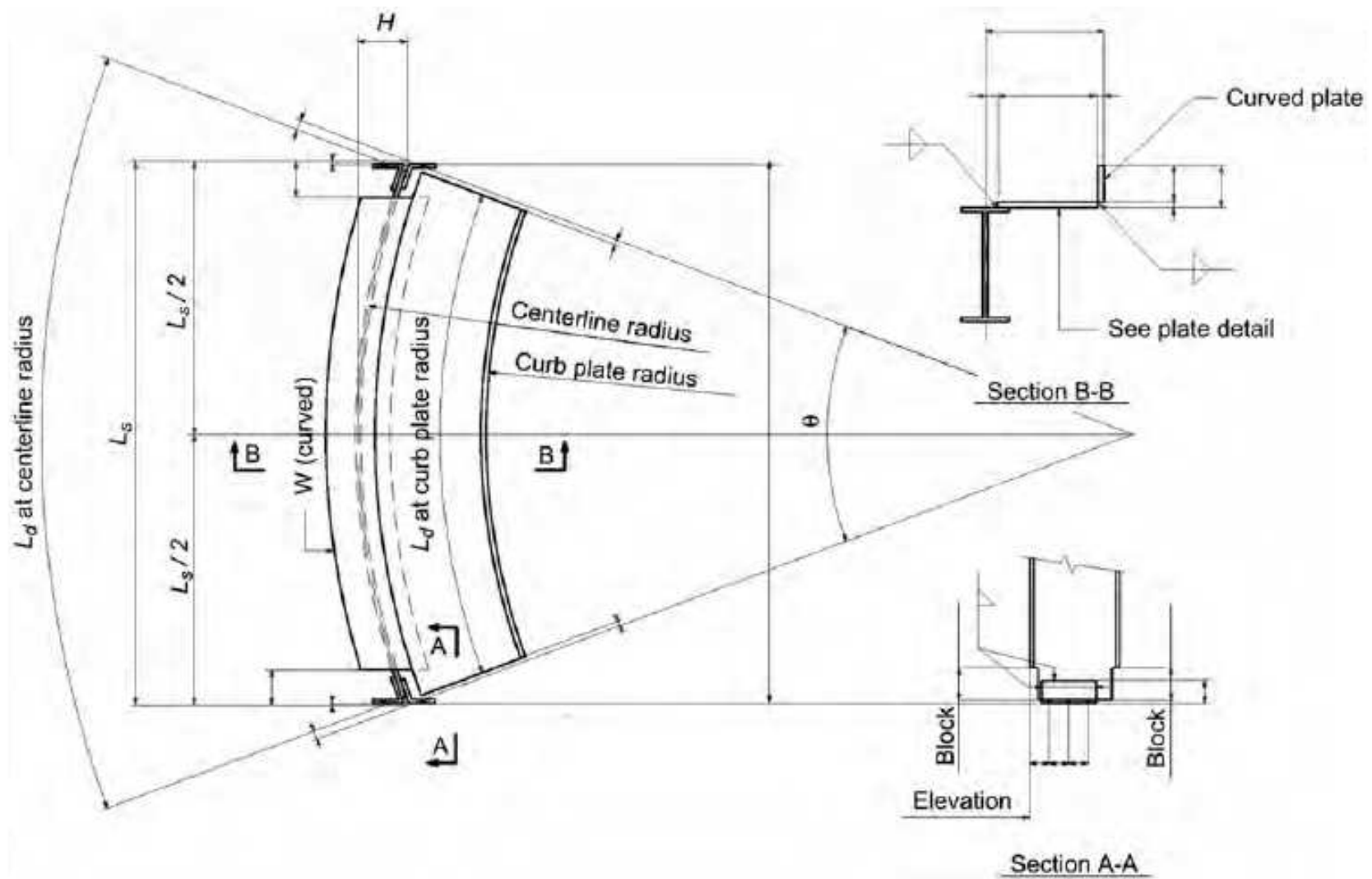


Fig. 4-5(a). Horizontally curved beam.

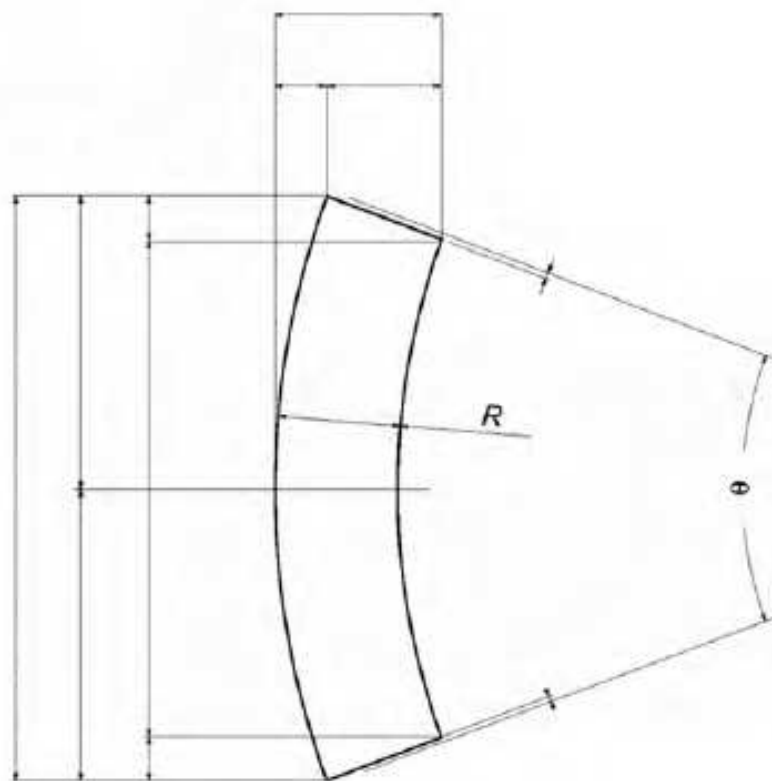


Fig. 4-5(b). Curved beam curb plate.

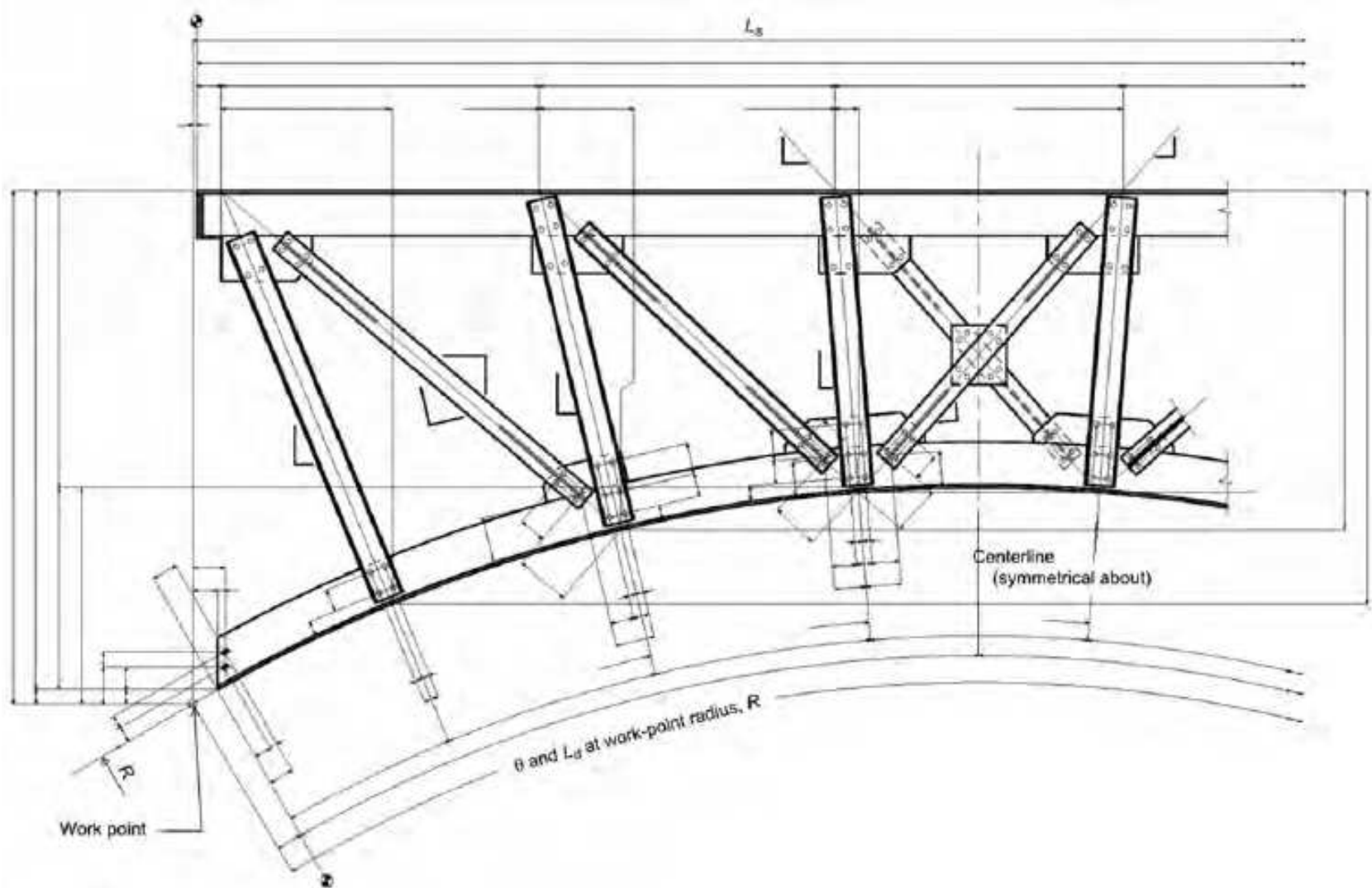


Fig. 4-6. Truss with curved bottom chord.

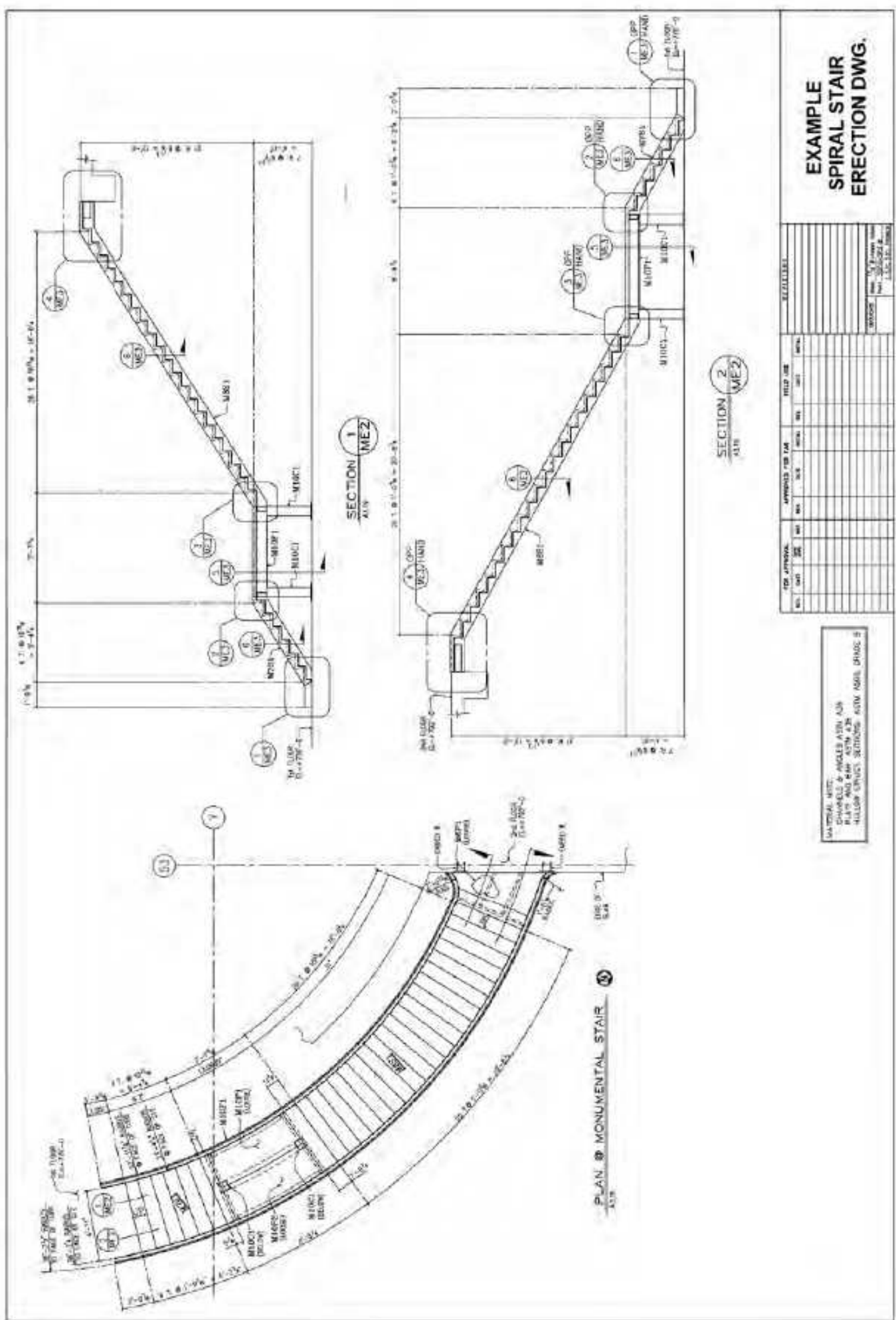
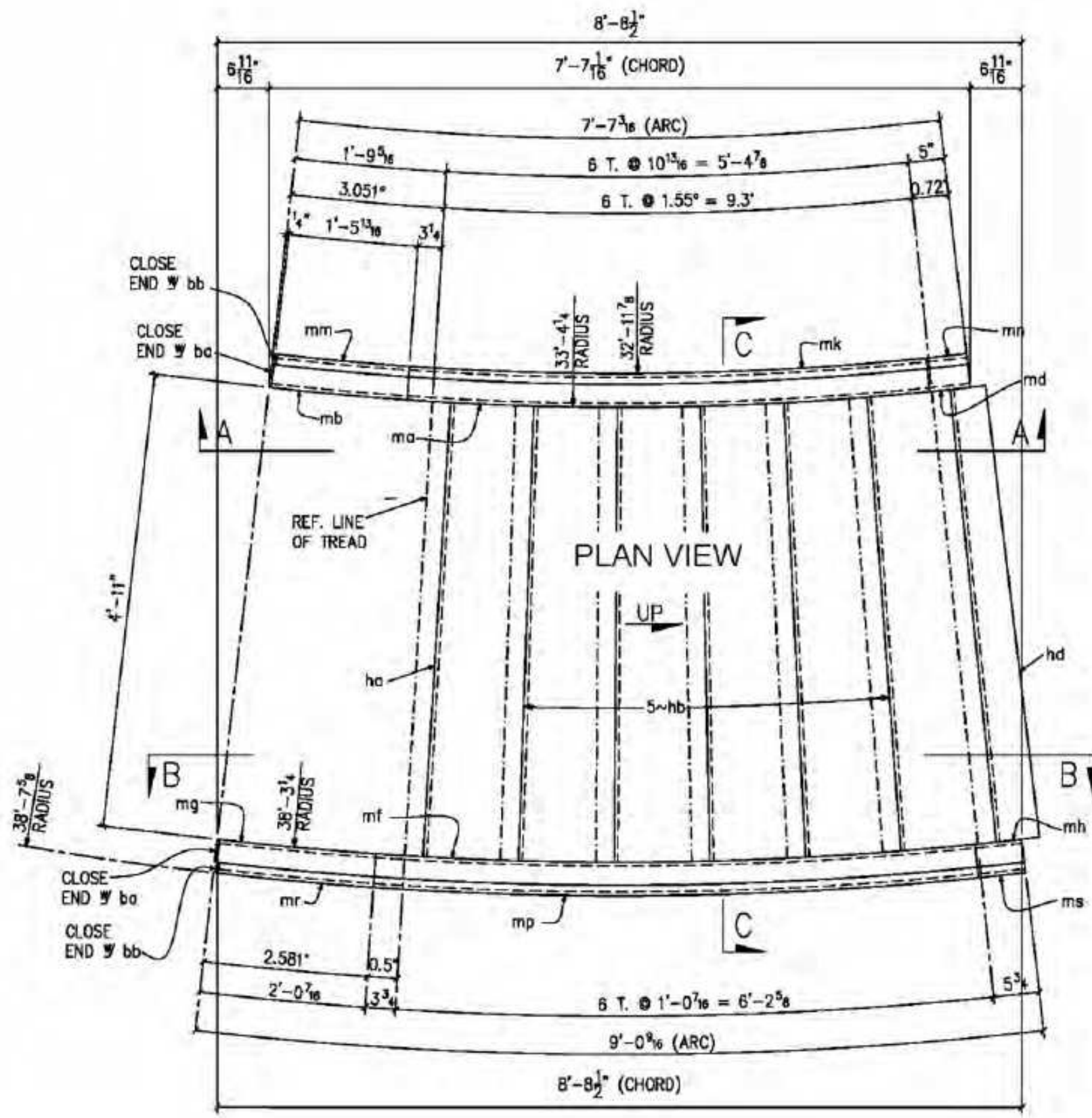
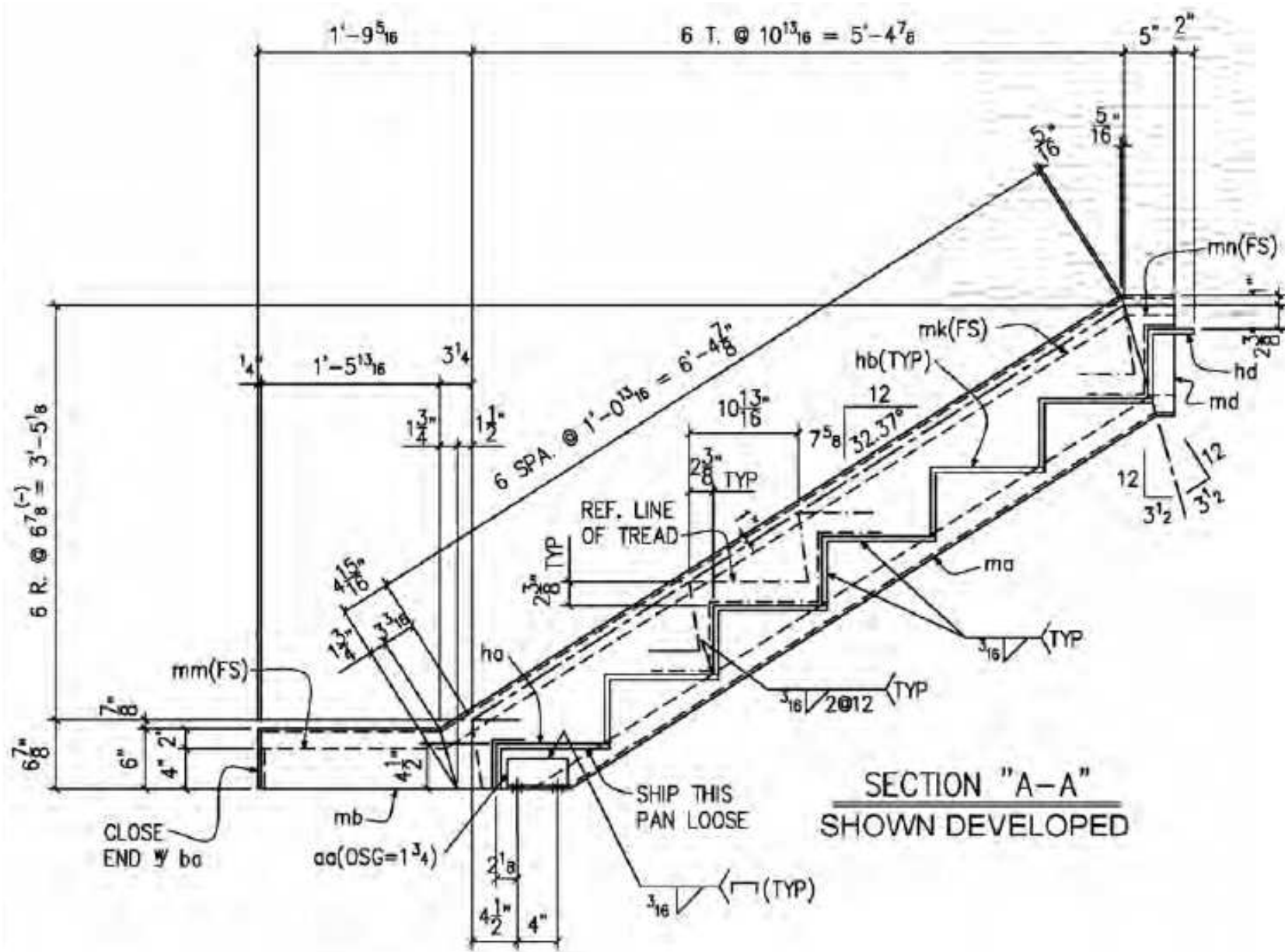
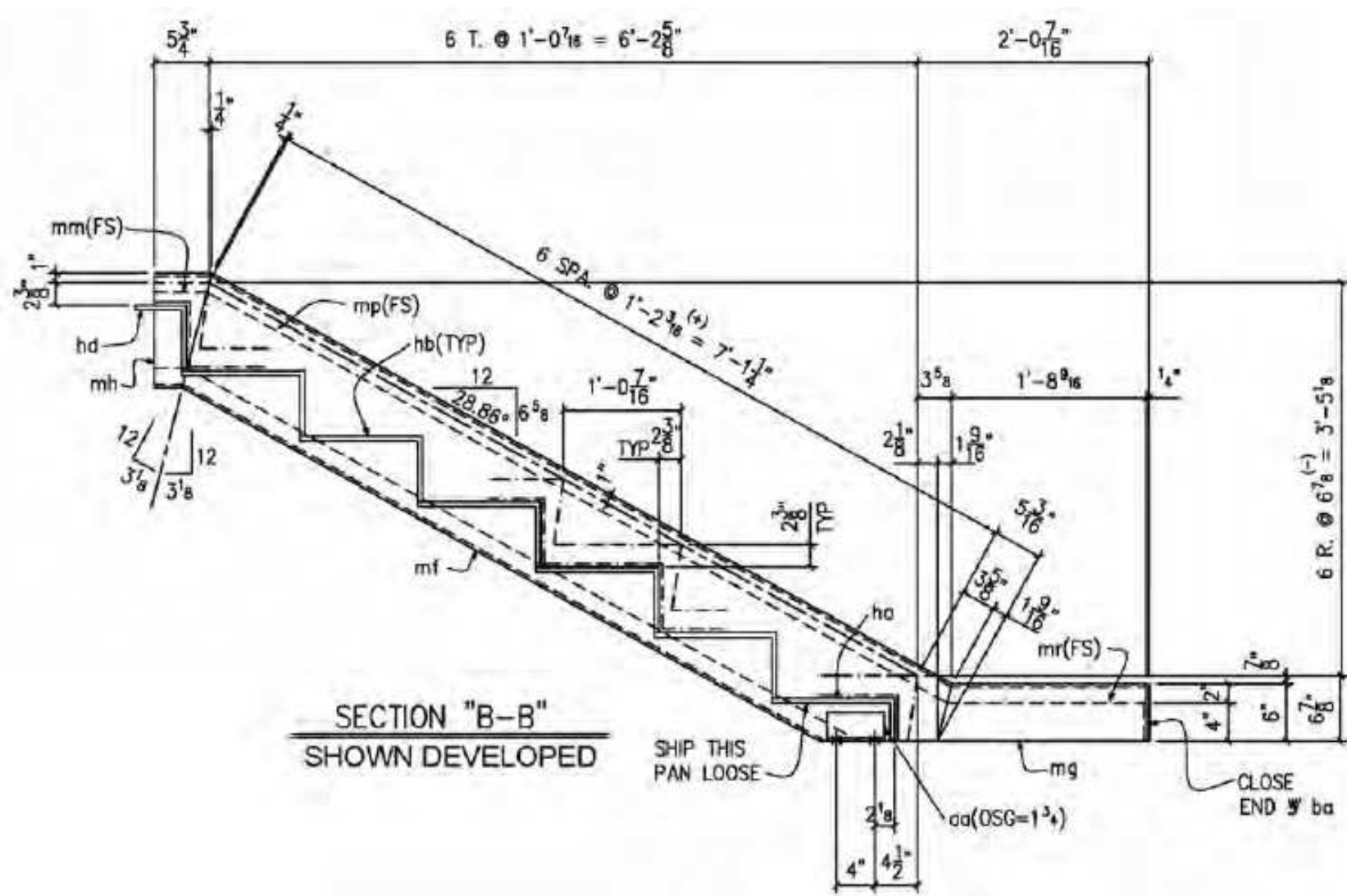


Fig. 4-7. Spiral stair contract drawing.

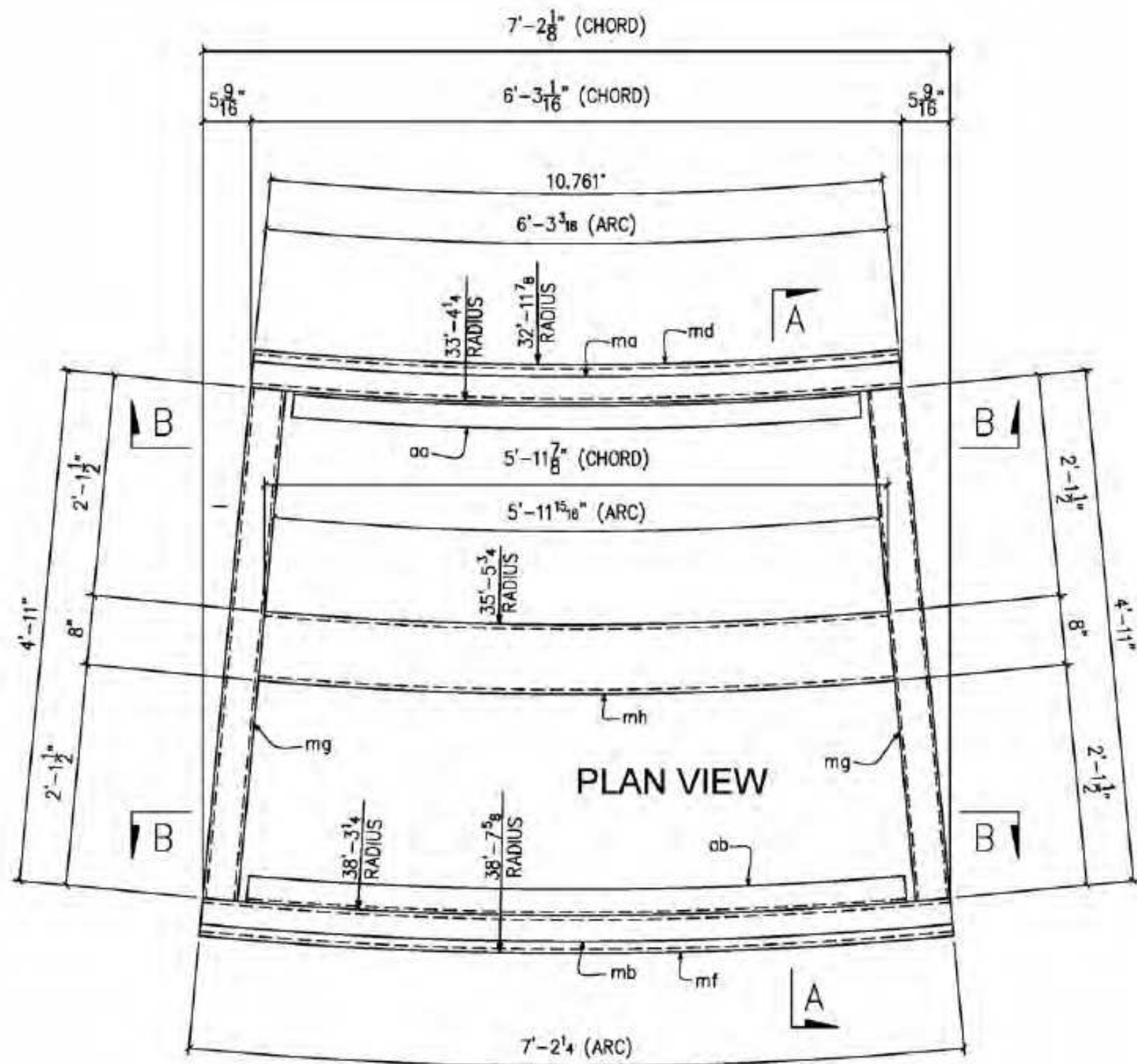




*Fig. 4-9. Spiral stair developed lower segment inner stringer.*



*Fig. 4-10. Spiral stair developed lower segment outer stringer.*



M10F1

Fig. 4-11. Spiral stair landing.

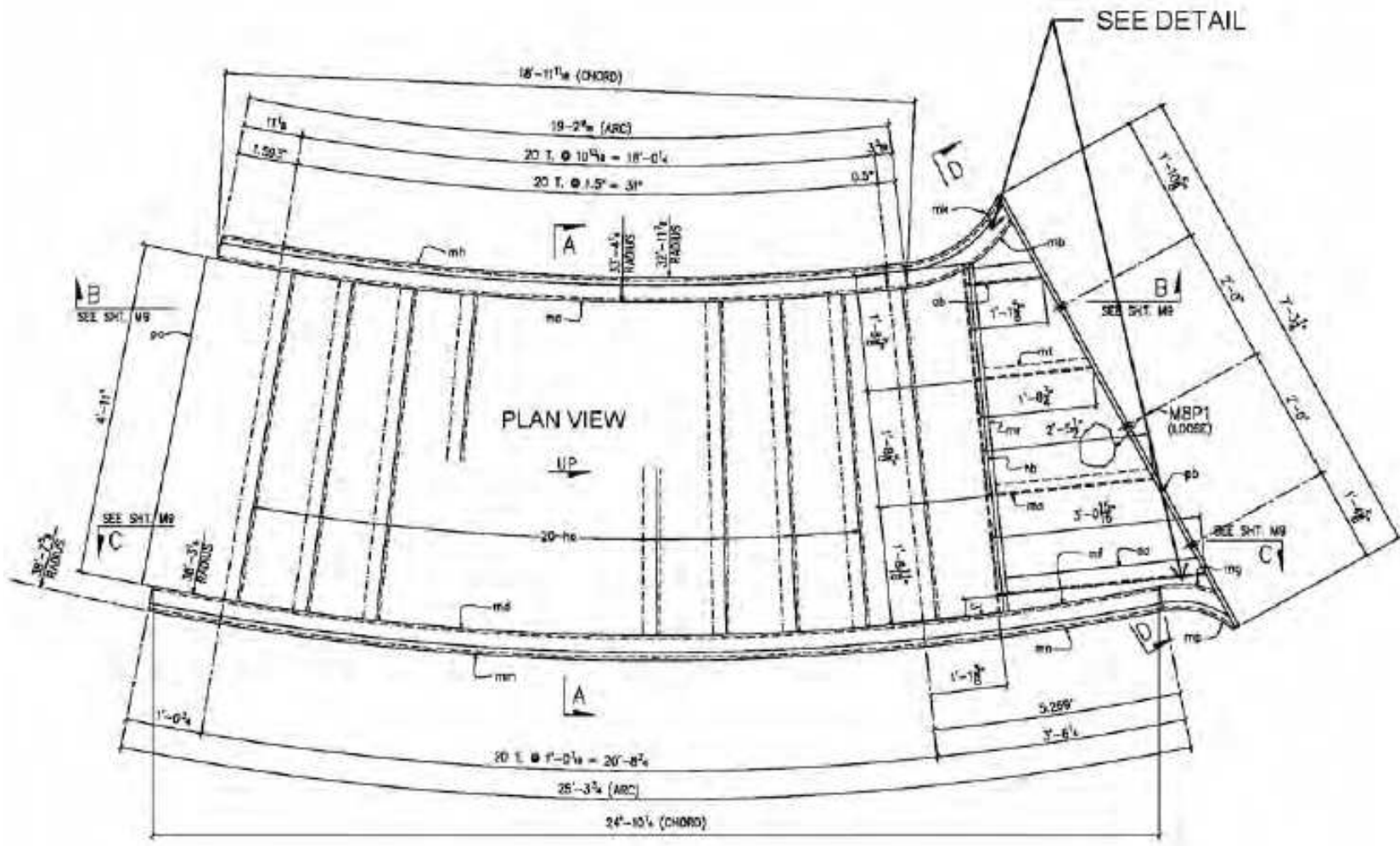


Fig. 4-12. Spiral stair plan at upper segment.

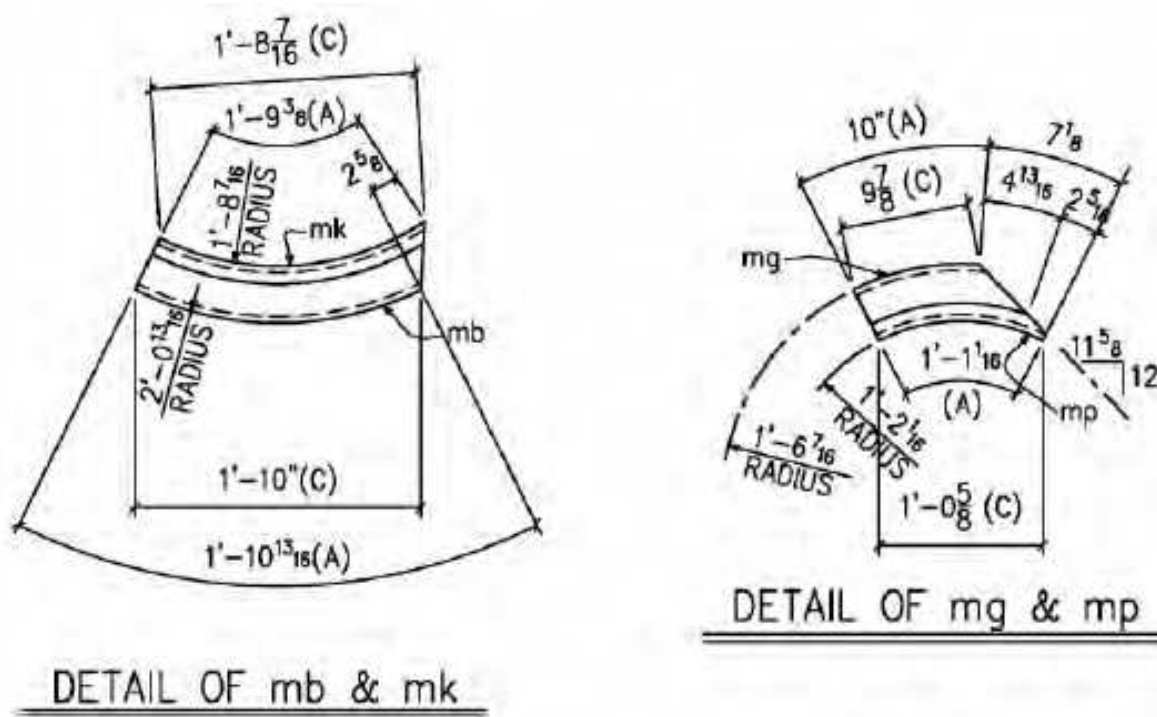


Fig. 4-13. Spiral stair upper segment ornate detail pieces.



# Chapter 5

## General Design Issues

### 5.1 INTRODUCTION

This chapter discusses several considerations that, in some cases, may affect the design of curved members. Section 5.2 discusses potential changes in material properties caused by the bending process and their effects on the structural behavior of curved members. Under normal conditions for building construction, ductility and toughness reductions can usually be neglected. However, for members subjected to high bending strains, the ductility and toughness can be significantly reduced.

Other design considerations for curved members are residual stresses (Section 5.3), nonlinear flexural stresses (Section 5.4), and cross-sectional distortion caused by the bending operation (Section 5.5). However, these differences affect the member strength only in special cases. Any changes to the residual stresses caused by the bending operation are typically beneficial and can usually be neglected. Nonlinear flexural stresses are significant only for members with very low  $R/D$  ratios that are uncommon in building construction. The effect of cross-sectional distortion needs to be evaluated only where the specified tolerances are exceeded.

Section 5.6 provides information that should be included in the contract documents to ensure the expected product is supplied. Ideally, a bender/roller company will be involved early in the design process, but the final contract documents must contain enough information to allow the fabricator and bender/roller to provide accurate cost and schedule estimates.

### 5.2 MATERIAL PROPERTIES

Cold bending involves inelastic straining of the member, which affects the material properties. These changes are primarily attributed to strain hardening and strain aging, which increases the yield stress, ultimate stress and hardness, and decreases the ductility and toughness. For curved members in buildings, the strains induced during the cold-bending process rarely exceed the potential strains induced in the manufacturing process of straight members. For example, webs of rotary-straightened I-shaped members and corners of rectangular HSS members are extensively cold worked. Gag-straightened members and round HSS are cold worked to a lesser degree. However, under some conditions where ductility and toughness are critical to the structural performance, the effect of bending on the material properties should be considered.

### 5.2.1 General Design Considerations

Most fabrication operations have the effect of reducing the ductility of the virgin steel. For example, punching and shearing cold work the material, and the heat caused by flame cutting and welding hardens the material in the heat affected zone. Because the material certification requirements are performed before fabrication, the post-fabrication material properties are typically unknown. Essentially, fabrication is controlled to provide the ductility required for the structure to perform as intended. For example, because bridges are subjected to low temperatures and fatigue loading, the *AASHTO/NSBA Steel Bridge Fabrication Guide Specifications* (AASHTO/NSBA, 2008) has special requirements that are more stringent than those in the *AISC Specification* (AISC, 2016c).

Members subjected to high strain levels during the bending process and unfavorable loading, fabrication or service conditions (see Section 5.2.4) may require special considerations. Significant judgment is required to assess the susceptibility to brittle fracture where members are subjected to conditions that may cause an increase in ductility demand and/or a decrease in ductility. Ductile performance is dependent on many variables, including the virgin material properties, level of cold work, service temperature, nature of loading (static/blast/impact/cyclic), level of working stress, level of redundancy, consequences of failure, fabrication quality, and geometry of details (stress concentrations). The *AISC Manual* (AISC, 2017) has further information on avoiding brittle fracture.

For steel previously strained to approximately 2% or higher, the ductility and toughness can be reduced by strain aging over a long period at room temperature (Boyd, 1970). For cold-worked members that are subsequently heated in the range of 250°F to 850°F, strain aging is accelerated. Temperatures in this range can be caused by welding, thermal cutting, heat straightening, or hot dip galvanizing. The critical factors affecting strain aging are the strain magnitude and the amount of time the strained material is subjected to the critical temperature range (Taylor, 2001).

Due to high cold work strains induced during manufacturing, cold-formed HSS members and members that are fabricated from cold-bent plates may require special attention. For common rectangular HSS sizes, the corner cold-bending strain can vary between 8.70 and 16.7% (Ritakallio and Bjork, 2014). Cold-bending strains for bent-plate members are dependent on the bending radius and are generally

much lower than for HSS corners. The seismic ductility of ASTM A500 rectangular HSS shapes is well documented for special concentrically braced frame (SCBF) seismic force-resisting systems, where HSS braces must endure several cycles of inelastic buckling before rupture. However, when these members are subsequently curved by bending, the already-reduced corner ductility can be further reduced by the bending strains. If cold-formed square or rectangular HSS is curved by bending, ASTM A1085 (ASTM, 2016) is preferable to ASTM A500, especially when used with unfavorable loading, fabrication or service conditions. ASTM A1085 is similar to ASTM A500 but provides improved geometric tolerances, an upper yield stress of 70 ksi, a lower limit on the corner radii, and a minimum Charpy V-notch (CVN) toughness of 25 ft-lb @ +40°F.

Under normal conditions for building construction, strain demands applied in service will be much less than those during the bending operation. Therefore, in most cases, curved members can be expected to perform as intended without accounting for any material property changes. The increased yield strength should not be considered in design, and for most structures, the decrease in ductility will not affect the structural behavior.

The modulus of elasticity remains unchanged after bending. However, where the applied service load is opposite of that induced in the bending operation, yielding occurs at a lower stress than for the virgin material due to the Bauschinger effect. Lange and Grages (2009) showed that this effect can increase service level load deflections of cold-cambered beams by about 20% over non-cambered rolled beams due to early deviation from the linear portion of the moment-rotation curve. Similar behavior was observed by Brockenbrough (1970b), where the stiffness reduction was caused by the additional residual stresses induced by heat curving of rolled beams and welded built-up plate girders. However, at service level loads, any slight variation from the theoretical elastic stress-strain curve should have a negligible effect on the predicted deflection of a cold-bent member (Kloiber, 1989).

### 5.2.2 Idealized Material Behavior

Although tension tests do not necessarily represent the behavior of a tension element in a real structure, they provide useful information that can be indicative of the actual behavior. Material property changes caused by flexural strains are similar to those caused by axial strains (Tor et al., 1951); therefore, the idealized uniaxial stress-strain curve can be used to predict the yield strength and ductility after the bending operation has been completed.

The stress-strain curve for every specimen is different because the behavior depends on several variables, including the orientation of the specimen relative to the rolling direction, the location of the specimen within the member,

any cold-working of the member, the chemistry of the steel, the cooling rate after rolling, and the toughness of the steel. However, the simplified analysis method discussed in this section is in reasonable agreement with the experimental results of Spoorenberg et al. (2012a), Kaufmann et al. (2001), Schlim (1987), and Blondeau et al. (1984).

An idealized engineering stress-strain curve for a structural steel tension specimen is shown in Figure 5-1 (FEMA, 2000). The curve is characterized by linear behavior in the elastic range and a well-defined yield point, as is represented by loading Path A-B. After yielding, the material has a flat yield plateau from Points B to C, followed by strain hardening. The material reaches ultimate strength at Point D and ruptures at Point E.

Materials subjected to inelastic strains up to about 1.5% remain on the yield plateau and unload along Path F-G. For members that are symmetric about the curved axis, this strain corresponds to  $R/D \geq 33$ , where  $R$  is the centroidal radius of curvature and  $D$  is the member depth in the plane of curvature. The residual strain, A-G, is relatively small in this range, causing only a minor ductility reduction (at 1.5% strain, the theoretical ductility reduction is approximately 7%).

For materials in the strain-hardening range, yield stress increases and ductility decreases with decreasing  $R/D$  ratios. In this case, the material unloads along Path H-I. Theoretically, upon reloading the material behaves linearly between points I and H. However, the experiments by Spoorenberg et al. (2012a) showed a slight nonlinearity as the loading approaches Point H, making for a less well-defined yield point. In this case, the yield strength is best defined using a 0.2% offset.

At 5% strain ( $R/D=10$  for members that are symmetric about the curved axis) the material will be in the strain-hardening range, with a theoretical yield stress increase of about 24% and a ductility decrease of about 25%. Strain aging can further increase the yield and tensile strengths, and reduce the ductility (Chajes et al., 1963; Kaufmann et al., 2001).

Because the material properties in this section are based on idealized conditions, empirical equations developed for cold-bent members (Spoorenberg et al., 2012b) are likely to be more accurate within the range of experimental variables. However, accurate predictions may not be warranted because, as with straight members, the material properties in cold-bent members vary throughout the cross section (Spoorenberg et al., 2012a).

### 5.2.3 Ductility and Toughness

Ductility and toughness must be adequate for the structure to perform as intended. Typical design assumptions and AISC *Specification* equations assume a minimum level of ductility to allow compact flexural members to reach the plastic

capacity of the section and to allow localized tensile yielding without rupture at stress concentrations. Under normal conditions with static loading in building construction, any ductility and toughness reductions caused by bending can be neglected in design. However, the effects of bending may need to be addressed to ensure proper performance of structures with unfavorable loading, fabrication or service conditions (see Section 5.2.4).

#### Cold Bending

Although ductility reductions can be significant at very high cold-work strains, ASTM elongation requirements for the virgin steel are usually met for cold-work strains up to 8% (Kaufmann et al., 2001). For steel plate bending, the ASME *Boiler and Pressure Vessel Code* (ASME, 2015) specifies a 5% strain limit for non-heat-treated vessel walls. Several studies have suggested higher allowable strain limits (Bala and Malik, 1983; Blondeau et al., 1984; Keating and Christian, 2007).

Strains less than 2% are usually insufficient to cause significant work hardening (Shank, 1957), and it is generally accepted that structural shapes with cold-bending strains up to approximately 3% can be used without considering material property changes (Barnshaw, 2009). For statically loaded building members with welded attachments, holes or stress concentrations, Riviezzi (1984) recommended a cold-bending strain limit of 4%. The limit can be increased to 5% for statically loaded members without welded attachments, holes or stress concentrations and should be decreased to 2% for structures subjected to impact, fatigue or cyclic loading.

Because any significant cold bending strain will cause a reduction in toughness, the strain limits in the preceding paragraph assume the toughness of the virgin material is greater than the required toughness of the curved member. The reduction in CVN absorbed energy is highly variable. For example, cold bending strains of 2% have resulted in CVN reductions between 0 and 35% (Kaufmann et al., 2001). Small-radius bends approaching the limits for cold

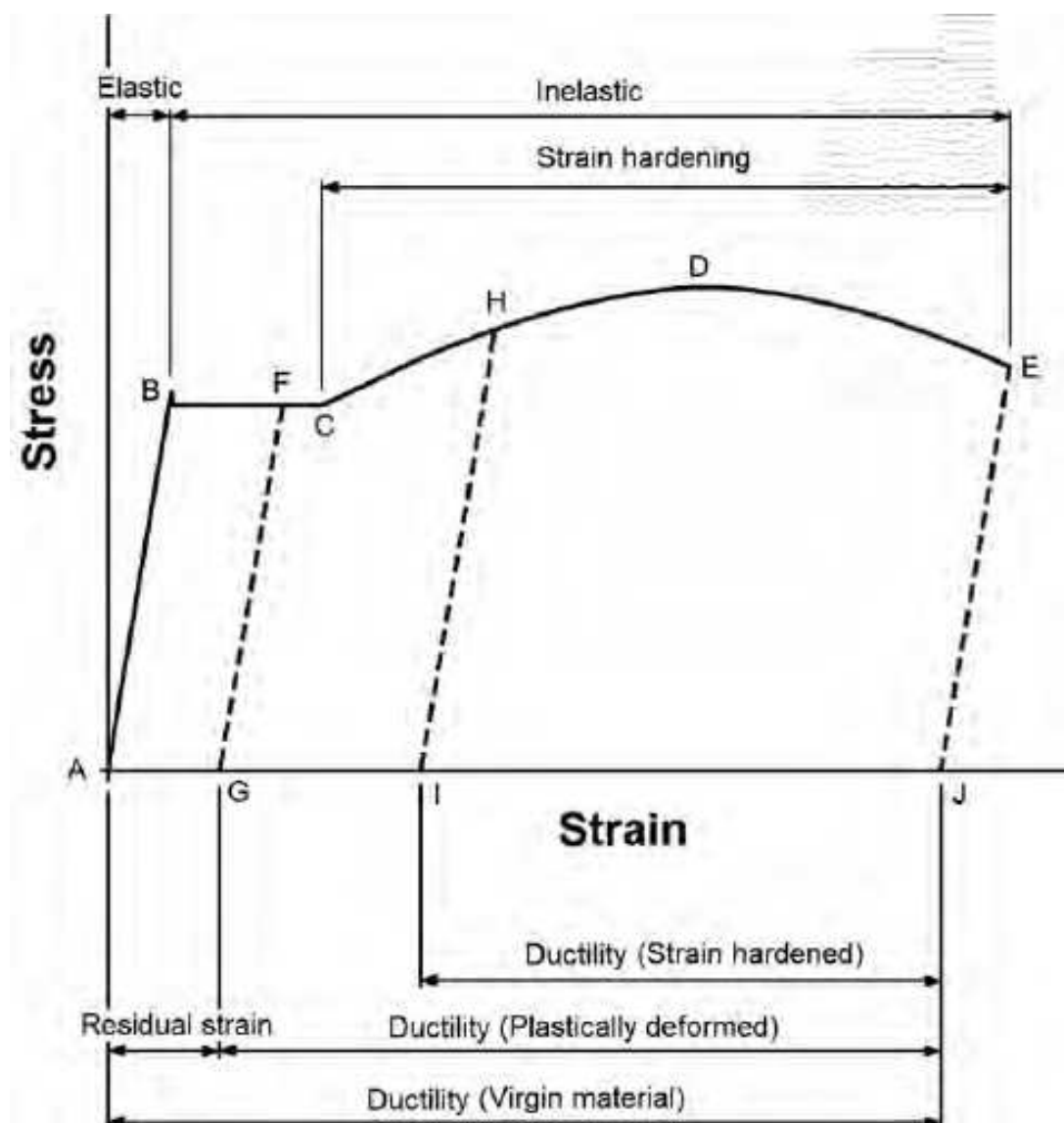


Fig. 5-1. Idealized stress-strain curve.

bending (see Table 3-2) can reduce the absorbed energy by as much as 50%. Based on the CVN measurements of straight wide-flange members (Cattan, 1996), even a 50% reduction in toughness is not likely to affect the performance of curved members subjected to static loading in typical building construction.

#### *Hot Bending and Heat Curving*

Changes to the material properties due to the application of heat are insignificant if the temperature limits in AISC *Specification* Section M2.1 are followed. Because these maximum temperatures are below the transformation temperatures, no detrimental metallurgical change will occur due to heat application alone.

In most cases, for the range of bending strains induced during the hot bending of shapes, the application of heat combined with the force required for bending is not detrimental to the properties. However, experimental results on hot-bent plates with significantly higher strains (9% to 15%) showed that ductility and toughness reduces with increasing strain (Keating and Christian, 2007).

Heat can be applied to adjust the geometry of a cold bent member with plastic strains up to 100 times the yield strain without significantly compromising the material properties (Sharma, 2005). Because any material property changes are caused primarily by the cold work, the yield strength, tensile strength and ductility are similar to cold-worked members without heat applied (Avent et al., 2000; Connor et al., 2008). The effect of heat application is similar to heat treatment, partially restoring the properties to that of the virgin steel (Connor et al., 2008; Varma and Kowalkowski, 2004). Heat application after cold bending has an insignificant effect on toughness and fatigue performance (Avent et al., 2000; Connor et al., 2008).

#### *Induction Bending*

For induction-bent members, changes in material properties occur due to recrystallization at the bending temperature (1,500 to 1,950°F). Because the bending process is inherently a form of heat treatment, with proper control of the essential variables (see Section 5.6), material properties can be enhanced by induction bending, eliminating the need for stress relieving in most applications (Riviezzi, 1984). Induction coils provide accurate temperature control and the cooling rates can be controlled to minimize the risk of unanticipated metallurgical changes. In some cases, especially for structures with unfavorable loading, fabrication or service conditions, a bending procedure qualification test may be necessary to verify the material properties after bending.

As discussed in Section 2.3.3, most induction bends are formed as the straight member moves through the coil at a constant rate. In this case, the material properties are uniform

throughout the arc. Members that are bent with incremental heating will have short segments where the material properties are affected by the induction heat, causing nonuniform material properties along the arc length. Under some conditions, varying material properties around the cross-sectional perimeter can be caused by uneven heating.

#### **5.2.4 Unfavorable Conditions**

For members with unfavorable conditions, more stringent design and/or fabrication techniques may be required. Generally, this includes members with cold-bending strains greater than 5% and structures with unfavorable loading, fabrication, or service conditions with cold-bending strains greater than 2%.

For some projects, especially those requiring multiple bends with similar strains, material properties can be evaluated using specimens extracted from highly strained areas of qualification bend test members. It may be desirable to provide an additional arc length to production members so the qualification bend tests can be cut from the production member end.

The effects of cold work on the strength, residual stresses, ductility and toughness can be reduced with heat treatment. Due to the additional time and expense involved, this option should be specified only where necessary. Properties can be partially restored by stress relieving the member; however, normalizing is the only heat treatment method that consistently restores the ductility and toughness to values similar to the virgin material. Properly controlled induction bending may also produce the material properties required.

Another option that may eliminate the need for heat treatment is to reduce the available strength from those specified in the AISC *Specification*. In many practical situations, the ductility and toughness requirements can be relaxed for members designed to a lower portion of their available strength. For yield strengths of 50 ksi and lower, Riviezzi (1984) recommended the available strength reductions in Table 5-1 for statically loaded members.

#### *Low Service Temperatures*

Generally, for statically loaded straight members, low temperature service is a consideration only when the lowest anticipated service temperature (LAST) is less than -30°F. Cold bending can cause an upward shift of the transition temperature, potentially making values for LAST less than +30°F detrimental for statically loaded members with high cold-bending strains.

The increase in transition temperature with cold-work strain is approximately linear, but the range is highly variable. For example, cold-bending strains of 2% have resulted in an upward shift between 0°F and 25°F (Kaufmann et al., 2001; Blondeau et al., 1984). Strains of 5% and greater

Table 5-1. Available Strength Reductions (Riviezzi, 1984)		
Member Description	Cold Bending Strain	Strength Reduction Factor
Members with no welded attachments, holes or stress concentrations	$\epsilon \leq 5\%$	1.0
	$\epsilon > 5\%$	0.60
Members with welded attachments, holes or stress concentrations	$\epsilon \leq 4\%$	1.0
	$\epsilon > 4\%$	0.60

increase the transition temperature appreciably (Shank, 1957), causing an upward shift as high as 60°F for specimens with 7% strain (Blondeau et al., 1984). However, cold bending structural members to 7% strain is rare and is typically limited to HSS shapes (see Table 3-2).

These effects can be almost completely suppressed by stress relieving (Blondeau et al., 1984) or properly controlled induction bending. Lower service temperatures may be possible while avoiding stress-relief if strength reduction factors similar to those in Table 5-1 are used in design. However, unfavorable loading, fabrication or service conditions can significantly increase the minimum applicable service temperatures.

### Galvanizing

As discussed in Section 5.2.1, strain aging can be accelerated, reducing the ductility and toughness of cold-bent members that are subsequently heated to galvanizing temperatures. The factors that can lead to embrittlement are discussed in ASTM A143/A143M-07(2014) (ASTM, 2014). As much as is practical, notches should be avoided for these members.

Although reported cases with cold bending and subsequent galvanizing have been successful (Wendt, 2010), careful post-galvanizing inspection of the member is important (Bjorhovde, 2006). For cold-bending strains greater than approximately 2%, the member may need to be stress relieved at 1,100°F for one hour for every inch of section thickness before galvanizing (Rahrig and Krzywicki, 2005). To avoid excessive grain growth, a maximum stress-relieving temperature of 1,100°F should be used (ASTM, 2014). Alternatively, the member can be normalized at temperatures from 1,600°F to 1,700°F (ASTM, 2014). Properly controlled induction bending may also produce the material properties required.

## 5.3 RESIDUAL STRESSES

Residual stresses are self-equilibrating stresses that are built into members as a result of manufacturing and fabrication operations. Thermally induced residual stresses can be caused by uneven cooling of the material after hot rolling, welding, flame cutting, heat curving and induction bending. Mechanically induced residual stresses can be caused

by punching, grinding, cold bending, and other fabrication operations. When multiple operations produce residual stresses in a member, the final residual stresses are determined primarily by the final stress-inducing operation with previous residual stresses of secondary importance (Macgregor, 1954).

The typical residual stress pattern for rolled I-shaped members, shown in Figure 5-2(a), is characterized by compression residual stresses at the flange edges that can vary from about 20% to 80% of the yield stress, depending on the flange thickness. Equilibrium is maintained by compression residual stresses at the mid-depth of the web and tensile residual stresses at the mid-width of the flanges.

Welded and oxyfuel flame-cut members typically have tensile residual stresses at the location of the heat input. The magnitude of the tensile residual stresses are typically at least equal to the yield stress of the material and are generally around 60 to 70 ksi, regardless of the original material properties (Bjorhovde et al., 2001). The parts that cool first will have residual compression; those that cool last will have residual tension.

Hot-formed HSS members have negligible longitudinal residual stresses (Sherman, 1992). Square and rectangular cold-formed HSS have yield-level tensile residual stresses along the weld seam and compression residual stresses in the corners as shown in Figure 5-2(b). The maximum tensile residual stress at the non-welded sides is approximately 50% of the yield stress (Sherman, 1969), and the maximum compression residual stresses are between 10% and 50% of the yield stress (Sherman, 1997; Key and Hancock, 1985; Sherman, 1969). Round HSS have yield-level tensile residual stresses along the weld seam and maximum compression residual stresses localized adjacent to the weld seam. Residual stresses are negligible for the remaining circumference (Ross and Chen, 1976).

### 5.3.1 Theoretical Residual Stresses

The cold-bending process induces a permanent deformation that alters the residual stress pattern. After the bending loads are released, the elastic fibers have a tendency to recover their original shape. Elastic spring-back forces are required for equilibrium of the section, but the spring-back is partially restrained by the inelastic fibers, which have a permanent

set. Superposition of the loading and spring-back stresses results in the final residual stresses remaining after unloading (Timoshenko, 1956).

This process is illustrated in Figure 5-3 for a perfectly plastic beam free of initial residual stresses and bent to the fully plastic condition. When the load is released, the spring-back stress,  $\sigma_s$ , adds to the yield stress,  $\sigma_y$ , resulting in the final residual stress pattern with tension stress,  $\sigma_{rt}$ , and compression stress,  $\sigma_{rc}$ , at the inner and outer extreme fibers, respectively. The resulting residual stresses at the extreme fibers are of opposite direction to the stresses induced during the bending operation. The residual stresses throughout the cross section are  $\sigma_r = \sigma_s + \sigma_y$ , and the residual stress magnitudes at the extreme fibers are  $\sigma_{rc} = \sigma_{rt} = \sigma_y(f - 1)$ , where  $f$  is the shape factor. For a rectangular member,  $f = 1.5$  and  $\sigma_{rc} = \sigma_{rt} = 0.50\sigma_y$ .

### 5.3.2 Actual Residual Stresses

The analysis method presented in Section 5.3.1 is oversimplistic because it does not account for three-dimensional effects, strain hardening material behavior, partially plastic stress distributions, or residual stresses that are present before bending. The cold-bending operation has a significant influence on the final residual stress pattern because it is usually the final operation affecting the residual stresses. However, the prebend residual stresses are only modified, not fully suppressed. For partially plastic stresses and strain-hardening material models, the residual stresses can be calculated by subtracting the elastic spring-back stresses from the inelastic stresses, where both are based on the moment applied during the cold-bending operation (Nitta and Thurlmann, 1960; Baldwin, 1949).

Residual stress changes due to cold bending occur only in the sections along the member that were yielded during the bending operation. Pyramid roller bending applies a uniform moment along the arc length; therefore, the residual stresses are constant along the curved length. For bending methods that concentrate the moment at discrete locations along the length, such as incremental step bending, ram bending, and gag pressing, the altered residual stress patterns are localized at these locations.

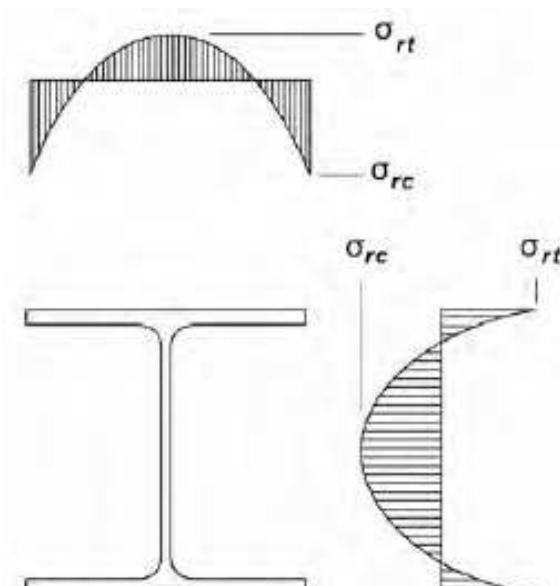
#### I-Shape Bent the Hard Way

A simplified residual stress pattern for an I-shaped member bent the hard way is shown in Figure 5-4 (Spoorenberg et al., 2011). Both the cold-bending effects and the initial residual stresses have a significant effect on the final residual stresses. Although the bending radius was found to have no clear influence on the residual stresses, the simplified pattern is valid only within the range investigated:  $10 \leq R/D \leq 40$ .

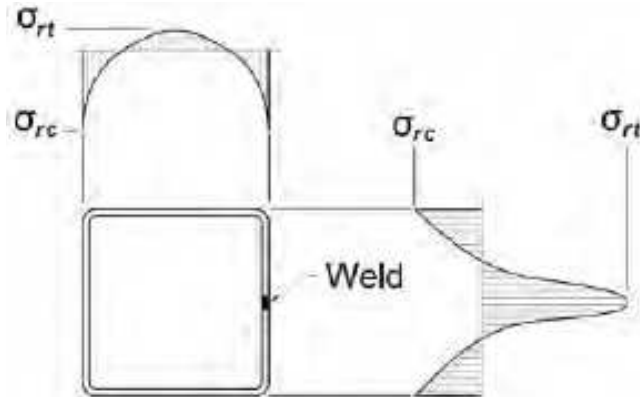
At the inner flange, the tension and compression residual stresses are  $\sigma_{rt} = 0.70\sigma_y$  and  $\sigma_{rc} = 0.35\sigma_y$ , respectively. At the outer flange, the magnitude of both the tension and compression residual stresses are  $\sigma_{rt} = \sigma_{rc} = 0.20\sigma_y$ . The magnitude of the residual stresses in the web are based on equilibrium and are dependent on the cross-section dimensions. For common wide-flange shapes, the web residual stresses required for equilibrium are approximately  $\sigma_{rt} = 0.25\sigma_y$  and  $\sigma_{rc} = 0.50\sigma_y$ .

#### I-Shape Bent the Easy Way

A simplified residual stress pattern for an I-shape bent the easy way is shown in Figure 5-5. This pattern agrees well with the measured residual stresses for rolled I-shaped



(a) Rolled I-shape



(b) Rectangular HSS

Fig. 5-2. Residual stress pattern for straight members.

members bent the easy way (Yoo et al., 1986) and rotary-straightened I-shaped members (Adams, 1966; Arnold et al., 1968; Beedle and Tall, 1960; Huber, 1958; Yura and Lu, 1968). A similar pattern was recommended by ECCS (1976), with  $\sigma_{rt} = \sigma_{rc} = 0.20\sigma_y$ , for rotary-straightened members. Lay and Ward (1969) noted that thermal residual stresses due to rolling were reduced by approximately 50% in roller-straightened members.

Heat curving about the weak axis produces a residual stress pattern with tension at the flange edges approximately equal to the yield stress (Brockenbrough, 1970a). Similar patterns result from the simultaneous application of heat and force, which is required for hot bending (Avent et al., 2001).

#### Hollow Structural Sections (HSS)

The residual stress pattern for cold-formed rectangular and square HSS members that are subsequently curved by cold bending is shown in Figure 5-6. Contrary to the theoretical residual stress discussion in Section 5.3.1, the residual stresses caused by cold bending are nonlinear across the flange width (Yanfei et al., 2015). These stresses, combined with the residual stresses in the member before bending [Figure 5-2(b)], result in tension residual stresses at the corners of the inner flange and compression residual stresses at the mid-depth of the web (Yanfei et al., 2015). Chiew et al. (2016) proposed a simplified, linear approximation similar to Figure 5-6, with equations to calculate the residual

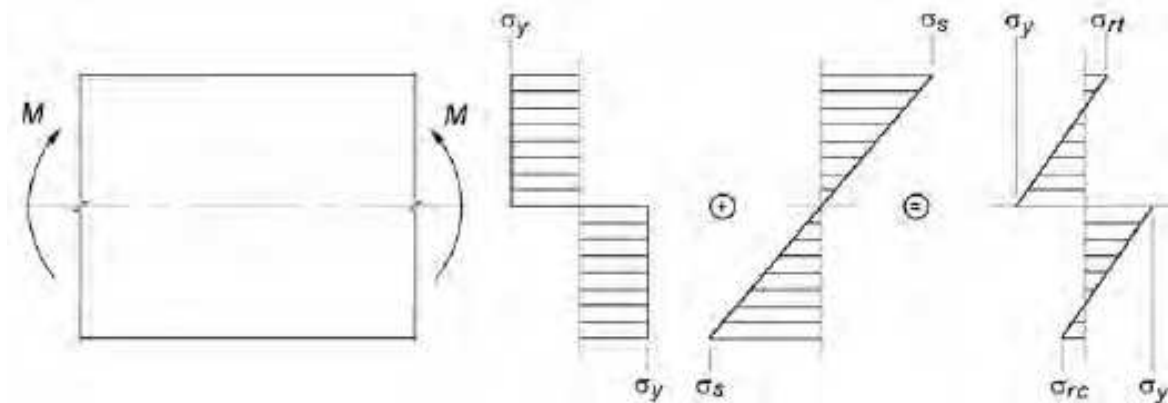


Fig. 5-3. Theoretical cold-bending residual stresses.

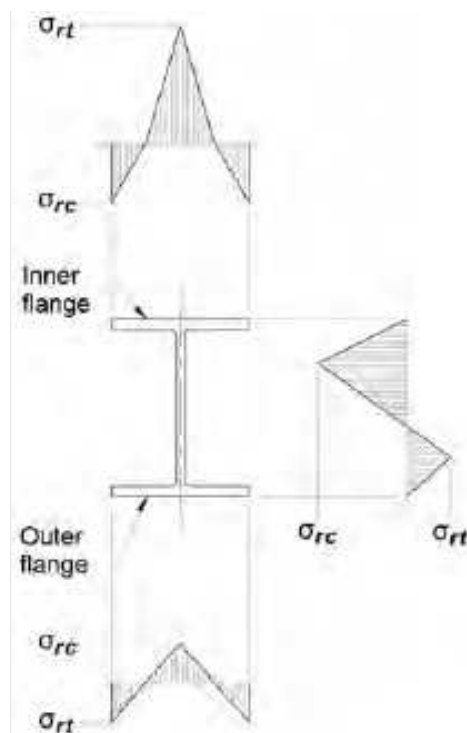


Fig. 5-4. Residual stress pattern for an I-shape bent the hard way.

stress magnitudes that are dependent on the cross-sectional dimensions and the bending radius. The maximum longitudinal residual stresses in both tension and compression are approximately  $0.60\sigma_y$  (Seddeik, 1985).

For round HSS members, cold-bending residual stresses vary around the perimeter. For very small  $R/D$  ratios typical of piping systems, the maximum longitudinal residual stresses are approximately  $0.50\sigma_y$  for draw bent members and  $1.0\sigma_y$  for hot bent members (Ding et al., 2014).

Induction bending induces maximum longitudinal residual stresses below  $0.50\sigma_y$ . Differential cooling causes a narrow band of through-thickness flexural residual stress to form around the perimeter of the final heated segment (at the last formed tangent). These flexural residual stresses, which exceed the yield stress, are caused by radial contraction of the water-cooled section, which is constrained by the adjacent straight segment.

### 5.3.3 Effect on Structural Performance

Cold bending tends to act as a form of mechanical stress relief (Lay and Ward, 1969), usually reducing the thermal residual stresses induced by the manufacturing process (hot rolling or cold forming and welding) of the straight member (Kloiber, 1989). When a bending method is used that concentrates the strains at discrete sections along the member length (incremental step bending, gag pressing), Adams (1966) noted that “it has been common practice to neglect any influence of cold bending on the behavior of members.”

Residual stresses have no effect on the plastic strength of a member; however, both the local and global buckling strength of compression members can be affected. For hot-rolled I-shaped members bent the hard way, changes to the residual stresses caused by cold bending increase the flexural buckling strength (Spoorenberg et al., 2012c). Similar results are expected for other cases; therefore, the change in

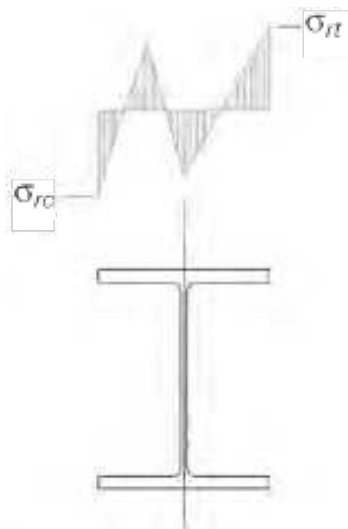


Fig. 5-5. Residual stress pattern for an I-shape bent the easy way.

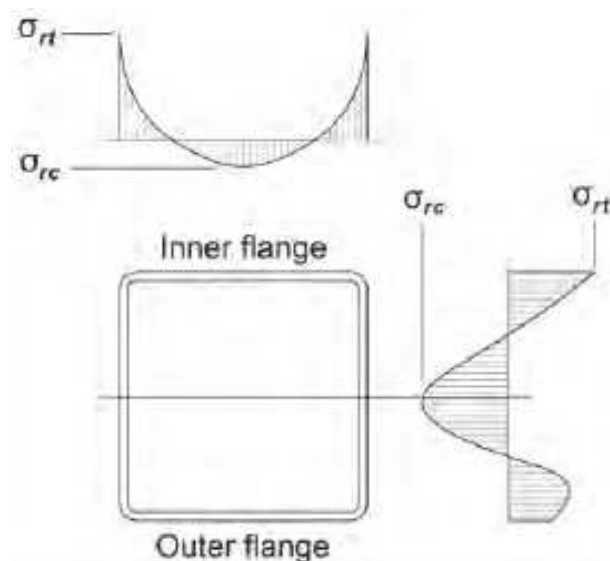


Fig. 5-6. Residual stress pattern for a bent cold-formed rectangular HSS.

residual stresses should be beneficial, or at worst, negligible for all cold-bent members.

The maximum residual stresses induced by heat curving and hot bending are similar to those caused by welding and oxyfuel flame cutting. For welded plate girders that were curved about the horizontal axis by heat curving, White et al. (2001) showed a negligible (about 1.5%) decrease in the flexural strength when the residual stresses caused by heat curving (Culver and Nasir, 1971) were used in lieu of the residual stresses caused by flame cutting and welding the flanges. Except for the through-thickness flexural residual stresses discussed in Section 5.3.2 for round HSS members, the heat induced in the induction bending process tends to act as a thermal stress relief, reducing the residual stresses.

Although residual stresses can influence fatigue performance, they are not considered in design because their effect is implicitly included in the provisions of AISC *Specification* Appendix 3. The Appendix 3 equations are calibrated using specimens with appropriate residual stresses; therefore, the fatigue life is calculated with the stress range as the sole stress parameter. Generally, the change in residual stresses caused by bending can be neglected when evaluating the fatigue performance.

#### 5.4 NONLINEAR FLEXURAL STRESSES

For members with radii typical of curved steel construction, flexural stresses can be calculated using the straight beam equation,  $\sigma = Mc/I$  (Boresi et al., 1993). However, when members curved to a very small radius are subjected

to flexure in the plane of curvature, the simplifying assumptions used to derive the straight beam equation are no longer valid. For curved members, the neutral axis lies between the centroidal axis and the center of curvature, and the flexural stresses are nonlinear as shown in Figure 5-7 (Fuller and Johnston, 1919). As the radius decreases, the neutral axis moves closer to the center of curvature.

The stresses at the extreme fibers are:

$$\sigma_c = \sigma_s \alpha \quad (5-1)$$

where

$\alpha$  = curved member/straight member flexural stress ratio

$\sigma_c$  = flexural stress at the extreme fibers of a curved member, ksi

$\sigma_s$  = flexural stress at the extreme fibers of an equivalent straight member, ksi

An approximate equation for the flexural stress ratio,  $\alpha$ , is (Cook and Young, 1985):

$$\alpha = \frac{R}{r} \quad (5-2)$$

where

$R$  = centroidal radius, in.

$r$  = radius to the point of interest, in.

For doubly symmetric members, the stress ratios at the inner and outer extreme fibers can be estimated using Equations 5-3a and 5-3b, respectively.

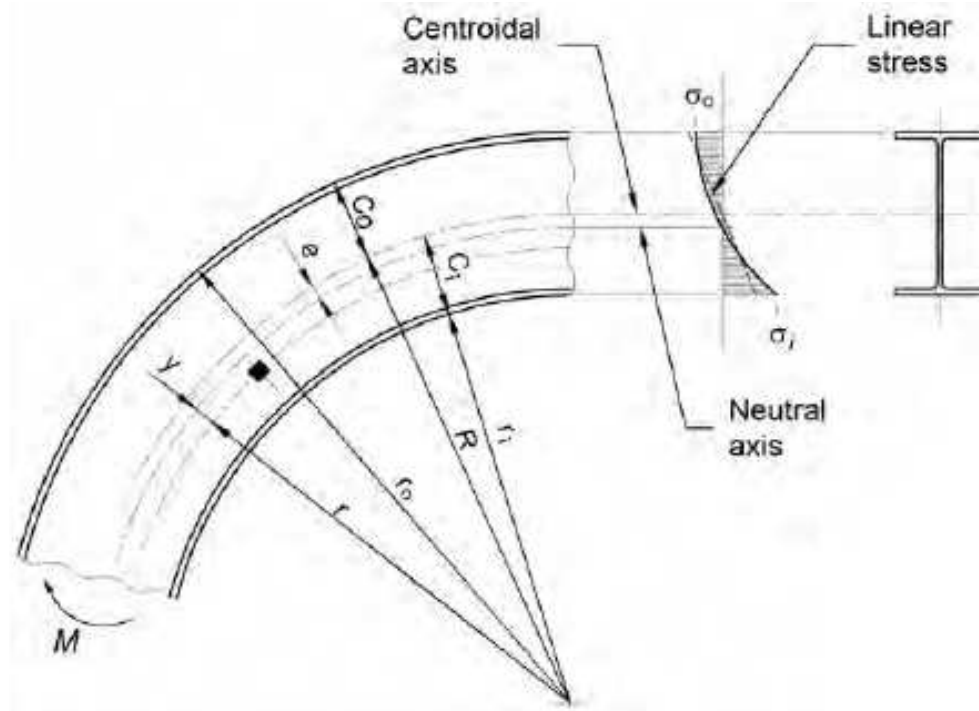


Fig. 5-7. Flexural stresses in the plane of curvature.

$$\alpha_i = \frac{1}{1 - \frac{D}{2R}} \quad (5-3a)$$

$$\alpha_o = \frac{1}{1 + \frac{D}{2R}} \quad (5-3b)$$

where

$D$  = member depth in the plane of curvature, in.

$\alpha_i$  = curved member/straight member flexural stress ratio at the inner fiber

$\alpha_o$  = curved member/straight member flexural stress ratio at the outer fiber

Equations 5-2 and 5-3 are conservative for all common structural steel shapes; however, more accurate calculations can account for the influence of the cross-sectional dimensions perpendicular to the plane of curvature. For members with relative large radii typical of curved steel construction, the stress ratio at the inner fiber is more accurately calculated with Equation 5-4, which is based on the work of Wilson and Quereau (1928):

$$\alpha_i = 1 + \frac{4I}{RBD^2} \quad (5-4)$$

where

$B$  = member width perpendicular to the plane of curvature, in.

$I$  = moment of inertia about the bending axis, in.<sup>4</sup>

Using Equation 5-4 for I-shaped members curved the hard way with  $R/D=10$ , the stress at the inner fiber is a maximum of 1% higher than that of a straight beam. For solid

rectangular shapes, I-shaped members curved the easy way, and tee-shapes with  $R/D=10$ , the stress at the inner fiber is a maximum of 3% higher than that of a straight beam. Therefore, for  $R/D \leq 10$ , structural steel members can be designed without consideration of the effect of curvature on the flexural stresses.

## 5.5 STRUCTURAL EFFECTS OF CROSS-SECTIONAL DISTORTION

Section 3.4 discusses cross-sectional distortion caused by the bending operation, and Section 4.3.3 discusses tolerances on these sectional dimensions. Unless the specified tolerances are exceeded, the effect of distortion can usually be neglected in design.

### 5.5.1 Rectangular Elements

The out-of-flatness tolerance implied by the limiting width-to-thickness ratios for noncompact/slender elements in AISC *Specification* Table B4.1b is  $(\delta_o/t)_{max} = 0.264$ . Based on equations developed by Dowswell (2010) and Soares (1988), the strength reduction for elements with  $\delta_o/t > 0.264$  can be calculated with Equation 5-5, which is applicable to all flat elements in AISC *Specification* Tables B4.1a and B4.1b. The reduction in local buckling strength according to Equation 5-5 is shown in Figure 5-8.

$$C_\delta = 1.23 - 0.95 \frac{\delta_o}{t} + 0.30 \left( \frac{\delta_o}{t} \right)^2 \quad (5-5)$$

In design, the local buckling strength for elements with  $\delta_o/t > 0.264$  can be addressed with an effective width-to-thickness ratio,  $\lambda_e$ , defined by Equation 5-6. The

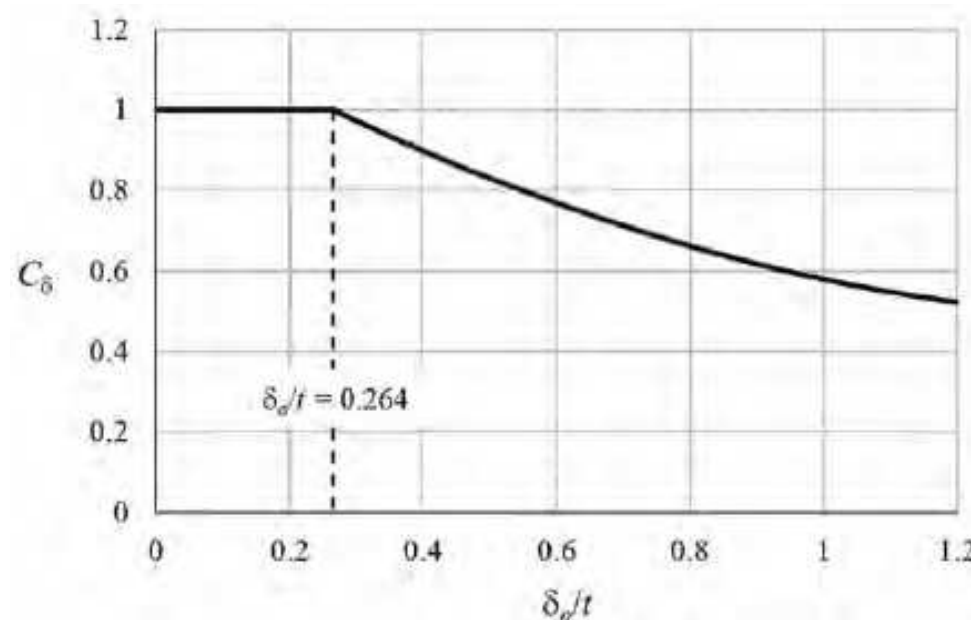


Fig. 5-8. Local buckling strength versus normalized out-of-flatness.

**Table 5-2. Section Property Ratios for Various Ovalization Parameters**

Section Property <sup>a</sup>	Equation	$\rho$				
		4%	5%	8%	10%	12%
$I_x/I$	$1 + 0.760\rho$	1.03	1.04	1.06	1.08	1.09
$I_y/I$	$1 - 0.741\rho$	0.970	0.963	0.940	0.926	0.911
$S_x/S$	$1 + 0.242\rho$	1.01	1.01	1.02	1.02	1.03
$S_y/S$	$1 - 0.261\rho$	0.990	0.987	0.980	0.974	0.969
$Z_x/Z$	$1 + 0.369\rho$	1.01	1.02	1.03	1.03	1.04
$Z_y/Z$	$1 - 0.313\rho$	0.987	0.984	0.974	0.968	0.962
$r_x/r$	$1 + 0.365\rho$	1.01	1.02	1.03	1.04	1.04
$r_y/r$	$1 - 0.386\rho$	0.985	0.981	0.969	0.962	0.954

<sup>a</sup> The x axis is the major axis, and the y axis is the minor axis.

width-to-thickness ratios required for the bending operation are usually more stringent than those required to resist service loads. Therefore, in most cases, reasonable cross-sectional distortions have a negligible structural effect. For example, if the flange of an I-shaped member is selected to meet  $\lambda < \lambda_{hd}$  to minimize distortion during the bending operation, the member can be designed for service loads using  $\lambda_p$  with a flange distortion  $\delta_o = 0.85t$ . With this large out-of-flatness distortion,  $C_\delta = 0.64$ ,  $\lambda = \lambda_{hd}$  and  $\lambda_e = \lambda_p$ .

$$\lambda_e = \frac{\lambda}{\sqrt{C_\delta}} \quad (5-6)$$

where

$b$  = element width, in.

$t$  = element thickness, in.

$\delta_o$  = initial out-of-flatness, in.

$\lambda = b/t$

### 5.5.2 Round HSS Ovality

The effect of ovalization on round HSS sectional properties is shown in Table 5-2. The moment of inertia, section modulus, plastic modulus, and radius of gyration were calculated for the major and minor axis of an ellipse for various ovalization parameters defined by Equation 3-5 in Section 3.4.4. In the second column of Table 5-2, an equation is provided for estimating each property ratio.

For  $\rho=8\%$ , using the nominal section properties results in errors of approximately  $\pm 3\%$  and  $\pm 6\%$  for the flexural strength and stiffness, respectively. It may be appropriate to neglect these differences in design, partially because the calculated member stiffness can be considered only an approximation due to the Bauschinger effect and the revised residual stress patterns caused by the bending operation. Additionally, the design recommendations in Chapters 6 and 7 require

more significant, generally conservative, reductions in the flexural properties for conditions where ovalization is critical under service loads. For  $\rho > 8\%$ , the ovalization factors in Chapters 6 and 7 can be used with the adjusted properties based on coefficients in Table 5-2 in lieu of the nominal properties.

### 5.6 CONTRACT DOCUMENTS

To ensure the expected product is supplied, requirements for curved members must be specified in the contract documents. The bid documents should contain enough information to allow an accurate cost estimate for bending services. Because the bender/roller usually acts as a subcontractor to the fabricator, the selection of the bender/roller generally occurs after the fabrication contract has been awarded. Therefore, any special bending requirements must be carefully considered by the design professional and conveyed to the fabricator. Any special requirements, such as weld seam grinding and lifting/erection aids, should be specified in the contract. Ideally, a bender/roller will be involved early in the design process.

Dimensional inspections should be performed at the bender/roller shop in the unstressed condition. Unless specified, only visual inspection for cracking is typically performed (Feldman, 2008). The contract documents must specify any specialized post-bend nondestructive testing or inspection procedures that are required.

All architecturally exposed structural steel (AESS) members must be identified in the contract documents. Each member designated AECC must be assigned a category defined in AISC *Code of Standard Practice* Section 10.1.1 (AISC, 2016a). Because the acceptable distortion decreases with increasing category, the bending cost usually increases. For both AECC and non-AECC members, the cross-sectional distortion tolerances should be specified. Often,

the cross-sectional element thickness required for strength is less than that required to limit distortion during the bending operation; therefore, member sizes shown on the design drawings should consider bending requirements. A bender/roller can be consulted regarding the cross-sectional element thicknesses required to limit distortion. Cross-sectional distortion and tolerances are discussed in Sections 3.4 and 4.3, respectively.

As with the fabrication of straight members, any splices required to limit the member length for handling, shipping or galvanizing should be shown in the contract documents. Additionally, any limitations caused by the bending machine or the bender/roller shop layout must be considered when locating the splices.

Geometric limitations should be checked to ensure proper functionality of horizontally curved monorail beams. Small-radius bends can cause binding of the trolley while traveling around the curve. It may be worth establishing the trolley manufacturer early in the design phase and working with them to verify the clearances. Because the trolley wheels roll along the bottom flange, a flange distortion tolerance should be included in the contract documents.

If post-bend heat treatment is required, the procedures must be specified in the contract documents. As discussed in Section 5.2, heat treatment is required only for structures with unfavorable loading, fabrication or service conditions. Due to the additional time and expense involved, this option should be specified only where necessary. For heat-curved or hot-bent members, the temperature limits in AISC *Specification* Section M2.1 must be followed to ensure the virgin mechanical properties are retained in the bent member.

Because induction-bent members are heated to between 1,500°F and 1,950°F, recrystallization can significantly affect the material properties. As discussed in Section 5.2.3, properties are usually enhanced by induction bending, but the temperature and the cooling rates must be closely

controlled to minimize the risk of unanticipated metallurgical changes. For structures with unfavorable loading, fabrication or service conditions, a bending procedure qualification test may be necessary to verify the material properties after bending. If a bending procedure qualification test is conducted, the production bending process can be revised as necessary to produce a product that meets the required properties. Because induction bending is a specialized process, the contract documents should be developed with significant input from a bender/roller company with experience in induction bending. TPA (1998) contains recommended standard practices for qualification of bending procedures for round tubular shapes conveying pressurized fluids. A standard qualification procedure is not available for structural members; however, many of the TPA recommendations can be used without modification, or they can be modified for use with structural members. For example, in pressurized piping, hoop stresses often control the design. However, in most structural applications, longitudinal material properties are of primary importance; therefore, coupons for destructive qualification tests should be oriented parallel to the member axis. Generally, a bending procedure will include the following information:

- Essential variables and tolerances for production bending, including member geometry, bending speed, bending temperature, power, frequency and coolant information (ISO, 2009).
- Information on post-bend heat treatment, if required.
- Details of any bending procedure qualification tests required. The contract documents must specify the required material properties and the location and orientation of the coupons for each test. Requirements for retesting should be specified.
- Post-bending inspection and nondestructive testing requirements.

# Chapter 6

## Vertically Curved Members

### 6.1 INTRODUCTION

Arches are efficient structural forms that resist loads primarily by axial compression. In practice, pure axial compression without moment cannot exist due to imperfections, eccentricities, support spreading and unsymmetrical loading. True arches rarely occur in buildings because they rely on large horizontal end thrusts, which can result in costly end connections and additional structural members to provide the required strength and stiffness. Therefore, vertically curved members in building structures are designed for combined axial compression and in-plane flexural loads. For shorter distances that are optimally spanned by flexural members, vertically curved beams are often used for the aesthetic effect.

This chapter discusses the behavior and strength of arches and beams loaded in the plane of curvature. The design method uses AISC *Specification* (AISC, 2016c) equations for straight members to design curved members subjected to axial compression and in-plane flexure. This method will allow the use of existing software for curved member design by modifying effective length factors and lateral-torsional buckling modification factors to account for the curvature. These recommendations are not intended for cambered beams, where the minor curvatures are neglected in design.

The accuracy of the proposed design method is dependent on the similarities between curved members and straight members regarding residual stresses, geometric imperfections, and inelastic flexural behavior. As discussed in Section 5.3, residual stresses are usually reduced by the bending operation, and the tolerances in the AISC *Code of Standard Practice* (AISC, 2016a) for curved members are similar to those for straight members. If the local strength considerations in Section 6.7 are satisfied, the inelastic flexural behavior of curved members will be similar to that of straight members. Therefore, the AISC *Specification* provisions for straight members can be applied to curved members.

### 6.2 ARCH GEOMETRY

A funicular shape is the geometry resulting exclusively in axial loads in a member when subjected to a particular load system. A funicular tension member, shown in Figure 6-1(a), takes the shape of a weightless cable under load. The funicular arch under the same load system is symmetrical about a horizontal plane to the funicular cable as shown in Figure 6-1(b). A funicular arch has the shape of the moment diagram of a straight beam of identical span and loads. This results in a polygon for the system of concentrated forces

in Figure 6-1(b) and a parabola for the uniform load in Figure 6-1(c).

Where the arch geometry deviates from the funicular geometry, the moment and shear at any point in the member can be calculated using the offset from the two curves as shown for the curved member in Figure 6-1(d) (Cooper and Chen, 1985). At the only location where the curved member meets the funicular polygon, the moment is zero. For other locations on the arch, the moment is the product of the axial load in the funicular member and the offset distance between the funicular curve and the arch member.

Arch geometry is often described using the rise-to-span ratio,  $H/L_s$ , where  $H$  is the arch rise and  $L_s$  is the arch span. Rise-to-span ratios between  $\frac{1}{6}$  and  $\frac{1}{5}$  are the most efficient structurally (Gambhir, 2004). For arched roof structures supported at the floor level, rise-to-span ratios between  $\frac{1}{4}$  and  $\frac{1}{3}$  provide the most economical compromise between structural efficiency and usable enclosed area (AISC, 1963).

### 6.3 AXIAL COMPRESSION

As discussed in Section 6.1, arches resist loads primarily by axial compression; however, flexural loads are almost always present in vertically curved members. As with straight members, curved members are designed using interaction equations, which require the axial and flexural strengths to be calculated independently. The provisions for local buckling in AISC *Specification* Chapters B and E can be used without modification for most curved members in buildings. Section 5.5 discusses a case where these provisions may not be applicable due to excessive cross-sectional distortion during the bending operation.

For the circular arch in Figure 6-2(a) with a radial uniform load,  $q$ , along the arc, the axial compression load is:

$$P_r = qR \quad (6-1)$$

where

$R$  = radius, in.

$q$  = radial uniform force per unit length along a circularly curved axis, kip/in.

For a uniformly loaded parabolic arch as shown in Figure 6-2(b), the maximum axial load, which occurs at the supports, is:

$$P_r = \frac{wL_s^2}{8H} \sqrt{1 + 16\left(\frac{H}{L_s}\right)^2} \quad (6-2)$$

where

$H$  = rise, in.

$L_s$  = chord, span, in.

$w$  = linear uniform force per unit length along the span, kip/in.

Under compression, the arch member shortens, causing a vertical deflection at the apex. For in-plane deflection, arch behavior is similar to that of a beam-column. Second-order deflections can usually be estimated by amplifying the first-order deflection according to Equation 6-3. Where deflections are significant, a second-order analysis with geometric nonlinearities, including the effect of member axial shortening, is required to properly determine the second-order effects.

$$\Delta_2 = \frac{\Delta_1}{1 - \frac{P_r}{P_{ei}}} \quad (6-3)$$

where

$P_{ei}$  = elastic in-plane critical buckling load, kips

$P_r$  = required axial strength, kips

$\Delta_1$  = first-order deflection, in.

$\Delta_2$  = second-order deflection, in.

### 6.3.1 In-Plane Strength

Because arch loads are carried primarily by compression, the in-plane strength is dependent on the support stiffness (Pi et al., 2007). Support spreading significantly reduces the

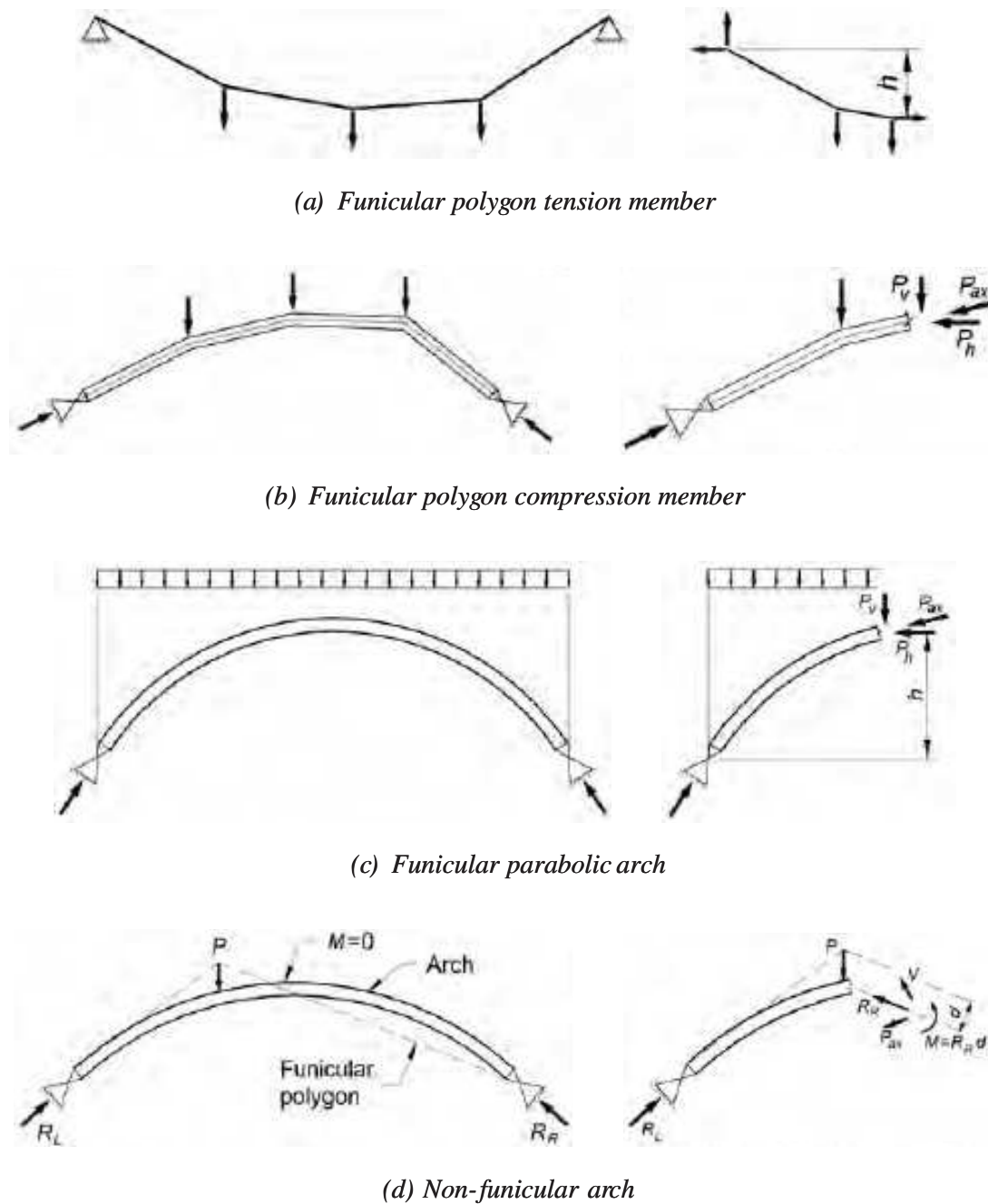


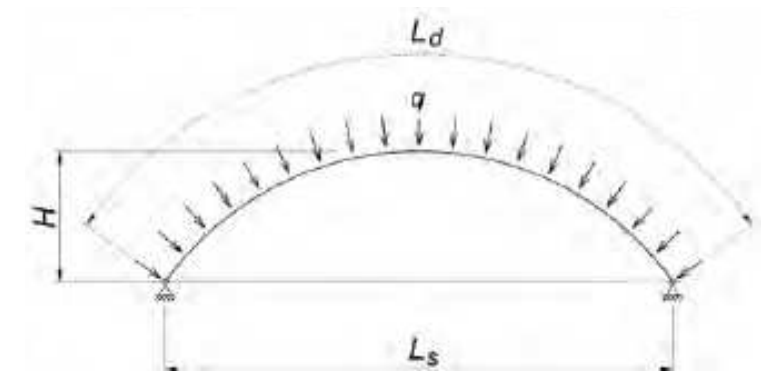
Fig. 6-1. Funicular and non-funicular shapes.

strength, causing large vertical deflections at the apex, potentially leading to collapse. This is illustrated in Figure 6-3(a), where the lateral supports are flexible. In this case, the support flexibility must be included in the structural analysis model, and the curved member will likely behave similar to a beam with a relatively low compression force. Completely rigid supports are difficult to obtain in practice, and additional members are often required to provide support stiffness. In Figure 6-3(b), the horizontal member acts as a tension tie, preventing arch spreading; however, these ties often interfere with the functionality and aesthetic quality of the structure. Figure 6-3(c) shows a vertical truss system designed to resist the horizontal thrust. Due to the high stiffness demand and large horizontal forces at arch supports, vertically curved members are often modeled as beams.

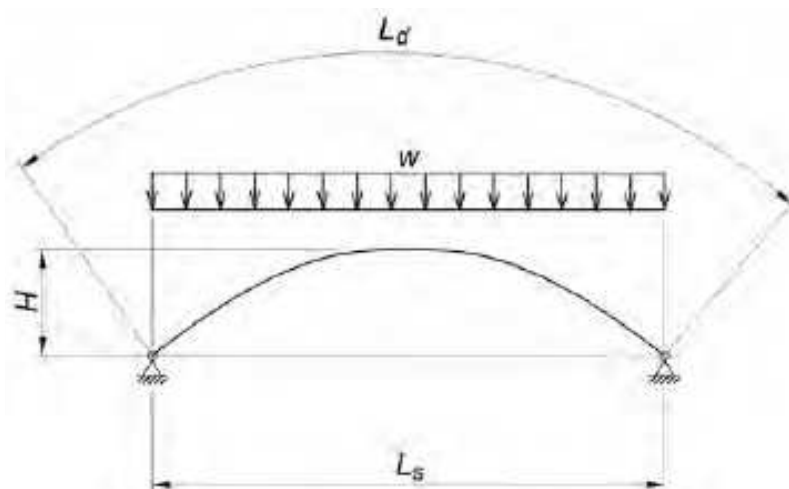
Flexible supports and a low rise-to-span ratio can lead to high in-plane arch deflections. Where deflections are significant, a second-order analysis with geometric nonlinearities is required to determine the second-order arch loads. In this case, the analysis must properly account for in-plane deformations, including the effect of member axial shortening and the horizontal support flexibility. The second-order effects

are not captured with a traditional  $P-\Delta$  analysis because arch deformations cause vertical, not horizontal, translation of the gravity loads. If the first-order deflection,  $\Delta_1$ , calculated using factored loads for LRFD or 1.6 times the service loads for ASD, is less than  $H/40$ , a first-order analysis is sufficiently accurate (King and Brown, 2001). This criterion assumes the analysis includes the effect of support flexibility. For arches with rise-to-span ratios less than 0.1, accurate modeling of support stiffness and second-order effects is critical.

Arches must be designed to prevent snap-through buckling, which is a type of in-plane instability that is sensitive to second-order effects and support spreading. Snap-through buckling can occur in a symmetric mode or an asymmetric mode, shown by deformed shapes C and B in Figure 6-4(a), respectively. Shape A in Figure 6-4(a) shows the deflected shape at imminent buckling. Because this limit state is difficult to predict, arches are preferably proportioned so that any in-plane instability will be limited by the asymmetric buckling modes shown in Figures 6-4(b) and 6-4(c). Snap-through buckling can be prevented by ensuring the span slenderness,  $L_s/r_i$ , exceeds a minimum critical value, where  $L_s$  is the span distance and  $r_i$  is the in-plane radius of gyration (CEN, 2009;

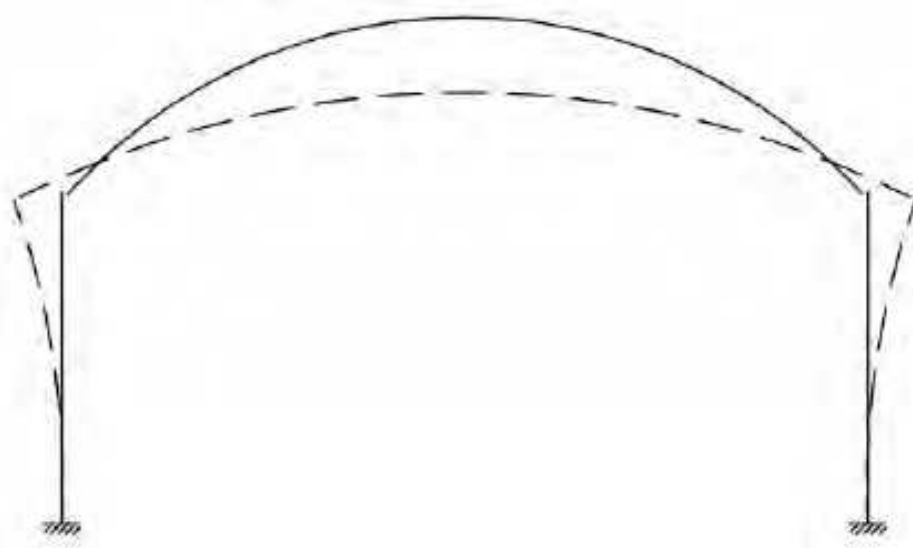


(a) Circular

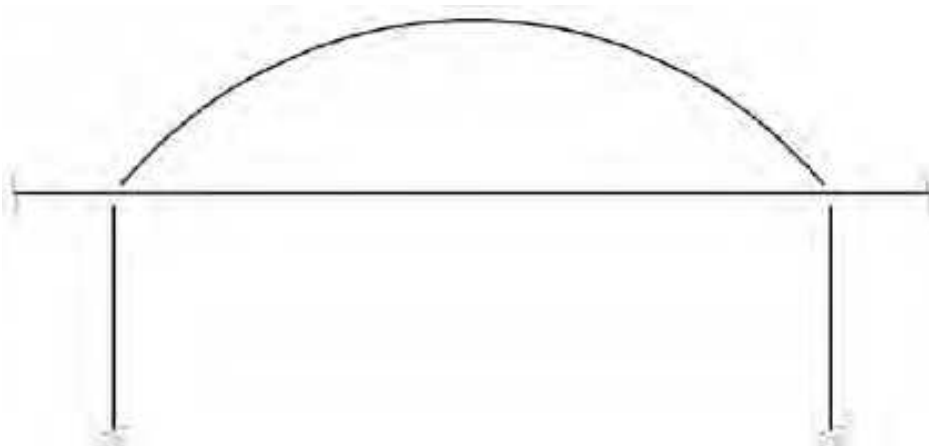


(b) Parabolic

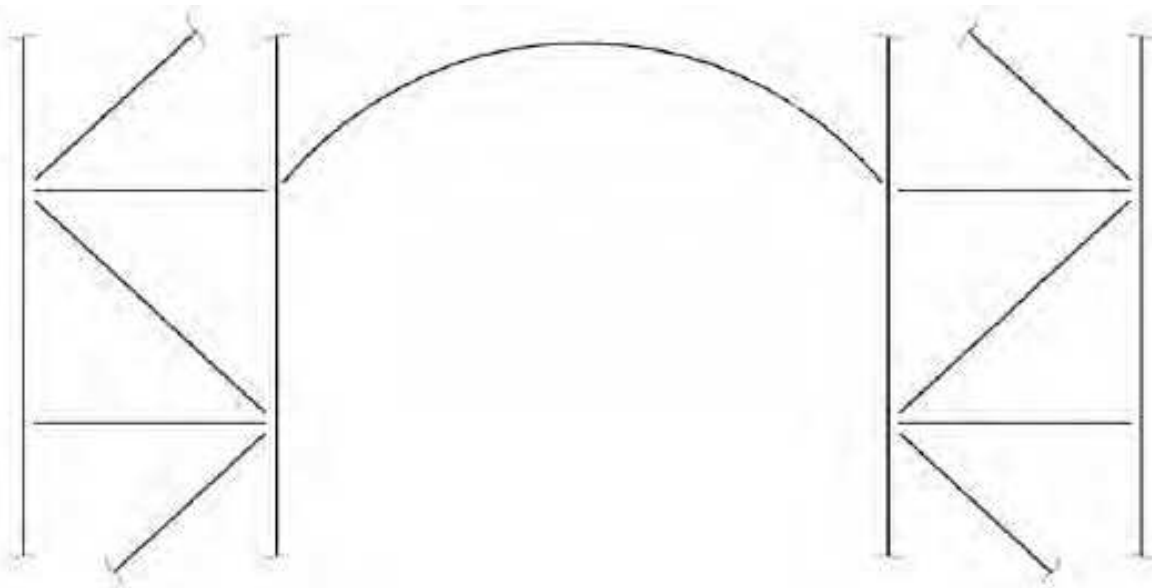
Fig. 6-2. Standard arch forms.



(a) *Support spreading*



(b) *Tension tie*



(c) *Vertical truss*

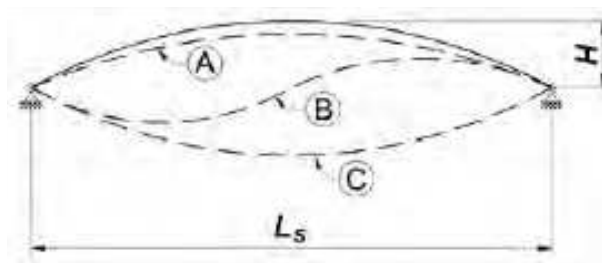
Fig. 6-3. *Support horizontal stiffness.*

Table 6-1. Minimum Span Slenderness, $(L_s/r_i)_{crit}$			
End Conditions	$H/L_s$		
	0.10	0.15	0.20
Pinned	59	36	35
Fixed	150	71	68

Pi et al., 2002; Schreyer and Masur, 1966). Minimum span slenderness values,  $(L_s/r_i)_{crit}$ , for pinned and fixed-end conditions and rise-to-span ratios,  $H/L_s$ , between 0.1 and 0.2 are listed in Table 6-1. Generally, snap-through buckling is not critical for arches with rigid supports and rise-to-span ratios greater than 0.2.

When snap-through buckling is prevented, arches buckle in the asymmetric modes shown in Figures 6-4(b) and 6-4(c) for pinned and fixed arches, respectively. These buckling modes are less sensitive to second-order effects and support spreading. The buckling strength can be predicted using the flexural buckling provisions of AISC *Specification* Chapter E, with modified effective length factors that consider the effect of curvature.

Although the axial load can vary along the arc, the arch member can be designed as a straight column with a uniform axial load throughout its length equal to the maximum load at any section within the arch. Table 6-2 lists the appropriate effective length factors for use with the flexural buckling provisions in AISC *Specification* Chapter E. In the *Specification* equations, the developed length of the arch,  $L_d$ , must be used in lieu of the straight-member unbraced length,  $L$ . The effective length factors in Table 6-2 are valid when  $H/L_s > 0.2$  or when  $0.1 \leq H/L_s \leq 0.2$  and the minimum span slenderness values in Table 6-1 are satisfied (Karnovsky, 2012; CEN, 2009; Pi et al., 2002; Gambhir, 2004; Timoshenko and Gere, 1961). The elastic in-plane critical buckling load is:



(a) Snap-through buckling



(b) Pinned arch



(c) Fixed arch

Fig. 6-4. In-plane buckling shapes.

Table 6-2. In-Plane Effective Length Factor, $K_i$			
Arch Form	End Conditions	$H/L_s$	$K_i$
Circular	Pinned	$0.1 \leq H/L_s < 0.3$	0.55
		$0.3 \leq H/L_s \leq 0.5$	0.60
	Fixed	All	0.40
Parabolic	Pinned	All	0.50
		$0.1 \leq H/L_s < 0.3$	0.40
	Fixed	$0.3 \leq H/L_s \leq 1.0$	0.35

$$P_{ei} = \frac{\pi^2 EI_i}{(K_i L_d)^2} \quad (6-4)$$

where

$E$  = modulus of elasticity, ksi

$I_i$  = moment of inertia about the axis of curvature, in.<sup>4</sup>

$K_i$  = effective length factor for in-plane buckling

$L_d$  = developed length (arc length) of the arch, in.

### 6.3.2 Out-of-Plane Strength

Figure 6-5 shows a potential out-of-plane buckling mode for arches under axial compression, where the buckled shape is characterized by out-of-plane translation and twisting. Free-standing arches, which are braced only at the ends, rely on end rotational restraints to provide out-of-plane stability and resistance to out-of-plane loads. In practice, most arches are braced against out-of-plane translation by continuous or discrete bracing systems. Solutions for buckling of continuously restrained arches were derived by Pi and Bradford (2002).

In the case of discrete braces, each segment can buckle between brace points. The buckling strength is dependent on the developed length along the arch between braces,  $L_{db}$ , shown in Figure 6-6. Although the member buckles in a flexural-torsional mode, the flexural buckling provisions in AISC *Specification* Chapter E can be used with an effective length factor modified to account for torsional effects. In the AISC *Specification* equations, the developed length between brace points,  $L_{db}$ , must be used in lieu of the straight-member unbraced length,  $L$ . The elastic out-of-plane critical buckling load is:

$$P_{eo} = \frac{\pi^2 EI_o}{(K_o L_{db})^2} \quad (6-5)$$

where

$I_o$  = moment of inertia perpendicular to the axis of curvature, in.<sup>4</sup>

$K_o$  = effective length factor for out-of-plane buckling

$L_{db}$  = developed length (arc length) along the arch between out-of-plane bracing, in.

For circular arches formed of doubly symmetric shapes, the effective length factor, developed from the work of Papageorgiou and Trahair (1987), is:

$$K_o = \frac{\sqrt{1 + \frac{1}{C_o} \left( \frac{\theta_b}{\pi} \right)^2}}{1 - \left( \frac{\theta_b}{\pi} \right)^2} \quad (6-6)$$

where

$$C_o = \frac{1}{I_o} \left[ \frac{GJ}{E} + C_w \left( \frac{\pi}{L_{db}} \right)^2 \right] \quad (6-7)$$

$C_w$  = warping constant, in.<sup>6</sup>

$G$  = shear modulus, ksi

$J$  = torsional constant, in.<sup>4</sup>

$\theta_b$  = subtended angle between braces, rad

For parabolic arches with doubly symmetric shapes and  $H_b/L_{sb} \leq 0.2$ , the buckling strength is similar to that of a circular arch (Moon et al., 2009). In this case, the effective length factor can be calculated using Equation 6-6 with an equivalent angle between braces according to Equation 6-8. When  $H_b/L_{sb} > 0.2$ , Equation 6-8 is conservative.

$$\cos\left(\frac{\theta_b}{2}\right) = 1 - \frac{8}{4 + \left(\frac{L_{sb}}{H_b}\right)^2} \quad (6-8)$$

where

$H_b$  = rise dimension between the brace points and the apex of the arch segment, in.

$L_{sb}$  = span length (chord length) between out-of-plane bracing, in.

Because members with high  $J/I_o$  ratios provide the most efficient out-of-plane buckling resistance, closed sections should be considered when this limit state controls the

design. For HSS shapes with  $\theta_b \leq 45^\circ$  (or  $H_b/L_{sb} \leq 0.10$ ), a conservative value for the effective length factor is  $K_o = 1.30$ . Equation 6-6 should always be used for open shapes, where  $K_o$  can be much higher—especially where the member is curved about the weak axis.

Further information on the out-of-plane buckling strength of arches is published in the SSRC Guide (Ziemian, 2010). For out-of-plane buckling solutions for singly symmetric shapes, refer to Trahair and Papangelis (1987).

#### 6.4 FLEXURE

As discussed in Section 6.1, vertically curved members in building structures are designed for combined axial compression and in-plane flexural loads. Although the effect of curvature on the lateral-torsional buckling strength is significant, the provisions for yielding and local buckling in AISC *Specification* Chapters B and F can be used without modification for most curved members in buildings. Chapter 5 discusses conditions where the AISC *Specification* provisions may not be applicable.

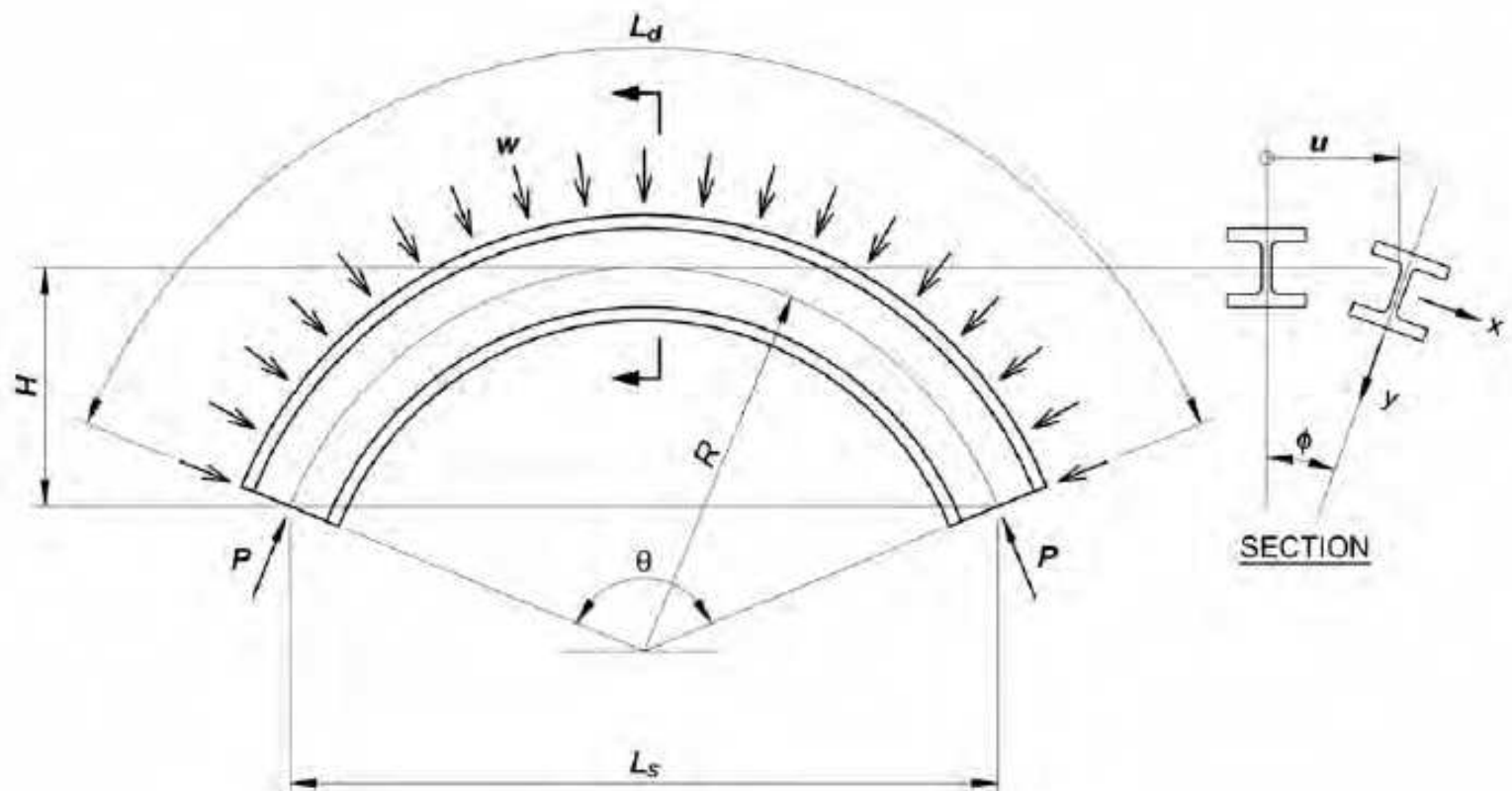


Fig. 6-5. Flexural-torsional buckling.

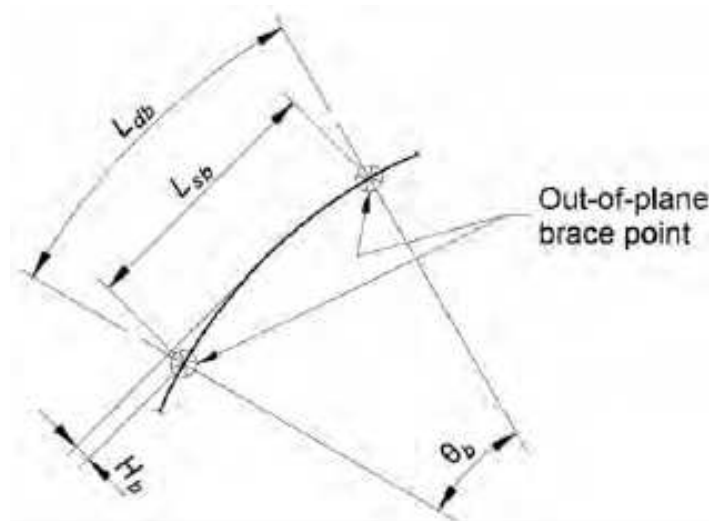


Fig. 6-6. Discrete bracing.

#### 6.4.1 Second-Order Effects

Second-order moments can be calculated either by using a second-order analysis as described in Section 6.3.1 or by amplifying the moments from a first-order analysis. The amplification factors in AISC *Specification* Appendix 8 for straight members are also accurate for curved members (Pi and Bradford, 2004; Pi and Trahair, 1999). The required in-plane flexural strength based on the amplified first-order moment is:

$$M_{ri} = B_i M_{i1} \quad (6-9)$$

where

$$B_i = \frac{1}{1 - \alpha \frac{P_r}{P_{ei}}} \quad (6-10)$$

$M_{i1}$  = first-order moment about the axis of curvature causing in-plane flexure, kip-in.

$P_{ei}$  = elastic in-plane critical buckling load, kips

$P_r$  = required axial load, kips

$\alpha$  = 1.0 (LRFD); 1.6 (ASD)

#### 6.4.2 Lateral-Torsional Buckling

Flexure in the plane of curvature can cause member instability with a buckled shape characterized by out-of-plane translation and twisting as shown in Figure 6-7. The buckling strength is highly dependent on the loading direction. For closing moments,  $M_{ic}$ , which are moments that induce compression at the inner flange, the buckling strength is greater

than that of an equivalent straight member. For members with opening moments,  $M_{io}$ , which are moments that induce compression at the outer flange, the buckling strength is less than that of an equivalent straight member.

For doubly symmetric members with equal end moments, the elastic critical lateral-torsional buckling moment is (Vacharajittiphan and Trahair, 1975; King and Brown, 2001):

$$M_{ei} = \sqrt{\left(\frac{C_y + C_z}{2R}\right)^2 + \left(\frac{\pi^2}{L_{db}^2} - \frac{1}{R^2}\right)C_y C_z} \pm \frac{C_y + C_z}{2R} \quad (6-11a)$$

where

$$C_y = EI_o \quad (6-11b)$$

$$C_z = GJ + \frac{\pi^2 E C_w}{L_{db}^2} \quad (6-11c)$$

$L_{db}$  = developed length (arc length) along the arch between points that are either braced against lateral displacement of the compression flange or braced against twist of the cross section, in.

The positive root in Equation 6-11a is for closing moments, and the negative root is for opening moments. In practice, most curved members are braced against lateral-torsional buckling by continuous or discrete bracing systems. Solutions for buckling of continuously restrained arches were derived by Pi and Bradford (2002).

In the case of discrete braces, each segment can buckle between brace points. The buckling strength is dependent on

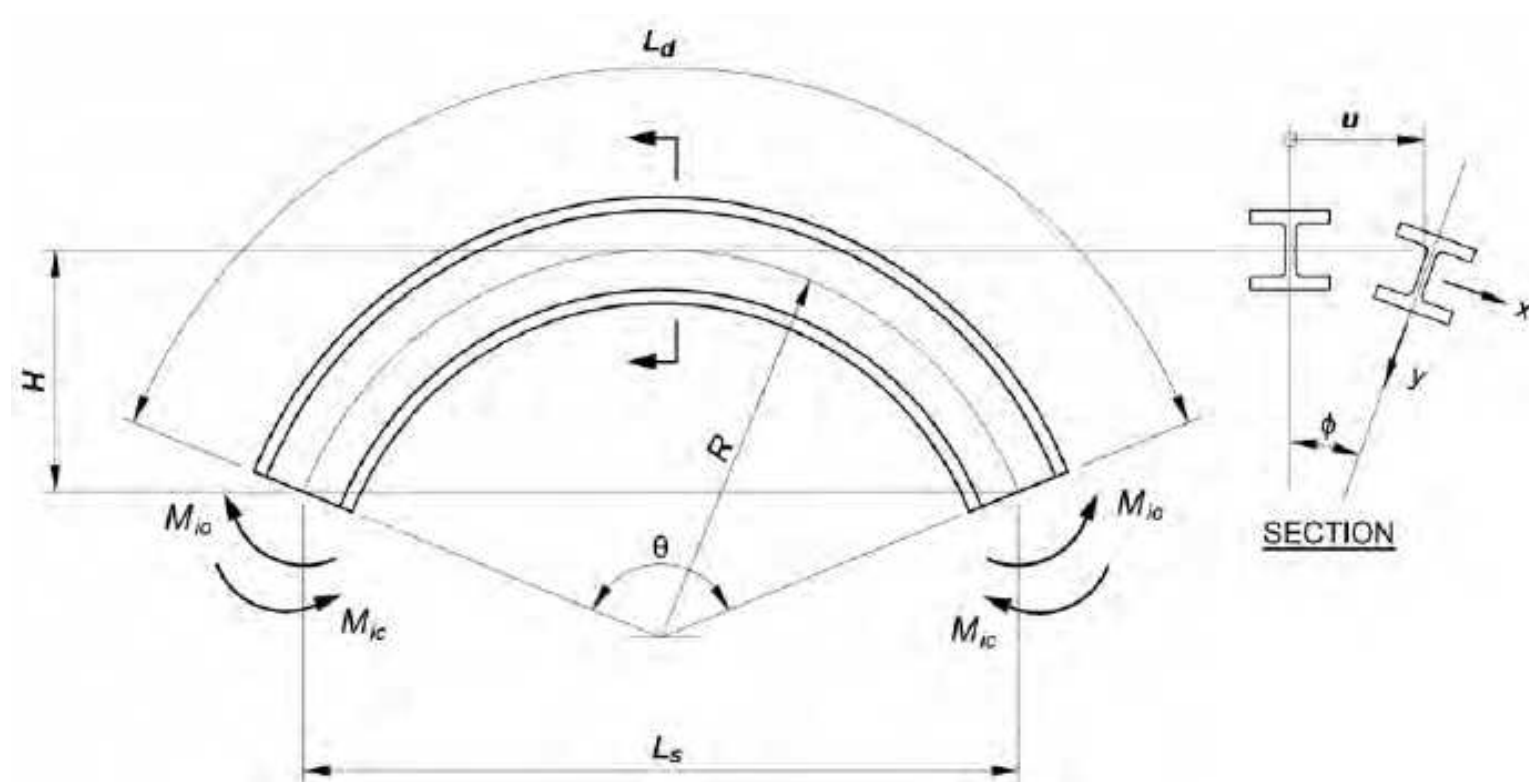


Fig. 6-7. Lateral-torsional buckling.

the developed length along the member between braces,  $L_{db}$ , shown in Figure 6-6. To properly consider member behavior in the inelastic range, the lateral-torsional buckling provisions in AISC *Specification* Chapter F can be used with the lateral-torsional buckling modification factor,  $C_b$ , revised to consider the effects of curvature. In the AISC *Specification* equations, the developed length between brace points,  $L_{db}$ , must be used in lieu of the straight-member unbraced length,  $L_b$ . The revised lateral-torsional buckling modification factor,  $C_{bi}$ , is:

$$C_{bi} = C_{bs} \left[ \sqrt{1 + C_a^2 - \left( \frac{EI_o}{R^2 M_{es}^2} \right) \left( GJ + \frac{\pi^2}{L_{db}^2} EC_w \right)} \pm C_a \right]$$

$$= C_{bs} \left( \sqrt{1 + C_a^2 - \frac{C_y C_z}{R^2 M_{es}^2}} \pm C_a \right) \quad (6-12a)$$

where

$$C_a = \frac{EI_o + GJ + \frac{\pi^2}{L_{db}^2} EC_w}{2RM_{es}}$$

$$= \frac{C_y + C_z}{2RM_{es}} \quad (6-12b)$$

$C_{bs}$  = lateral-torsional buckling modification factor for an equivalent straight member

$M_{es}$  = elastic critical lateral-torsional buckling moment of the equivalent straight member subjected to uniform moment with a length equal to  $L_{db}$ , kip-in.

$$= \frac{\pi}{L_{db}} \sqrt{EI_o GJ + \left( \frac{\pi E}{L_{db}} \right)^2 I_o C_w} \quad (6-13)$$

For parabolically curved doubly symmetric members with  $H_b/L_{sb} \leq 0.2$ , the lateral-torsional buckling strength is similar to that of circularly curved members (Moon et al., 2009). An equivalent radius,  $R_e$ , for use with Equations 6-11 and 6-12 can be calculated with Equation 6-14. Although this method is accurate only when  $H_b/L_{sb} \leq 0.2$ , it can be used to provide a conservative estimate of the flexural strength of members with opening moments when  $H_b/L_{sb} > 0.2$ . For members with closing moments and  $H_b/L_{sb} > 0.2$ , the equivalent radius method is unconservative, but a conservative estimate of the member strength can be calculated using the equivalent straight member with a length equal to  $L_{db}$ .

$$R_e = \frac{4H_b^2 + L_{sb}^2}{8H_b} \quad (6-14)$$

For lateral-torsional buckling solutions for singly symmetric shapes, refer to Trahair and Papangelis (1987).

## 6.5 COMBINED AXIAL AND FLEXURAL LOADS

The strength of curved members under the actions of combined axial and flexural loads can be calculated with AISC *Specification* Chapter H. The required in-plane flexural strength,  $M_{ri}$ , should be based on a second-order analysis or an amplified first-order moment as discussed in Section 6.4.1. Member strength should be verified at each unbraced segment along the length.

Because the axial load can vary along the member, careful selection of the proper axial load ratio,  $P_r/P_c$ , is essential. For in-plane buckling, there is only one axial load ratio for the arch, which is calculated with the required axial load,  $P_r$ , equal to the maximum axial load within the arch. For out-of-plane buckling, both the required load and the available load,  $P_c$ , can vary between unbraced segments within a curved member. The governing axial load ratio for each arch segment is the maximum of the out-of-plane axial load ratio for that segment and the in-plane axial load ratio for the entire arch.

For several idealized loading conditions, a design procedure for circular arches is available in the SSRC Guide (Ziemian, 2010). The equations were originally developed by Pi and Trahair (1999) and Pi and Bradford (2004) for in-plane strength, and by Pi and Trahair (1998; 2000) and Pi and Bradford (2005) for out-of-plane strength. A linear interaction equation is used to combine the maximum moment and the maximum axial load within the arch. To account for the load variation along the arch, the required loads are reduced by modification factors. In practice, the many different load cases typically required for final design cannot be covered by the idealized solutions presented; however, they may be useful for preliminary member sizing.

## 6.6 STRUCTURAL ANALYSIS MODELS

Generally, only straight beam elements are available in commercial structural analysis programs; therefore, curved members are modeled with a series of straight segments. The accuracy increases with the number of elements. Between 10 and 20 elements is adequate for modeling most semi-circular members (King and Brown, 2001). For shallow arches and other highly nonlinear structures requiring a second-order analysis, a convergence study may be required to determine the appropriate number of elements.

## 6.7 LOCAL STRENGTH CONSIDERATIONS

When curved members are subjected to in-plane flexure, the flexural strength and stiffness can be affected by cross-sectional distortion. For the I-shaped member in Figure 6-8(a), which is subjected to strong axis in-plane flexure, the flange forces,  $F_f$ , are shown in Figure 6-8(b). To maintain equilibrium of the curved flanges, radial forces at the web-to-flange interfaces are required. Because the inner radius

is smaller than the outer radius, the radial force at the inner flange,  $q_i$ , is larger than the radial force at the outer flange,  $q_o$ . However, using the centroidal radius,  $R$ , at both flanges will usually provide sufficient accuracy. In this case, the radial force per unit length is:

$$q = \frac{F_f}{R} = \frac{M_i}{R(d - t_f)} \quad (6-15)$$

where

$F_f = M_i/(d - t_f)$  = flange force, kips

$M_i$  = moment about the axis of curvature causing in-plane flexure, kip-in.

$R$  = centroidal radius, in.  
 $d$  = member depth, in.  
 $t_f$  = member flange thickness, in.

The radial flange-force component can cause local bending of the flanges and local buckling of the web. The radial-load effects are similar for other members with flat cross-sectional elements, including square and rectangular HSS, as well as the stiffened and unstiffened elements in Figure 6-9. For round HSS, radial forces can cause ovalization, reducing the strength and stiffness.

### 6.7.1 Out-of-Plane Bending of Rectangular Elements

Local flange bending caused by radial loads in curved rectangular elements is shown in Figures 6-10(a) and 6-10(b)

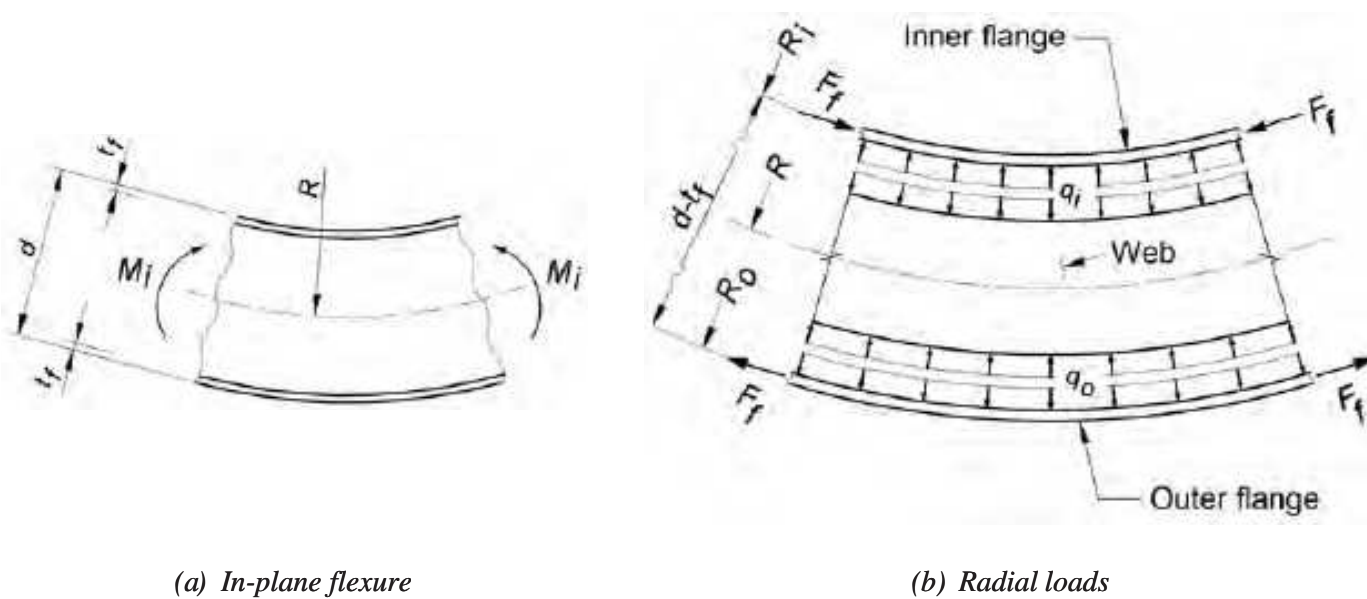


Fig. 6-8. Local loads for a curved I-shape.

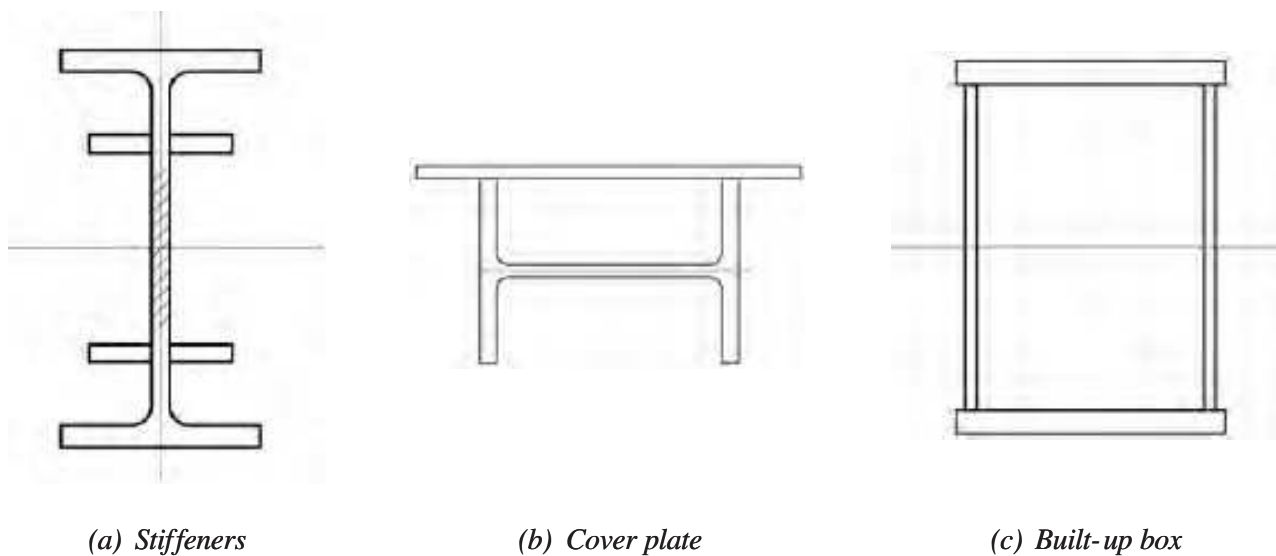


Fig. 6-9. Flat cross-sectional elements subjected to radial loads.

for I-shaped members and HSS members, respectively. The ultimate strength limit state is characterized by simultaneous plastic collapse about the member axis and local plastic collapse of the flange, near the flange-to-web interface (Mandal, 1992; Vandepitte, 1983; Vandepitte, 1982; Save and Massonet, 1972). Because the local and sectional strengths are interdependent, two methods are available to evaluate the member:

1. The local bending strength of the element can be evaluated considering the potential reduction caused by longitudinal flexural stresses resulting from the required member moment,  $M_{ri}$ . This method is applicable to all stiffened and unstiffened elements.
2. The member flexural section properties can be reduced to account for the local bending stresses caused by the radial loads. This method is applicable only to I-shape, HSS, and built-up box members, but it may reduce the number of iterations required for member selection.

#### Local Bending Strength

For unstiffened elements, the design model is shown in Figure 6-11(a), where the radial uniform force per unit area,  $\sigma$ , acts transverse to the flange. Figure 6-11(b) shows the moment diagram for half of the flange, where  $w_f$  is the force per unit length and  $l$  is the cantilever beam length. The maximum moment per unit length at the fixed end of the beam is:

$$m_f = \frac{\sigma l^2}{2} \quad (6-16)$$

The radial uniform force per unit area is:

$$\begin{aligned} \sigma &= \frac{F_f}{Rb_f} \\ &= \frac{\sigma_z t_f}{R} \end{aligned} \quad (6-17)$$

Substituting Equation 6-17 into Equation 6-16 results in a required flexural strength per unit length of:

$$m_r = \frac{\sigma_z t_f l^2}{2R} \quad (6-18)$$

Neglecting the flange-to-web fillet, the fixed end of the cantilever is at the face of the web and  $l=b$ . The nominal flexural strength per unit length is:

$$m_n = k_u F_y \frac{t_f^2}{4} \quad (6-19)$$

where  $k_u$  is a reduction factor that accounts for the effect of the longitudinal flexural stresses caused by the member moment about the axis of curvature,  $M_i$ .

$$k_u = 4.60 - 4.40 \frac{\sigma_z}{F_y} \leq 1.0 \quad (6-20)$$

where

$F_y$  = specified minimum yield stress, ksi

$l$  = beam length for element out-of-plane bending, in.

$\sigma$  = radial uniform force per unit area, ksi

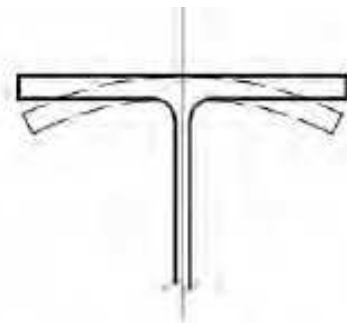
$\sigma_z$  = longitudinal flexural stress in the beam =  $M_i c / I \leq F_y$ , ksi

For LRFD,  $\phi = 0.90$ , and for ASD,  $\Omega = 1.67$ .

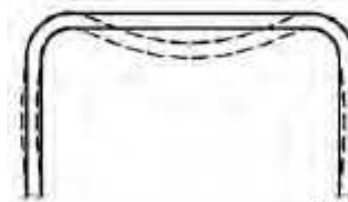
The design model for stiffened elements is shown in Figure 6-12(a). For HSS flanges and other cases where the element is continuous at the edges, the local flange moment can be calculated with a fixed-end beam model as shown in Figure 6-12(b). The maximum required flexural strength per unit length is:

$$m_r = \frac{\sigma_z t_f l^2}{12R} \quad (6-21)$$

For built-up box shapes with limited continuity between the flanges and the webs due to relatively thin webs or partial-strength welds at the flange-to-web interface, flange bending



(a) I-shape



(b) Rectangular HSS

Fig. 6-10. Flange-bending due to radial loads.

should be based on the simply supported beam model shown in Figure 6-12(c). In this case, the maximum required flexural strength per unit length is:

$$m_r = \frac{\sigma_z t_f l^2}{8R} \quad (6-22)$$

Assuming the flange spans between the web centerlines,  $l = B - t_w$ . The nominal flexural strength per unit length is:

$$m_n = k_s F_y \frac{t_f^2}{4} \quad (6-23)$$

where  $k_s$  is a reduction factor that accounts for the effect of the longitudinal flexural stresses caused by the member moment about the axis of curvature,  $M_i$ .

$$k_s = 2.06 - 1.86 \frac{\sigma_z}{F_y} \leq 1.0 \quad (6-24)$$

#### Reduced Flexural Section Properties

As an alternative to verifying the local bending strength of elements explicitly, curved-member flexural section properties can be reduced to account for the local bending stresses caused by the radial loads. The effective section modulus about the axis of curvature is:

$$S_{ei} = k_f S_i \quad (6-25)$$

The effective plastic modulus about the axis of curvature is:

$$Z_{ei} = k_f Z_i \quad (6-26)$$

The effective moment of inertia about the axis of curvature is:

$$I_{ei} = k_f I_i \quad (6-27)$$

For I-shaped members, the reduction factor is:

$$k_f = \frac{9.20}{8.80 + \frac{b_f^2}{R t_f}} \leq 1.00 \quad (6-28)$$

For sections with full corner continuity, including square and rectangular HSS, the reduction factor is:

$$k_f = \frac{8.24}{7.44 + \frac{(B - t_w)^2}{R t_f}} \leq 1.00 \quad (6-29)$$

For built-up box shapes with limited continuity between the flanges and the webs due to relatively thin webs or partial-strength welds at the flange-to-web interface, the reduction factor is:

$$k_f = \frac{9.20}{8.80 + \frac{(B - t_w)^2}{R t_f}} \leq 1.00 \quad (6-30)$$

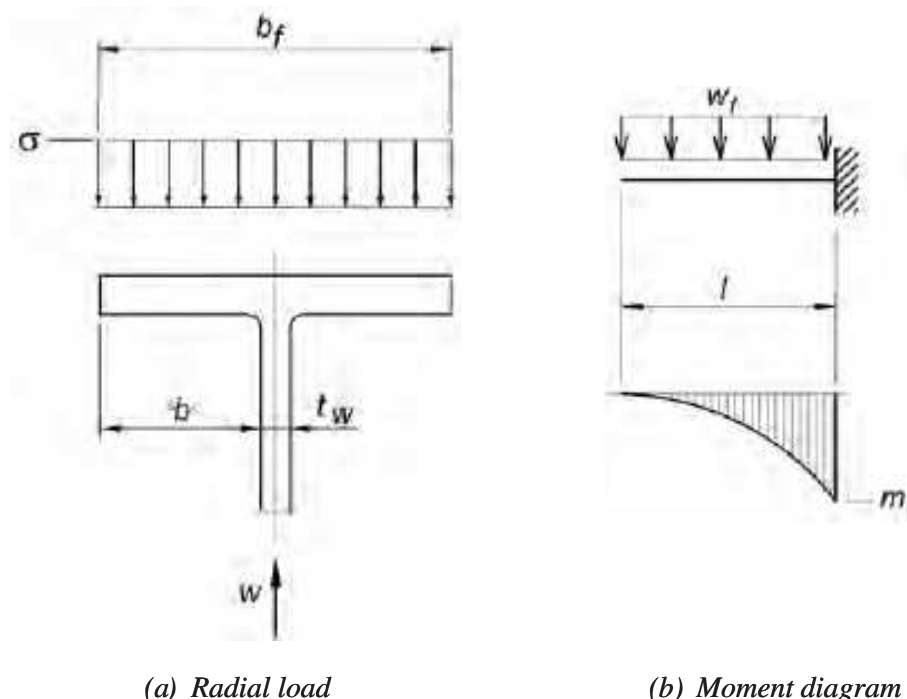


Fig. 6-11. Flange-bending design model for unstiffened elements.

where

- $I_i$  = moment of inertia about the axis of curvature, in.<sup>4</sup>
- $S_i$  = section modulus about the axis of curvature, in.<sup>3</sup>
- $Z_i$  = plastic modulus about the axis of curvature, in.<sup>3</sup>
- $t_w$  = thickness of the web, in.

### 6.7.2 Web Bend-Buckling

For closing moments that induce compression at the inner flange [Figure 6-8(a)], the radial components of the flange forces cause compression in the web. For members with small-radius bends and thin webs, these loads can cause web bend-buckling, which is a local stability failure where the flat depth of the web buckles as shown in Figure 6-13. The nominal in-plane flexural strength for the web bend-buckling limit state is:

$$M_{ni} = \frac{2ERt_w^3}{3h} \quad (6-31)$$

where

- $h$  = clear distance between fillets, in.

For LRFD,  $\phi = 0.90$ , and for ASD,  $\Omega = 1.67$ .

Generally, cold-bent members are not susceptible to this limit state because cold bending of members with small radii and thin webs would cause excessive web distortion during the bending operation. Therefore, this limit state is applicable only to special cases, such as when the cut-to-curve method is used to fabricate a plate girder. For all ASTM A992 (ASTM, 2016) rolled I-shaped members in AISC *Manual Part 1* (AISC, 2017), web bend-buckling is a concern only when  $R/d < 10$ .

### 6.7.3 Ovalization of Round HSS

Flexural deformations cause ovalization in both straight and curved round HSS members, causing a decrease in strength and stiffness and localized stresses in the circumferential (hoop) direction. Ovalization also causes a deviation from the longitudinal linear-elastic stress distribution assumed in elementary bending theory. These effects were considered in the development of AISC *Specification* Section F8 for straight members, where ovalization is caused by flexure-induced curvature. However, for curved members, ovalization is amplified and the effects must be considered in design. Figure 6-14 shows the deformed shapes caused by in-plane bending, which are dependent on the loading direction. The major axis of the ovalized shape is in the plane of curvature for opening moments,  $M_{io}$ , and the minor axis is in the plane of curvature for closing moments,  $M_{ic}$ .

The flexural section properties are functions of the flexibility characteristic,  $c_r$ , which is defined by Equation 6-32. The equations in this section assume infinitely long members and consider the effect of circumferential stresses. They are accurate for geometries common to structural steel members. Where ovalization is restrained by flanges, connections, or a straight HSS segment, the factors are conservative. Because significant nonlinear ovalization can occur when the member is loaded beyond the effective yield moment (Kim and Oh, 2006),  $M_{yi} = S_{ei}F_y$ , limiting the nominal flexural strength of AESS members to  $M_{yi}$  may be appropriate.

$$c_r = \frac{4Rt}{(D-t)^2} \quad (6-32)$$

The effective section modulus is (Kellogg, 1957):

$$S_{ei} = k_{si}S \quad (6-33)$$

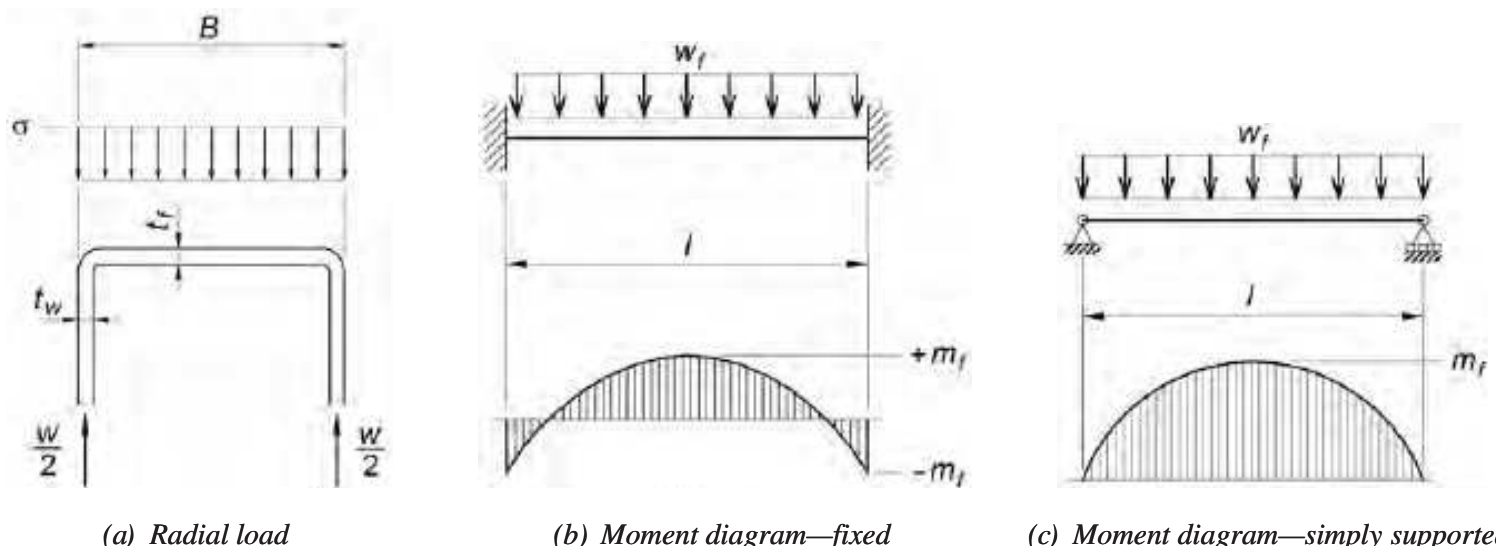


Fig. 6-12. Flange-bending design model for stiffened elements.

where

$$k_{si} = 1.19 c_r^{2/3} \leq 1.00 \quad (6-34)$$

The effective plastic modulus is (Spence and Findlay, 1973):

$$Z_{ei} = k_{zi} Z \quad (6-35)$$

where

$$k_{zi} = \frac{c_r}{\sqrt{1 + c_r^2}} \quad (6-36)$$

The effective moment of inertia is (Kellogg, 1957):

$$I_e = k_i I \quad (6-37)$$

where

$$k_i = \frac{1}{1 + \frac{9}{12c_r^2 + 1}} \quad (6-38)$$

Because the circumferential stresses were considered in the development of the effective plastic modulus according to Equation 6-35, their calculation is not required for routine design problems. However, when fatigue or local strength is an issue, the circumferential stresses can be calculated with a multiplier on the longitudinal flexural stress according to Equation 6-39 (Kellogg, 1957).

$$\sigma_{ci} = k_{ci} \frac{M_i}{S} \quad (6-39)$$

where

$D$  = outside diameter, in.

$I$  = moment of inertia of the HSS member, in.<sup>4</sup>

$S$  = section modulus of the HSS member, in.<sup>3</sup>

$Z$  = plastic modulus of the HSS member, in.<sup>3</sup>

$$k_{ci} = \frac{1.80}{c_r^{2/3}} \quad (6-40)$$

$t$  = wall thickness, in.

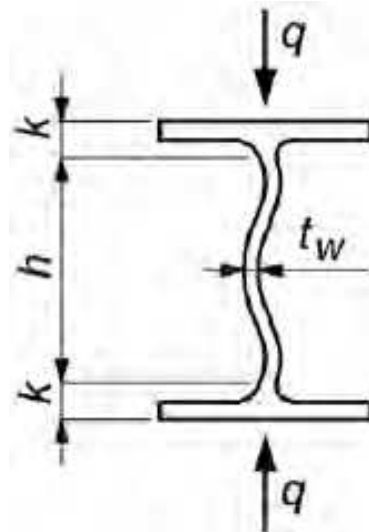


Fig. 6-13. Web bend-buckling.

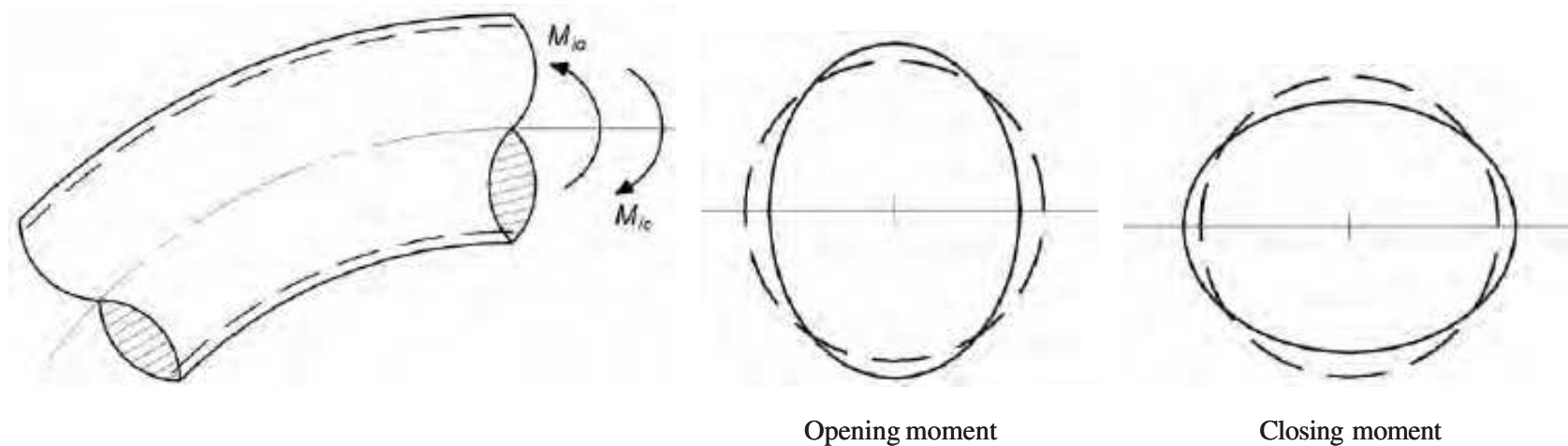


Fig. 6-14. Ovalization of a round HSS member.

## 6.8 CONNECTIONS

As discussed in Section 6.3.1, the in-plane strength of arches is dependent on the horizontal stiffness of the supports. Excessive connection flexibility in the horizontal direction can significantly reduce the arch in-plane strength, potentially leading to collapse. Therefore, special connection detailing may be appropriate to ensure the boundary conditions assumed in the structural analysis model are consistent with the connections provided.

As with end connections for straight beams, the out-of-plane stability of arches and vertically curved beams is dependent on the torsional stiffness at the ends. In many cases, these members are also subjected to out-of-plane loads causing a horizontal shear perpendicular to the plane of curvature. Because of this and the potentially high axial compression loads, single-plate shear connections are usually unsuitable for curved members. End-plate connections transfer compression loads efficiently; however, the ends must be cut accurately to minimize any field fit-up gap.

For the arch in Figure 6-3(b), the horizontal stiffness requirement can be satisfied with the end-plate connection in Figure 6-15. The stiffness can be increased by specifying a slip-critical joint where the curved member bolts to the horizontal member (tension tie). The horizontal arch reaction transfers directly into the tension tie, and the vertical reaction transfers through the web of the horizontal member into the cap plate of the vertical member.

Resistance to the horizontal thrust for the arch in Figure 6-3(c) must pass through the column into the strut on the opposite side. The end-plate connection in Figure 6-16 is efficient in transferring the horizontal arch reaction into the column by bearing, and the vertical reaction is transferred into the column through the bolts. Other than the closing of any erection gaps between the end plate and the column flange, this connection is very stiff in horizontal compression. Due to column placement tolerances, column cross-sectional tolerances, and fabrication tolerances for the curved member, some adjustability should be provided for erection. This can

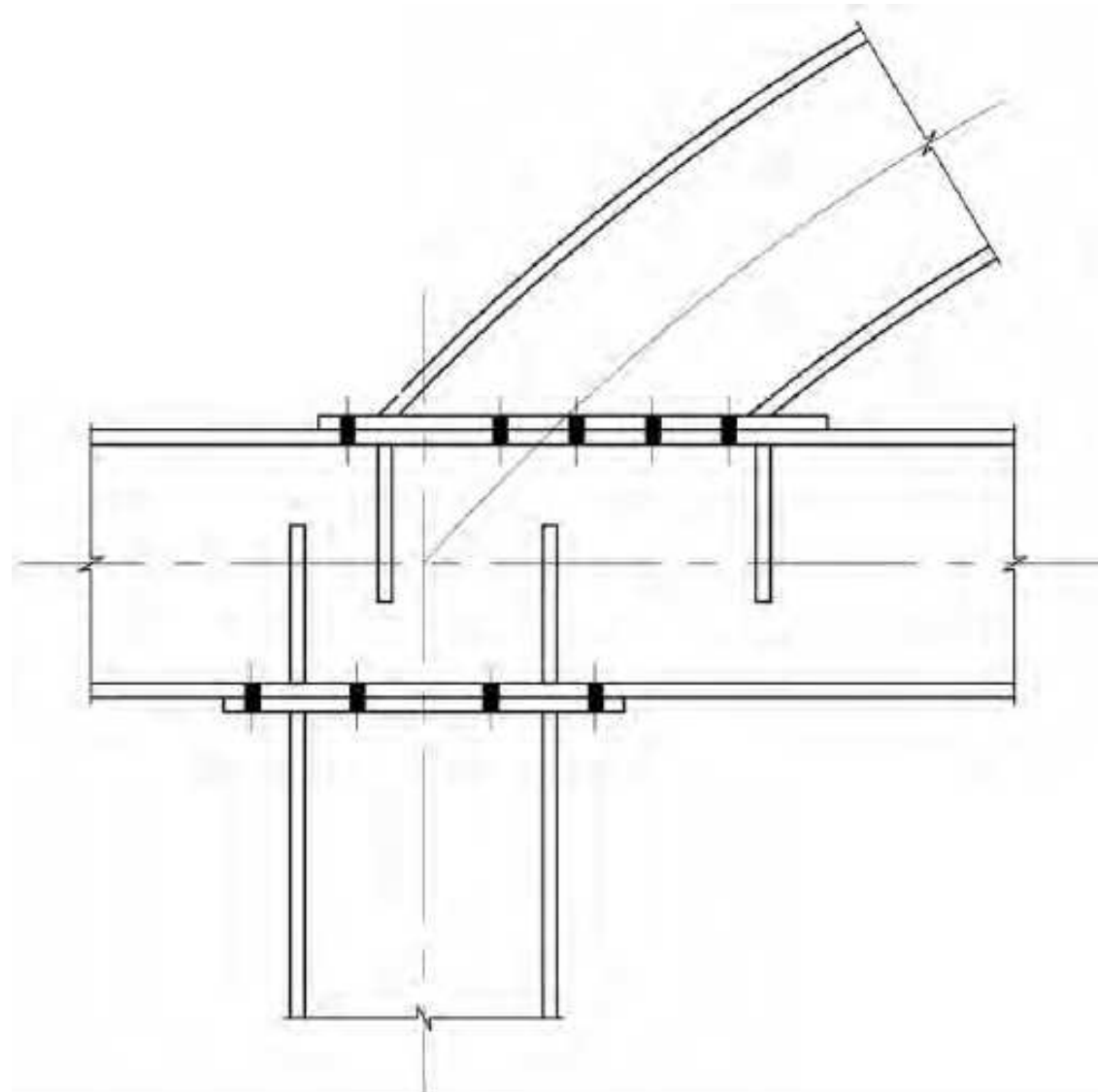


Fig. 6-15. Arch-to-tension tie connection.

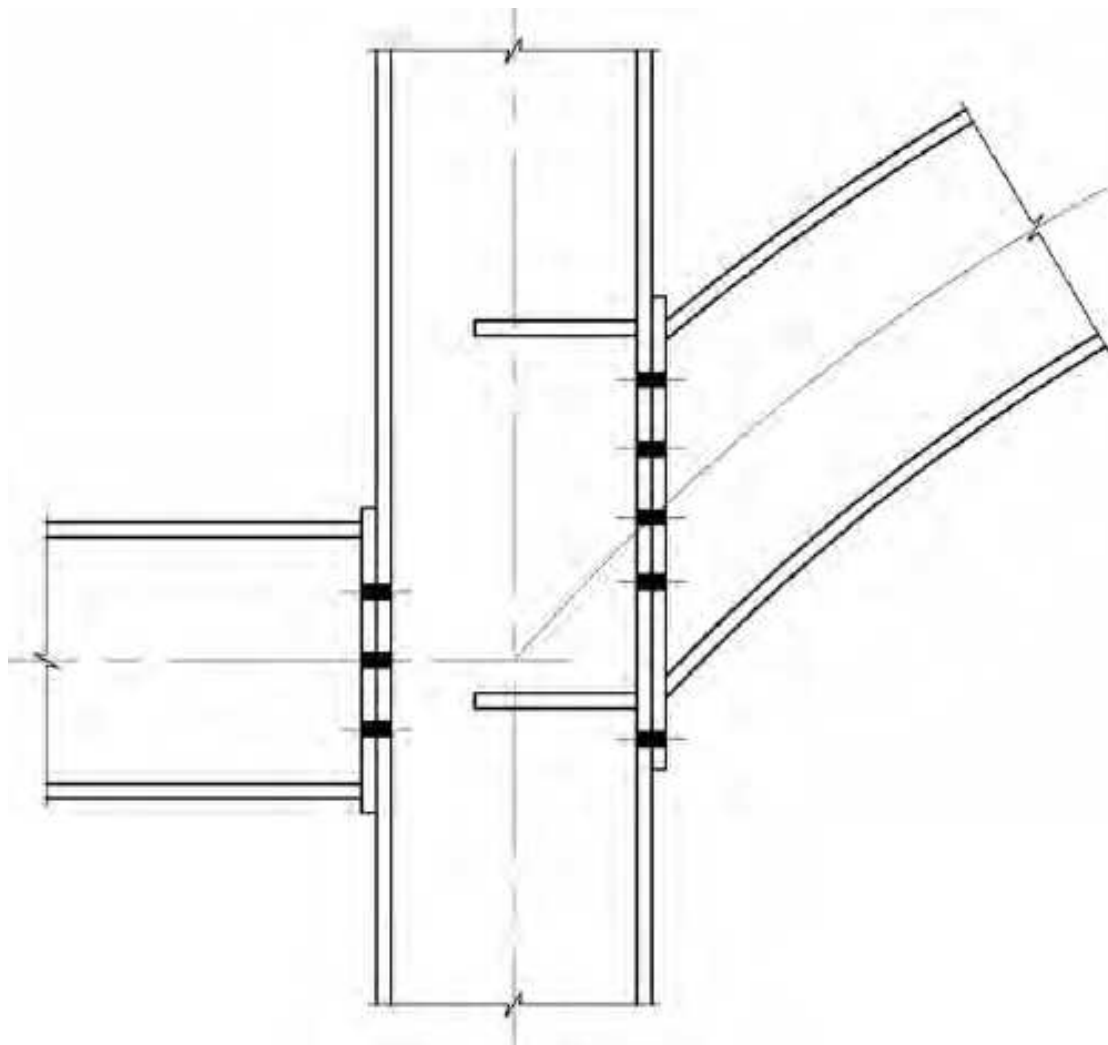


Fig. 6-16. Arch-to-column connection.

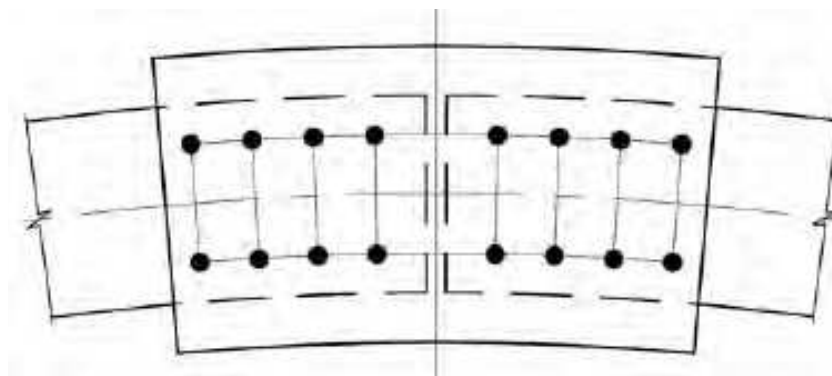


Fig. 6-17. Flange-plate splice.

be done with a splice in the curved member or with shim packs between the end plate and the column flange.

Section 4.4 discusses splice requirements for curved members. Similar to columns, arch stability is dependent on the flexural stiffness at the splice; however, arch in-plane stability is also sensitive to the axial stiffness. Therefore, any splices must be capable of maintaining member flexural and axial continuity. Either welded or bolted slip-critical splices should be considered. End-plate splices can also be efficient.

Figure 6-17 shows a simple flange-plate splice for an I-shaped member curved about its weak axis. The member ends can be finished to bear, or the splice can be designed

with a gap. A disadvantage to flange-plate splices, and other splices requiring bolt holes in the curved member, is the inefficiency of forming the holes after bending.

An alternative bolted splice for an I-shaped member curved about its strong axis is shown in Figure 6-18. This connection is efficient for fabrication because a precise cut is not required at the member ends and bolt holes are not required in the curved member. Four inner plates are shop welded to the curved members, which are bolted together in the field using the outer plates. Depending on the joint length, hand holes may be required to allow proper access to the bolts between the flanges.

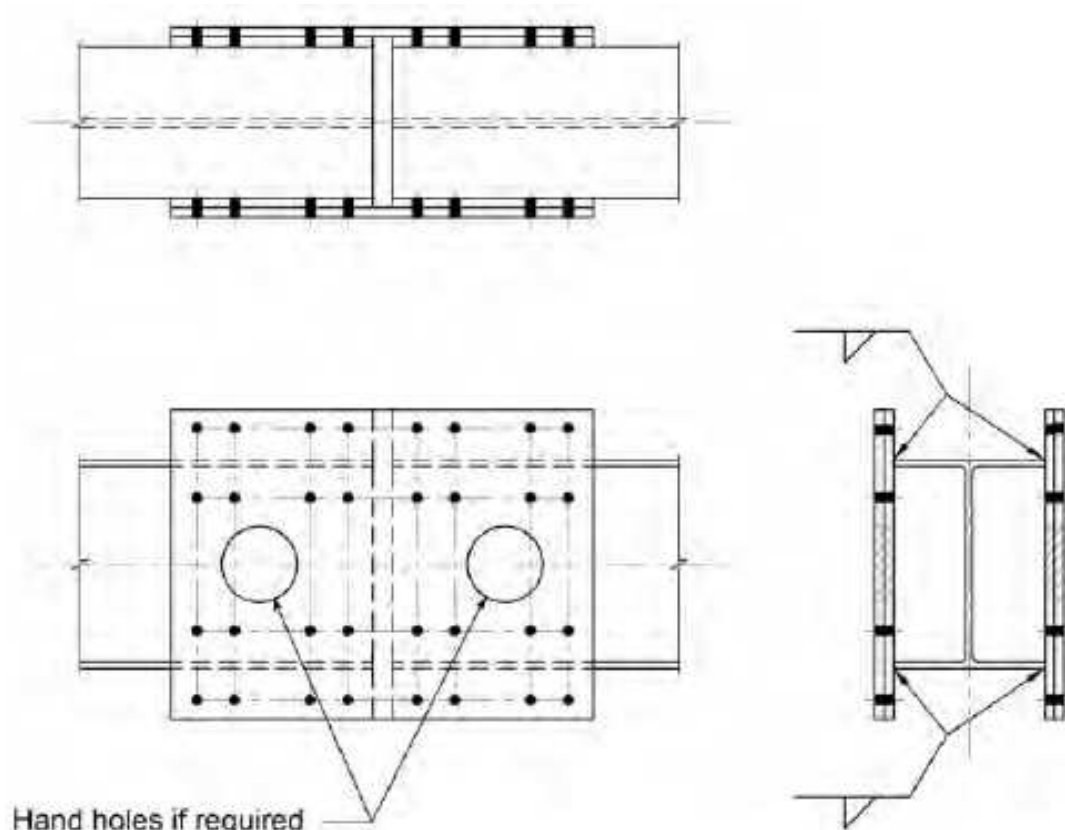


Fig. 6-18. Alternative bolted splice.



# Chapter 7

## Horizontally Curved Members

### 7.1 INTRODUCTION

This chapter discusses the strength and behavior of beams loaded perpendicular to the plane of curvature as shown in Figure 7-1. Horizontally curved beams must resist both flexural and torsional moments and are subject to the same limit states as straight beams. In most cases, torsional rotations lead to a design controlled by serviceability considerations.

### 7.2 BEHAVIOR

The deflected shape of a horizontally curved beam is characterized by vertical and horizontal translation, and torsional rotation of the cross section. Second-order effects and potential yielding of the beam cause nonlinear deformations until failure occurs by excessive deformations and/or yielding of the member. Due to their high torsional stiffness, closed sections provide efficient resistance to these deformations.

The behavior of curved beams is dependent on the span angle,  $\theta_s$ , in Figure 7-1. Beams with span angles less than  $1^\circ$  are dominated by flexure, acting as a nominally straight beam with an initial geometric imperfection. For beams with span angles between  $1^\circ$  and  $20^\circ$ , both bending and torsion have a significant influence on the behavior. When the span angle is greater than  $20^\circ$ , the behavior is affected primarily by torsion (Pi et al., 2000).

Because torsional deformations dominate the behavior of beams with span angles greater than  $20^\circ$ , efficient framing systems typically utilize infill members to provide torsional

restraint. Where the curved member is continuous across torsional supports, as shown in Figure 7-2, warping restraint increases the torsional efficiency. Analogous to the flexural behavior of a continuous beam, warping restraint is provided by equal and opposite warping moments in the adjacent span. The total resisting moment at the end of the infill beam is the sum of the torsional loads at the end of each span,  $M_e$ , shown in Figure 7-2(c). Connections between the curved member and the infill beams are discussed in Section 7.9.

### 7.3 STRUCTURAL ANALYSIS

Several methods are available to calculate the required loads in a curved beam. The finite element method is generally used for final design. Both the  $M/R$  method and the eccentric-load method are accurate enough for use in final design; however, they may be more appropriate for preliminary design in cases where complicated geometry and loadings are required. Also, these methods can provide valuable insight into the fundamental behavior of horizontally curved beams.

The required loads can also be calculated using equations published by Lebet and Hirt (2013), Young and Budynas (2002) and Nakai and Yoo (1988); however, the equations are cumbersome for design office use, and they are available only for a limited number of idealized cases. For the simplest case shown in Figure 7-2(a), where the beam is subjected to equal and opposite flexural moments,  $M_x$ , at the ends of the unbraced segment, the flexural moment is (Pi et al., 2000):

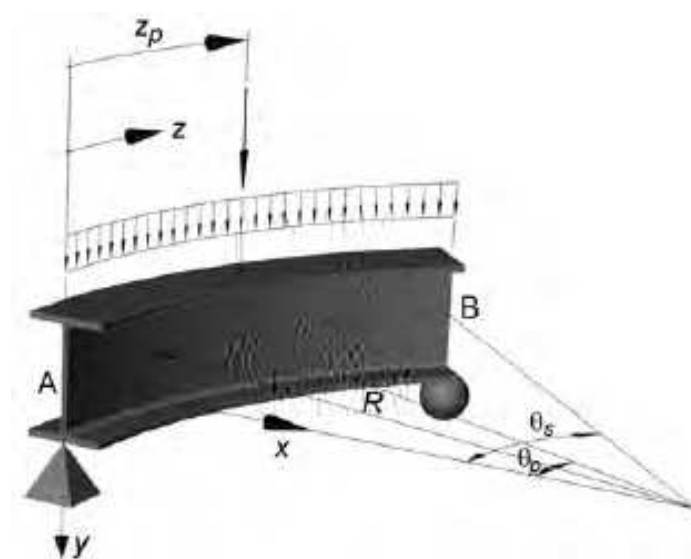


Fig. 7-1. Horizontally curved beam.

$$M_{x\theta} = \frac{M_x \cos\left(\frac{\theta_b}{2} - \theta_z\right)}{\cos\left(\frac{\theta_b}{2}\right)} \quad (7-1)$$

where

$\theta_b$  = angle between torsional restraints, rad

$\theta_z$  = angle from the end of the segment to the location of interest, rad

The torsional moment is:

$$M_{z\theta} = \frac{M_x \sin\left(\frac{\theta_b}{2} - \theta_z\right)}{\cos\left(\frac{\theta_b}{2}\right)} \quad (7-2)$$

The maximum flexural moment, which occurs at the mid-span, is:

$$M_{xm} = \frac{M_x}{\cos\left(\frac{\theta_b}{2}\right)} \quad (7-3)$$

The maximum torsional moment, which occurs at the ends, is:

$$M_{ze} = M_x \tan\left(\frac{\theta_b}{2}\right) \quad (7-4)$$

In addition to shear and axial loads, helical members are subjected to biaxial flexure and torsion. Several solutions are available for calculating the loads in spiral stairs of various geometries (Bangash and Bangash, 1999; Abdul-Baki and Bartel, 1969; Bergman, 1956). However, the equations are cumbersome for design office use and they are available only for a limited number of idealized cases. Because the solutions were derived by modeling the treads and stringers as a

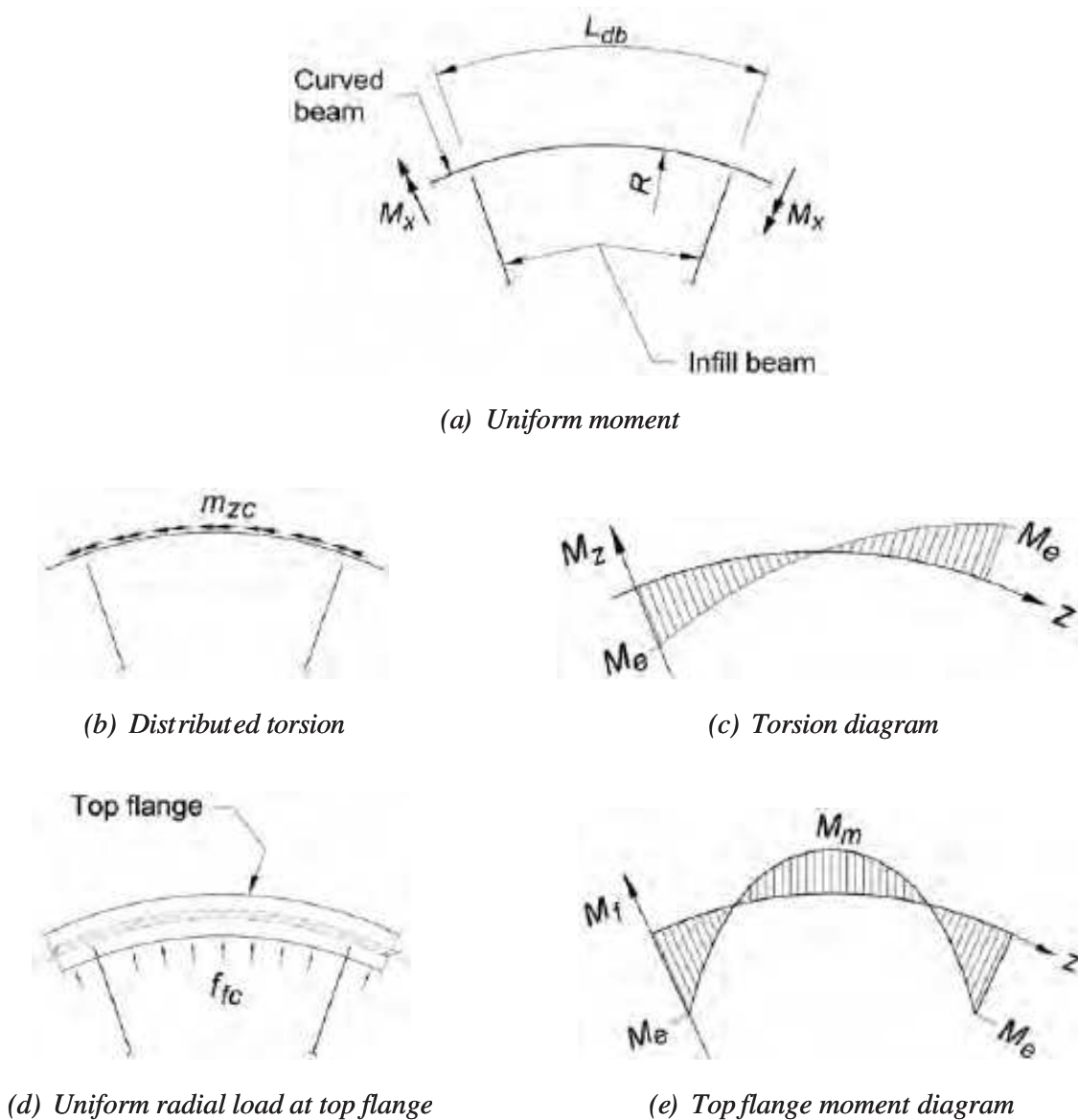


Fig. 7-2. Curved beam continuous across torsional supports.

single member, they are applicable to steel stairs only in special cases. A finite element model may be the best method to determine the required member loads. A conservative model can be obtained by neglecting the treads and modeling the stringers as independent spiral members. In many cases, this will be extremely conservative because the treads can provide significant torsional restraint to the stringer. The level of torsional restraint provided by the treads is dependent on the tread type, arrangement and connection details.

### 7.3.1 Finite Element Models

Either a two- or three-dimensional finite element model can be used to model the structural behavior of horizontally curved beams. As discussed in Section 6.6, curved members are usually modeled with a series of straight elements. Although a three-dimensional model requires a greater engineering effort, the accuracy may only be slightly better than a two-dimensional analysis with similar element sizes (Nevling et al., 2006).

#### Two-Dimensional Finite Element Model

A two-dimensional segmented finite element model, with several straight beam elements representing the curved member will usually provide the accuracy required for design purposes. The accuracy increases with the number of elements. Between 10 and 20 elements is adequate for modeling most semi-circular members (King and Brown, 2001). For models with highly nonlinear behavior, a convergence study may be required to determine the appropriate number of elements.

Most commercial finite element programs use the basic beam finite element formulation, which does not have the capability to model the warping stiffness. In this case, only the St. Venant stiffness is utilized in the analysis, which causes an overestimate of the torsional deformations for most open cross sections. The accuracy can be improved by using equivalent torsion constants (Ahmed and Weisgerber, 1996; White and Coletti, 2013). For members with warping fixed at both ends of the span, the equivalent torsion constant is:

$$J_e = \frac{J}{1 - \frac{\sinh \gamma}{\gamma} + \frac{(\cosh \gamma - 1)^2}{\gamma \sinh \gamma}} \quad (7-5)$$

where

$J$  = torsional constant, in.<sup>4</sup>

$$\gamma = L_{db} \sqrt{\frac{GJ}{EC_w}} \quad (7-6)$$

and where

$C_w$  = warping constant, in.<sup>6</sup>

$E$  = modulus of elasticity, ksi

$G$  = shear modulus, ksi

$L_{db}$  = developed length (arc length) along the curved member between torsional restraints, in.

For members with warping fixed at one end of the span and warping free at the other end, the equivalent torsion constant is:

$$J_e = \frac{J}{1 - \frac{\sinh \gamma}{\gamma \cosh \gamma}} \quad (7-7)$$

Because torsion in closed cross sections is resisted primarily by St. Venant torsion, accurate results can be expected for closed sections when the warping stiffness is neglected.

#### Three-Dimensional Finite Element Model

A three-dimensional finite element model uses several elements to make up the cross section. The webs are typically modeled with plate elements, but can also be modeled with shell or solid elements. The flanges of I-shaped members are typically modeled with beam elements, but can also be modeled with plate, shell or solid elements (FHWA, 2015; AASHTO/NSBA, 2014; King and Brown, 2001). The warping stiffness is addressed properly in these models without the need for modified torsion constants.

Infill members and cross frames that are rigidly connected to restrain torsion can be connected to nodes at the top and bottom flanges of the curved member. They can be modeled with beam elements or with plate/shell/solid elements (FHWA, 2015; AASHTO/NSBA, 2014).

Any deck or slab can be modeled with plate, shell or solid elements. If plate or shell elements are used, the elements should be offset vertically above the top flange of the curved member using linking elements. For example, a composite slab can be modeled with eight-node solid elements attached to the curved member top flange with beam elements representing the shear headed stud anchors (FHWA, 2015).

If the flanges of the curved member are modeled with beam elements, the required stresses from the model can be compared with the available stresses in the AISC *Specification* (AISC, 2016c) and AISC Design Guide 9 *Torsional Analysis of Structural Steel Members* (Seaburg and Carter, 1997). However, the available strengths in the AISC *Specification* were not developed to be compared to the results from finite element models built with plate, shell or solid elements. The ASD safety factors and LRFD resistance factors in the AISC *Specification* were calibrated to provide a specific target reliability when compared with required loads calculated using truss and beam elements in the structural analysis model, not plate, shell or solid elements. If the results of a model with plate, shell or solid elements are used with the AISC *Specification* provisions, the required member loads should be determined by summing the element stresses over the

entire cross section. This will complicate the calculations and will likely produce similar results compared to a model with beam elements used for the flanges.

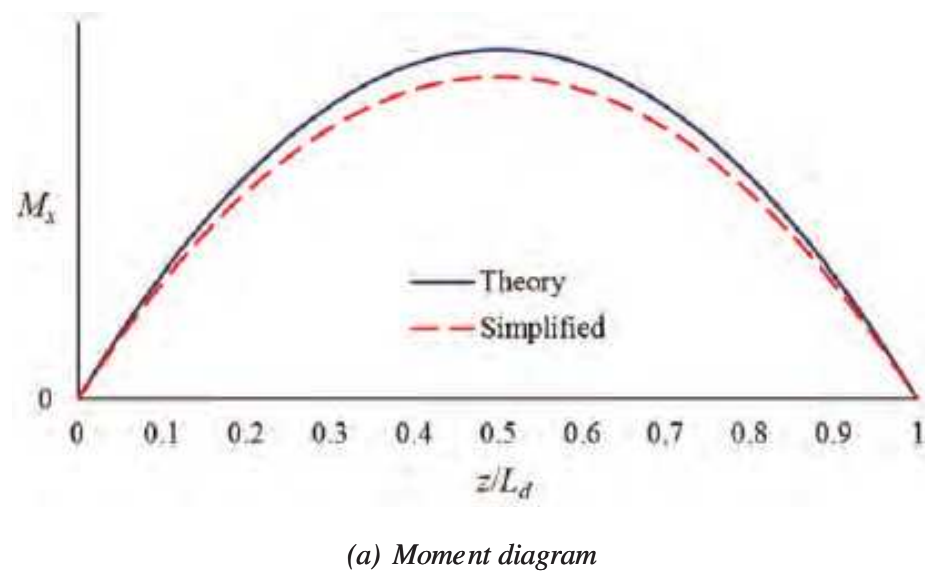
### 7.3.2 $M/R$ Method

The  $M/R$  method (Tung and Fountain, 1970) has been used extensively in design where the curved beam is modeled as a straight member with a length equal to the developed span length,  $L_{ds} = R\theta_s$ , where  $R$  is the radius and  $\theta_s$  is the span angle in radians. The shear force,  $V$ , and the out-of-plane flexural moment,  $M_x$ , are calculated as for a straight beam. Figure 7-3(a) shows the bending moment diagram for a horizontally curved, simply supported, uniformly loaded beam. The solid line shows the moment for the exact solution (Lebet and Hirt, 2013), and the dashed line shows the moment calculated using the straight beam approximation. The bending moment diagrams for a horizontally curved, simply supported beam with a midspan concentrated load is shown in Figure 7-4(a). In both cases, the developed member length,  $L_d$ , is equal to the developed span length,  $L_{ds}$ .

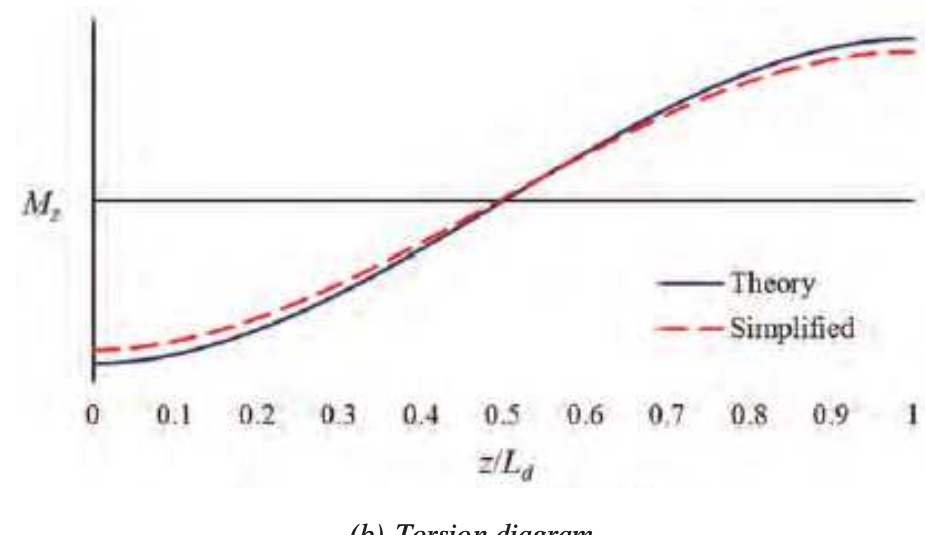
The torsional moment per unit length resulting from the beam curvature can be estimated with Equation 7-8. Torsion diagrams can be constructed in a manner similar to the method used for shear and moment diagrams, where the change in torsional moment,  $M_z$ , between two points along the developed beam length is equal to the summation of  $m_{zc}$  over the segment of interest. Because  $m_{zc}$  accounts only for shear-center loads caused by the beam curvature, any additional torsional moments should be added algebraically to  $m_{zc}$ .

$$m_{zc} = \frac{M_x}{R} \quad (7-8)$$

For the curved beam in Figure 7-2(a),  $m_{zc}$  is shown in Figure 7-2(b) and the torsion diagram is shown in Figure 7-2(c). Because the torsion diagram is shown on a curved axis, the diagram is curved; however, the variation in torsional moment is linear along the member arc. The torsion diagrams for the bending moment diagrams in Figures 7-3(a)



(a) Moment diagram



(b) Torsion diagram

Fig. 7-3. Moment and torsion diagrams for a horizontally curved, simply supported, uniformly loaded beam.

and 7-4(a) are shown in Figures 7-3(b) and 7-4(b), respectively. In both cases, torsional restraints are located only at the supports ( $L_d = L_{ds} = L_{db}$ ).

The required shear calculated using the straight beam model is equal to the theoretical value; however, the flexural and torsional moments are under-predicted. When  $\theta_s \leq \pi/6$  (30°), the error for the simplified method is less than 3%. For  $\theta_s > \pi/6$  (30°), the flexural and torsional moments can be calculated using correction factors according to Equations 7-9 and 7-10, respectively.

$$M_{xc} = CM_x \quad (7-9)$$

$$M_{zc} = CM_z \quad (7-10)$$

where

$$C = 1 - \frac{\theta_s}{30} + \frac{\theta_s^2}{6.2} \quad (7-11)$$

### Idealized Cases

For several idealized cases, the  $M/R$  method can be used to develop equations for the torsional moment at any location along the member. For all cases discussed, torsional restraints are located only at the supports ( $L_d = L_{ds} = L_{db}$ ). For a horizontally curved, simply supported, uniformly loaded beam, the torsional moment represented by the diagram in Figure 7-3(b) is:

$$M_z = \frac{w}{24R} [L_d^3 - z^2(6L_d - 4z)] \quad (7-12)$$

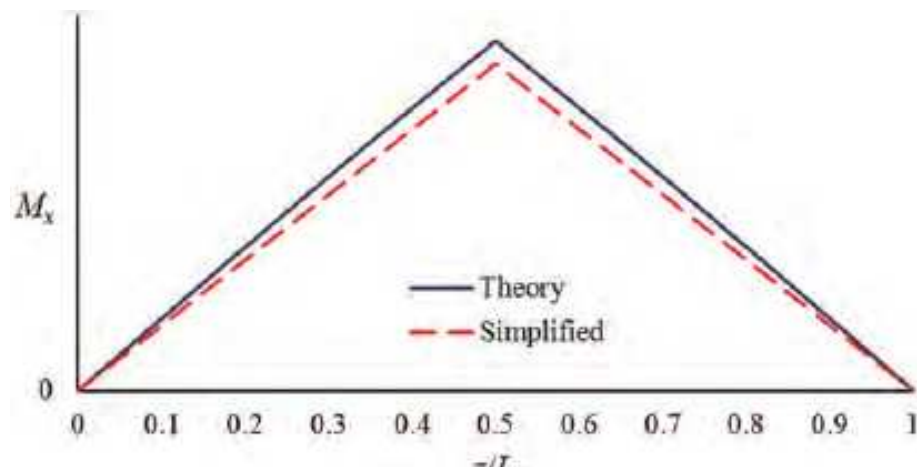
where

$L_d$  = developed beam length, in.

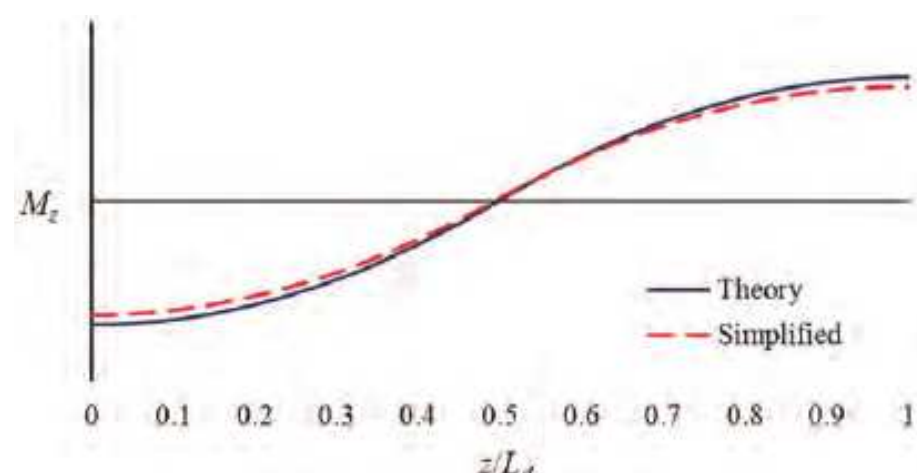
$w$  = uniform load, kip/in.

$z$  = distance along the developed beam length, in.

The torsional moment is zero at the midspan and the maximum/minimum values at the ends are:



(a) Moment diagram



(b) Torsion diagram

Fig. 7-4. Moment and torsion diagrams for a horizontally curved, simply supported beam with a midspan concentrated load.

$$M_z = \pm \frac{wL_d^3}{24R} \quad (7-13)$$

For a horizontally curved, simply supported beam with a midspan concentrated load, the torsional moment represented by the diagram in Figure 7-4(b) is:

$$M_z = \frac{P}{16R} (L_d^2 - 4z^2) \quad \text{for } z \leq \frac{L_d}{2} \quad (7-14)$$

where

$P$  = concentrated load, kips

The torsional moment is zero at the midspan and the maximum/minimum values at the ends are:

$$M_z = \pm \frac{PL_d^2}{16R} \quad (7-15)$$

For a horizontally curved, fixed-end, uniformly loaded beam, the torsional moment is:

$$M_z = \frac{wz}{12R} (3L_d z - L_d^2 - 2z^2) \quad (7-16)$$

The torsional moment is zero at the ends and midspan. The maximum/minimum values at  $z=0.211L_d$  and  $z=0.789L_d$  are:

$$M_z = \pm \frac{wL_d^3}{125R} \quad (7-17)$$

For a horizontally curved, fixed-end beam with a midspan concentrated load, the torsional moment is:

$$M_z = \frac{Pz}{8R} (2z - L_d) \quad \text{for } z \leq \frac{L_d}{2} \quad (7-18)$$

The torsional moment is zero at the ends and midspan. The maximum/minimum values at  $z=L_d/4$  and  $z=3L_d/4$  are:

$$M_z = \pm \frac{PL_d^2}{64R} \quad (7-19)$$

### 7.3.3 Eccentric Load Method

A simple method to approximate the torsional loads on a horizontally curved beam is based on the horizontal eccentricity from the load to a chord drawn between the supports (Heins and Firmage, 1979). For members that are loaded along their curved shear center axis, the equivalent eccentricity is the distance perpendicular to the chord, from the chord to the centroid of the load. For uniformly distributed loads, the equivalent eccentricity is:

$$e_w = R \left[ \cos\left(\frac{\theta_s}{4}\right) - \cos\left(\frac{\theta_s}{2}\right) \right] \quad (7-20)$$

And the uniformly distributed torsion is:

$$m_z = we_w \quad (7-21)$$

For midspan concentrated loads, the equivalent eccentricity is:

$$e_p = R \left[ 1 - \cos\left(\frac{\theta_s}{2}\right) \right] \quad (7-22)$$

And the concentrated midspan torsion is:

$$M_z = Pe_p \quad (7-23)$$

The support moments are accurately predicted with the eccentric load method; however, the span moments are only approximate. Use of these approximate span moments results in a linear torsion diagram, which is advantageous in design because the required cases for these loading conditions are available in AISC Design Guide 9, Appendix B.

## 7.4 FLEXURAL STRENGTH

The local buckling provisions in AISC *Specification* Chapter B are applicable to horizontally curved beams without modification. As discussed in Section 7.2, the behavior at ultimate strength is characterized by excessive vertical, horizontal and torsional deformations rather than a classical lateral-torsional buckling failure. However, as with straight beams, the flexural strength of curved beams is reduced for members that are susceptible to lateral-torsional buckling (Yoo et al., 1996; Nishida et al., 1978). Because closed sections have a high torsional rigidity, they are typically not subject to lateral-torsional buckling.

The effect of curvature on the lateral-torsional buckling strength is negligible when the angle between torsional restraints,  $\theta_b$ , is equal to or less than  $\pi/8$  (22.5°). In this case, AISC *Specification* Chapter F is applicable. For doubly symmetric I-shaped members with  $\theta_b > \pi/8$  (22.5°), the provisions of Chapter F can be used with a revised lateral-torsional buckling modification factor according to Equation 7-24 (adapted from Yoo et al., 1996). In the AISC *Specification* equations, the developed length along the beam between torsional restraints,  $L_{db}=R\theta_b$ , must be used in lieu of the straight-member unbraced length,  $L_b$ .

$$C_{bo} = C_{bs} \left[ 1 - \left( \frac{\theta_b}{\pi} \right)^2 \right]^2 \quad (7-24)$$

where

$C_{bs}$  = lateral-torsional buckling modification factor for an equivalent straight member  
 $\theta_b$  = angle between torsional restraints, rad

## 7.5 TORSIONAL STRENGTH

After the required torsional loading diagrams have been constructed using one of the structural analysis methods in Section 7.3, the torsional strength can be determined with one of the methods in this section. Because both torsion and flexure are present in curved beams, the second-order effects and interaction equations in Section 7.6 are required to verify the member strength. In all cases, the torsional strength is calculated for an equivalent straight member, based on the developed length between torsional restraints,  $L_{db}$ , and properly accounting for any warping restraints.

### 7.5.1 Elastic Method

AISC Design Guide 9 can be used to calculate the elastic torsional strength of an equivalent straight member. Because the torsion diagrams for curved beams are typically nonlinear, conservative assumptions are usually required to accommodate the design charts in Appendix B of the Design Guide. The simplest loading case with a uniform moment over the unbraced length, as shown in Figure 7-2(a), results in a uniformly distributed torsion, as shown in Figure 7-2(b). For this loading condition, the torsional functions can be determined with Case 4 or Case 7, depending on the warping boundary conditions at the supports. For simply supported beams subjected to uniformly distributed loads, the maximum value of  $m_{zc}$  within the span can be used as a conservative estimate of the uniform torsion per unit length. Using this simplification with Case 4 for a beam with free warping at the boundaries results in an overestimate of torsional rotations by 23%.

For composite I-shaped beams, as shown in Figure 7-5(a), the torsional properties are based on the idealized transformed section shown in Figure 7-5(b) (Heins and Kuo, 1972). The normalized warping functions and warping statical moments are shown in Figures 7-5(c) and 7-5(d), respectively. The torsional constant is:

$$J = \frac{1}{3} \left( b_f t_f^3 + d_e t_w^3 + \frac{b_e t_c^3}{m} \right) \quad (7-25)$$

The warping constant is:

$$C_w = \frac{1}{12} \left[ y^2 b_e^3 t_e + (d_e - y)^2 b_f^3 t_f \right] \quad (7-26)$$

The normalized warping function for the slab is:

$$W_{nc} = \frac{y b_e}{2} \quad (7-27)$$

The normalized warping function for the steel section is:

$$W_{ns} = \frac{(d_e - y) b_f}{2} \quad (7-28)$$

The warping statical moment for the slab is:

$$S_{ws} = \frac{y b_e^2 t_e}{8} \quad (7-29)$$

The warping statical moment for the steel section is:

$$S_{ws} = \frac{(d_e - y) b_f^2 t_f}{8} \quad (7-30)$$

The shear center location is:

$$y = \frac{b_f^3 t_f d_e}{b_e^3 t_e + b_f^3 t_f} \quad (7-31)$$

where

- $E$  = modulus of elasticity of the steel section, ksi
- $E_c$  = modulus of elasticity of the slab, ksi
- $G$  = shear modulus of the steel section, ksi
- $G_c$  = shear modulus of the slab, ksi
- $b_e$  = effective slab width, in.
- $b_f$  = flange width, in.
- $d_e = d + (t_e - t_f)/2$  = distance between flange centroids of the idealized section, in.
- $m = G/G_c$  = shear modular ratio
- $n = E/E_c$  = modular ratio
- $t_c$  = slab thickness, in.
- $t_e = t_c/n$  = transformed slab thickness, in.
- $t_f$  = flange thickness, in.

### 7.5.2 Isolated Flange Method

If the St. Venant torsion is neglected, the torsional loads are resisted exclusively by warping. For I-shaped members, the warping strength can be approximated by isolating the flanges and treating them as independent rectangular beams loaded in the horizontal plane by a distributed radial force per unit length calculated with Equation 7-32. The radial force is applied toward the center of curvature at the tension flange and away from the center of curvature at the compression flange as shown in Figure 7-6.

$$f_{fc} = \frac{m_{zc}}{h_o} = \frac{M_x}{R h_o} \quad (7-32)$$

where

$h_o$  = distance between flange centroids, in.

The flexural boundary conditions of the isolated flange are based on the warping boundary conditions of the curved member. If warping is restrained at the support, the isolated flange will be modeled with a flexurally fixed end. For free warping, the isolated flange will be modeled with a flexurally pinned end. For sections with compact flanges, the nominal flexural strength of the isolated flange is:

$$M_{nw} = F_y Z_f \quad (7-33)$$

The plastic modulus about the strong axis of the flange is:

$$Z_f = \frac{t_f b_f^2}{4} \quad (7-34)$$

where

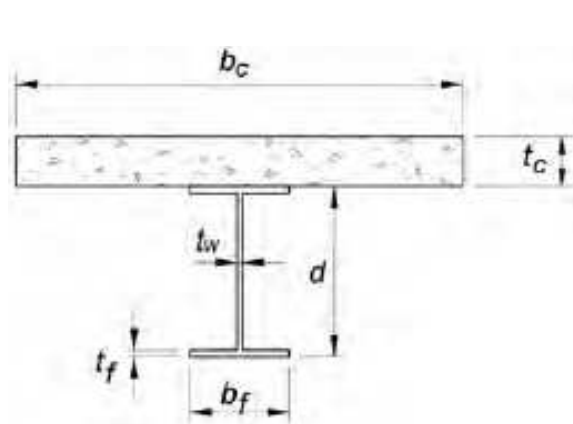
$b_f$  = flange width, in.

$t_f$  = flange thickness, in.

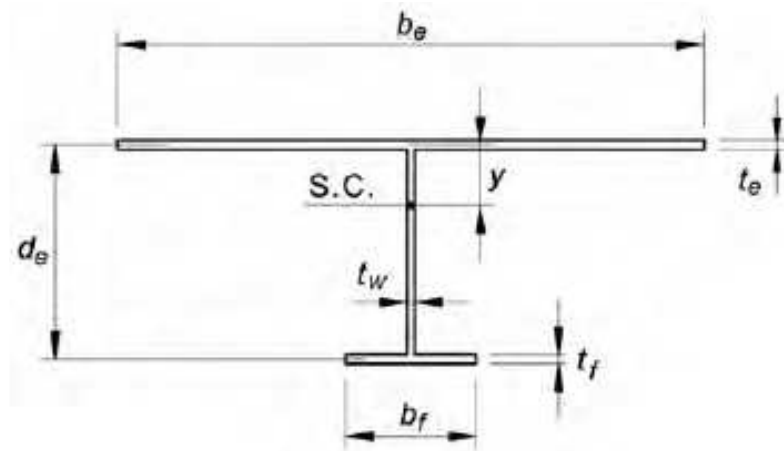
For the beam in Figure 7-2(a), the moment diagram for the isolated top flange, shown in Figure 7-2(e), is based on the compression flange radial load shown in Figure 7-2(d). Because the member is continuous across the infill beams, warping is restrained at the ends of the unbraced segment. For this condition, the moment diagram for the equivalent straight beam isolated flange is based on a fixed-fixed uniformly loaded beam.

The basic steps for the isolated flange method are:

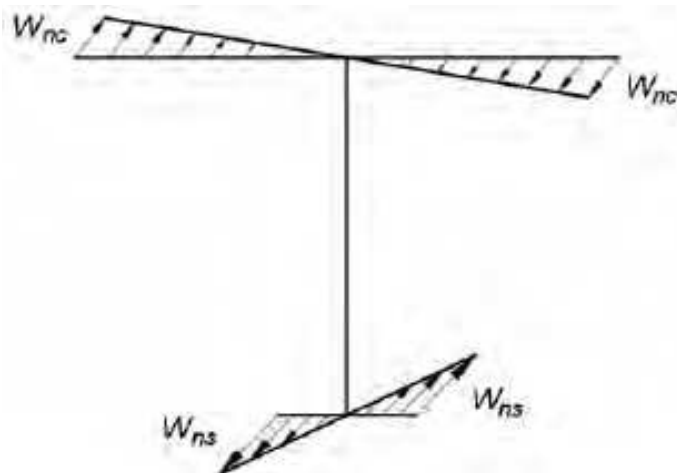
1. Construct the primary moment diagram for the equivalent straight beam segment between points of torsional restraint,  $L_{db}$ .
2. Convert the warping boundary conditions to the appropriate flexural boundary conditions for the isolated flange.
3. Using the primary moment diagram and Equation 7-32, calculate the distributed radial force per unit length,  $f_{fc}$ , to be applied to the isolated flange.
4. Construct the moment diagram for the isolated flange.



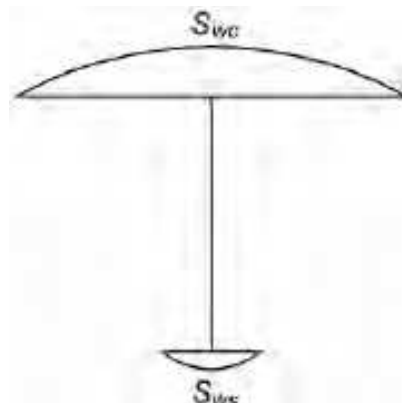
(a) Dimensions



(b) Idealized section



(c) Normalized warping function



(d) Warping statical moment

Fig. 7-5. Torsional properties of a composite beam.

- Evaluate both flanges under the combined actions, including second-order effects, as discussed in Section 7.6.

## 7.6 COMBINED FLEXURE AND TORSION

As with straight members, curved members subjected to both flexure and torsion must consider the effects of load interaction. After the required flexural and torsional moments are determined, the available member strength is calculated either by combining the stresses or by combining the load ratios in an interaction equation. In either case, second-order effects must be considered.

### 7.6.1 Second-Order Effects

Second-order torsional moments and rotations can be calculated either by using a rigorous second-order analysis or by amplifying the results of a first-order analysis. Amplification factors similar to those in AISC *Specification* Appendix 8 for straight members can be used for curved members (Rettie, 2015; AASHTO, 2014; Ashkinadze, 2008; Lindner and Glitsch, 2005; Boissonnade et al., 2002; Trahair and Teh, 2000; Pi and Trahair, 1994). For open sections subjected to both torsion and strong-axis flexure, the second-order torsional rotation is:

$$\theta_2 = B_o \theta_1 \quad (7-35)$$

The second-order torsional moment is:

$$M_{rz} = B_o M_z \quad (7-36)$$

The amplification factor is:

$$B_o = \frac{0.85}{1 - \alpha \frac{M_{ro}}{M_{eo}}} \geq 1.0 \quad (7-37)$$

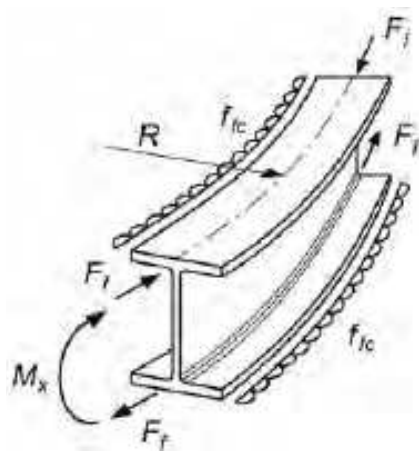


Fig. 7-6. The isolated flange method (adapted from King and Brown, 2001).

where

$M_{eo}$  = elastic critical lateral-torsional buckling moment for out-of-plane flexure, kip-in.

$M_{ro}$  = required out-of-plane flexural moment, kip-in.

$M_z$  = first-order torsional moment, kip-in.

$\theta_1$  = first-order torsional rotation, rad

$\alpha$  = 1.0 (LRFD); 1.6 (ASD)

Where compression flange bracing is spaced close enough to satisfy  $L_b \leq L_p$  according to AISC *Specification* Chapter F, torsional moments can be based on a first-order analysis. Because closed sections are typically not subject to lateral-torsional buckling, the second-order contribution to the torsional moment is negligible for these members.

### 7.6.2 Noncomposite I-Shaped Members

Noncomposite I-shaped members can be evaluated using either the elastic method or the isolated flange method, which are discussed in Sections 7.5.1 and 7.5.2, respectively. When the isolated flange method is used to determine the flange warping moment, the out-of-plane moment can be combined with the flange warping moment by adapting AISC *Specification* Equation H1-1a:

$$\frac{M_{ro}}{M_{co}} + \frac{8}{9} \frac{M_{rw}}{M_{cw}} \leq 1.0 \quad (7-38)$$

where

$M_{co}$  = available out-of-plane flexural strength of the member, kip-in.

$M_{cw}$  = available flexural strength of the isolated flange, kip-in.

$= \phi M_{nw}$  (LRFD)

$= M_{nw}/\Omega$  (ASD)

$M_{nw}$  = nominal flexural strength of the isolated flange, kip-in.

$M_{ro}$  = required out-of-plane flexural strength of the member, kip-in.

$M_{rw}$  = required second-order flexural strength of the isolated flange, kip-in.

$\Omega$  = 1.67

$\phi$  = 0.90

When the elastic method is used, the warping stresses calculated with AISC Design Guide 9 can be combined with the member flexural stresses by adapting AISC *Specification* Equation H1-1a for elastic stresses according to Equation 7-39. The 16/27 value for the constant is the result of dividing 8/9, which is the constant from Equation H1-1a, by 3/2, which is the shape factor of the flange.

$$\frac{\sigma_{ro}}{\sigma_{co}} + \frac{16}{27} \frac{\sigma_{rw}}{\sigma_{cw}} \leq 1.0 \quad (7-39)$$

where

- $\sigma_{co}$  = available out-of-plane flexural stress, ksi
- $\sigma_{cw}$  = available warping stress, ksi
- $= \phi F_y$  (LRFD)
- $= F_y/\Omega$  (ASD)
- $\sigma_{ro}$  = required out-of-plane flexural stress, ksi
- $\sigma_{rw}$  = required second-order warping stress, ksi
- $\Omega = 1.67$
- $\phi = 0.90$

#### Analysis by Finite Element model

For finite element models with the flanges modeled as rectangular beam elements, the strong axis of the element will be oriented vertically with the warping stresses varying across the element depth. The analysis will result in both axial and flexural loads on the element due to out-of-plane flexure and warping of the curved beam, respectively. The elements can be evaluated using the equations in *Specification* Section H1. For finite element models with the flanges modeled as plate, shell or solid elements, the required member loads for use with the equations in AISC *Specification* Section H1 should be determined by summing the stresses over the element as discussed in Section 7.3.1.

#### 7.6.3 HSS and Box-Shaped Members

Round, square and rectangular HSS members and box-shaped members can be designed according to AISC *Specification* Section H3.2. For combined flexure, shear and torsion, Equation H3-6 reduces to:

$$\frac{M_{ro}}{M_{co}} + \left( \frac{V_r}{V_c} + \frac{M_{rz}}{M_{cz}} \right)^2 \leq 1.0 \quad (7-40)$$

where

- $M_{cz}$  = available torsional strength, kip-in.
- $M_{rz}$  = required torsional strength, kip-in.
- $V_c$  = available shear strength, kips
- $V_r$  = required shear strength, kips

For evaluation using stresses, Equation 7-40 can be expressed using the stress ratios:

$$\frac{\sigma_{ro}}{\sigma_{co}} + \left( \frac{\tau_{rv}}{\tau_{cv}} + \frac{\tau_{rt}}{\tau_{ct}} \right)^2 \leq 1.0 \quad (7-41)$$

where

- $\tau_{ct}$  = available shear stress for torsional loads, ksi
- $\tau_{cv}$  = available shear stress for shear loads, ksi
- $\tau_{rt}$  = required shear stress due to torsional loads, ksi
- $\tau_{rv}$  = required shear stress due to shear loads, ksi

#### 7.6.4 Composite I-Shaped Members

For partially and fully composite straight and curved beams

subjected to torsion, the concrete slab provides most of the torsional resistance. The steel member enhances the slab strength by restraining the longitudinal deformation. Torsional strength increases when the member is subjected to flexural loading because flexural compression in the slab partially opposes the torsional tensile stresses, which decreases the concrete cracking (Tan and Uy, 2011; Tan and Uy, 2009; Nie et al., 2009). Therefore, the interaction between torsion and flexure can be neglected for partially and fully composite beams, and the torsional and flexural strengths can be verified independently.

#### 7.7 SERVICEABILITY

As discussed in Sections 7.1 and 7.2, large vertical, horizontal and torsional deformations at ultimate strength often result in designs based on serviceability rather than strength. A reasonable limit on the maximum angle of rotation will ensure nonstructural elements are not damaged by excessive rotations. There are no formal limits in building codes; therefore, judgment should be used to define the appropriate deflection and rotation limits based on the type of building elements supported by the beam. When Equation 7-37 is used to calculate the second-order amplification factor for serviceability conditions,  $\alpha = 1.00$  can be used for both LRFD and ASD. Additional considerations, such as floor vibrations, may result in other serviceability performance criteria.

In the serviceability evaluation, the maximum normal stress in the member should be limited to the first-yield stress (Bremault et al., 2008; Driver and Kennedy, 1989). Alternatively, for I-shaped members in the inelastic range, the torsional rotation,  $\theta_{2i}$ , can be estimated with Equation 7-42a (Pi and Trahair, 1994). For closed shapes, a strength evaluation according to Equation 7-40 or 7-41 will ensure nominally elastic behavior and the elastic deformations can be used to evaluate serviceability limits.

$$\theta_{2i} = \frac{\theta_2}{1 - \frac{\alpha_t}{2}} \quad (7-42a)$$

where

- $\alpha_t$  = ratio of required torsional moment to plastic torsional strength

The value of  $\alpha_t$  can be estimated with Equations 7-42b and 7-42c for the isolated flange method and the elastic method, respectively:

$$\alpha_t = \frac{M_{rw}}{M_{cw}} \quad (7-42b)$$

$$\alpha_t = \frac{2 \sigma_{rw}}{3 \sigma_{cw}} \quad (7-42c)$$

## 7.8 OVALIZATION OF ROUND HSS

When curved round HSS members are subjected to out-of-plane flexure, the flexural strength and stiffness can be reduced by ovalization of the cross section. Figure 7-7 shows the deformed shape caused by out-of-plane bending, where the major axis of the ovalized shape is skewed at an angle of approximately  $35^\circ$  to  $45^\circ$  from the axis of flexure (Mourad and Younan, 2002).

The flexural section properties are functions of the flexibility characteristic,  $c_r$ , which is defined by Equation 6-32. The equations in this section assume infinitely long members and consider the effect of circumferential stresses. They are accurate for geometries common to structural steel members. Where ovalization is restrained by flanges, connections, or a straight HSS segment, the factors are conservative. Because significant nonlinear ovalization can occur when the member is loaded beyond the effective yield moment (Mourad and Younan, 2001),  $M_{yo} = S_{eo}F_y$ , limiting the nominal flexural strength of AESS members to  $M_{yo}$  may be appropriate. The effective section modulus is (Kellogg, 1957):

$$S_{eo} = k_{so}S \quad (7-43)$$

where

$$k_{so} = 0.926c_r^{2/3} \leq 1.00 \quad (7-44)$$

The effective plastic modulus, developed from the work of Spence and Findlay (1973) and Rodabaugh, (1979), is:

$$Z_{eo} = k_{zo}Z \quad (7-45)$$

where

$$k_{zo} = \frac{1.2c_r}{\sqrt{1 + c_r^2}} \quad (7-46)$$

For out-of-plane bending, the effective moment of inertia is identical to that of in-plane bending, which is calculated with Equation 6-37 (Kellogg, 1957). Because the circumferential stresses were considered in the development of the

effective plastic modulus according to Equation 7-45, their calculation is not required for routine design problems. However, when fatigue or local strength is an issue, the circumferential stresses can be calculated with a multiplier on the longitudinal flexural stress according to Equation 7-47 (Kellogg, 1957).

$$\sigma_{co} = k_{co} \frac{M_o}{S} \quad (7-47)$$

where

$M_o$  = moment perpendicular to the axis of curvature causing out-of-plane flexure, kip-in.

$S$  = section modulus of the HSS member, in.<sup>3</sup>

$Z$  = plastic modulus, in.<sup>3</sup>

$$k_{co} = \frac{1.50}{c_r^{2/3}} \quad (7-48)$$

## 7.9 CONNECTIONS

The primary difference in connections for straight beams and horizontally curved beams is the required torsional resistance. If the structural analysis model assumes warping restraints at the support, special connection considerations are required to ensure the modeled boundary conditions are consistent with the connections provided.

For curved members that are continuous across torsional supports as for the beam in Figure 7-2(a), the connection between the infill beams and the curved member must provide the required torsional resistance. The total connection moment is the sum of the torsional loads at the end of each curved segment,  $M_e$ , shown in Figure 7-2(c).

For I-shaped curved members, infill beams can be connected with nonconventional single-plane shear connections similar to the detail in Figure 7-8(a). An extended single-plate connection will allow simple erection of the infill beam. Multiple vertical bolt rows may be required to resist the torsional moment. Fitting the plate and welding to the curved-beam flanges will prevent local bending deformation of the

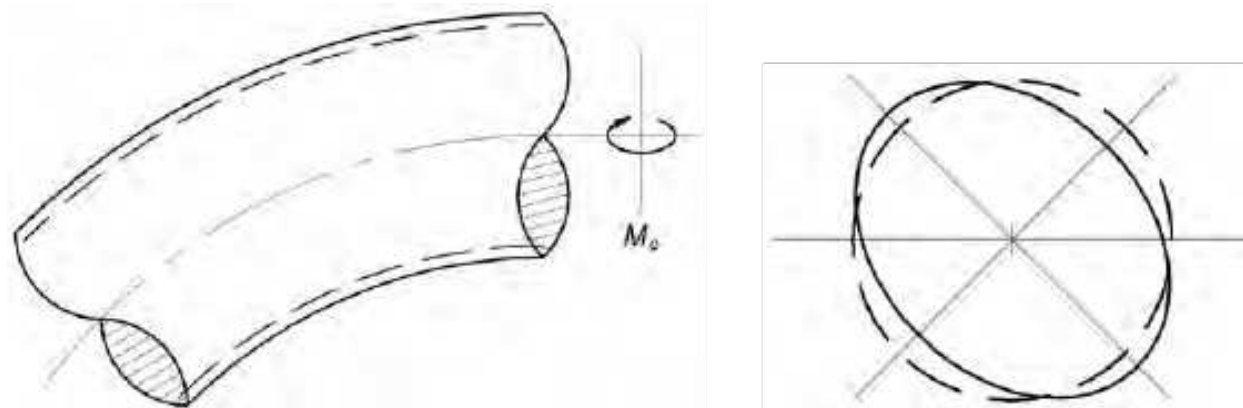
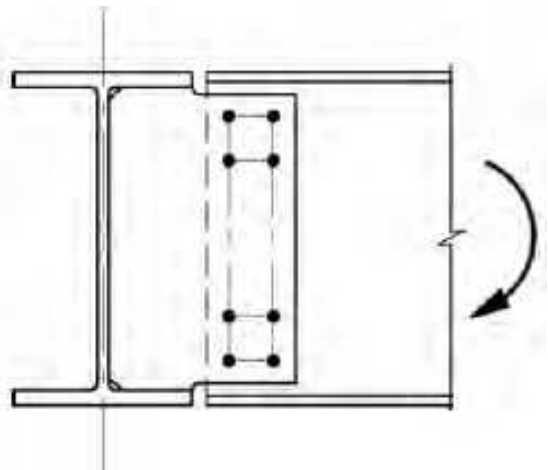
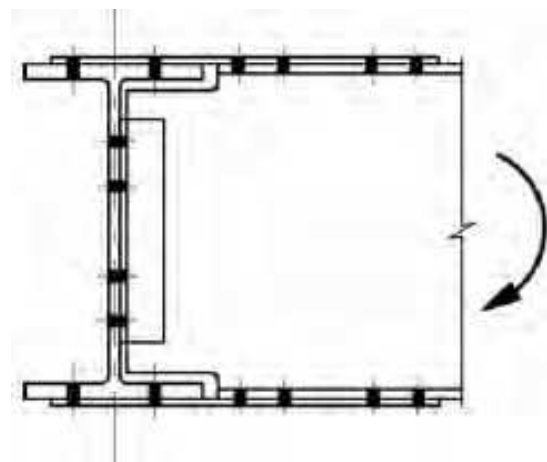


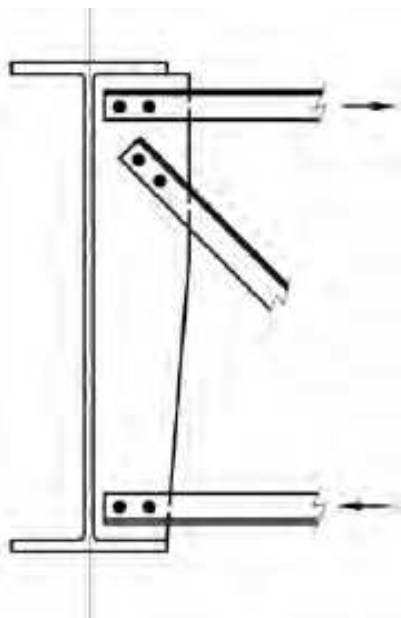
Fig. 7-7. Ovalization of a round HSS member.



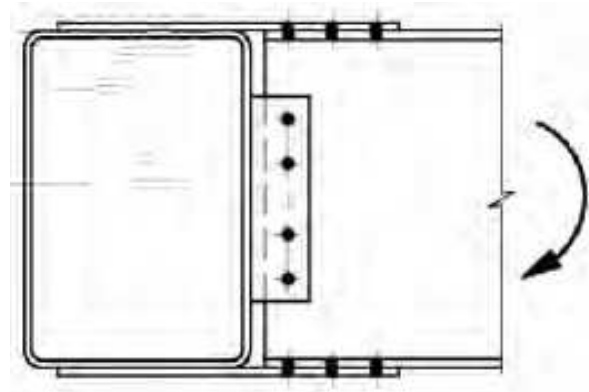
(a) Single-plate connection



(b) Flange-plate connection



(c) Cross-frame bracing



(d) Flange plate-to-HSS curved member connection

Fig. 7-8. Infill beam connections to curved members.

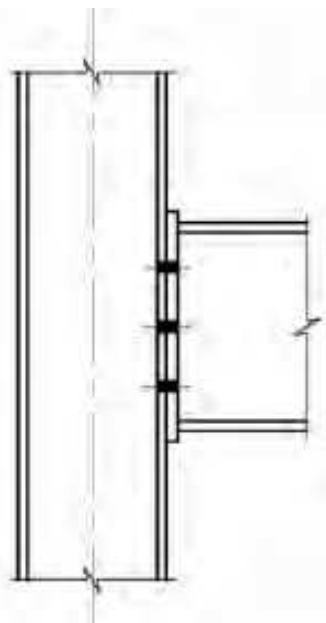
curved-beam web. If a single-plate connection is not adequate, flange plates can be added as shown in Figure 7-8(b). Although clip angles are used for the web connection, a single-plate connection can also be used to provide fit-up tolerances and eliminate hole forming in the curved-member web. Figure 7-8(c) shows a cross-frame bracing system that may be more efficient for deep curved beams with large torsional loads.

Due to the limited local wall bending strength and stiffness, single-plane shear connections acting alone are usually unsuitable for providing torsional restraint to curved square and rectangular HSS beams. If the torsional resistance is provided by flange plates, as shown in Figure 7-8(d), the

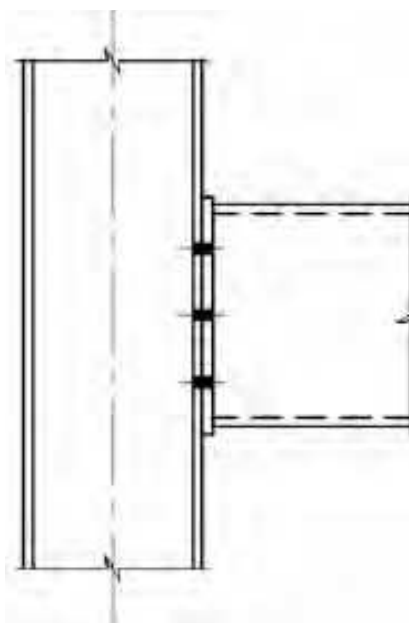
single-plate shear connection can be designed only for the beam shear load.

For equilibrium, the torsional moment at the end of curved beam spans must be transferred through the connection. For I-shaped members, the local web strength limits the torsional resistance (Grundy et al., 1983); therefore, any significant torsion must be resisted by connecting the flanges. Additionally, most common web shear connections, especially single-plate shear connections, are capable of only limited torsional resistance (Bennetts et al., 1981).

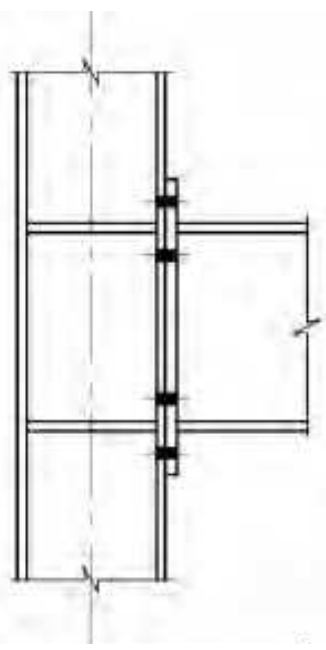
Figures 7-9(a) and 7-9(b) show flush end plate beam-to-column connections for I-shape and HSS beams, respectively. These connections are capable of transferring significant



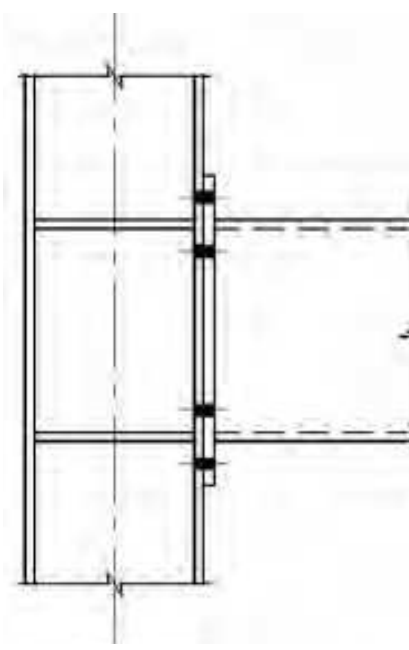
(a) I-shaped beam with flush end plate



(b) HSS beam with flush end plate



(c) I-shaped beam with extended end plate



(d) HSS beam with extended end plate

Fig. 7-9. End-plate connections.

torsional moments into the supporting member and can be designed as pinned connections for flexure. In Figure 7-9(b), the column flange must be substantially wider than the HSS beam to allow proper bolting clearances. The extended end plate connections in Figures 7-9(c) and 7-9(d) are capable of transferring large torsional moments as well as strong-axis moments. These connections can also be designed to transfer warping moments into the column.

If warping restraint is required, often the most practical option is to provide a connection to resist only the torsional load at the support, but eliminate warping from the connection by locating a warping stiffener near the member end. Both box stiffeners, shown in Figure 7-10(a), and cross stiffeners, shown in Figure 7-10(b), provide effective warping resistance (Smith, 1995; Szewczak et al., 1983; Vacharajit-tiphan and Trahair, 1974).

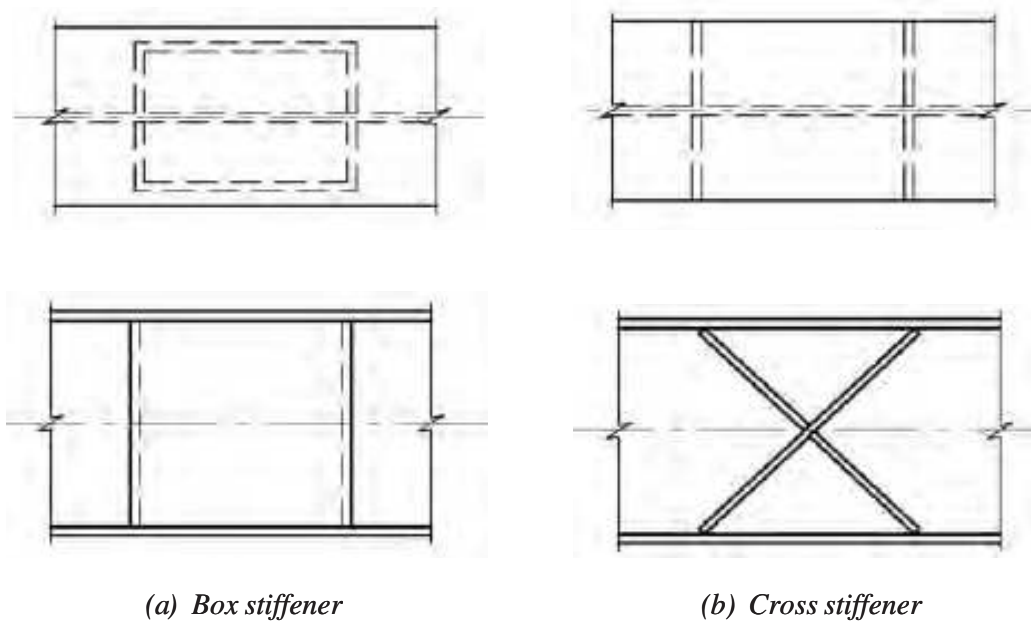


Fig. 7-10. Warping stiffeners.

# Chapter 8

## Design Examples

### Example 8.1—Vertically Curved Member

#### Given:

A W18×86 is bent the hard way to form the circular arch in Figure 8-1, which is subjected to three concentrated loads. The supports are restrained against translation in all directions and rotationally free in all directions. Verify that the W18×86 is adequate for the imposed loading. Bracing, which prevents out-of-plane translation and torsional rotation, is provided at five locations. The loads are:

LRFD	ASD
$P_{1u} = 120$ kips	$P_{1a} = 80$ kips
$P_{2u} = 75$ kips	$P_{2a} = 50$ kips

W-shape member material: ASTM A992

Plate material: ASTM A36

Bolts:  $\frac{3}{8}$ -in.-diameter Group A, threads not excluded from the shear plane (thread condition N), slip-critical Class A

Holes: oversized  $1\frac{1}{16}$ -in. diameter

Weld strength: 70 ksi

#### Solution:

From AISC *Manual* Tables 2-4 and 2-5, the material properties are as follows:

ASTM A992

$F_y = 50$  ksi

$F_u = 65$  ksi

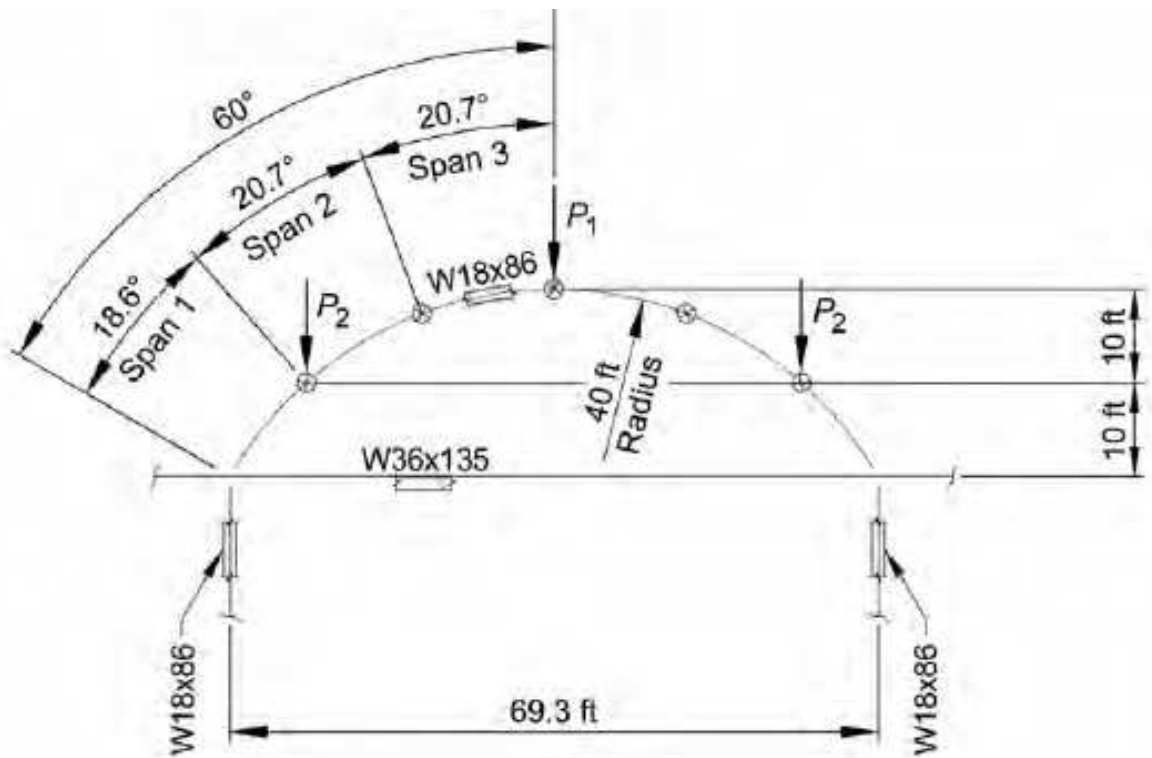


Fig. 8-1. Vertically curved member.

ASTM A36

$F_y = 36$  ksi

$F_u = 58$  ksi

From AISC *Manual* Table 1-1, the geometric properties are as follows:

**W18x86**

$A = 25.3$ in. <sup>2</sup>	$d = 18.4$ in.	$t_w = 0.480$ in.	$b_f = 11.1$ in.
$t_f = 0.770$ in.	$b_f/2t_f = 7.20$	$h/t_w = 33.4$	$I_x = 1,530$ in. <sup>4</sup>
$S_x = 166$ in. <sup>3</sup>	$r_x = 7.77$ in.	$Z_x = 186$ in. <sup>3</sup>	$I_y = 175$ in. <sup>4</sup>
$r_y = 2.63$ in.	$r_{ts} = 3.05$ in.	$h_o = 17.6$ in.	$J = 4.10$ in. <sup>4</sup>
$C_w = 13,600$ in. <sup>6</sup>			

**W36x135**

$d = 35.6$ in.	$t_w = 0.600$ in.	$t_f = 0.790$ in.	$k_{des} = 1.54$ in.
$h/t_w = 54.1$			

### Arch Geometry

Radius:

$$R = (40 \text{ ft})(12 \text{ in./ft}) \\ = 480 \text{ in.}$$

Arch angle:

$$\theta = (120^\circ) \left( \frac{\pi \text{ rad}}{180^\circ} \right) \\ = (2\pi/3) \text{ rad}$$

Chord span:

$$L_s = (69.3 \text{ ft})(12 \text{ in./ft}) \\ = 832 \text{ in.}$$

Rise:

$$H = (20 \text{ ft})(12 \text{ in./ft}) \\ = 240 \text{ in.}$$

Developed arc length:

$$L_d = (40 \text{ ft})[(2\pi/3) \text{ rad}](12 \text{ in./ft}) \\ = 1,010 \text{ in.}$$

$$\frac{H}{L_s} = \frac{240 \text{ in.}}{832 \text{ in.}} \\ = 0.288$$

### Structural Analysis

The loads were calculated using the finite element model shown in Figure 8-2 with a first-order analysis. Each span was segmented using straight beam elements with approximately a 3° arc between nodes.

The analysis resulted in the deflected shape in Figure 8-3 with a vertical deflection at the apex of:

LRFD	ASD
$\Delta_1 = 1.07$ in.	$\Delta_1 = 0.715$ in.

According to Section 6.3.1, if the first-order deflection,  $\Delta_1$ , calculated using factored loads for LRFD, or 1.6 times the service loads for ASD, is less than  $H/40$ , a first-order finite element analysis is sufficiently accurate.

$$\frac{H}{40} = \frac{240 \text{ in.}}{40} = 6.00 \text{ in.}$$

LRFD	ASD
1.07 in. < 6.00 in. <b>o.k.</b>	1.6(0.715 in.) = 1.14 in. < 6.00 in. <b>o.k.</b>

Therefore, a first-order analysis is adequate.

The vertical ( $y$ ) and horizontal ( $x$ ) support reactions are:

LRFD	ASD
$R_{ux} = 117 \text{ kips}$	$R_{ax} = 77.7 \text{ kips}$
$R_{uy} = 140 \text{ kips}$	$R_{ay} = 93.6 \text{ kips}$

The member loads are summarized in Table 8-1. The axial load varies along the member and is greatest at the supports. The moment diagram shown in Figure 8-4 shows reverse curvature, with closing moments in Spans 1 and 2 and an opening moment at the apex.

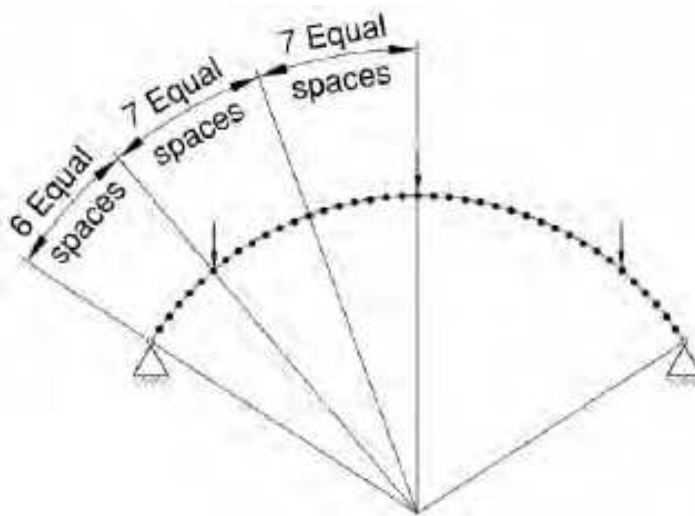


Fig. 8-2. Finite element model for Example 8.1.

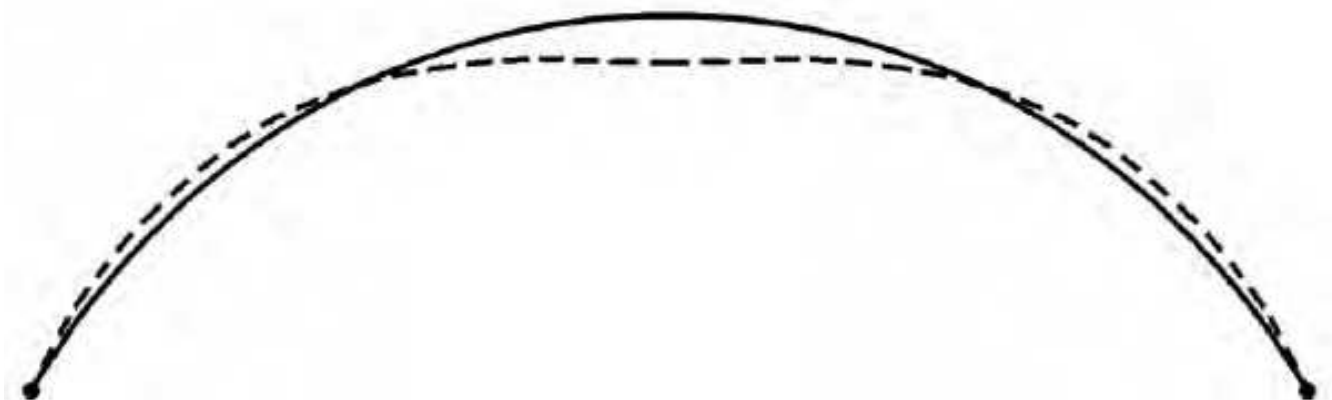


Fig. 8-3. Deflected shape for Example 8.1.

Table 8-1. Member Loads from Structural Analysis Model						
Location	Axial Load, $P_r$ kips		Moment, $M_{rx}$ kip-in.		Shear, $V_r$ kips	
	$P_u$	$P_a$	$M_{ux}$	$M_{ax}$	$V_u$	$V_a$
Supports	182	121	0	0	25.8	17.2
Apex	118	78.6	-5,360	-3,570	57.5	38.3
Maximum at Span 3	131	87.0	+1,380 -5,360	+918 -3,570	57.5	38.3
Maximum at Span 2	132	88.2	+1,880	+1,250	26.0	17.3
Maximum at Span 1	182	121	+1,270	+845	25.8	17.2

### Local Buckling—Flexure

Flanges:

$$\lambda_f = \frac{b_f}{2t_f} = 7.20$$

Web:

$$\lambda_w = \frac{h}{t_w} = 33.4$$

From AISC *Specification* Table B4.1b, the limiting width-to-thickness ratios are as follows.

Flanges:

$$\lambda_{pf} = 0.38 \sqrt{\frac{E}{F_y}} = 0.38 \sqrt{\frac{29,000 \text{ ksi}}{50 \text{ ksi}}} = 9.15$$

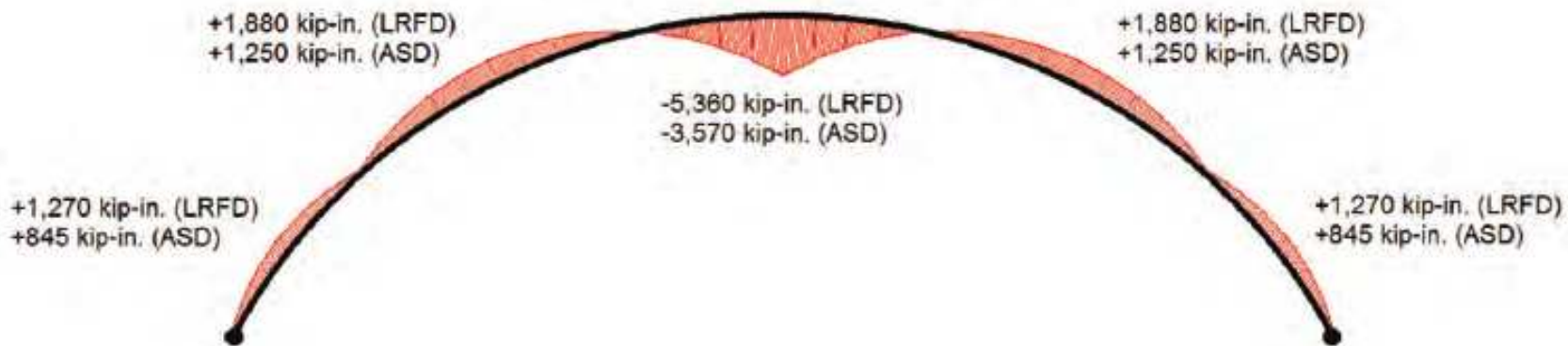


Fig. 8-4. Moment diagram for Example 8.1.

Web:

$$\begin{aligned}\lambda_{pw} &= 3.76 \sqrt{\frac{E}{F_y}} \\ &= 3.76 \sqrt{\frac{29,000 \text{ ksi}}{50 \text{ ksi}}} \\ &= 90.6\end{aligned}$$

Because  $\lambda_f < \lambda_{pf}$  and  $\lambda_w < \lambda_{pw}$ , the W18x86 has compact flanges and web.

#### *Local Buckling—Axial Compression*

Flanges:

$$\begin{aligned}\lambda_f &= \frac{b_f}{2t_f} \\ &= 7.20\end{aligned}$$

Web:

$$\begin{aligned}\lambda_w &= \frac{h}{t_w} \\ &= 33.4\end{aligned}$$

From AISC *Specification* Table B4.1a, the limiting width-to-thickness ratios are as follows.

Flanges:

$$\begin{aligned}\lambda_{rf} &= 0.56 \sqrt{\frac{E}{F_y}} \\ &= 0.56 \sqrt{\frac{29,000 \text{ ksi}}{50 \text{ ksi}}} \\ &= 13.5\end{aligned}$$

Web:

$$\begin{aligned}\lambda_{rw} &= 1.49 \sqrt{\frac{E}{F_y}} \\ &= 1.49 \sqrt{\frac{29,000 \text{ ksi}}{50 \text{ ksi}}} \\ &= 35.9\end{aligned}$$

Because  $\lambda_f < \lambda_{rf}$  and  $\lambda_w < \lambda_{rw}$ , the W18x86 has nonslender flanges and web.

#### *Shear Strength*

The available shear strength of the W18x86 is determined from AISC *Specification* Section G2.1 as follows:

$$h/t_w = 33.4$$

$$\begin{aligned}2.24 \sqrt{\frac{E}{F_y}} &= 2.24 \sqrt{\frac{29,000 \text{ ksi}}{50 \text{ ksi}}} \\ &= 53.9\end{aligned}$$

Because  $h/t_w < 2.24\sqrt{\frac{E}{F_y}}$  :

$$C_{v1} = 1.0$$

(Spec. Eq. G2-2)

The area of the web is:

$$\begin{aligned} A_w &= dt_w \\ &= (18.4 \text{ in.})(0.480 \text{ in.}) \\ &= 8.83 \text{ in.}^2 \end{aligned}$$

The nominal shear strength,  $V_n$ , is:

$$\begin{aligned} V_n &= 0.6F_y A_w C_{v1} \\ &= 0.6(50 \text{ ksi})(8.83 \text{ in.}^2)(1.0) \\ &= 265 \text{ kips} \end{aligned} \quad (\text{Spec. Eq. G2-1})$$

And the available shear strength is:

LRFD	ASD
$\phi_v V_n = 1.00(265 \text{ kips})$ $= 265 \text{ kips} > V_u = 57.5 \text{ kips} \quad \text{o.k.}$	$\frac{V_n}{\Omega_v} = \frac{265 \text{ kips}}{1.50}$ $= 177 \text{ kips} > V_a = 38.3 \text{ kips} \quad \text{o.k.}$

Alternatively, the available shear strength could have been taken from AISC *Manual* Table 6-2.

#### Out-of-Plane Bending of W18 Flanges

The effect of out-of-plane bending of the flanges is determined using reduced section properties according to Section 6.7.1 with a reduction factor according to Equation 6-28.

$$\begin{aligned} k_f &= \frac{9.20}{8.80 + \frac{b_f^2}{Rt_f}} \leq 1.00 \\ &= \frac{9.20}{8.80 + \frac{(11.1 \text{ in.})^2}{(480 \text{ in.})(0.770 \text{ in.})}} \leq 1.00 \\ &= 1.01 > 1.00 \end{aligned} \quad (6-28)$$

Therefore,  $k_f = 1.00$ .

Because  $k_f = 1.00$ , flange bending will not occur, and the effective flexural properties are equal to the straight-member properties.

#### In-Plane Axial Buckling Strength

The in-plane axial buckling strength is calculated using AISC *Specification* Section E3 with the recommendations in Section 6.3.1. For a circular arch with pinned end conditions and  $H/L_s = 0.288$ , the effective length factor from Table 6-2 is  $K_i = 0.55$ . The unbraced length is  $L_d = 1,010 \text{ in.}$ , and the radius of gyration about the axis of curvature is  $r_i = r_x = 7.77 \text{ in.}$

$$\begin{aligned} \frac{L_c}{r} &= \frac{K_i L_d}{r_i} \\ &= \frac{(0.55)(1,010 \text{ in.})}{7.77 \text{ in.}} \\ &= 71.5 \end{aligned}$$

The elastic buckling stress is determined from AISC *Specification* Section E3 as follows:

$$\begin{aligned}
 F_e &= \frac{\pi^2 E}{\left(\frac{L_c}{r}\right)^2} & (\text{Spec. Eq. E3-4}) \\
 &= \frac{\pi^2 (29,000 \text{ ksi})}{(71.5)^2} \\
 &= 56.0 \text{ ksi}
 \end{aligned}$$

$$4.71 \sqrt{\frac{E}{F_y}} = 4.71 \sqrt{\frac{29,000 \text{ ksi}}{50 \text{ ksi}}} = 113$$

Because  $\frac{L_c}{r} < 4.71 \sqrt{\frac{E}{F_y}}$ , AISC *Specification* Equation E3-2 is used to determine the critical stress,  $F_{cr}$ :

$$\begin{aligned}
 F_{cr} &= \left[ 0.658 \frac{F_y}{F_e} \right] F_y & (\text{Spec. Eq. E3-2}) \\
 &= \left[ 0.658 \left( \frac{50 \text{ ksi}}{56.0 \text{ ksi}} \right) \right] (50 \text{ ksi}) \\
 &= 34.4 \text{ ksi}
 \end{aligned}$$

The nominal compressive strength,  $P_{ni}$ , is:

$$\begin{aligned}
 P_{ni} &= F_{cr} A_g & (\text{from Spec. Eq. E3-1}) \\
 &= (34.4 \text{ ksi})(25.3 \text{ in.}^2) \\
 &= 870 \text{ kips}
 \end{aligned}$$

And the available compressive strength due to in-plane buckling is:

LRFD	ASD
$\phi_c P_{ni} = 0.90(870 \text{ kips}) = 783 \text{ kips}$	$\frac{P_{ni}}{\Omega_c} = \frac{870 \text{ kips}}{1.67} = 521 \text{ kips}$

#### Second-Order Deflection

The elastic in-plane critical buckling load is:

$$\begin{aligned}
 P_{ei} &= F_e A_g \\
 &= (56.0 \text{ ksi})(25.3 \text{ in.}^2) \\
 &= 1,420 \text{ kips}
 \end{aligned}$$

The serviceability deflection at the apex is calculated using Equation 6-3 with  $P_r = 121$  kips, which is the maximum axial service load in the arch, and  $\Delta_1$  for ASD based on service-level loads.

$$\begin{aligned}
\Delta_2 &= \frac{\Delta_1}{1 - \frac{P_r}{P_{ei}}} & (6-3) \\
&= \frac{0.715 \text{ in.}}{1 - \left( \frac{121 \text{ kips}}{1,420 \text{ kips}} \right)} \\
&= 0.782 \text{ in.}
\end{aligned}$$

#### Out-of-Plane Axial Buckling Strength

The out-of-plane axial buckling strength is calculated using AISC *Specification* Section E3 with the recommendations in Section 6.3.2. The moment of inertia perpendicular to the axis of curvature is  $I_o = I_y = 175 \text{ in.}^4$ , and the radius of gyration perpendicular to the axis of curvature is  $r_o = r_y = 2.63 \text{ in.}$

#### Span 1

$$\begin{aligned}
\theta_b &= (18.6^\circ) \left( \frac{\pi \text{ rad}}{180^\circ} \right) \\
&= 0.325 \text{ rad}
\end{aligned}$$

$$\begin{aligned}
L_{db} &= R\theta_b \\
&= (480 \text{ in.})(0.325 \text{ rad}) \\
&= 156 \text{ in.}
\end{aligned}$$

$$\begin{aligned}
C_o &= \frac{1}{I_o} \left[ \frac{GJ}{E} + C_w \left( \frac{\pi}{L_{db}} \right)^2 \right] & (6-8) \\
&= \frac{1}{175 \text{ in.}^4} \left[ \frac{(11,200 \text{ ksi})(4.10 \text{ in.}^4)}{29,000 \text{ ksi}} + (13,600 \text{ in.}^6) \left( \frac{\pi}{156 \text{ in.}} \right)^2 \right] \\
&= 0.0406
\end{aligned}$$

$$\begin{aligned}
K_o &= \frac{\sqrt{1 + \frac{1}{C_o} \left( \frac{\theta_b}{\pi} \right)^2}}{1 - \left( \frac{\theta_b}{\pi} \right)^2} & (6-6) \\
&= \frac{\sqrt{1 + \left( \frac{1}{0.0406} \right) \left( \frac{0.325 \text{ rad}}{\pi} \right)^2}}{1 - \left( \frac{0.325 \text{ rad}}{\pi} \right)^2} \\
&= 1.14
\end{aligned}$$

$$\begin{aligned}
\frac{L_c}{r} &= \frac{K_o L_{db}}{r_o} \\
&= \frac{(1.14)(156 \text{ in.})}{2.63 \text{ in.}} \\
&= 67.6
\end{aligned}$$

The elastic buckling stress is determined from AISC *Specification* Section E3 as follows:

$$\begin{aligned}
F_e &= \frac{\pi^2 E}{\left(\frac{L_c}{r}\right)^2} & (Spec. Eq. E3-4) \\
&= \frac{\pi^2 (29,000 \text{ ksi})}{(67.6)^2} \\
&= 62.6 \text{ ksi}
\end{aligned}$$

$$\begin{aligned}
4.71 \sqrt{\frac{E}{F_y}} &= 4.71 \sqrt{\frac{29,000 \text{ ksi}}{50 \text{ ksi}}} \\
&= 113
\end{aligned}$$

Because  $\frac{L_c}{r} < 4.71 \sqrt{\frac{E}{F_y}}$ , AISC Specification Equation E3-2 is used to determine the critical stress,  $F_{cr}$ :

$$\begin{aligned}
F_{cr} &= \left( 0.658 \frac{F_y}{F_e} \right) F_y & (Spec. Eq. E3-2) \\
&= \left[ 0.658 \left( \frac{50 \text{ ksi}}{62.6 \text{ ksi}} \right) \right] (50 \text{ ksi}) \\
&= 35.8 \text{ ksi}
\end{aligned}$$

The nominal compressive strength,  $P_{no}$ , is:

$$\begin{aligned}
P_{no} &= F_{cr} A_g & (\text{from Spec. Eq. E3-1}) \\
&= (35.8 \text{ ksi})(25.3 \text{ in.}^2) \\
&= 906 \text{ kips}
\end{aligned}$$

And the available compressive strength due to out-of-plane buckling is:

LRFD	ASD
$\phi_c P_{no} = 0.90(906 \text{ kips})$ $= 815 \text{ kips} > P_u = 182 \text{ kips} \text{ o.k.}$	$\frac{P_{no}}{\Omega_c} = \frac{906 \text{ kips}}{1.67}$ $= 543 \text{ kips} > P_a = 121 \text{ kips} \text{ o.k.}$

Spans 2 and 3

$$\begin{aligned}
\theta_b &= (20.7^\circ) \left( \frac{\pi \text{ rad}}{180^\circ} \right) \\
&= 0.361 \text{ rad}
\end{aligned}$$

$$\begin{aligned}
L_{db} &= R\theta_b \\
&= (480 \text{ in.})(0.361 \text{ rad}) \\
&= 173 \text{ in.}
\end{aligned}$$

$$\begin{aligned}
C_o &= \frac{1}{I_o} \left[ \frac{GJ}{E} + C_w \left( \frac{\pi}{L_{db}} \right)^2 \right] & (6-8) \\
&= \frac{1}{175 \text{ in.}^4} \left[ \frac{(11,200 \text{ ksi})(4.10 \text{ in.}^4)}{29,000 \text{ ksi}} + (13,600 \text{ in.}^6) \left( \frac{\pi}{173 \text{ in.}} \right)^2 \right] \\
&= 0.0347
\end{aligned}$$

$$\begin{aligned}
K_o &= \frac{\sqrt{1 + \frac{1}{C_o} \left( \frac{\theta_b}{\pi} \right)^2}}{1 - \left( \frac{\theta_b}{\pi} \right)^2} & (6-6) \\
&= \frac{\sqrt{1 + \frac{1}{0.0347} \left( \frac{0.361 \text{ rad}}{\pi} \right)^2}}{1 - \left( \frac{0.361 \text{ rad}}{\pi} \right)^2} \\
&= 1.19
\end{aligned}$$

$$\begin{aligned}
\frac{L_c}{r} &= \frac{K_o L_{db}}{r_o} \\
&= \frac{(1.19)(173 \text{ in.})}{2.63 \text{ in.}} \\
&= 78.3
\end{aligned}$$

The elastic buckling stress is determined from AISC *Specification* Section E3 as follows:

$$\begin{aligned}
F_e &= \frac{\pi^2 E}{\left( \frac{L_c}{r} \right)^2} & (\text{Spec. Eq. E3-4}) \\
&= \frac{\pi^2 (29,000 \text{ ksi})}{(78.3)^2} \\
&= 46.7 \text{ ksi} \\
4.71 \sqrt{\frac{E}{F_y}} &= 4.71 \sqrt{\frac{29,000 \text{ ksi}}{50 \text{ ksi}}} \\
&= 113
\end{aligned}$$

Because  $\frac{L_c}{r} < 4.71 \sqrt{\frac{E}{F_y}}$ , AISC *Specification* Equation E3-2 is used to determine the critical stress,  $F_{cr}$ :

$$\begin{aligned}
F_{cr} &= \left( 0.658 \frac{F_y}{F_e} \right) F_y & (\text{Spec. Eq. E3-2}) \\
&= \left[ 0.658 \left( \frac{50 \text{ ksi}}{46.7 \text{ ksi}} \right) \right] (50 \text{ ksi}) \\
&= 31.9 \text{ ksi}
\end{aligned}$$

The nominal compressive strength,  $P_{no}$ , is:

$$\begin{aligned}
P_{no} &= F_{cr} A_g & (\text{from Spec. Eq. E3-1}) \\
&= (31.9 \text{ ksi})(25.3 \text{ in.}^2) \\
&= 807 \text{ kips}
\end{aligned}$$

And the available compressive strength due to out-of-plane buckling is:

LRFD	ASD
$\phi_c P_{no} = 0.90(807 \text{ kips})$ $= 726 \text{ kips} > P_u = 132 \text{ kips} \text{ o.k.}$	$\frac{P_{no}}{\Omega_c} = \frac{807 \text{ kips}}{1.67}$ $= 483 \text{ kips} > P_a = 88.2 \text{ kips} \text{ o.k.}$

Note that the available strength is compared to the maximum axial load in span 2 because it is slightly larger than that of span 3.

#### Flexural Strength

##### Second-order effects

The first-order moments from the structural analysis model are amplified as discussed in Section 6.4.1. The amplification factor is determined using Equation 6-10, as follows:

LRFD	ASD
$\alpha = 1.0$ $B_i = \frac{1}{1 - \alpha \frac{P_u}{P_{ei}}}$ $= \frac{1}{1 - (1.0) \left( \frac{182 \text{ kips}}{1,420 \text{ kips}} \right)}$ $= 1.15$	$\alpha = 1.6$ $B_i = \frac{1}{1 - \alpha \frac{P_a}{P_{ei}}}$ $= \frac{1}{1 - (1.6) \left( \frac{121 \text{ kips}}{1,420 \text{ kips}} \right)}$ $= 1.16$

The moments in Table 8-1 are multiplied by  $B_i$ , resulting in the second-order moments provided in Table 8-2.

#### Lateral-Torsional Buckling

The lateral-torsional buckling strength is calculated using AISC *Specification* Section F2 with the recommendations in Section 6.4.2. The moment of inertia perpendicular to the axis of curvature is  $I_o = I_y = 175 \text{ in.}^4$

$$\begin{aligned}
 M_p &= F_y Z_x && (\text{Spec. Eq. F2-1}) \\
 &= (50 \text{ ksi})(186 \text{ in.}^3) \\
 &= 9,300 \text{ kip-in.}
 \end{aligned}$$

#### Span 1

$$\begin{aligned}
 \theta_b &= (18.6^\circ) \left( \frac{\pi \text{ rad}}{180^\circ} \right) \\
 &= 0.325 \text{ rad} \\
 L_{db} &= R\theta_b \\
 &= (40 \text{ ft})(0.325 \text{ rad})(12 \text{ in./ft}) \\
 &= 156 \text{ in.}
 \end{aligned}$$

Table 8-2. Second-Order Moments		
Location	Moment, $M_{rx2}$ kip-in.	
	$M_{ux2}$	$M_{ax2}$
Supports	0	0
Apex	-6,160	-4,140
Maximum at Span 3	+1,590 -6,160	+1,060 -4,140
Maximum at Span 2	+2,160	+1,450
Maximum at Span 1	+1,460	+980

From Section 6.4.2:

$$\begin{aligned}
 M_{es} &= \frac{\pi}{L_{db}} \sqrt{EI_o GJ + \left( \frac{\pi E}{L_{db}} \right)^2 I_o C_w} \\
 &= \frac{\pi}{156 \text{ in.}} \sqrt{(29,000 \text{ ksi})(175 \text{ in.}^4)(11,200 \text{ ksi})(4.10 \text{ in.}^4) + \left[ \frac{\pi(29,000 \text{ ksi})}{156 \text{ in.}} \right]^2 (175 \text{ in.}^4)(13,600 \text{ in.}^6)} \\
 &= 20,600 \text{ kip-in.}
 \end{aligned} \tag{6-13}$$

$$\begin{aligned}
 C_y &= EI_o \\
 &= (29,000 \text{ ksi})(175 \text{ in.}^4) \\
 &= 5,080,000 \text{ kip-in.}^2
 \end{aligned} \tag{6-11b}$$

$$\begin{aligned}
 C_z &= GJ + \frac{\pi^2 E C_w}{L_{db}^2} \\
 &= (11,200 \text{ ksi})(4.10 \text{ in.}^4) + \frac{\pi^2 (29,000 \text{ ksi})(13,600 \text{ in.}^6)}{(156 \text{ in.})^2} \\
 &= 206,000 \text{ kip-in.}^2
 \end{aligned} \tag{6-11c}$$

$$\begin{aligned}
 C_a &= \frac{C_y + C_z}{2RM_{es}} \\
 &= \frac{5,080,000 \text{ kip-in.}^2 + 206,000 \text{ kip-in.}^2}{(2)(480 \text{ in.})(20,600 \text{ kip-in.})} \\
 &= 0.267
 \end{aligned} \tag{6-12b}$$

Span 1 is subjected to closing moments; therefore, the positive root will be used in Equation 6-12a. Use  $C_{bs} = 1.0$ .

$$\begin{aligned}
 C_{bi} &= C_{bs} \left( \sqrt{1 + C_a^2 - \frac{C_y C_z}{R^2 M_{es}^2}} + C_a \right) \quad (\text{from Eq. 6-12a}) \\
 &= (1.0) \left[ \sqrt{1 + (0.267)^2 - \frac{(5,080,000 \text{ kip-in.}^2)(206,000 \text{ kip-in.}^2)}{(480 \text{ in.})^2 (20,600 \text{ kip-in.})^2}} + 0.267 \right] \\
 &= 1.30
 \end{aligned}$$

Use AISC *Specification* Section F2 with  $L_b = L_{db} = (156 \text{ in.})/(12 \text{ in./ft}) = 13.0 \text{ ft}$  and  $C_b = C_{bi} = 1.30$ . From AISC *Manual Table 3-6*, for a W18x86:

$$L_p = 9.29 \text{ ft}$$

$$L_r = 28.6 \text{ ft}$$

Because  $L_p < L_b < L_r$ , AISC *Specification* Equation F2-2 is used to determine the nominal flexural strength,  $M_n$ :

$$\begin{aligned} M_n &= C_b \left[ M_p - (M_p - 0.7F_yS_x) \left( \frac{L_b - L_p}{L_r - L_p} \right) \right] \leq M_p \\ &= (1.30) \left\{ 9,300 \text{ kip-in.} - \left[ 9,300 \text{ kip-in.} - (0.7)(50 \text{ ksi})(166 \text{ in.}^3) \right] \left[ \frac{13.0 \text{ ft} - 9.29 \text{ ft}}{28.6 \text{ ft} - 9.29 \text{ ft}} \right] \right\} \leq 9,300 \text{ kip-in.} \\ &= 11,200 \text{ kip-in.} > 9,300 \text{ kip-in.} \end{aligned} \quad (\text{Spec. Eq. F2-2})$$

Therefore:

$$M_n = 9,300 \text{ kip-in.}$$

And the available flexural strength is:

LRFD	ASD
$\phi_b M_n = 0.90(9,300 \text{ kip-in.})$ $= 8,370 \text{ kip-in.} > M_u = 1,460 \text{ kip-in. o.k.}$	$\frac{M_n}{\Omega_b} = \frac{9,300 \text{ kip-in.}}{1.67}$ $= 5,570 \text{ kip-in.} > M_a = 980 \text{ kip-in. o.k.}$

Span 2

$$\begin{aligned} \theta_b &= (20.7^\circ) \left( \frac{\pi \text{ rad}}{180^\circ} \right) \\ &= 0.361 \text{ rad} \end{aligned}$$

$$\begin{aligned} L_{db} &= R\theta_b \\ &= (40 \text{ ft})(0.361 \text{ rad})(12 \text{ in./ft}) \\ &= 173 \text{ in.} \end{aligned}$$

From Section 6.4.2:

$$\begin{aligned} M_{es} &= \frac{\pi}{L_{db}} \sqrt{EI_o GJ + \left( \frac{\pi E}{L_{db}} \right)^2 I_o C_w} \\ &= \frac{\pi}{173 \text{ in.}} \sqrt{(29,000 \text{ ksi})(175 \text{ in.}^4)(11,200 \text{ ksi})(4.10 \text{ in.}^4) + \left[ \frac{\pi(29,000 \text{ ksi})}{173 \text{ in.}} \right]^2 (175 \text{ in.}^4)(13,600 \text{ in.}^6)} \\ &= 17,200 \text{ kip-in.} \end{aligned} \quad (6-13)$$

$$\begin{aligned} C_y &= EI_o \\ &= (29,000 \text{ ksi})(175 \text{ in.}^4) \\ &= 5,080,000 \text{ kip-in.}^2 \end{aligned} \quad (6-11b)$$

$$\begin{aligned}
C_z &= GJ + \frac{\pi^2 EC_w}{L_{db}^2} \\
&= (11,200 \text{ ksi})(4.10 \text{ in.}^4) + \frac{\pi^2 (29,000 \text{ ksi})(13,600 \text{ in.}^6)}{(173 \text{ in.})^2} \\
&= 176,000 \text{ kip-in.}^2
\end{aligned} \tag{6-11c}$$

$$\begin{aligned}
C_a &= \frac{C_y + C_z}{2RM_{es}} \\
&= \frac{5,080,000 \text{ kip-in.}^2 + 176,000 \text{ kip-in.}^2}{(2)(480 \text{ in.})(17,200 \text{ kip-in.})} \\
&= 0.318
\end{aligned} \tag{6-12b}$$

Span 2 is subjected to closing moments; therefore, the positive root will be used in Equation 6-12a. Use  $C_{bs} = 1.0$ .

$$\begin{aligned}
C_{bi} &= C_{bs} \left( \sqrt{1 + C_a^2 - \frac{C_y C_z}{R^2 M_{es}^2}} + C_a \right) \quad (\text{from Eq. 6-12a}) \\
&= (1.0) \left[ \sqrt{1 + (0.318)^2 - \frac{(5,080,000 \text{ kip-in.}^2)(176,000 \text{ kip-in.}^2)}{(480 \text{ in.})^2 (17,200 \text{ kip-in.})^2}} + 0.318 \right] \\
&= 1.36
\end{aligned}$$

Use AISC *Specification* Section F2 with  $L_b = L_{db} = (173 \text{ in.})/(12 \text{ in./ft}) = 14.4 \text{ ft}$  and  $C_b = C_{bi} = 1.36$ . From AISC *Manual Table 3-6*, for a W18×86:

$$\begin{aligned}
L_p &= 9.29 \text{ ft} \\
L_r &= 28.6 \text{ ft}
\end{aligned}$$

Because  $L_p < L_b < L_r$ , AISC *Specification* Equation F2-2 is used to determine the nominal flexural strength,  $M_n$ :

$$\begin{aligned}
M_n &= C_b \left[ M_p - (M_p - 0.7F_y S_x) \left( \frac{L_b - L_p}{L_r - L_p} \right) \right] \leq M_p \quad (\text{Spec. Eq. F2-2}) \\
&= (1.36) \left\{ 9,300 \text{ kip-in.} - \left[ 9,300 \text{ kip-in.} - (0.7)(50 \text{ ksi})(166 \text{ in.}^3) \right] \left( \frac{14.4 \text{ ft} - 9.29 \text{ ft}}{28.6 \text{ ft} - 9.29 \text{ ft}} \right) \right\} \leq 9,300 \text{ kip-in.} \\
&= 11,400 \text{ kip-in.} > 9,300 \text{ kip-in.}
\end{aligned}$$

Therefore,

$$M_n = 9,300 \text{ kip-in.}$$

And the available flexural strength is:

LRFD	ASD
$ \begin{aligned} \phi_b M_n &= 0.90(9,300 \text{ kip-in.}) \\ &= 8,370 \text{ kip-in.} > M_u = 2,160 \text{ kip-in.} \text{ o.k.} \end{aligned} $	$ \begin{aligned} \frac{M_n}{\Omega_b} &= \frac{9,300 \text{ kip-in.}}{1.67} \\ &= 5,570 \text{ kip-in.} > M_a = 1,450 \text{ kip-in.} \text{ o.k.} \end{aligned} $

Span 3

Due to the moment reversal in Span 3, using  $C_{bs} = 1.0$  would be overly conservative, and therefore  $C_{bs}$  is calculated for the equivalent straight member using the second-order moments from the structural analysis model:

$$C_{bs} = \frac{12.5M_{max}}{2.5M_{max} + 3M_A + 4M_B + 3M_C}$$

(from Spec. Eq. F1-1)

LRFD	ASD
$M_{max} = 6,160 \text{ kip-in.}$	$M_{max} = 4,140 \text{ kip-in.}$
$M_A = 453 \text{ kip-in.}$	$M_A = 296 \text{ kip-in.}$
$M_B = 1,230 \text{ kip-in.}$	$M_B = 816 \text{ kip-in.}$
$M_C = 3,560 \text{ kip-in.}$	$M_C = 2,370 \text{ kip-in.}$
$12.5M_{max} = 12.5(6,160 \text{ kip-in.})$ = 77,000 kip-in.	$12.5M_{max} = 12.5(4,140 \text{ kip-in.})$ = 51,800 kip-in.
$2.5M_{max} = 2.5(6,160 \text{ kip-in.})$ = 15,400 kip-in.	$2.5M_{max} = 2.5(4,140 \text{ kip-in.})$ = 10,400 kip-in.
$3M_A = 3(453 \text{ kip-in.})$ = 1,360 kip-in.	$3M_A = 3(296 \text{ kip-in.})$ = 888 kip-in.
$4M_B = 4(1,230 \text{ kip-in.})$ = 4,920 kip-in.	$4M_B = 4(816 \text{ kip-in.})$ = 3,260 kip-in.
$3M_C = 3(3,560 \text{ kip-in.})$ = 10,700 kip-in.	$3M_C = 3(2,370 \text{ kip-in.})$ = 7,110 kip-in.
$C_{bs} = \frac{77,000 \text{ kip-in.}}{15,400 \text{ kip-in.} + 1,360 \text{ kip-in.} + 4,920 \text{ kip-in.} + 10,700 \text{ kip-in.}}$ = 2.38	$C_{bs} = \frac{51,800 \text{ kip-in.}}{10,400 \text{ kip-in.} + 888 \text{ kip-in.} + 3,260 \text{ kip-in.} + 7,110 \text{ kip-in.}}$ = 2.39

Span 3 is subjected to opening moments; therefore, the negative root will be used in Equation 6-12a. For  $C_a$ ,  $C_y$ ,  $C_z$  and  $M_{es}$ , see calculations for Span 2.

$$\begin{aligned}
 C_{bi} &= C_{bs} \left( \sqrt{1 + C_a^2 - \frac{C_y C_z}{R^2 M_{es}^2}} - C_a \right) && \text{(from Eq. 6-12a)} \\
 &= (2.39) \left[ \sqrt{1 + (0.318)^2 - \frac{(5,080,000 \text{ kip-in.}^2)(176,000 \text{ kip-in.}^2)}{(480 \text{ in.})^2 (17,200 \text{ kip-in.})^2}} - 0.318 \right] \\
 &= 1.73
 \end{aligned}$$

Use AISC *Specification* Section F2 with  $L_b = L_{db} = 14.4 \text{ ft}$  and  $C_b = C_{bi} = 1.73$ . From AISC *Manual* Table 3-6, for a W18×86:

$$L_p = 9.29 \text{ ft}$$

$$L_r = 28.6 \text{ ft}$$

Because  $L_p < L_b < L_r$ , AISC *Specification* Equation F2-2 is used to determine the nominal flexural strength,  $M_n$ :

$$\begin{aligned}
 M_n &= C_b \left[ M_p - (M_p - 0.7F_y S_x) \left( \frac{L_b - L_p}{L_r - L_p} \right) \right] \leq M_p && \text{(Spec. Eq. F2-2)} \\
 &= (1.73) \left\{ 9,300 \text{ kip-in.} - \left[ 9,300 \text{ kip-in.} - (0.7)(50 \text{ ksi})(166 \text{ in.}^3) \right] \left( \frac{14.4 \text{ ft} - 9.29 \text{ ft}}{28.6 \text{ ft} - 9.29 \text{ ft}} \right) \right\} \leq 9,300 \text{ kip-in.} \\
 &= 14,500 \text{ kip-in.} > 9,300 \text{ kip-in.}
 \end{aligned}$$

Therefore,

$$M_n = 9,300 \text{ kip-in.}$$

And the available flexural strength is:

LRFD	ASD
$\phi_b M_n = 0.90(9,300 \text{ kip-in.})$ $= 8,370 \text{ kip-in.} > M_u = 6,160 \text{ kip-in. o.k.}$	$\frac{M_n}{\Omega_b} = \frac{9,300 \text{ kip-in.}}{1.67}$ $= 5,570 \text{ kip-in.} > M_a = 4,140 \text{ kip-in. o.k.}$

### Combined Loading

Based on the recommendations in Section 6.5, the axial and flexural loads are combined using AISC *Specification* Section H1. The required axial and flexural loads are taken from Tables 8-1 and 8-2, respectively.

#### In-plane

The axial load ratio is based on the largest axial load within the arch, which is at the supports. The largest flexural load ratio is at the apex and the available compressive strength was previously determined.

LRFD	ASD
$\frac{P_r}{P_{ci}} = \frac{P_u}{\phi_c P_{ni}}$ $= \frac{182 \text{ kips}}{783 \text{ kips}}$ $= 0.232$	$\frac{P_r}{P_{ci}} = \frac{P_a}{P_{ni}/\Omega_c}$ $= \frac{121 \text{ kips}}{521 \text{ kips}}$ $= 0.232$

Because  $P_r/P_{ci} > 0.2$ , AISC *Specification* Equation H1-1a is applicable:

LRFD	ASD
$\frac{P_u}{\phi_c P_{ni}} + \frac{8}{9} \left( \frac{M_u}{\phi_b M_n} \right) \leq 1.0$ $0.232 + \left( \frac{8}{9} \right) \left( \frac{6,160 \text{ kip-in.}}{8,370 \text{ kip-in.}} \right) \leq 1.0$ $0.886 < 1.0 \text{ o.k.}$	$\frac{P_a}{P_{ni}/\Omega_c} + \frac{8}{9} \left( \frac{M_a}{M_n/\Omega_b} \right) \leq 1.0$ $0.232 + \left( \frac{8}{9} \right) \left( \frac{4,140 \text{ kip-in.}}{5,570 \text{ kip-in.}} \right) \leq 1.0$ $0.893 < 1.0 \text{ o.k.}$

#### Span 1 out-of-plane

LRFD	ASD
$\frac{P_r}{P_{co}} = \frac{P_u}{\phi_c P_{no}}$ $= \frac{182 \text{ kips}}{815 \text{ kips}}$ $= 0.223$	$\frac{P_r}{P_{co}} = \frac{P_a}{P_{no}/\Omega_c}$ $= \frac{121 \text{ kips}}{543 \text{ kips}}$ $= 0.223$

Because  $P_r/P_{ci} < 0.2$ , AISC Specification Equation H1-1a is applicable:

LRFD	ASD
$\frac{P_u}{\phi_c P_{no}} + \frac{8}{9} \left( \frac{M_u}{\phi_b M_n} \right) \leq 1.0$ $0.223 + \left( \frac{8}{9} \right) \left( \frac{1,460 \text{ kip-in.}}{8,370 \text{ kip-in.}} \right) \leq 1.0$ $0.378 < 1.0 \quad \text{o.k.}$	$\frac{P_a}{P_{no}/\Omega_c} + \frac{8}{9} \left( \frac{M_a}{M_n/\Omega_b} \right) \leq 1.0$ $0.223 + \left( \frac{8}{9} \right) \left( \frac{980 \text{ kip-in.}}{5,570 \text{ kip-in.}} \right) \leq 1.0$ $0.379 < 1.0 \quad \text{o.k.}$

Span 2 out-of-plane

LRFD	ASD
$\frac{P_r}{P_{co}} = \frac{P_u}{\phi_c P_{no}}$ $= \frac{132 \text{ kips}}{726 \text{ kips}}$ $= 0.182$	$\frac{P_r}{P_{co}} = \frac{P_a}{P_{no}/\Omega_c}$ $= \frac{88.2 \text{ kips}}{483 \text{ kips}}$ $= 0.183$

Because  $P_r/P_{ci} < 0.2$ , AISC Specification Equation H1-1b is applicable:

LRFD	ASD
$\frac{P_u}{2\phi_c P_{no}} + \frac{M_u}{\phi_b M_n} \leq 1.0$ $\frac{0.182}{2} + \frac{2,160 \text{ kip-in.}}{8,370 \text{ kip-in.}} \leq 1.0$ $0.349 < 1.0 \quad \text{o.k.}$	$\frac{P_a}{2P_{no}/\Omega_c} + \frac{M_a}{M_n/\Omega_b} \leq 1.0$ $\frac{0.183}{2} + \frac{1,450 \text{ kip-in.}}{5,570 \text{ kip-in.}} \leq 1.0$ $0.352 < 1.0 \quad \text{o.k.}$

Span 3 out-of-plane

LRFD	ASD
$\frac{P_r}{P_{co}} = \frac{P_u}{\phi_c P_{no}}$ $= \frac{131 \text{ kips}}{726 \text{ kips}}$ $= 0.180$	$\frac{P_r}{P_{co}} = \frac{P_a}{P_{no}/\Omega_c}$ $= \frac{87.0 \text{ kips}}{483 \text{ kips}}$ $= 0.180$

Because  $P_r/P_{ci} < 0.2$ , AISC Specification Equation H1-1b is applicable:

LRFD	ASD
$\frac{P_u}{2\phi_c P_{no}} + \frac{M_u}{\phi_b M_n} \leq 1.0$ $\frac{0.180}{2} + \frac{6,160 \text{ kip-in.}}{8,370 \text{ kip-in.}} \leq 1.0$ $0.826 < 1.0 \quad \text{o.k.}$	$\frac{P_a}{2P_{no}/\Omega_c} + \frac{M_a}{M_n/\Omega_b} \leq 1.0$ $\frac{0.180}{2} + \frac{4,140 \text{ kip-in.}}{5,570 \text{ kip-in.}} \leq 1.0$ $0.833 < 1.0 \quad \text{o.k.}$

### End Connection Design

The end-plate connection shown in Figure 8-5 is efficient in transferring compression loads from the arch member to the W36 beam. Oversize holes are used to provide for tolerances in the horizontal plane. If vertical adjustment is required, shims (fillers) could be added between the end plate and the W36 flange. In that case, bolt strength and slip resistance may be reduced according to AISC *Specification* Sections J5.2 and J3.8, respectively.

#### Bolt shear strength

From AISC *Manual* Table 7-1, the available shear strength per bolt for  $\frac{7}{8}$ -in.-diameter Group A bolts with threads not excluded from the shear plane (thread condition N) is:

LRFD	ASD
$\phi r_n = 24.3 \text{ kips/bolt}$ $\phi R_n = n\phi r_n$ $= (12 \text{ bolts})(24.3 \text{ kips/bolt})$ $= 292 \text{ kips} > 117 \text{ kips} \text{ o.k.}$	$\frac{r_n}{\Omega} = 16.2 \text{ kips/bolt}$ $\frac{R_n}{\Omega} = n \frac{r_n}{\Omega}$ $= (12 \text{ bolts})(16.2 \text{ kips/bolt})$ $= 194 \text{ kips} > 77.7 \text{ kips} \text{ o.k.}$

#### Bolt slip resistance strength

From AISC *Manual* Table 7-3, with  $\frac{7}{8}$ -in.-diameter Group A bolts with Class A faying surfaces in oversized holes, the available slip resistance strength is:

LRFD	ASD
$\phi r_n = 11.2 \text{ kips/bolt}$ $\phi R_n = n\phi r_n$ $= (12 \text{ bolts})(11.2 \text{ kips/bolt})$ $= 134 \text{ kips} > 117 \text{ kips} \text{ o.k.}$	$\frac{r_n}{\Omega} = 7.51 \text{ kips/bolt}$ $\frac{R_n}{\Omega} = n \frac{r_n}{\Omega}$ $= (12 \text{ bolts})(7.51 \text{ kips/bolt})$ $= 90.1 \text{ kips} > 77.7 \text{ kips} \text{ o.k.}$

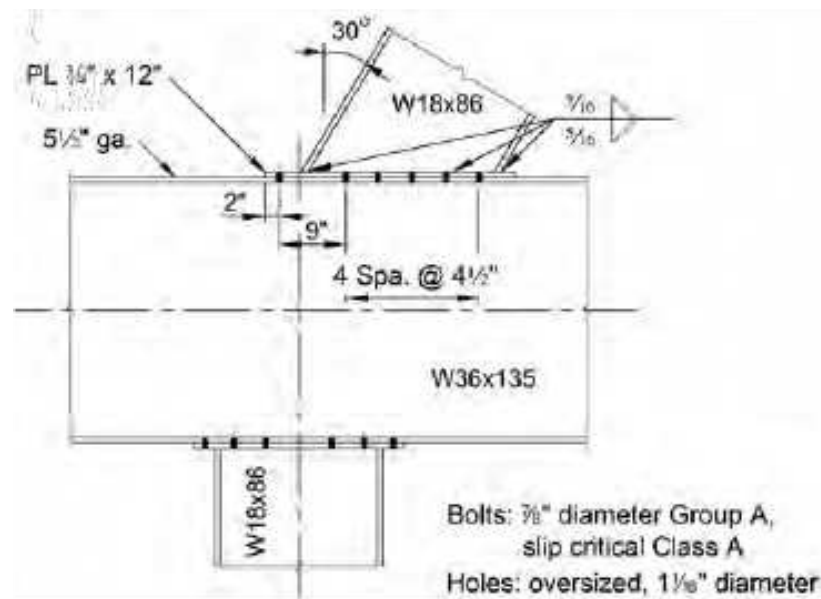


Fig. 8-5. End connections for Example 8.1.

### Bolt bearing and tearout at the end plate

The nominal bearing strength of the end plate is determined from AISC *Specification* Section J3.10, assuming deformation at service load is a design consideration:

$$\begin{aligned} r_n &= 2.4dtF_u && \text{(Spec. Eq. J3-6a)} \\ &= 2.4(\frac{3}{8} \text{ in.})(\frac{3}{4} \text{ in.})(58 \text{ ksi}) \\ &= 91.4 \text{ kips/bolt} \end{aligned}$$

The nominal tearout strength of the end plate is determined from AISC *Specification* Section J3.10, assuming deformation at service load is a design consideration:

$$\begin{aligned} l_c &= s - d_h \\ &= 4\frac{1}{2} \text{ in.} - 1\frac{1}{16} \text{ in.} \\ &= 3.44 \text{ in.} \end{aligned}$$

$$\begin{aligned} r_n &= 1.2l_c t F_u && \text{(Spec. Eq. J3-6c)} \\ &= 1.2(3.44 \text{ in.})(\frac{3}{4} \text{ in.})(58 \text{ ksi}) \\ &= 180 \text{ kips/bolt} \end{aligned}$$

Therefore, bearing controls over tearout for the end plate. The available bolt bearing strength is:

LRFD	ASD
$\begin{aligned} \phi R_n &= n\phi r_n \\ &= (12 \text{ bolts})(0.75)(91.4 \text{ kips/bolt}) \\ &= 823 \text{ kips} > 117 \text{ kips} \quad \text{o.k.} \end{aligned}$	$\begin{aligned} \frac{R_n}{\Omega} &= n \frac{r_n}{\Omega} \\ &= (12 \text{ bolts}) \left( \frac{91.4 \text{ kips/bolt}}{2.00} \right) \\ &= 548 \text{ kips} > 77.7 \text{ kips} \quad \text{o.k.} \end{aligned}$

### Bolt bearing and tearout at the W36 beam flange

The nominal bearing strength of the beam flange is determined from AISC *Specification* Section J3.10, assuming deformation at service load is a design consideration:

$$\begin{aligned} r_n &= 2.4dtF_u && \text{(Spec. Eq. J3-6a)} \\ &= 2.4(\frac{3}{8} \text{ in.})(0.790 \text{ in.})(65 \text{ ksi}) \\ &= 108 \text{ kips/bolt} \end{aligned}$$

The nominal tearout strength of the beam flange is determined from AISC *Specification* Section J3.10, assuming deformation at service load is a design consideration:

$$\begin{aligned} l_c &= s - d_h \\ &= 4\frac{1}{2} \text{ in.} - 1\frac{1}{16} \text{ in.} \\ &= 3.44 \text{ in.} \end{aligned}$$

$$\begin{aligned} r_n &= 1.2l_c t F_u && \text{(Spec. Eq. J3-6c)} \\ &= 1.2(3.44 \text{ in.})(0.790 \text{ in.})(65 \text{ ksi}) \\ &= 212 \text{ kips/bolt} \end{aligned}$$

Therefore, bearing controls over tearout for the beam flange. The available bolt bearing strength is:

LRFD	ASD
$\begin{aligned} \phi R_n &= n\phi r_n \\ &= (12 \text{ bolts})(0.75)(108 \text{ kips/bolt}) \\ &= 972 \text{ kips} > 117 \text{ kips} \quad \text{o.k.} \end{aligned}$	$\begin{aligned} \frac{R_n}{\Omega} &= n \frac{r_n}{\Omega} \\ &= (12 \text{ bolts}) \left( \frac{108 \text{ kips/bolt}}{2.00} \right) \\ &= 648 \text{ kips} > 77.7 \text{ kips} \quad \text{o.k.} \end{aligned}$

### Weld end plate to W18 web

The plate-to-web weld is designed to resist both the vertical and horizontal reaction because the end of the W18 is not finished to bear. If the end of the W18 is finished to bear, the vertical compression force can be neglected in the weld design. In that case, the vertical load is carried by bearing between the W18 and the end plate, and the weld would be designed to resist only the horizontal reaction. The W18 flanges are welded to the end plate to provide out-of-plane flexural stiffness.

LRFD	ASD
$R_u = \sqrt{(117 \text{ kips})^2 + (140 \text{ kips})^2}$ $= 182 \text{ kips}$	$R_a = \sqrt{(77.7 \text{ kips})^2 + (93.6 \text{ kips})^2}$ $= 122 \text{ kips}$

The weld length is:

$$l_w = \frac{d - 2t_f}{\cos \theta}$$

$$= \frac{18.4 \text{ in.} - 2(0.770 \text{ in.})}{\cos 30^\circ}$$

$$= 19.5 \text{ in.}$$

The available strength for a two-sided  $\frac{5}{16}$ -in. fillet weld is determined using AISC *Manual* Equation 8-2a or 8-2b as follows:

LRFD	ASD
$\phi R_n = (2 \text{ welds})(1.392 \text{ kip/in.}) Dl_w$ $= (2 \text{ welds})(1.392 \text{ kip/in.})(5)(19.5 \text{ in.})$ $= 271 \text{ kips} > 182 \text{ kips} \text{ o.k.}$	$\frac{R_n}{\Omega} = (2 \text{ welds})(0.928 \text{ kip/in.}) Dl_w$ $= (2 \text{ welds})(0.928 \text{ kip/in.})(5)(19.5 \text{ in.})$ $= 181 \text{ kips} > 122 \text{ kips} \text{ o.k.}$

### Web local yielding at W36 beam

The available web local yielding strength of the W36×135 beam is determined using AISC *Specification* Section J10.2. The available bearing length is the distance along the W36 between the W18 flange outer surface plus twice the end plate thickness:

$$l_b = \frac{18.4 \text{ in.}}{\cos 30^\circ} + 2(\frac{3}{4} \text{ in.})$$

$$= 22.7 \text{ in.}$$

Because the force is applied at a distance from the beam end that is greater than the depth of the beam, use AISC *Specification* Equation J10-2 to determine the available strength.

$$R_n = F_{yw} t_w (5k + l_b) \quad (\text{Spec. Eq. J10-2})$$

$$= (50 \text{ ksi})(0.600 \text{ in.})[5(1.54 \text{ in.}) + 22.7 \text{ in.}]$$

$$= 912 \text{ kips}$$

LRFD	ASD
$\phi R_n = 1.00(912 \text{ kips})$ $= 912 \text{ kips} > 140 \text{ kips} \text{ o.k.}$	$\frac{R_n}{\Omega} = \frac{912 \text{ kips}}{1.50}$ $= 608 \text{ kips} > 93.6 \text{ kips} \text{ o.k.}$

### Web local crippling at W36 beam

Because the force is applied at a distance from the beam end that is greater than or equal to half the depth of the beam, use AISC *Specification* Equation J10-4 to determine the available strength.

$Q_f = 1.0$  (for wide-flange sections)

$$R_n = 0.80t_w^2 \left[ 1 + 3 \left( \frac{l_b}{d} \right) \left( \frac{t_w}{t_f} \right)^{1.5} \right] \sqrt{\frac{EF_{yw}t_f}{t_w}} Q_f \quad (\text{Spec. Eq. J10-4})$$

$$= 0.80(0.600 \text{ in.})^2 \left[ 1 + 3 \left( \frac{22.7 \text{ in.}}{35.6 \text{ in.}} \right) \left( \frac{0.600 \text{ in.}}{0.790 \text{ in.}} \right)^{1.5} \right] \sqrt{\frac{(29,000 \text{ ksi})(50 \text{ ksi})(0.790 \text{ in.})}{0.600 \text{ in.}}} (1.0)$$

$$= 902 \text{ kips}$$

LRFD	ASD
$\phi R_n = 0.75(902 \text{ kips})$ $= 677 \text{ kips} > 140 \text{ kips} \quad \text{o.k.}$	$\frac{R_n}{\Omega} = \frac{902 \text{ kips}}{2.00}$ $= 451 \text{ kips} > 93.6 \text{ kips} \quad \text{o.k.}$

### Web compression buckling at W36 beam

The available strength for the limit state of web compression buckling of the W36×135 beam is determined using AISC *Specification* Section J10.5.

$$h = (h/t_w)t_w$$

$$= (54.1)(0.600 \text{ in.})$$

$$= 32.5 \text{ in.}$$

$Q_f = 1.0$  (for wide-flange sections)

$$R_n = \left( \frac{24t_w^3 \sqrt{EF_{yw}}}{h} \right) Q_f \quad (\text{Spec. Eq. J10-8})$$

$$= \left[ \frac{24(0.600 \text{ in.})^3 \sqrt{(29,000 \text{ ksi})(50 \text{ ksi})}}{32.5 \text{ in.}} \right] (1.0)$$

$$= 192 \text{ kips}$$

LRFD	ASD
$\phi R_n = 0.90(192 \text{ kips})$ $= 173 \text{ kips} > 140 \text{ kips}$	$\frac{R_n}{\Omega} = \frac{192 \text{ kips}}{1.67}$ $= 115 \text{ kips} > 93.6 \text{ kips} \quad \text{o.k.}$

### Advanced Finite Element Analysis

Although a first-order finite element analysis is adequate for this example, this section uses advanced analysis techniques to illustrate the similarities between the results of both methods. A second-order geometrically nonlinear analysis resulted in a service-load deflection at the apex of 0.731 in., which is only 2% greater than the 0.715-in. first-order deflection. The second-order moments, summarized in Table 8-3, are all between 1% and 3% greater than the first-order moments in Table 8-1.

**Table 8-3. Moments from Second-Order Geometrically Nonlinear Analysis**

Location	Moment, $M_x$ kip-in.	
	$M_{ux}$	$M_{ax}$
Minimum at Span 3	-5,420	-3,610
Maximum at Span 2	+1,920	+1,280
Maximum at Span 1	+1,300	+867

**Table 8-4. Required Second-Order Moments**

Location	Moment, $M_{rx2}$ kip-in.	
	$M_{ux2}$	$M_{ax2}$
Minimum at Span 3	-6,020	-4,010
Maximum at Span 2	+2,130	+1,420
Maximum at Span 1	+1,440	+962

The second-order geometrically nonlinear analysis includes only the change in geometry caused by the loads. Any change in geometry caused by buckling instability must also be included in the analysis. In this example, these deformations were addressed using an amplified first-order analysis, where the first-order moments and deformations were multiplied by an in-plane second-order amplification factor,  $B_i$ . A similar amplification factor can be calculated using the results of an elastic buckling analysis. Using a finite element buckling analysis, the mode 1 [Figure 6-4(b)] critical load factors for in-plane buckling are 10.4 and 15.6 for LRFD loads and ASD loads, respectively. The service-load deflection can be calculated with an amplification factor of:

$$B_i = \frac{1}{1 - \frac{1}{15.6}} \\ = 1.07$$

Therefore, the second-order deflection at the apex is:

$$\Delta_2 = (1.07)(0.731 \text{ in.}) \\ = 0.782 \text{ in.}$$

This value is 0.3% greater than the amplified first-order value of 0.780 in.; however, both amplification factors are conservative because the deflected shape (Figure 8-3) is different from the mode 1 buckled shape shown in Figure 6-4(b). The required second-order moments can be calculated with amplification factors based on the buckling multipliers.

LRFD	ASD
$B_i = \frac{1}{1 - (1.0)\left(\frac{1}{10.4}\right)} \\ = 1.11$	$B_i = \frac{1}{1 - (1.6)\left(\frac{1}{15.6}\right)} \\ = 1.11$

The moments in Table 8-3 are multiplied by  $B_i$ , resulting in the second-order moments in Table 8-4.

The moments in Table 8-4 are all between 1% and 3% less than those in Table 8-2, indicating that, for this problem, the amplified first-order analysis is slightly conservative compared to the results using more advanced modeling techniques.

### Example 8.2—Horizontally Curved Continuous Member

#### Given:

The horizontally curved W21x101 beam in Figure 8-6 forms a circular curve with a 30-ft radius and a total angle of  $90^\circ$  between the W14x90 columns. The beam is continuous across an HSS column at the midspan, where torsion of the curved beam is restrained by the W21x55 beam. The member end connections to the W14x90 columns are restrained against torsional rotation but provide no flexural or warping restraint. Determine if the W21x101 beam is adequate for the loading cases given. The uniformly distributed load along the member circumference including the beam self-weight is:

LRFD	ASD
$w_u = 0.750 \text{ kip/ft}$	$w_a = 0.500 \text{ kip/ft}$

Two loading cases will be considered:

Case 1: Both spans loaded

Case 2: Only one span loaded

The required vertical shear reaction at the W21x55 is:

LRFD	ASD
$R_u = 30 \text{ kips}$	$R_a = 20 \text{ kips}$

W-shape member material: ASTM A992

Plate material: ASTM A36

Bolts:  $\frac{3}{4}$ -in.-diameter Group A bolts with threads not excluded from the shear plane (thread condition N)

Holes: standard,  $\frac{13}{16}$ -in. diameter

Weld strength: 70 ksi

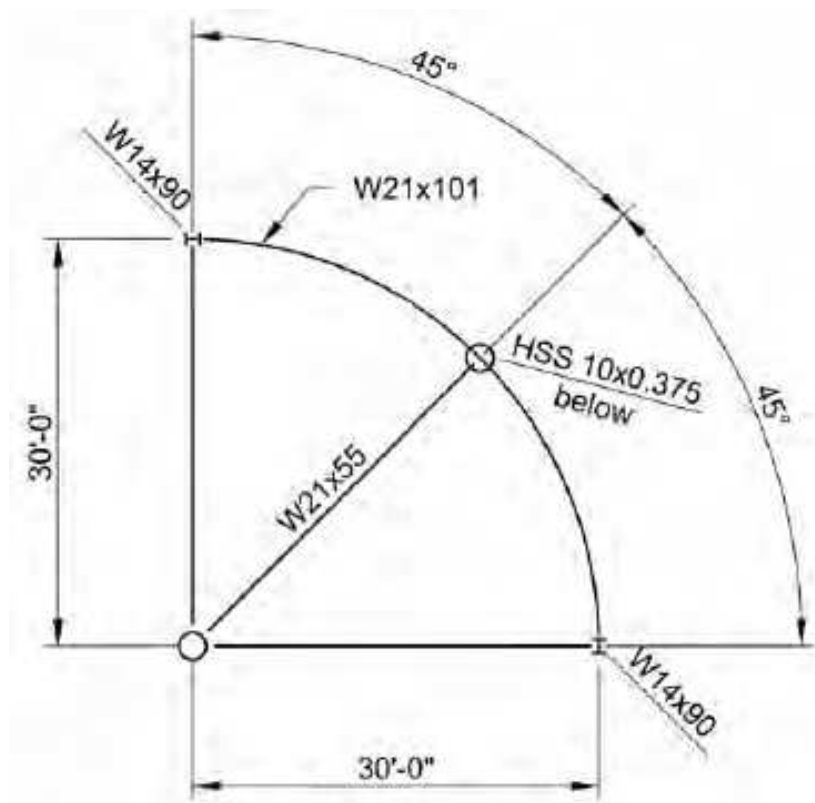


Fig. 8-6. Horizontally curved member for Example 8.2.

**Solution:**

From AISC *Manual* Tables 2-4 and 2-5, the material properties are as follows:

ASTM A992

$$F_y = 50 \text{ ksi}$$

$$F_u = 65 \text{ ksi}$$

ASTM A36

$$F_y = 36 \text{ ksi}$$

$$F_u = 58 \text{ ksi}$$

From AISC *Manual* Table 1-1, the geometric properties are as follows:

Beam

W21x101

$$d = 21.4 \text{ in.}$$

$$t_w = 0.500 \text{ in.}$$

$$b_f = 12.3 \text{ in.}$$

$$t_f = 0.800 \text{ in.}$$

$$k_{des} = 1.30 \text{ in.}$$

$$b_f/2t_f = 7.68$$

$$h/t_w = 37.5$$

$$I_x = 2,420 \text{ in.}^4$$

$$S_x = 227 \text{ in.}^3$$

$$Z_x = 253 \text{ in.}^3$$

$$r_{ts} = 3.35 \text{ in.}$$

$$h_o = 20.6 \text{ in.}$$

$$J = 5.21 \text{ in.}^4$$

$$C_w = 26,200 \text{ in.}^6$$

Column

W14x90

$$b_f = 14.5 \text{ in.}$$

$$t_f = 0.710 \text{ in.}$$

Beam

W21x55

$$t_w = 0.375 \text{ in.}$$

**Beam Geometry**

Radius:

$$R = (30 \text{ ft})(12 \text{ in./ft})$$

$$= 360 \text{ in.}$$

Span angle:

$$\theta_s = (45^\circ) \left( \frac{\pi \text{ rad}}{180^\circ} \right)$$
$$= \frac{\pi}{4} \text{ rad}$$

Angle between torsional restraints:

$$\theta_b = (45^\circ) \left( \frac{\pi \text{ rad}}{180^\circ} \right)$$
$$= \frac{\pi}{4} \text{ rad}$$

Developed span length:

$$L_{ds} = (30 \text{ ft}) \left( \frac{\pi}{4} \text{ rad} \right) (12 \text{ in./ft})$$
$$= 283 \text{ in.}$$

Developed length between braces:

$$L_{db} = (30 \text{ ft}) \left( \frac{\pi}{4} \text{ rad} \right) (12 \text{ in./ft})$$
$$= 283 \text{ in.}$$

## Flexural Loads

### Load Case 1

For Load Case 1, both spans are loaded. The beam end reactions are determined using AISC *Manual* Table 3-23, Case 12. The reaction at the pinned end is:

LRFD	ASD
$R_u = \frac{3w_u L_{ds}}{8}$ $= \frac{3(0.750 \text{ kip/ft})(23.6 \text{ ft})}{8}$ $= 6.64 \text{ kips}$	$R_a = \frac{3w_a L_{ds}}{8}$ $= \frac{3(0.500 \text{ kip/ft})(23.6 \text{ ft})}{8}$ $= 4.43 \text{ kips}$

The reaction at the continuous support is:

LRFD	ASD
$R_u = \frac{5w_u L_{ds}}{8}$ $= \frac{5(0.750 \text{ kip/ft})(23.6 \text{ ft})}{8}$ $= 11.1 \text{ kips}$	$R_a = \frac{5w_a L_{ds}}{8}$ $= \frac{5(0.500 \text{ kip/ft})(23.6 \text{ ft})}{8}$ $= 7.38 \text{ kips}$

The flexural moment as a function of  $z$  is:

$$M_{xz} = \frac{wz}{2} \left( \frac{3L_{ds}}{4} - z \right)$$

The maximum positive moment, at  $z = 3L_s/8$ , is:

LRFD	ASD
$M_{ux} = \frac{9w_u L_{ds}^2}{128}$ $= \frac{9(0.750 \text{ kip/ft})(23.6 \text{ ft})^2 (12 \text{ in./ft})}{128}$ $= 352 \text{ kip-in.}$	$M_{ax} = \frac{9w_a L_{ds}^2}{128}$ $= \frac{9(0.500 \text{ kip/ft})(23.6 \text{ ft})^2 (12 \text{ in./ft})}{128}$ $= 235 \text{ kip-in.}$

The maximum negative moment, located at the continuous support, is:

LRFD	ASD
$M_{ux} = -\frac{w_u L_{ds}^2}{8}$ $= -\frac{(0.750 \text{ kip/ft})(23.6 \text{ ft})^2 (12 \text{ in./ft})}{8}$ $= -627 \text{ kip-in.}$	$M_{ax} = -\frac{w_a L_{ds}^2}{8}$ $= -\frac{(0.500 \text{ kip/ft})(23.6 \text{ ft})^2 (12 \text{ in./ft})}{8}$ $= -418 \text{ kip-in.}$

### Load Case 2

For Load Case 2, only one span is loaded. The beam end reactions are determined using AISC *Manual* Table 3-23, Case 29. The reaction at the pinned end is:

LRFD	ASD
$R_u = \frac{7w_u L_{ds}}{16}$ $= \frac{7(0.750 \text{ kip/ft})(23.6 \text{ ft})}{16}$ $= 7.74 \text{ kips}$	$R_a = \frac{7w_a L_{ds}}{16}$ $= \frac{7(0.500 \text{ kip/ft})(23.6 \text{ ft})}{16}$ $= 5.16 \text{ kips}$

The reaction at the continuous support is:

LRFD	ASD
$R_u = \frac{5w_u L_{ds}}{8}$ $= \frac{5(0.750 \text{ kip/ft})(23.6 \text{ ft})}{8}$ $= 11.1 \text{ kips}$	$R_a = \frac{5w_a L_{ds}}{8}$ $= \frac{5(0.500 \text{ kip/ft})(23.6 \text{ ft})}{8}$ $= 7.38 \text{ kips}$

The flexural moment as a function of  $z$  is:

$$M_{xz} = \frac{wz}{16} (7L_{ds} - 8z)$$

The maximum positive moment, at  $z = 7L_s/16$ , is:

LRFD	ASD
$M_{ux} = \frac{49w_u L_{ds}^2}{512}$ $= \frac{49(0.750 \text{ kip/ft})(23.6 \text{ ft})^2(12 \text{ in./ft})}{512}$ $= 480 \text{ kip-in.}$	$M_{ax} = \frac{49w_a L_{ds}^2}{512}$ $= \frac{49(0.500 \text{ kip/ft})(23.6 \text{ ft})^2(12 \text{ in./ft})}{512}$ $= 320 \text{ kip-in.}$

The maximum negative moment, located at the continuous support, is:

LRFD	ASD
$M_{ux} = -\frac{w_u L_{ds}^2}{16}$ $= -\frac{(0.750 \text{ kip/ft})(23.6 \text{ ft})^2(12 \text{ in./ft})}{16}$ $= -313 \text{ kip-in.}$	$M_{ax} = -\frac{w_a L_{ds}^2}{16}$ $= -\frac{(0.500 \text{ kip/ft})(23.6 \text{ ft})^2(12 \text{ in./ft})}{16}$ $= -209 \text{ kip-in.}$

### Torsional Loads

Torsional loads are calculated with the  $M/R$  method discussed in Section 7.3.2. Figures 8-7 and 8-8 show the diagrams generated with the  $M/R$  method. The out-of-plane flexural moment diagrams for the beam are shown in Figures 8-7(a) and 8-8(a) for Load Cases 1 and 2, respectively.

The distributed torsional loading diagrams for the beam are developed using the out-of-plane flexural moment diagrams with Equation 7-8. The torsional loading diagrams are shown in Figures 8-7(b) and 8-8(b) for Load Cases 1 and 2, respectively.

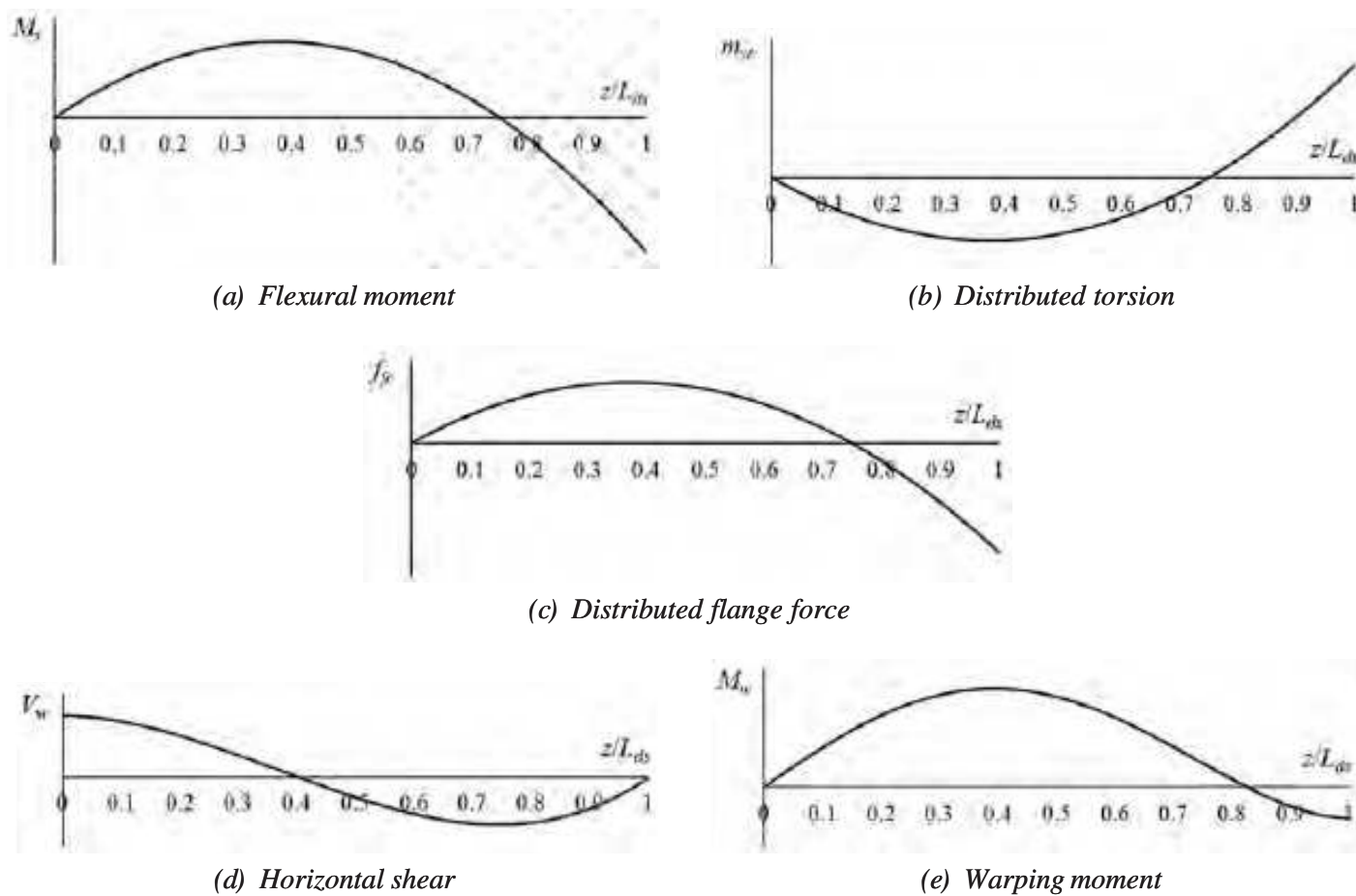


Fig. 8-7. M/R diagrams for Load Case 1.

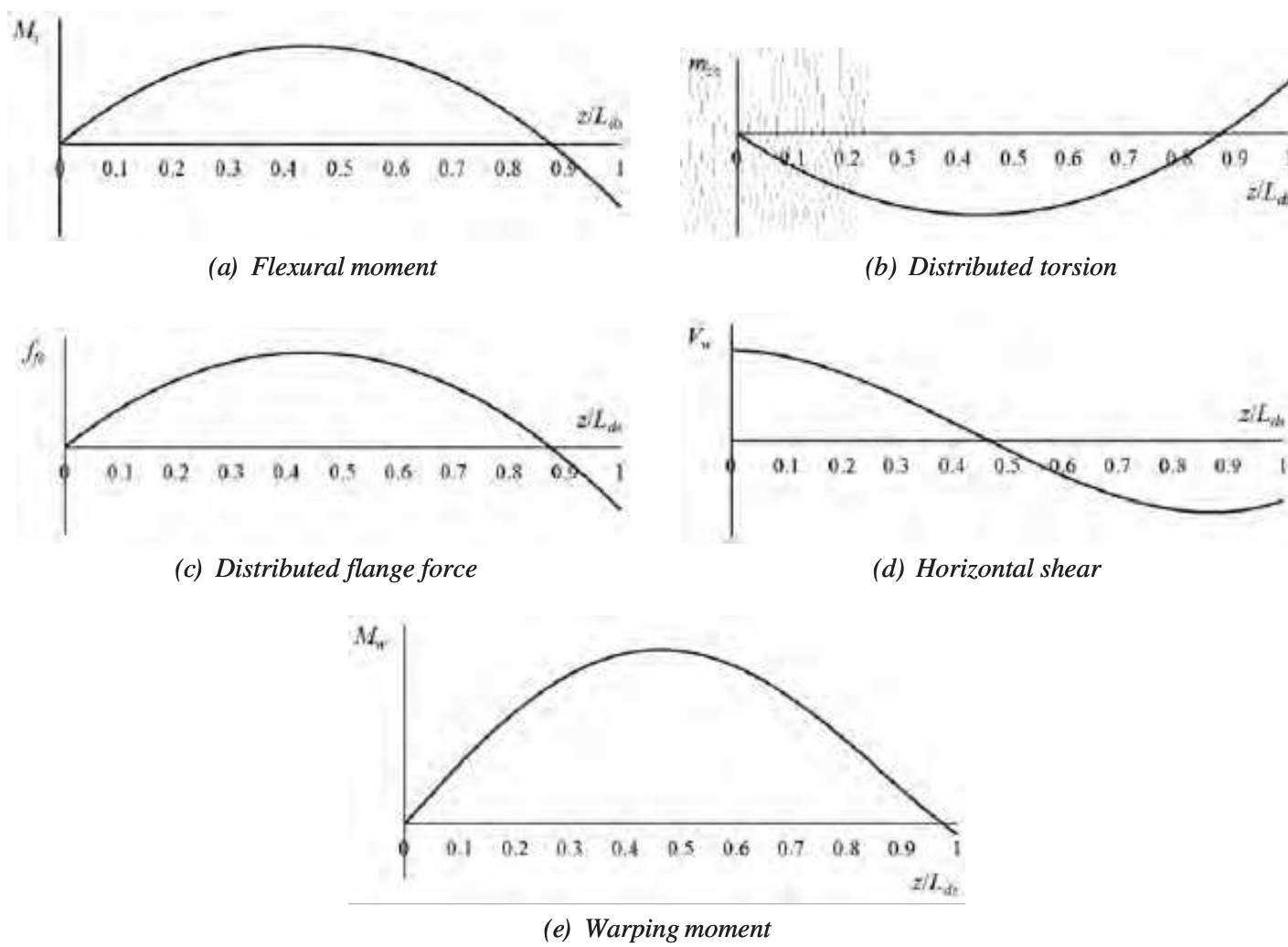


Fig. 8-8. M/R diagrams for Load Case 2.

**Table 8-5. Torsional Loads from  $M/R$  Analysis**

		<b>LRFD</b>	<b>ASD</b>
Case 1	Maximum $M_w$ (at $z = 0.39L_{ds}$ )	253	169
	Minimum $M_w$ (at continuous support)	-78.9	-52.6
	$V_w$ at simply supported end	3.73	2.49
	$V_w$ at continuous end	-0.120	-0.080
	Maximum $f_{fc}$ (at $z = 0.38L_{ds}$ )	0.0474	0.0316
Case 2	Maximum $M_w$ (at $z = 0.46L_{ds}$ )	476	317
	Minimum $M_w$ (at continuous support)	-27.9	-18.6
	$V_w$ at simply supported end	5.95	3.97
	$V_w$ at continuous end	-3.91	-2.60
	Maximum $f_{fc}$ (at $z = 0.44L_{ds}$ )	0.0645	0.0430

$M_w$  = flange warping moment, kip-in.  
 $V_w$  = flange horizontal shear, kips

Because the torsional strength is based on the isolated flange method discussed in Section 7.5.2, the distributed radial flange force diagram is developed using the distributed torsional loading diagrams with Equation 7-32. The distributed radial flange force diagrams for the beam are shown in Figures 8-7(c) and 8-8(c) for Load Cases 1 and 2, respectively.

The shear diagrams for the isolated flange are shown in Figures 8-7(d) and 8-8(d) for Load Cases 1 and 2, respectively. The moment diagrams for the isolated flange are shown in Figures 8-7(e) and 8-8(e) for Load Cases 1 and 2, respectively. All loads are summarized in Table 8-5.

#### Corrected Moments

A correction factor is applied to the moments according to Section 7.3.2. The critical combination is for Load Case 2, where the flexural and warping moments are:

<b>LRFD</b>	<b>ASD</b>
$M_{ux} = 480$ kip-in. (previously calculated)	$M_{ax} = 320$ kip-in. (previously calculated)
$M_{uw} = 476$ kip-in. (from Table 8-5)	$M_{aw} = 317$ kip-in. (from Table 8-5)

According to Equation 7-11, the correction factor is:

$$\begin{aligned}
 C &= 1 - \frac{\theta_s}{30} + \frac{\theta_s^2}{6.2} \\
 &= 1 - \frac{\pi/4}{30} + \frac{(\pi/4)^2}{6.2} \\
 &= 1.07
 \end{aligned} \tag{7-11}$$

The corrected moments are determined using Equation 7-9:

<b>LRFD</b>	<b>ASD</b>
$M_{uxc} = (1.07)(480 \text{ kip-in.})$ $= 514 \text{ kip-in.}$	$M_{axc} = (1.07)(320 \text{ kip-in.})$ $= 342 \text{ kip-in.}$
$M_{uwc} = (1.07)(476 \text{ kip-in.})$ $= 509 \text{ kip-in.}$	$M_{awc} = (1.07)(317 \text{ kip-in.})$ $= 339 \text{ kip-in.}$

### Shear Strength

The available shear strength of the curved W21x101 is determined using AISC *Specification* Section G2.1.

$$h/t_w = 37.5$$

$$2.24 \sqrt{\frac{E}{F_y}} = 2.24 \sqrt{\frac{29,000 \text{ ksi}}{50 \text{ ksi}}}$$

$$= 53.9$$

Because  $h/t_w < 2.24 \sqrt{\frac{E}{F_y}}$ :

$$C_{v1} = 1.0$$

(*Spec. Eq. G2-2*)

The area of the web is:

$$A_w = dt_w$$

$$= (21.4 \text{ in.})(0.500 \text{ in.})$$

$$= 10.7 \text{ in.}^2$$

The nominal shear strength,  $V_n$ , is:

$$V_n = 0.6F_y A_w C_{v1}$$

$$= 0.6(50 \text{ ksi})(10.7 \text{ in.}^2)(1.0)$$

$$= 321 \text{ kips}$$

(*Spec. Eq. G2-1*)

And the available shear strength is:

LRFD	ASD
$\phi_v V_n = 1.00(321 \text{ kips})$ $= 321 \text{ kips} > 11.1 \text{ kips} \text{ o.k.}$	$\frac{V_n}{\Omega_v} = \frac{321 \text{ kips}}{1.50}$ $= 214 \text{ kips} > 7.38 \text{ kips} \text{ o.k.}$

### Flexural Strength

The available flexural strength of the curved W21x101 is determined using AISC *Specification* Section F2.

#### Local buckling

For the W21x101:

$$\lambda_f = \frac{b_f}{2t_f}$$

$$= 7.68$$

$$\lambda_w = \frac{h}{t_w}$$

$$= 37.5$$

From AISC *Specification* Table B4.1b, the limiting width-to-thickness ratios are:

$$\lambda_{pf} = 0.38 \sqrt{\frac{E}{F_y}}$$

$$= 0.38 \sqrt{\frac{29,000 \text{ ksi}}{50 \text{ ksi}}}$$

$$= 9.15$$

$$\begin{aligned}
\lambda_{pw} &= 3.76 \sqrt{\frac{E}{F_y}} \\
&= 3.76 \sqrt{\frac{29,000 \text{ ksi}}{50 \text{ ksi}}} \\
&= 90.6
\end{aligned}$$

Because  $\lambda_f < \lambda_{pf}$  and  $\lambda_w < \lambda_{pw}$ , the section is compact.

#### Lateral-torsional buckling

The plastic bending moment for a W21x101 is:

$$\begin{aligned}
M_p &= F_y Z_x \\
&= (50 \text{ ksi})(253 \text{ in.}^3) \\
&= 12,700 \text{ kip-in.}
\end{aligned} \tag{Spec. Eq. F2-1}$$

Using Equation 7-24 with  $C_{bs} = 1.0$

$$\begin{aligned}
C_{bo} &= C_{bs} \left[ 1 - \left( \frac{\theta_b}{\pi} \right)^2 \right]^2 \\
&= (1.0) \left[ 1 - \left( \frac{\pi/4}{\pi} \right)^2 \right]^2 \\
&= 0.879
\end{aligned} \tag{7-24}$$

Use AISC *Specification* Section F2 with  $L_b = L_{db} = (283 \text{ in.})/(12 \text{ in./ft}) = 23.6 \text{ ft}$  and  $C_b = C_{bo} = 0.879$ . From AISC *Manual Table 3-6*, for a W21x101:

$$\begin{aligned}
L_p &= 10.2 \text{ ft} \\
L_r &= 30.1 \text{ ft}
\end{aligned}$$

Because  $L_p < L_b < L_r$ , AISC *Specification* Equation F2-2 is used to determine the nominal flexural strength,  $M_n$ :

$$\begin{aligned}
M_n &= C_b \left[ M_p - (M_p - 0.7F_y S_x) \left( \frac{L_b - L_p}{L_r - L_p} \right) \right] \leq M_p \\
&= (0.879) \left\{ 12,700 \text{ kip-in.} - \left[ 12,700 \text{ kip-in.} - (0.7)(50 \text{ ksi})(227 \text{ in.}^3) \right] \left( \frac{23.6 \text{ ft} - 10.2 \text{ ft}}{30.1 \text{ ft} - 10.2 \text{ ft}} \right) \right\} \leq 12,700 \text{ kip-in.} \\
&= 8,350 \text{ kip-in.} < 12,700 \text{ kip-in.}
\end{aligned} \tag{Spec. Eq. F2-2}$$

Therefore, the nominal flexural strength is:

$$M_n = 8,350 \text{ kip-in.}$$

And the available flexural strength is:

LRFD	ASD
$ \begin{aligned} M_{co} &= \phi_b M_n \\ &= 0.90(8,350 \text{ kip-in.}) \\ &= 7,520 \text{ kip-in.} \end{aligned} $	$ \begin{aligned} M_{co} &= \frac{M_n}{\Omega_b} \\ &= \frac{8,350 \text{ kip-in.}}{1.67} \\ &= 5,000 \text{ kip-in.} \end{aligned} $

### Second-Order Effects

The elastic critical lateral-torsional buckling moment,  $M_{eo}$ , is calculated with  $F_{cr}$  from AISC *Specification* Equation F2-4 using the modified lateral-torsional buckling modification factor,  $C_{bo}$ , and  $c = 1$ :

$$F_{cr} = \frac{C_{bo}\pi^2 E}{\left(\frac{L_b}{r_{ts}}\right)^2} \sqrt{1 + 0.078 \frac{Jc}{S_x h_o} \left(\frac{L_b}{r_{ts}}\right)^2} \quad (\text{from Spec. Eq. F2-4})$$

$$= \frac{(0.879)\pi^2(29,000 \text{ ksi})}{\left(\frac{283 \text{ in.}}{3.35 \text{ in.}}\right)^2} \sqrt{1 + 0.078 \frac{(5.21 \text{ in.}^4)(1)}{(227 \text{ in.}^3)(20.6 \text{ in.})} \left(\frac{283 \text{ in.}}{3.35 \text{ in.}}\right)^2}$$

$$= 44.9 \text{ ksi}$$

$$M_{eo} = F_{cr} S_x$$

$$= (44.9 \text{ ksi})(227 \text{ in.}^3)$$

$$= 10,200 \text{ kips-in.}$$

The second-order amplification factor,  $B_o$ , is calculated using Equation 7-37 with  $M_{ro} = M_{xc}$ .

LRFD	ASD
$\alpha = 1.0$ $B_o = \frac{0.85}{1 - \alpha \frac{M_{uxc}}{M_{eo}}} \geq 1.0$ $= \frac{0.85}{1 - (1.0) \left( \frac{514 \text{ kip-in.}}{10,200 \text{ kip-in.}} \right)} \geq 1.0$ $= 0.895 < 1.0$  Therefore, $B_o = 1.0$ .	$\alpha = 1.6$ $B_o = \frac{0.85}{1 - \alpha \frac{M_{axc}}{M_{eo}}} \geq 1.0$ $= \frac{0.85}{1 - (1.6) \left( \frac{342 \text{ kip-in.}}{10,200 \text{ kip-in.}} \right)} \geq 1.0$ $= 0.898 < 1.0$  Therefore, $B_o = 1.0$ .

The required second-order flange warping moment is:

LRFD	ASD
$M_{uw} = B_o M_{awc}$ $= (1.0)(509 \text{ kip-in.})$ $= 509 \text{ kip-in.}$	$M_{aw} = B_o M_{awc}$ $= (1.0)(339 \text{ kip-in.})$ $= 339 \text{ kip-in.}$

### Warping Strength

The isolated flange plastic modulus,  $Z_f$ , for a W21x101 is calculated with Equation 7-34:

$$Z_f = \frac{t_f b_f^2}{4} \quad (7-34)$$

$$= \frac{(0.800 \text{ in.})(12.3 \text{ in.})^2}{4}$$

$$= 30.3 \text{ in.}^3$$

The nominal flexural strength of the isolated flange,  $M_{nw}$ , is calculated with Equation 7-33:

$$\begin{aligned} M_{nw} &= F_y Z_f \\ &= (50 \text{ ksi})(30.3 \text{ in.}^3) \\ &= 1,520 \text{ kips-in.} \end{aligned} \quad (7-33)$$

The available flexural strength of the isolated flange is:

LRFD	ASD
$\begin{aligned} M_{cw} &= \phi_b M_{nw} \\ &= 0.90(1,520 \text{ kip-in.}) \\ &= 1,370 \text{ kip-in.} \end{aligned}$	$\begin{aligned} M_{cw} &= \frac{M_{nw}}{\Omega_b} \\ &= \frac{1,520 \text{ kip-in.}}{1.67} \\ &= 910 \text{ kip-in.} \end{aligned}$

### Combined Loads

The out-of-plane flexural moment is combined with the flange warping moment using Equation 7-38.

LRFD	ASD
$\begin{aligned} \frac{M_{uxc}}{M_{co}} + \frac{8}{9} \frac{M_{uw}}{M_{cw}} &\leq 1.0 \\ \frac{514 \text{ kip-in.}}{7,520 \text{ kip-in.}} + \left(\frac{8}{9}\right) \left(\frac{509 \text{ kip-in.}}{1,370 \text{ kip-in.}}\right) &\leq 1.0 \\ 0.399 < 1.00 &\quad \text{o.k.} \end{aligned}$	$\begin{aligned} \frac{M_{axc}}{M_{co}} + \frac{8}{9} \frac{M_{aw}}{M_{cw}} &\leq 1.0 \\ \frac{342 \text{ kip-in.}}{5,000 \text{ kip-in.}} + \left(\frac{8}{9}\right) \left(\frac{339 \text{ kip-in.}}{910 \text{ kip-in.}}\right) &\leq 1.0 \\ 0.400 < 1.00 &\quad \text{o.k.} \end{aligned}$

### Serviceability

As discussed in Section 7.7, serviceability evaluations should be based on a first-yield criterion. The isolated flange section modulus is:

$$\begin{aligned} S_f &= \frac{t_f b_f^2}{6} \\ &= \frac{(0.800 \text{ in.})(12.3 \text{ in.})^2}{6} \\ &= 20.2 \text{ in.}^3 \end{aligned}$$

The service-load warping stress is:

$$\begin{aligned} \sigma_{rw} &= \frac{M_{aw}}{S_f} \\ &= \frac{339 \text{ kip-in.}}{20.2 \text{ in.}^3} \\ &= 16.8 \text{ ksi} \end{aligned}$$

The service-level, out-of-plane flexural stress is:

$$\begin{aligned} \sigma_{ro} &= \frac{M_{axc}}{S_x} \\ &= \frac{342 \text{ kip-in.}}{227 \text{ in.}^3} \\ &= 1.51 \text{ ksi} \end{aligned}$$

$$\begin{aligned}
\sigma &= \sigma_{rw} + \sigma_{ro} \\
&= 16.8 \text{ ksi} + 1.51 \text{ ksi} \\
&= 18.3 \text{ ksi} < 50 \text{ ksi} \quad \text{o.k.}
\end{aligned}$$

A conservative estimate of the torsional rotation can be calculated with the horizontal flange deflection, using the distributed flange force,  $f_{fc}$ , as a uniform load. Because  $f_{fc}$  varies along the beam length, as shown in Figures 8-7(c) and 8-8(c), the maximum positive service-load value is used. The maximum ASD value in Table 8-5 is for Case 2:  $f_{fc} = 0.0430 \text{ kip/in.}$  The St. Venant stiffness is neglected, further contributing to the conservatism of this method. The isolated flange moment of inertia is:

$$\begin{aligned}
I_f &= \frac{t_f b_f^3}{12} \\
&= \frac{(0.800 \text{ in.})(12.3 \text{ in.})^3}{12} \\
&= 124 \text{ in.}^4
\end{aligned}$$

From AISC *Manual* Table 3-23, Case 12:

$$\begin{aligned}
\Delta_{max} &= \frac{f_{fc} L_{ds}^4}{185 E I_f} \\
&= \frac{(0.0430 \text{ kip/in.})(283 \text{ in.})^4}{(185)(29,000 \text{ ksi})(124 \text{ in.}^4)} \\
&= 0.415 \text{ in.}
\end{aligned}$$

The first-order torsional rotation is:

$$\begin{aligned}
\theta_1 &= \tan^{-1} \left( \frac{2\Delta_{max}}{h_o} \right) \\
&= \tan^{-1} \left( \frac{(2)(0.415 \text{ in.})}{20.6 \text{ in.}} \right) \\
&= 2.31^\circ
\end{aligned}$$

The second-order multiplier under service loads (unfactored loads) is calculated using Equation 7-37 with  $\alpha = 1.0$  and  $M_{ro} = M_{axc}$ :

$$\begin{aligned}
B_o &= \frac{0.85}{1 - \alpha \frac{M_{axc}}{M_{eo}}} \geq 1.0 \quad (\text{from Eq. 7-37}) \\
&= \frac{0.85}{1 - (1.00) \left( \frac{342 \text{ kip-in.}}{10,200 \text{ kip-in.}} \right)} \geq 1.00 \\
&= 0.879 < 1.00; \text{ therefore, } B_o = 1.00.
\end{aligned}$$

The second-order torsional rotation under service loads,  $\theta_2$ , is calculated using Equation 7-35:

$$\begin{aligned}
\theta_2 &= B_o \theta_1 \quad (7-35) \\
&= (1.00)(2.31^\circ) \\
&= 2.31^\circ
\end{aligned}$$

#### Connection Design at Pinned End

The end-plate connection shown in Figure 8-9 is efficient in transferring torsion from the curved beam to the W14 column. Because the torsional moment is transferred by horizontal shear forces at the beam flanges, the flanges are welded to the end plate. An 8-in. gage is used to provide efficient resistance to torsional loads and to reduce the strong-axis rotational stiffness.

### Loads

Calculate the torsional moment based on the flange horizontal shear. From Table 8-5, the maximum value for  $V_w$  occurs for Load Case 2.

LRFD	ASD
$V_{uw} = 5.95$ kips	$V_{aw} = 3.97$ kips

The torsional moment is:

LRFD	ASD
$M_{uz} = V_{uw}h_o$ $= (5.95 \text{ kips})(20.6 \text{ in.})$ $= 123 \text{ kip-in.}$	$M_{az} = V_{aw}h_o$ $= (3.97 \text{ kips})(20.6 \text{ in.})$ $= 81.8 \text{ kip-in.}$

The vertical reaction at the pinned end is highest for Load Case 2, as previously calculated.

LRFD	ASD
$R_{uc} = 7.74$ kips	$R_{ac} = 5.16$ kips

### Bolt shear

From AISC *Manual* Table 7-1, the available shear strength per bolt for  $\frac{3}{4}$ -in.-diameter Group A bolts with threads not excluded from the shear plane (thread condition N) is:

LRFD	ASD
$\phi r_n = 17.9$ kips/bolt	$\frac{r_n}{\Omega} = 11.9$ kips/bolt

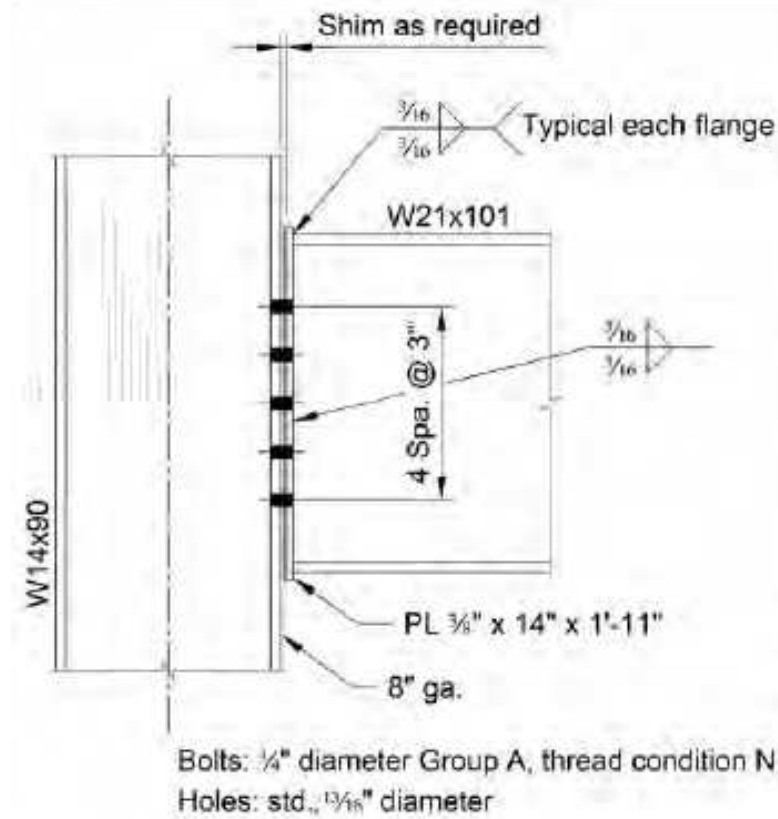


Fig. 8-9. Connection at simply supported end for Example 8.2.

The available strength of the bolt group is determined using the instantaneous center of rotation method (ICR). Eccentricity of loading on the bolt group is determined as follows:

LRFD	ASD
$e_x = \frac{M_{uz}}{R_{uc}}$ $= \frac{123 \text{ kip-in.}}{7.74 \text{ kips}}$ $= 15.9 \text{ in.}$	$e_x = \frac{M_{az}}{R_{ac}}$ $= \frac{81.8 \text{ kip-in.}}{5.16 \text{ kips}}$ $= 15.9 \text{ in.}$

Interpolating from AISC *Manual* Table 7-9, with Angle = 0°,  $e_x = 15.9$  in.,  $s = 3$  in., and  $n = 5$ :

$$C = 3.00$$

The available strength of the bolt group is determined as follows. The available strength is reduced by 0.85; this is the maximum reduction factor for fillers (shims) required by AISC *Specification* Section J5.2.

LRFD	ASD
$\phi R_n = C \phi r_n (0.85)$ $= 3.00(17.9 \text{ kips/bolt})(0.85)$ $= 45.6 \text{ kips} > 7.74 \text{ kips} \quad \text{o.k.}$	$\frac{R_n}{\Omega} = C \frac{r_n}{\Omega} (0.85)$ $= 3.00(11.9 \text{ kips/bolt})(0.85)$ $= 30.3 \text{ kips} > 5.16 \text{ kips} \quad \text{o.k.}$

#### *Bolt bearing and tearout at the plate*

The nominal bearing strength of the end plate is determined from AISC *Specification* Section J3.10, assuming deformation at service load is a design consideration:

$$\begin{aligned}
 r_n &= 2.4dtF_u && \text{(Spec. Eq. J3-6a)} \\
 &= 2.4(\frac{3}{4} \text{ in.})(\frac{3}{8} \text{ in.})(58 \text{ ksi}) \\
 &= 39.2 \text{ kips/bolt}
 \end{aligned}$$

The nominal tearout strength of the plate is determined from AISC *Specification* Section J3.10, assuming deformation at service load is a design consideration. The clear distance from the edge of the hole to the edge of the plate is:

$$\begin{aligned}
 l_c &= s - \frac{d_h}{2} \\
 &= 3.00 \text{ in.} - \frac{\frac{13}{16} \text{ in.}}{2} \\
 &= 2.59 \text{ in.}
 \end{aligned}$$

The clear distance between holes at 3-in. spacing is:

$$\begin{aligned}
 l_c &= s - d_h \\
 &= 3.00 \text{ in.} - \frac{13}{16} \text{ in.} \\
 &= 2.19 \text{ in.}
 \end{aligned}$$

The clear distance between holes will control over the clear distance to the edge. The available tearout strength is:

$$\begin{aligned}
 r_n &= 1.2l_c t F_u && \text{(Spec. Eq. J3-6c)} \\
 &= 1.2(2.19 \text{ in.})(\frac{3}{8} \text{ in.})(58 \text{ ksi}) \\
 &= 57.2 \text{ kips/bolt}
 \end{aligned}$$

Therefore, bearing controls over tearout for the plate. The available bolt bearing strength is:

LRFD	ASD
$\phi R_n = C \phi r_n$ $= (3.00)(0.75)(39.2 \text{ kips/bolt})$ $= 88.2 \text{ kips} > 7.74 \text{ kips o.k.}$	$\frac{R_n}{\Omega} = C \frac{r_n}{\Omega}$ $= (3.00) \frac{39.2 \text{ kips/bolt}}{2.00}$ $= 58.8 \text{ kips} > 5.16 \text{ kips o.k.}$

#### Bolt bearing and tearout at the W14 column flange

The nominal bearing strength of the column flange is determined from AISC *Specification* Section J3.10, assuming deformation at service load is a design consideration:

$$\begin{aligned}
 r_n &= 2.4dtF_u && \text{(Spec. Eq. J3-6a)} \\
 &= 2.4(\frac{3}{4} \text{ in.})(0.710 \text{ in.})(65 \text{ ksi}) \\
 &= 83.1 \text{ kips/bolt}
 \end{aligned}$$

The nominal tearout strength of the column flange is determined from AISC *Specification* Section J3.10, assuming deformation at service load is a design consideration. The clear distance from the edge of the hole to the edge of the column flange is:

$$\begin{aligned}
 l_c &= s - \frac{d_h}{2} \\
 &= \frac{(14.5 \text{ in.} - 8.00 \text{ in.})}{2} - \frac{\frac{13}{16} \text{ in.}}{2} \\
 &= 2.84 \text{ in.}
 \end{aligned}$$

The clear distance between holes at 3-in. spacing is:

$$\begin{aligned}
 l_c &= s - d_h \\
 &= 3.00 \text{ in.} - \frac{13}{16} \text{ in.} \\
 &= 2.19 \text{ in.}
 \end{aligned}$$

The clear distance between holes will control. The available tearout strength is:

$$\begin{aligned}
 r_n &= 1.2l_c t F_u && \text{(Spec. Eq. J3-6c)} \\
 &= 1.2(2.19 \text{ in.})(0.710 \text{ in.})(65 \text{ ksi}) \\
 &= 121 \text{ kips/bolt}
 \end{aligned}$$

Therefore, bearing controls over tearout for the column flange. The available bolt bearing strength is:

LRFD	ASD
$\phi R_n = C \phi r_n$ $= (3.00)(0.75)(83.1 \text{ kips/bolt})$ $= 187 \text{ kips} > 7.74 \text{ kips o.k.}$	$\frac{R_n}{\Omega} = C \frac{r_n}{\Omega}$ $= (3.00) \left( \frac{83.1 \text{ kips/bolt}}{2.00} \right)$ $= 125 \text{ kips} > 5.16 \text{ kips o.k.}$

#### Weld end plate to W21 flanges

The available weld strength at the beam flange is determined using AISC *Manual* Equation 8-2a or 8-2b. The length of weld is:

$$\begin{aligned}
 l &= 2b_f - t_w \\
 &= 2(12.3 \text{ in.}) - 0.500 \text{ in.} \\
 &= 24.1 \text{ in.}
 \end{aligned}$$

For a  $\frac{3}{16}$ -in. weld, the available strength is:

LRFD	ASD
$\begin{aligned}\phi R_n &= (1.392 \text{ kip/in.}) Dl \\ &= (1.392 \text{ kip/in.})(3)(24.1 \text{ in.}) \\ &= 101 \text{ kips} > 5.95 \text{ kips} \quad \text{o.k.}\end{aligned}$	$\begin{aligned}\frac{R_n}{\Omega} &= (0.928 \text{ kip/in.}) Dl \\ &= (0.928 \text{ kip/in.})(3)(24.1 \text{ in.}) \\ &= 67.1 \text{ kips} > 3.97 \text{ kips} \quad \text{o.k.}\end{aligned}$

#### *Weld end plate to W21 web*

The available weld strength at the beam web is determined using AISC *Manual* Equation 8-2a or 8-2b. The length of weld is:

$$\begin{aligned}l &= d - 2k \\ &= 21.4 \text{ in.} - 2(1.30 \text{ in.}) \\ &= 18.8 \text{ in.}\end{aligned}$$

LRFD	ASD
$\begin{aligned}\phi R_n &= (1.392 \text{ kip/in.}) Dl(2 \text{ sides}) \\ &= (1.392 \text{ kip/in.})(3)(18.8 \text{ in.})(2 \text{ sides}) \\ &= 157 \text{ kips} > 7.74 \text{ kips} \quad \text{o.k.}\end{aligned}$	$\begin{aligned}\frac{R_n}{\Omega} &= (0.928 \text{ kip/in.}) Dl(2 \text{ sides}) \\ &= (0.928 \text{ kip/in.})(3)(18.8 \text{ in.})(2 \text{ sides}) \\ &= 105 \text{ kips} > 5.16 \text{ kips} \quad \text{o.k.}\end{aligned}$

#### *Connection Design at Continuous Support*

The single-plate shear connection shown in Figure 8-10 is economical to fabricate and facilitates efficient erection. The vertical beam reaction is transferred into the HSS column and the torsional reaction from each beam span is resisted by the single-plate connection. The connection must also resist the vertical end reaction at the W21×55 beam.

#### *Loads*

Calculate the torsional moment based on the flange horizontal shear. The load from both spans must be resisted by the connection; therefore, the maximum of  $2V_w$  for Load Case 1 or  $V_w$  for Load Case 2 will be used. From Table 8-5, the critical condition occurs for Load Case 2:

LRFD	ASD
$V_{uw} = 3.91 \text{ kips}$	$V_{aw} = 2.60 \text{ kips}$

The torsional moment is:

LRFD	ASD
$\begin{aligned}M_{uz} &= V_{uw} h_o \\ &= (3.91 \text{ kips})(20.6 \text{ in.}) \\ &= 80.5 \text{ kip-in.}\end{aligned}$	$\begin{aligned}M_{az} &= V_{aw} h_o \\ &= (2.60 \text{ kips})(20.6 \text{ in.}) \\ &= 53.6 \text{ kip-in.}\end{aligned}$

From the problem statement, the required vertical shear reaction at the W21×55 is:

LRFD	ASD
$R_u = 30 \text{ kips}$	$R_a = 20 \text{ kips}$

### *Maximum plate thickness*

From AISC *Manual* Part 10, determine the maximum plate thickness,  $t_{max}$ , that will result in the plate yielding before the bolts shear. Design Check 2, Exception b, for the extended configuration is applicable. Because  $l_{eh} = 2$  in. is greater than  $2d_b = 1.50$  in., the edge distance is adequate. From Table 10-9 with  $n = 5$ :

$$t_{max} = \frac{d}{2} + \frac{1}{16}$$

$$= \frac{\frac{3}{4} \text{ in.}}{2} + \frac{1}{16} \text{ in.}$$

$$= 0.438 \text{ in.}$$

Because 0.438 in. is greater than the actual plate thickness of 0.375 in., the connection has sufficient ductility.

### *Bolt shear*

From AISC *Manual* Table 7-1, the available shear strength per bolt for  $\frac{3}{4}$ -in.-diameter Group A bolts with threads not excluded from the shear plane (thread condition N) is:

LRFD	ASD
$\phi r_n = 17.9 \text{ kips/bolt}$	$\frac{r_n}{\Omega} = 11.9 \text{ kips/bolt}$

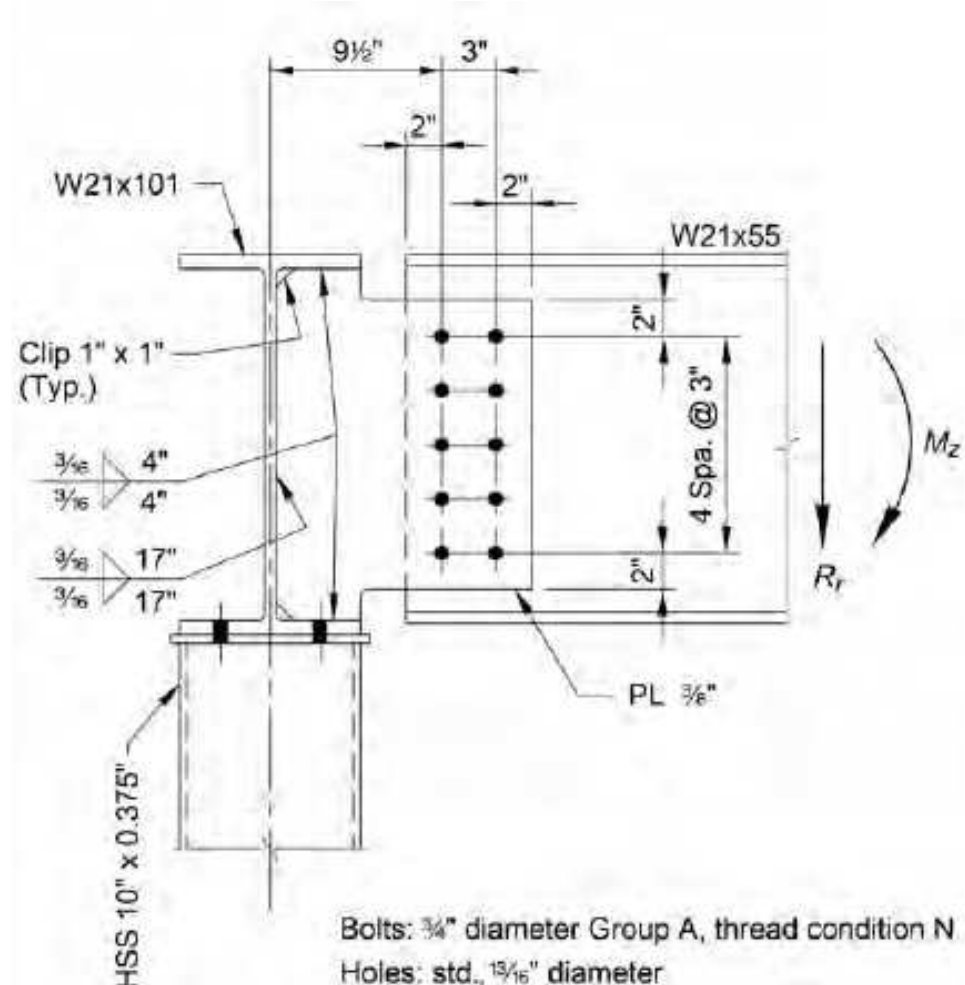


Fig. 8-10. Connection at continuous support for Example 8.2.

The available strength of the bolt group is determined using the instantaneous center of rotation method. Eccentricity of loading on the bolt group is determined as follows:

LRFD	ASD
$e_x = e + \frac{M_{uz}}{R_u}$ $= 11 \text{ in.} + \frac{80.5 \text{ kip-in.}}{30 \text{ kips}}$ $= 13.7 \text{ in.}$	$e_x = e + \frac{M_{az}}{R_a}$ $= 11 \text{ in.} + \frac{53.6 \text{ kip-in.}}{20 \text{ kips}}$ $= 13.7 \text{ in.}$

Interpolating from AISC *Manual* Table 7-7, with  $e_x = 13.7$  in.,  $s = 3$  in.,  $n = 5$  and Angle =  $0^\circ$ :

$$C = 2.68$$

The available strength of the bolt group is determined as follows:

LRFD	ASD
$\phi R_n = C \phi r_n$ $= (2.68)(17.9 \text{ kips/bolt})$ $= 48.0 \text{ kips} > 30 \text{ kips} \quad \text{o.k.}$	$\frac{R_n}{\Omega} = C \frac{r_n}{\Omega}$ $= (2.68)(11.9 \text{ kips/bolt})$ $= 31.9 \text{ kips} > 20 \text{ kips} \quad \text{o.k.}$

#### Bolt bearing and tearout at plate

The nominal bearing strength of the plate is determined from AISC *Specification* Section J3.10, assuming deformation at service load is a design consideration:

$$\begin{aligned}
 r_n &= 2.4dtF_u && \text{(Spec. Eq. J3-6a)} \\
 &= 2.4(\frac{3}{4} \text{ in.})(\frac{3}{8} \text{ in.})(58 \text{ ksi}) \\
 &= 39.2 \text{ kips/bolt}
 \end{aligned}$$

The nominal tearout strength of the plate is determined from AISC *Specification* Section J3.10, assuming deformation at service load is a design consideration. The clear distance from the edge of the hole to the edge of the plate is:

$$\begin{aligned}
 l_c &= l_e - \frac{d_b}{2} \\
 &= 2.00 \text{ in.} - \frac{\frac{13}{16} \text{ in.}}{2} \\
 &= 1.59 \text{ in.}
 \end{aligned}$$

$$\begin{aligned}
 r_n &= 1.2l_c t F_u && \text{(Spec. Eq. J3-6c)} \\
 &= 1.2(1.59 \text{ in.})(\frac{3}{8} \text{ in.})(58 \text{ ksi}) \\
 &= 41.5 \text{ kips/bolt}
 \end{aligned}$$

Therefore, bearing controls over tearout for the plate. The available bolt bearing strength is:

LRFD	ASD
$\phi R_n = C \phi r_n$ $= (2.68)(0.75)(39.2 \text{ kips/bolt})$ $= 78.8 \text{ kips} > 30 \text{ kips} \quad \text{o.k.}$	$\frac{R_n}{\Omega} = C \frac{r_n}{\Omega}$ $= (2.68) \left( \frac{39.2 \text{ kips/bolt}}{2.00} \right)$ $= 52.5 \text{ kips} > 20 \text{ kips} \quad \text{o.k.}$

### Bolt bearing and tearout at W21 beam web

The nominal bearing strength of the beam web is determined from AISC *Specification* Section J3.10, assuming deformation at service load is a design consideration:

$$\begin{aligned} r_n &= 2.4dtF_u \\ &= 2.4(\frac{3}{4} \text{ in.})(0.375 \text{ in.})(65 \text{ ksi}) \\ &= 43.9 \text{ kips/bolt} \end{aligned} \quad (\text{Spec. Eq. J3-6a})$$

The nominal tearout strength of the beam web is determined from AISC *Specification* Section J3.10, assuming deformation at service load is a design consideration. The clear distance from the edge of the hole to the edge of the web, including a  $\frac{1}{4}$ -in. tolerance to account for possible beam underrun, is:

$$\begin{aligned} l_c &= l_e - \frac{1}{4} \text{ in.} - \frac{d_b}{2} \\ &= 2.00 \text{ in.} - \frac{1}{4} \text{ in.} - \frac{\frac{13}{16} \text{ in.}}{2} \\ &= 1.34 \text{ in.} \end{aligned}$$

$$\begin{aligned} r_n &= 1.2l_c t F_u \\ &= 1.2(1.34 \text{ in.})(0.375 \text{ in.})(65 \text{ ksi}) \\ &= 39.2 \text{ kips/bolt} \end{aligned} \quad (\text{Spec. Eq. J3-6c})$$

Therefore, tearout controls over bearing for the beam web. The available bolt tearout strength is:

LRFD	ASD
$\begin{aligned} \phi R_n &= C\phi r_n \\ &= (2.68)(0.75)(39.2 \text{ kips/bolt}) \\ &= 78.8 \text{ kips} > 30 \text{ kips} \quad \text{o.k.} \end{aligned}$	$\begin{aligned} \frac{R_n}{\Omega} &= C \frac{r_n}{\Omega} \\ &= (2.68) \left( \frac{39.2 \text{ kips/bolt}}{2.00} \right) \\ &= 52.5 \text{ kips} > 20 \text{ kips} \quad \text{o.k.} \end{aligned}$

### W21x101 Web-to-plate weld

The available weld strength for a  $\frac{3}{16}$ -in., 17-in.-long weld is determined using AISC *Manual* Equation 8-2a or 8-2b.

LRFD	ASD
$\begin{aligned} \phi R_n &= (1.392 \text{ kip/in.}) D l (2 \text{ sides}) \\ &= (1.392 \text{ kip/in.})(3)(17.0 \text{ in.})(2 \text{ sides}) \\ &= 142 \text{ kips} > 30 \text{ kips} \quad \text{o.k.} \end{aligned}$	$\begin{aligned} \frac{R_n}{\Omega} &= (0.928 \text{ kip/in.}) D l (2 \text{ sides}) \\ &= (0.928 \text{ kip/in.})(3)(17.0 \text{ in.})(2 \text{ sides}) \\ &= 94.7 \text{ kips} > 20 \text{ kips} \quad \text{o.k.} \end{aligned}$

### W21x101 Web rupture at weld

The required thickness of the beam web to match the shear rupture strength of the weld is determined from AISC *Manual* Equation 9-2:

$$\begin{aligned} t_{min} &= \frac{3.09D}{F_u} \\ &= \frac{(3.09)(3)}{65 \text{ ksi}} \\ &= 0.143 \text{ in.} < 0.500 \text{ in.} \quad \text{o.k.} \end{aligned} \quad (\text{AISC Manual Eq. 9-2})$$

### W21x101 Flange-to-plate weld

The available weld strength for a  $\frac{3}{16}$ -in., 4-in.-long weld is determined using AISC *Manual* Equation 8-2a or 8-2b.

LRFD	ASD
$\begin{aligned}\phi R_n &= (1.392 \text{ kip/in.}) D l (2 \text{ sides}) \\ &= (1.392 \text{ kip/in.})(3)(4.00 \text{ in.})(2 \text{ sides}) \\ &= 33.4 \text{ kips} > 3.91 \text{ kips} \quad \text{o.k.}\end{aligned}$	$\begin{aligned}\frac{R_n}{\Omega} &= (0.928 \text{ kip/in.}) D l (2 \text{ sides}) \\ &= (0.928 \text{ kip/in.})(3)(4.00 \text{ in.})(2 \text{ sides}) \\ &= 22.3 \text{ kips} > 2.60 \text{ kips} \quad \text{o.k.}\end{aligned}$

### W21x101 Flange rupture at weld

The required thickness of the beam flange to match the shear rupture strength of the weld is determined from AISC *Manual* Equation 9-2:

$$\begin{aligned}t_{min} &= \frac{3.09D}{F_u} && \text{(AISC Manual Eq. 9-2)} \\ &= \frac{(3.09)(3)}{65 \text{ ksi}} \\ &= 0.143 \text{ in.} < 0.800 \text{ in.} \quad \text{o.k.}\end{aligned}$$

### Plate rupture at weld

The required thickness of the plate to match the shear rupture strength of the weld is determined from AISC *Manual* Equation 9-3:

$$\begin{aligned}t_{min} &= \frac{6.19D}{F_u} && \text{(AISC Manual Eq. 9-3)} \\ &= \frac{(6.19)(3)}{58 \text{ ksi}} \\ &= 0.320 \text{ in.} < \frac{3}{8} \text{ in.} \quad \text{o.k.}\end{aligned}$$

### Plate shear yielding

The available shear yielding strength of the plate is determined using AISC *Specification* Section J4.2.

$$\begin{aligned}A_{gv} &= l t_p \\ &= (16.0 \text{ in.})(\frac{3}{8} \text{ in.}) \\ &= 6.00 \text{ in.}^2\end{aligned}$$

$$\begin{aligned}R_n &= 0.60 F_y A_{gv} && \text{(Spec. Eq. J4-3)} \\ &= 0.60(36 \text{ ksi})(6.00 \text{ in.}^2) \\ &= 130 \text{ kips}\end{aligned}$$

LRFD	ASD
$\begin{aligned}\phi R_n &= 1.00(130 \text{ kips}) \\ &= 130 \text{ kips} > 30 \text{ kips} \quad \text{o.k.}\end{aligned}$	$\begin{aligned}\frac{R_n}{\Omega} &= \frac{130 \text{ kips}}{1.50} \\ &= 86.7 \text{ kips} > 20 \text{ kips} \quad \text{o.k.}\end{aligned}$

### Plate shear rupture

The available shear rupture strength of the plate is determined using AISC *Specification* Section J4.2.

$$\begin{aligned} A_{nv} &= [l - n(d_h + \frac{1}{16} \text{ in.})]t_p \\ &= [16.0 \text{ in.} - (5)(\frac{13}{16} \text{ in.} + \frac{1}{16} \text{ in.})](\frac{3}{8} \text{ in.}) \\ &= 4.36 \text{ in.}^2 \end{aligned}$$

$$\begin{aligned} R_n &= 0.60F_u A_{nv} && (\text{Spec. Eq. J4-3}) \\ &= 0.60(58 \text{ ksi})(4.36 \text{ in.}^2) \\ &= 152 \text{ kips} \end{aligned}$$

LRFD	ASD
$\phi R_n = 0.75(152 \text{ kips})$ $= 114 \text{ kips} > 30 \text{ kips} \quad \text{o.k.}$	$\frac{R_n}{\Omega} = \frac{152 \text{ kips}}{2.00}$ $= 76.0 \text{ kips} > 20 \text{ kips} \quad \text{o.k.}$

### Plate flexural yielding

The available flexural strength of the plate is checked for the applicable limit states of flexural yielding and flexural rupture as stipulated in AISC *Specification* Section J4.5.

The gross plastic modulus of the plate,  $Z_g$ , is:

$$\begin{aligned} Z_g &= \frac{(\frac{3}{8} \text{ in.})(16.0 \text{ in.})^2}{4} \\ &= 24.0 \text{ in.}^3 \end{aligned}$$

The nominal strength of the plate,  $M_n$ , is:

$$\begin{aligned} M_n &= F_y Z_g \\ &= (36 \text{ ksi})(24.0 \text{ in.}^3) \\ &= 864 \text{ kip-in.} \end{aligned}$$

And the available strength of the plate is:

LRFD	ASD
$\phi M_n = 0.90(864 \text{ kip-in.})$ $= 778 \text{ kip-in.}$  $M_u = R_u e_g + M_{uz}$ $= (30 \text{ kips})(9.50 \text{ in.}) + 80.5 \text{ kip-in.}$ $= 366 \text{ kip-in.} < 778 \text{ kip-in.} \quad \text{o.k.}$	$\frac{M_n}{\Omega} = \frac{864 \text{ kip-in.}}{1.67}$ $= 517 \text{ kip-in.}$  $M_a = R_a e_g + M_{az}$ $= (20 \text{ kips})(9.50 \text{ in.}) + 53.6 \text{ kip-in.}$ $= 244 \text{ kip-in.} < 517 \text{ kip-in.} \quad \text{o.k.}$

### Plate flexural rupture

The net plastic modulus of the plate,  $Z_n$ , is:

$$\begin{aligned} Z_n &= Z_g - t d'_h \sum y_i \\ &= 24.0 \text{ in.}^3 - (\frac{3}{8} \text{ in.})(\frac{13}{16} \text{ in.} + \frac{1}{16} \text{ in.})[(2)(3 \text{ in.} + 6 \text{ in.})] \\ &= 18.1 \text{ in.}^3 \end{aligned}$$

The nominal strength of the plate,  $M_n$ , is:

$$\begin{aligned} M_n &= F_u Z_n \\ &= (58 \text{ ksi})(18.1 \text{ in.}^3) \\ &= 1,050 \text{ kip-in.} \end{aligned}$$

And the available strength of the plate is:

LRFD	ASD
$\phi M_n = 0.75(1,050 \text{ kip-in.})$ $= 788 \text{ kip-in.}$	$\frac{M_n}{\Omega} = \frac{1,050 \text{ kip-in.}}{2.00}$ $= 525 \text{ kip-in.}$
$M_u = R_u e_g + M_{uz}$ $= (30 \text{ kips})(9.50 \text{ in.}) + 80.5 \text{ kip-in.}$ $= 366 \text{ kip-in.} < 788 \text{ kip-in.} \quad \text{o.k.}$	$M_a = R_a e_g + M_{az}$ $= (20 \text{ kips})(9.50 \text{ in.}) + 53.6 \text{ kip-in.}$ $= 244 \text{ kip-in.} < 525 \text{ kip-in.} \quad \text{o.k.}$

#### Plate block shear rupture

From AISC Specification Section J4.3, the block shear rupture strength of the plate is:

$$R_n = 0.6F_u A_{nv} + U_{bs}F_u A_{nt} \leq 0.6F_y A_{gv} + U_{bs}F_u A_{nt} \quad (\text{Spec. Eq. J4-5})$$

where

$$\begin{aligned} A_{gv} &= (\frac{3}{8} \text{ in.})(14 \text{ in.}) \\ &= 5.25 \text{ in.}^2 \end{aligned}$$

$$\begin{aligned} A_{nv} &= (\frac{3}{8} \text{ in.})[14 \text{ in.} - (4.5)(\frac{13}{16} \text{ in.} + \frac{1}{16} \text{ in.})] \\ &= 3.77 \text{ in.}^2 \end{aligned}$$

$$\begin{aligned} A_{nt} &= (\frac{3}{8} \text{ in.})[5 \text{ in.} - (1.5)(\frac{13}{16} \text{ in.} + \frac{1}{16} \text{ in.})] \\ &= 1.38 \text{ in.}^2 \end{aligned}$$

$$U_{bs} = 0.5$$

and then

$$\begin{aligned} R_n &= 0.6(65 \text{ ksi})(3.77 \text{ in.}^2) + 0.5(65 \text{ ksi})(1.38 \text{ in.}^2) \leq 0.6(36 \text{ ksi})(5.25 \text{ in.}^2) + 0.5(65 \text{ ksi})(1.38 \text{ in.}^2) \\ &= 192 \text{ kips} > 158 \text{ kips} \end{aligned}$$

Therefore,  $R_n = 158$  kips.

LRFD	ASD
$\phi = 0.75$ $\phi R_n = 0.75(158 \text{ kips})$ $= 119 \text{ kips} > 30 \text{ kips} \quad \text{o.k.}$	$\Omega = 2.00$ $\frac{R_n}{\Omega} = \frac{158 \text{ kips}}{2.00}$ $= 79.0 \text{ kips} > 20 \text{ kips} \quad \text{o.k.}$

#### Interaction of plate shear yielding and flexural yielding

From AISC Manual Part 10, the plate is checked for the interaction of shear yielding and flexural yielding.

$$\left(\frac{V_r}{V_c}\right)^2 + \left(\frac{M_r}{M_c}\right)^2 \leq 1.0 \quad (\text{Manual Eq. 10-5})$$

LRFD	ASD
<p>From the problem statement and the preceding calculations:</p> $V_r = R_u$ $= 30 \text{ kips}$ $V_c = \phi R_n$ $= 130 \text{ kips}$ $M_r = M_u$ $= 366 \text{ kip-in.}$ $M_c = \phi M_n$ $= 778 \text{ kip-in.}$ $\left(\frac{30 \text{ kips}}{130 \text{ kips}}\right)^2 + \left(\frac{366 \text{ kip-in.}}{778 \text{ kip-in.}}\right)^2 = 0.275 < 1.0 \quad \text{o.k.}$	<p>From the problem statement and the preceding calculations:</p> $V_r = R_a$ $= 20 \text{ kips}$ $V_c = \frac{R_n}{\Omega}$ $= 86.7 \text{ kips}$ $M_r = M_a$ $= 244 \text{ kip-in.}$ $M_c = \frac{M_n}{\Omega}$ $= 517 \text{ kip-in.}$ $\left(\frac{20 \text{ kips}}{86.7 \text{ kips}}\right)^2 + \left(\frac{244 \text{ kip-in.}}{517 \text{ kip-in.}}\right)^2 = 0.276 < 1.0 \quad \text{o.k.}$

#### Finite element models

The curved beam was modeled with both two- and three-dimensional finite element models, as described in Section 7.3.1. Both models were analyzed with a first-order analysis. The three-dimensional model was also analyzed with a second-order geometrically nonlinear analysis. Each model was loaded using both Case 1 and Case 2. Each span was modeled using 10 straight segments with a 4.5° arc between nodes.

For the two-dimensional analysis, the curved member was modeled with 10 beam elements per span. The beam was analyzed with both the actual torsional constant,  $J$ , and the equivalent torsional constant,  $J_e$ , which was calculated with Equations 7-6 and 7-7.

$$\gamma = L_{db} \sqrt{\frac{GJ}{EC_w}}$$

$$= (283 \text{ in.}) \sqrt{\frac{(11,200 \text{ ksi})(5.21 \text{ in.}^4)}{(29,000 \text{ ksi})(26,200 \text{ in.}^6)}}$$

$$= 2.48$$
(7-7)

$$J_e = \frac{J}{1 - \frac{\sinh \gamma}{\gamma \cosh \gamma}}$$

$$= \frac{5.21 \text{ in.}^4}{1 - \frac{\sinh(2.48)}{(2.48)\cosh(2.48)}}$$

$$= 8.65 \text{ in.}^4$$
(7-6)

For the three-dimensional analysis, the curved member was modeled with 10 rectangular beam elements per span at each flange and 10 plate elements at the web.

The maximum deformations occurred for Load Case 2, near the middle of the loaded span. Table 8-6 summarizes the maximum service-load vertical deflections,  $\Delta_s$ , and torsional rotations,  $\theta_s$ , for all cases. For the two-dimensional models, the use of  $J_e$  in lieu of  $J$  increased the accuracy; however, both of the two-dimensional models produced conservative deformations. The rotation calculated with the  $M/R$  method is in close agreement with the results of the three-dimensional finite element models. The

Table 8-6. Serviceability Deflections and Rotations		
	$\Delta_s$	$\theta_s$
M/R method	—	2.31°
2-D FE model using $J$	2.39 in.	6.07°
2-D FE model using $J_e$	1.46 in.	3.72°
3-D first-order FE model	0.915 in.	2.24°
3-D second-order FE model	0.939 in.	2.37°

second-order analysis resulted in a 3% increase in the vertical deflection and a 6% increase in the torsional rotation.

### Example 8.3—Horizontally Curved, Simply Supported Member

**Given:**

The horizontally curved W21x83 beams in Figure 8-11 form a circular curve with a 30-ft radius and a span angle of 30° between the columns. The member ends are restrained against torsional rotation but flexural and warping restraint is not provided. The service-load midspan rotation is limited to a maximum of 2°. Verify that the curved beam is adequate for the imposed loads. The uniformly distributed load along the member circumference including the beam self-weight, is:

LRFD	ASD
$w_u = 1.50 \text{ kip/ft}$	$w_a = 1.00 \text{ kip/ft}$

W-shape member material: ASTM A992

**Solution:**

From AISC *Manual* Tables 2-4, the material properties are as follows:

ASTM A992

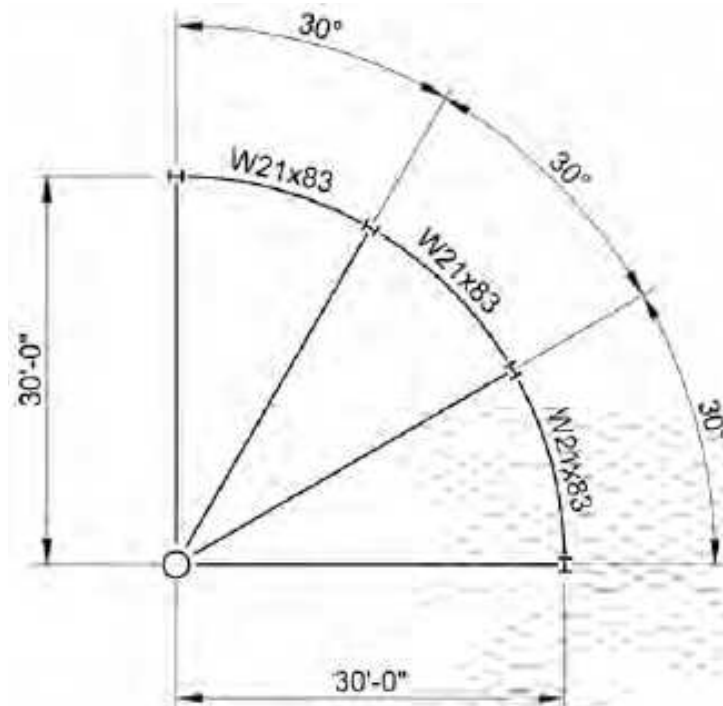


Fig. 8-11. Horizontally curved member for Example 8.3.

$$F_y = 50 \text{ ksi}$$

$$F_u = 65 \text{ ksi}$$

From AISC *Manual* Table 1-1, the geometric properties are as follows:

Beam

W21x83

$$\begin{aligned} d &= 21.4 \text{ in.} & t_w &= 0.515 \text{ in.} & b_f &= 8.36 \text{ in.} & t_f &= 0.835 \text{ in.} \\ b_f/2t_f &= 5.00 & h/t_w &= 36.4 & I_x &= 1,830 \text{ in.}^4 & S_x &= 171 \text{ in.}^3 \\ Z_x &= 196 \text{ in.}^3 & r_{ts} &= 2.21 \text{ in.} & h_o &= 20.6 \text{ in.} & J &= 4.34 \text{ in.}^4 \\ C_w &= 8,630 \text{ in.}^6 \end{aligned}$$

Additional properties from AISC Design Guide 9 (Seaburg and Carter, 1997) Appendix A, are as follows:

Beam

W21x83

$$\begin{aligned} a &= 71.8 \text{ in.} & W_{no} &= 43.0 \text{ in.}^2 & S_{w1} &= 75.0 \text{ in.}^4 & Q_f &= 34.2 \text{ in.}^3 \\ Q_w &= 98.0 \text{ in.}^3 \end{aligned}$$

### Beam Geometry

Radius:

$$\begin{aligned} R &= (30 \text{ ft})(12 \text{ in./ft}) \\ &= 360 \text{ in.} \end{aligned}$$

Span angle:

$$\begin{aligned} \theta_s &= (30^\circ) \left( \frac{\pi \text{ rad}}{180^\circ} \right) \\ &= \frac{\pi}{6} \text{ rad} \end{aligned}$$

Angle between torsional restraints:

$$\begin{aligned} \theta_b &= (30^\circ) \left( \frac{\pi \text{ rad}}{180^\circ} \right) \\ &= \frac{\pi}{6} \text{ rad} \end{aligned}$$

Developed span length:

$$\begin{aligned} L_{ds} &= (30 \text{ ft}) \left( \frac{\pi}{6} \text{ rad} \right) (12 \text{ in./ft}) \\ &= 188 \text{ in.} \end{aligned}$$

Developed length between braces:

$$\begin{aligned} L_{dd} &= (30 \text{ ft}) \left( \frac{\pi}{6} \text{ rad} \right) (12 \text{ in./ft}) \\ &= 188 \text{ in.} \end{aligned}$$

### Flexural Loads

For a simply supported uniformly loaded beam corresponding to AISC *Manual* Table 3-23, Case 1, the maximum moment, at the midspan, is:

LRFD	ASD
$\begin{aligned} M_{ux} &= \frac{w_u L_{ds}^2}{8} \\ &= \frac{(1.50 \text{ kip/ft})(188 \text{ in.})^2}{8(12 \text{ in./ft})} \\ &= 552 \text{ kip-in.} \end{aligned}$	$\begin{aligned} M_{ax} &= \frac{w_a L_{ds}^2}{8} \\ &= \frac{(1.00 \text{ kip/ft})(188 \text{ in.})^2}{8(12 \text{ in./ft})} \\ &= 368 \text{ kip-in.} \end{aligned}$

The maximum shear force, which occurs at the supports, is:

LRFD	ASD
$V_u = \frac{w_u L_{ds}}{2}$ $= \frac{(1.50 \text{ kip/ft})(188 \text{ in.})}{2(12 \text{ in./ft})}$ $= 11.8 \text{ kips}$	$V_a = \frac{w_a L_{ds}}{2}$ $= \frac{(1.00 \text{ kip/ft})(188 \text{ in.})}{2(12 \text{ in./ft})}$ $= 7.83 \text{ kips}$

### Shear Strength

The available shear strength is determined using AISC *Specification* Section G2.1.

$$2.24 \sqrt{\frac{E}{F_y}} = 2.24 \sqrt{\frac{29,000 \text{ ksi}}{50 \text{ ksi}}} = 53.9$$

$$h/t_w = 36.4$$

Because  $h/t_w < 2.24 \sqrt{\frac{E}{F_y}}$ :

$$C_{v1} = 1.0$$

(*Spec. Eq. G2-2*)

The area of the web,  $A_w$ , is:

$$A_w = dt_w$$

$$= (21.4 \text{ in.})(0.515 \text{ in.})$$

$$= 11.0 \text{ in.}^2$$

The nominal shear strength,  $V_n$ , is:

$$V_n = 0.6F_y A_w C_{v1} \quad (\text{Spec. Eq. G2-1})$$

$$= 0.6(50 \text{ ksi})(11.0 \text{ in.}^2)(1.0)$$

$$= 330 \text{ kips}$$

And the available shear strength is:

LRFD	ASD
$\phi_v V_n = 1.00(330 \text{ kips})$ $= 330 \text{ kips} > 11.8 \text{ kips} \quad \text{o.k.}$	$\frac{V_n}{\Omega_v} = \frac{330 \text{ kips}}{1.50}$ $= 220 \text{ kips} > 7.83 \text{ kips} \quad \text{o.k.}$

### Flexural Strength

The available flexural strength of the curved beam is determined using AISC *Specification* Section F2.

### Local buckling

$$\lambda_f = \frac{b_f}{2t_f}$$

$$= 5.00$$

$$\lambda_w = \frac{h}{t_w} = 36.4$$

From AISC *Specification* Table B4.1b, the limiting width-to-thickness ratios are:

$$\begin{aligned}\lambda_{pf} &= 0.38 \sqrt{\frac{E}{F_y}} \\ &= 0.38 \sqrt{\frac{29,000 \text{ ksi}}{50 \text{ ksi}}} \\ &= 9.15\end{aligned}$$

$$\begin{aligned}\lambda_{pw} &= 3.76 \sqrt{\frac{E}{F_y}} \\ &= 3.76 \sqrt{\frac{29,000 \text{ ksi}}{50 \text{ ksi}}} \\ &= 90.6\end{aligned}$$

Because  $\lambda_f < \lambda_{pf}$  and  $\lambda_w < \lambda_{pw}$ , the section is compact.

#### Lateral-torsional buckling

$$\begin{aligned}M_p &= F_y F_z && (\text{Spec. Eq. F2-1}) \\ &= (50 \text{ ksi})(196 \text{ in.}^3) \\ &= 9,800 \text{ kip-in.}\end{aligned}$$

Using Equation 7-24 with  $C_{bs} = 1.0$ :

$$\begin{aligned}C_{bo} &= C_{bs} \left[ 1 - \left( \frac{\theta_b}{\pi} \right)^2 \right]^2 \\ &= (1.0) \left[ 1 - \left( \frac{\pi/6}{\pi} \right)^2 \right]^2 \\ &= 0.945\end{aligned} \tag{7-24}$$

Using AISC *Specification* Section F2 with  $L_b = L_{db} = (188 \text{ in.})/(12 \text{ in./ft}) = 15.7 \text{ ft}$  and  $C_b = C_{bo} = 0.945$ . From AISC *Manual* Table 3-6, for a W21x83:

$$\begin{aligned}L_p &= 6.46 \text{ ft} \\ L_r &= 20.2 \text{ ft}\end{aligned}$$

Because  $L_p < L_b < L_r$ , AISC *Specification* Equation F2-2 is used to determine the nominal flexural strength,  $M_n$ :

$$\begin{aligned}M_n &= C_b \left[ M_p - (M_p - 0.7F_yS_x) \left( \frac{L_b - L_p}{L_r - L_p} \right) \right] \leq M_p && (\text{Spec. Eq. F2-2}) \\ &= (0.945) \left\{ 9,800 \text{ kip-in.} - \left[ 9,800 \text{ kip-in.} - (0.7)(50 \text{ ksi})(171 \text{ in.}^3) \right] \left( \frac{15.7 \text{ ft} - 6.46 \text{ ft}}{20.2 \text{ ft} - 6.46 \text{ ft}} \right) \right\} \leq 9,800 \text{ kip-in.} \\ &= 6,840 \text{ kip-in.} < 9,800 \text{ kip-in.}\end{aligned}$$

Therefore, the nominal flexural strength is:

$$M_n = 6,840 \text{ kip-in.}$$

And the available out-of-plane flexural strength is:

LRFD	ASD
$M_{co} = \phi M_n$ $= 0.90(6,840 \text{ kip-in.})$ $= 6,160 \text{ kip-in.}$	$M_{co} = \frac{M_n}{\Omega}$ $= \frac{6,840 \text{ kip-in.}}{1.67}$ $= 4,100 \text{ kip-in.}$

### Second-order effects

The elastic critical out-of-plane lateral-torsional buckling moment,  $M_{eo}$ , is calculated with  $F_{cr}$  from AISC Specification Equation F2-4 with  $c = 1$ :

$$F_{cr} = \frac{C_b \pi^2 E}{\left(\frac{L_b}{r_{ts}}\right)^2} \sqrt{1 + 0.078 \frac{J_c}{S_x h_o} \left(\frac{L_b}{r_{ts}}\right)^2}$$

$$= \frac{(0.945) \pi^2 (29,000 \text{ ksi})}{\left(\frac{188 \text{ in.}}{2.21 \text{ in.}}\right)^2} \sqrt{1 + 0.078 \frac{(4.34 \text{ in.}^4)(1)}{(171 \text{ in.}^3)(20.6 \text{ in.})} \left(\frac{188 \text{ in.}}{2.21 \text{ in.}}\right)^2}$$

$$= 48.7 \text{ ksi}$$

$$M_{eo} = F_{cr} S_x$$

$$= (48.7 \text{ ksi})(171 \text{ in.}^3)$$

$$= 8,330 \text{ kip-in.}$$

The second-order amplification factor,  $B_o$ , is calculated using Equation 7-37 with  $M_{ro} = M_{cx}$ .

LRFD	ASD
$\alpha = 1.0$ $B_o = \frac{0.85}{1 - \alpha \left( \frac{M_{ux}}{M_{eo}} \right)} \geq 1.0$ $= \frac{0.85}{1 - (1.0) \left( \frac{552 \text{ kip-in.}}{8,330 \text{ kip-in.}} \right)} \geq 1.0$ $= 0.910 < 1.0$ <p>Therefore, <math>B_o = 1.0</math></p>	$\alpha = 1.6$ $B_o = \frac{0.85}{1 - \alpha \left( \frac{M_{ax}}{M_{eo}} \right)} \geq 1.0$ $= \frac{0.85}{1 - (1.6) \left( \frac{368 \text{ kip-in.}}{8,330 \text{ kip-in.}} \right)} \geq 1.0$ $= 0.915 < 1.0$ <p>Therefore, <math>B_o = 1.0</math></p>

### Flexural stresses

The maximum normal stress is:

LRFD	ASD
$\sigma_{uo} = \frac{M_{ux}}{S_x}$ $= \frac{552 \text{ kip-in.}}{171 \text{ in.}^3}$ $= 3.23 \text{ ksi}$	$\sigma_{ao} = \frac{M_{ax}}{S_x}$ $= \frac{368 \text{ kip-in.}}{171 \text{ in.}^3}$ $= 2.15 \text{ ksi}$

The maximum shear stress at the web is:

LRFD	ASD
$\tau_{buw} = \frac{V_u Q_w}{I_x t_w}$ $= \frac{(11.8 \text{ kips})(98.0 \text{ in.}^3)}{(1,830 \text{ in.}^4)(0.515 \text{ in.})}$ $= 1.23 \text{ ksi}$	$\tau_{baw} = \frac{V_a Q_w}{I_x t_w}$ $= \frac{(7.83 \text{ kips})(98.0 \text{ in.}^3)}{(1,830 \text{ in.}^4)(0.515 \text{ in.})}$ $= 0.814 \text{ ksi}$

The maximum shear stress at the flanges is:

LRFD	ASD
$\tau_{buf} = \frac{V_u Q_f}{I_x t_f}$ $= \frac{(11.8 \text{ kips})(34.2 \text{ in.}^3)}{(1,830 \text{ in.}^4)(0.835 \text{ in.})}$ $= 0.264 \text{ ksi}$	$\tau_{baf} = \frac{V_a Q_f}{I_x t_f}$ $= \frac{(7.83 \text{ kips})(34.2 \text{ in.}^3)}{(1,830 \text{ in.}^4)(0.835 \text{ in.})}$ $= 0.175 \text{ ksi}$

### Torsional Loads

Torsional loads are calculated using the eccentric load method discussed in Section 7.3.3. The equivalent eccentricity is calculated using Equation 7-20:

$$\begin{aligned}
 e_w &= R \left[ \cos\left(\frac{\theta_s}{4}\right) - \cos\left(\frac{\theta_s}{2}\right) \right] & (7-20) \\
 &= (30 \text{ ft}) \left[ \cos\left(\frac{\pi/6}{4}\right) - \cos\left(\frac{\pi/6}{2}\right) \right] \\
 &= 0.766 \text{ ft}
 \end{aligned}$$

Combining Equations 7-21 and 7-36, the second-order uniformly distributed torsional force is:

LRFD	ASD
$m_{uz} = B_o w_u e_w$ $= (1.0)(1.50 \text{ kip/ft})(0.766 \text{ ft})$ $= 1.15 \text{ kip-ft/ft}$	$m_{az} = B_o w_a e_w$ $= (1.0)(1.00 \text{ kip/ft})(0.766 \text{ ft})$ $= 0.766 \text{ kip-ft/ft}$

The torsional moment at each end is:

LRFD	ASD
$M_{uz} = \frac{(1.15 \text{ kip-ft/ft})(15.7 \text{ ft})}{2}$ $= 9.03 \text{ kip-ft}$	$M_{az} = \frac{(0.766 \text{ kip-ft/ft})(15.7 \text{ ft})}{2}$ $= 6.01 \text{ kip-ft}$

### Torsional functions

The torsional functions are calculated using the equations in Moore and Mueller (2002). These values can also be found using AISC Design Guide 9, Appendix B, Case 4, with  $l/a = L_{ds}/a = 188 \text{ in.}/71.8 \text{ in.} = 2.62$ .

*Midspan*

$$\theta \left( \frac{GJ}{m_{rz}} \frac{1}{2a^2} \right) = 0.180$$

$$\theta' \left( \frac{GJ}{m_{rz}} \frac{L_{ds}}{10a^2} \right) = 0$$

$$\theta'' \left( \frac{GJ}{m_{rz}} \right) = -0.497$$

$$\theta''' \left( \frac{GJ}{m_{rz}} a \right) = 0$$

*Ends*

$$\theta \left( \frac{GJ}{m_{rz}} \frac{1}{2a^2} \right) = 0$$

$$\theta' \left( \frac{GJ}{m_{rz}} \frac{L_{ds}}{10a^2} \right) = \pm 0.117$$

$$\theta'' \left( \frac{GJ}{m_{rz}} \right) = 0$$

$$\theta''' \left( \frac{GJ}{m_{rz}} a \right) = \pm 0.864$$

*Torsional stresses*

*Midspan*

$$\begin{aligned} \theta'' &= (0.497) \left( \frac{m_{rz}}{GJ} \right) \\ &= \frac{0.497 m_{rz}}{GJ} \end{aligned}$$

The warping normal stress at the flanges is:

$$\begin{aligned} \sigma_{rw} &= EW_{no} \theta'' && \text{(AISC Design Guide 9, Eq. 4.3a)} \\ &= EW_{no} \left( \frac{0.497 m_{rz}}{GJ} \right) \\ &= \frac{0.497 EW_{no} m_{rz}}{GJ} \\ &= \frac{0.497 m_{rz} (29,000 \text{ ksi})(43.0 \text{ in.}^2)}{(11,200 \text{ ksi})(4.34 \text{ in.}^4)} \\ &= 12.8 m_{rz} \text{ ksi} \end{aligned}$$

LRFD	ASD
$\sigma_{uw} = 12.8m_{uz}$ $= (12.8)(1.15 \text{ kip-ft/ft})$ $= 14.7 \text{ ksi}$	$\sigma_{aw} = 12.8m_{az}$ $= (12.8)(0.766 \text{ kip-ft/ft})$ $= 9.81 \text{ ksi}$

Ends

$$\theta' = (0.177) \left( \frac{m_{rz}}{GJ} \frac{10a^2}{L_{ds}} \right)$$

$$= \frac{1.77m_{rz}a^2}{GJL_{ds}}$$

The torsional shear stress is:

$$\tau_t = Gt\theta' \quad (\text{AISC Design Guide 9, Eq. 4.1})$$

$$= Gt \left( \frac{1.77m_{rz}a^2}{GJL_{ds}} \right)$$

$$= \frac{1.77tm_{rz}a^2}{JL_{ds}}$$

$$= \frac{1.77tm_{rz}(71.8 \text{ in.})^2}{(4.34 \text{ in.}^4)(188 \text{ in.})}$$

$$= 11.2tm_{rz} \text{ ksi}$$

At the web,  $t = t_w = 0.515 \text{ in.}$

LRFD	ASD
$\tau_{tuw} = 11.2t_w m_{uz}$ $= (11.2)(0.515 \text{ in.})(1.15 \text{ kip-ft/ft})$ $= 6.63 \text{ ksi}$	$\tau_{taw} = 11.2t_w m_{az}$ $= (11.2)(0.515 \text{ in.})(0.766 \text{ kip-ft/ft})$ $= 4.42 \text{ ksi}$

At the flanges,  $t = t_f = 0.835 \text{ in.}$

LRFD	ASD
$\tau_{tuf} = 11.2t_f m_{uz}$ $= (11.2)(0.835 \text{ in.})(1.15 \text{ kip-ft/ft})$ $= 10.8 \text{ ksi}$	$\tau_{taf} = 11.2t_f m_{az}$ $= (11.2)(0.835 \text{ in.})(0.766 \text{ kip-ft/ft})$ $= 7.16 \text{ ksi}$

$$\theta''' = (0.864) \left( \frac{m_{rz}}{GJa} \right)$$

$$= \frac{0.864m_{rz}}{GJa}$$

The warping shear stress at the flanges is:

$$\begin{aligned}
 \tau_{ws} &= \frac{ES_{w1}\theta'''}{t_f} && \text{(AISC Design Guide 9, Eq. 4.2a)} \\
 &= \frac{ES_{w1}}{t_f} \left( \frac{0.864m_{rz}}{GJa} \right) \\
 &= \frac{0.864ES_{w1}m_{rz}}{GJa t_f} \\
 &= \frac{0.864m_{rz}(29,000 \text{ ksi})(75.0 \text{ in.}^4)}{(11,200 \text{ ksi})(4.34 \text{ in.}^4)(71.8 \text{ in.})(0.835 \text{ in.})} \\
 &= 0.645m_{rz} \text{ ksi}
 \end{aligned}$$

LRFD	ASD
$  \begin{aligned}  \tau_{uws} &= 0.645m_{uz} \\  &= (0.645)(1.15 \text{ kip-ft/ft}) \\  &= 0.742 \text{ ksi}  \end{aligned}  $	$  \begin{aligned}  \tau_{aws} &= 0.645m_{az} \\  &= (0.645)(0.766 \text{ kip-ft/ft}) \\  &= 0.494 \text{ ksi}  \end{aligned}  $

### Combined Stresses

#### Midspan normal stresses at the flanges

The available warping stress is:

LRFD	ASD
$  \begin{aligned}  \sigma_{cw} &= \phi F_y \\  &= 0.90(50 \text{ ksi}) \\  &= 45.0 \text{ ksi}  \end{aligned}  $	$  \begin{aligned}  \sigma_{cw} &= \frac{F_y}{\Omega} \\  &= \frac{50 \text{ ksi}}{1.67} \\  &= 29.9 \text{ ksi}  \end{aligned}  $

The available out-of-plane flexural stress is:

LRFD	ASD
$  \begin{aligned}  \sigma_{co} &= \frac{M_{co}}{S_x} \\  &= \frac{6,160 \text{ kip-in.}}{171 \text{ in.}^3} \\  &= 36.0 \text{ in.}^3  \end{aligned}  $	$  \begin{aligned}  \sigma_{co} &= \frac{M_{co}}{S_x} \\  &= \frac{4,100 \text{ kip-in.}}{171 \text{ in.}^3} \\  &= 24.0 \text{ in.}^3  \end{aligned}  $

The interaction is evaluated according to Equation 7-39:

LRFD	ASD
$  \begin{aligned}  \frac{\sigma_{uo}}{\sigma_{co}} + \frac{16}{27} \frac{\sigma_{uw}}{\sigma_{cw}} &\leq 1.0 \\  \frac{3.25 \text{ ksi}}{36.0 \text{ ksi}} + \left( \frac{16}{27} \right) \left( \frac{14.7 \text{ ksi}}{45.0 \text{ ksi}} \right) &= 0.284 \leq 1.0 \quad \text{o.k.}  \end{aligned}  $	$  \begin{aligned}  \frac{\sigma_{ao}}{\sigma_{co}} + \frac{16}{27} \frac{\sigma_{aw}}{\sigma_{cw}} &\leq 1.0 \\  \frac{2.16 \text{ ksi}}{24.0 \text{ ksi}} + \left( \frac{16}{27} \right) \left( \frac{9.81 \text{ ksi}}{29.9 \text{ ksi}} \right) &= 0.284 \leq 1.0 \quad \text{o.k.}  \end{aligned}  $

*End shear stresses at the web*

The available shear stress is:

LRFD	ASD
$\begin{aligned}\tau_c &= \phi \tau_n \\ &= \phi 0.6 F_y \\ &= (1.00)(0.6)(50 \text{ ksi}) \\ &= 30.0 \text{ ksi}\end{aligned}$	$\begin{aligned}\tau_c &= \frac{\tau_n}{\Omega} \\ &= \frac{0.6 F_y}{1.50} \\ &= \frac{(0.6)(50 \text{ ksi})}{1.50} \\ &= 20.0 \text{ ksi}\end{aligned}$

The total shear stress in the web is:

LRFD	ASD
$\begin{aligned}\tau_{uw} &= \tau_{buw} + \tau_{tuw} \\ &= 1.23 \text{ ksi} + 6.63 \text{ ksi} \\ &= 7.86 \text{ ksi} < 30.0 \text{ ksi} \quad \text{o.k.}\end{aligned}$	$\begin{aligned}\tau_{aw} &= \tau_{baw} + \tau_{taw} \\ &= 0.816 \text{ ksi} + 4.42 \text{ ksi} \\ &= 5.24 \text{ ksi} < 20.0 \text{ ksi} \quad \text{o.k.}\end{aligned}$

*End shear stresses at the flanges*

The total shear stress in the flanges is:

LRFD	ASD
$\begin{aligned}\tau_{uf} &= \tau_{buf} + \tau_{tuf} + \tau_{uws} \\ &= 0.264 \text{ ksi} + 10.8 \text{ ksi} + 0.742 \text{ ksi} \\ &= 11.8 \text{ ksi} < 30.0 \text{ ksi} \quad \text{o.k.}\end{aligned}$	$\begin{aligned}\tau_{af} &= \tau_{baf} + \tau_{taf} + \tau_{aws} \\ &= 0.176 \text{ ksi} + 7.16 \text{ ksi} + 0.494 \text{ ksi} \\ &= 7.83 \text{ ksi} < 20.0 \text{ ksi} \quad \text{o.k.}\end{aligned}$

*Serviceability*

As discussed in Section 7.7, serviceability evaluations should be based on a first-yield criterion.

$$\begin{aligned}\sigma &= \sigma_{aw} + \sigma_{ao} \\ &= 9.81 \text{ ksi} + 2.16 \text{ ksi} \\ &= 12.0 \text{ ksi} < 50 \text{ ksi} \quad \text{o.k.}\end{aligned}$$

The midspan service-load torsional rotation is:

$$\begin{aligned}\theta &= (0.180) \left( \frac{m_{az}}{GJ} 2a^2 \right) \\ &= (0.180) \left[ \frac{(0.766 \text{ kip-ft/ft})}{(11,200 \text{ ksi})(4.34 \text{ in.}^4)} (2)(71.8 \text{ in.})^2 \right] \left( \frac{1^\circ}{0.017453 \text{ rad}} \right) \\ &= 1.67^\circ < 2^\circ \quad \text{o.k.}\end{aligned}$$

# Glossary

*Arc.* Part of the circumference of a curve. The curved portion of a bend.

*Arc length.* The curved distance along a circumferential line. The length of the curved portion of a member.

*Bend radius.* The radius of curvature, measured to a reference point on the cross section.

*Center-to-center.* The distance between tangent points of two adjoining bends.

*Chord.* The straight distance between two points on a curve.

*Cold bending.* Any bending process where curvature is induced by load application at room temperature.

*Compound bend.* A curve made up of two or more arcs in the same plane, joined tangentially without reversal of curvature.

*Degree of bend.* The angle to which a bend is formed.

*Distortion.* A deviation from the original cross-sectional shape.

*Ductility.* The ability of the material to deform without fracture.

*Easy way.* The orientation of a member where bending occurs about the weak principal axis.

*Gag pressing.* A cold-bending method that uses hydraulic rams to simultaneously apply bending forces at discrete, widely-spaced, locations along the member. Also known as point bending.

*Grip.* An additional straight length at each end of a curved member required in the bending operation. Also known as hold and tail or lead and tail to emphasize the additional length is required at each end of the member.

*Hard way.* The orientation of a member where bending occurs about the strong principal axis.

*Heat curving.* A bending process that relies only on the application of heat in specific patterns to induce curvature.

*Horizontally curved member.* A member with curvature in the horizontal plane.

*Hot bending.* Any bending process where curvature is induced by load application at an elevated temperature.

*In-plane flexure.* Bending of a curved member where moment is applied about the axis of curvature. The primary flexural stresses and deflections are in the plane of curvature.

*Incremental step bending.* A cold-bending method that uses hydraulic rams to apply bending forces at several discrete, closely-spaced, locations along the member.

*Induction bending.* A hot-bending method that utilizes an electric induction coil to heat a short section of the member before it is curved by force.

*Local buckling.* A type of potential cross-sectional distortion that is caused by compression stresses in the member induced during the bending operation. Local buckling can be in the form of a single half-wave or a series of wrinkles along the entire bend length. Also known as waving or wrinkling.

*Mandrel.* A tool that can be inserted into a HSS member to support the walls and minimize cross-sectional distortion during the bending process.

*Multi-axis bend.* A bend with curvature about more than one axis. Also known as a multi-plane bend.

*Normalizing.* A thermal treatment where the member is heated to a suitable temperature above the upper transformation temperature, followed by cooling in still air at room temperature.

*Off-axis bend.* A bending orientation where the member is curved about a non-principal or non-geometric axis. Also known as conical rolling.

*Oil-canning.* A form of local buckling that can cause collapse of the cross section due to the combined effect of ovalization and local buckling in a single half-wave.

*Out-of-plane flexure.* Bending of a curved member where moment is applied in the plane of curvature. The primary flexural stresses and deflections are in perpendicular to the plane of curvature.

*Ovality.* The cross-sectional distortion of a round HSS where the deviation from the theoretical shape forms an oval.

*Pyramid roll bending.* A cold-bending operation where a member is bent progressively by repeatedly passing it through a set of three adjustable rolls in a pyramid arrangement.

*Reverse-compound bend.* A curve made up of two or more arcs in the same plane, joined tangentially with reversal of curvature. Also known as an S-curve or an offset bend.

*Rise.* The distance, perpendicular to the chord, between the mid-point of a chord and an arc. Also known as the mid-ordinate.

*Rotary-draw bending.* A bending method where the member is clamped to a form and bent by rotating it around a bend die.

*Slope.* The angle of an inclined member designated using the vertical (rise) and horizontal (run) distances between two points. Also known as bevel or pitch.

*Snap-through buckling.* A type of instability where the load-displacement diagram descends after reaching a limit point and the structure abruptly transforms from one equilibrium state to another remote equilibrium state on the ascending, stable portion of the curve.

*Spiral.* A three-dimensional curve with an arc in one plane and a constant slope in a perpendicular plane. Also known as a helix or helical curve. The curving process is often called sloped rolling or pitched rolling.

*Springback.* The deformation of a bent member immediately after a bending load is released, where a portion of the curvature is lost.

*Strake.* A protruding fin that can be connected to a structure to improve aerodynamic stability.

*Synchronized incremental cold bending.* A cold-bending process where synchronized forces are applied at several locations along the member.

*Tangent.* A straight line, perpendicular to the radius, which touches a curve at a single point. A straight member adjacent to a curved segment.

*Tangent point.* The start- or end-point of a curve.

*Variable-radius bend.* Parabolic, elliptical and other non-circular bends with variable radii. Also known as multi-radius and a non-circular bends.

*Vertically curved member.* A member with curvature in the vertical plane.

*Waving.* See *Local buckling*.

*Wrinkling.* See *Local buckling*.

*Yield point.* The curvature at which a member will deform permanently during bending.

# Symbols

$A_{fg}$	Gross area of tension flange, in. <sup>2</sup>	$H$	Rise, in.
$A_{fn}$	Net area of tension flange, in. <sup>2</sup>	$H_b$	Rise dimension between the brace points and the apex of the arch segment, in.
$A_w$	Area of web, in. <sup>2</sup>	$I$	Moment of inertia, in. <sup>4</sup>
$B$	Member width perpendicular to the plane of curvature, in.	$I_e$	Effective moment of inertia, in. <sup>4</sup>
$B_i$	In-plane second-order amplification factor	$I_{ei}$	Effective moment of inertia about the axis of curvature, in. <sup>4</sup>
$B_o$	Out-of-plane second-order amplification factor	$I_i$	Moment of inertia about the axis of curvature, in. <sup>4</sup>
$C$	Moment correction factor for horizontally curved beams	$I_o$	Moment of inertia perpendicular to the axis of curvature, in. <sup>4</sup>
$C_{bs}$	Lateral-torsional buckling modification factor for an equivalent straight member	$J$	Torsional constant, in. <sup>4</sup>
$C_{bi}$	Lateral-torsional buckling modification factor for a curved member subjected to in-plane flexure	$J_e$	Equivalent torsional constant, in. <sup>4</sup>
$C_{bo}$	Lateral-torsional buckling modification factor for a curved member subjected to out-of-plane flexure	$K_i$	Effective length factor for in-plane buckling
$C_{v1}$	Web shear strength coefficient	$K_o$	Effective length factor for out-of-plane buckling
$C_w$	Warping constant, in. <sup>6</sup>	$L$	Laterally unbraced length, in.
$C_\delta$	Local buckling strength coefficient	$L$	Developed member length, in.
$D$	Member depth in the plane of curvature, in.	$L_d$	Arc length, developed length, in.
$D$	Outside diameter of a round HSS, in.	$L_{db}$	Developed length (arc length) along the curved member between brace points, in.
$D_{max}$	Maximum outside diameter of the curved member, in.	$L_{ds}$	Developed span length, in.
$D_{min}$	Minimum outside diameter of the curved member, in.	$L_p$	Chord, span, in.
$D_n$	Nominal outside diameter of the straight member, before bending, in.	$L_s$	Chord, span, in.
$E$	Modulus of elasticity, ksi	$L_{sb}$	Span length (chord length) between out-of-plane bracing, in.
$E_c$	Modulus of elasticity of the slab, ksi	$M$	Moment, kip-in.
$F_e$	Elastic buckling stress, ksi	$M_{co}$	Available out-of-plane flexural strength, kip-in.
$F_{cr}$	Critical buckling stress, ksi	$M_{cw}$	Available flexural strength of the isolated flange, kip-in.
$F_f$	Flange force, kips	$M_{cz}$	Available torsional strength, kip-in.
$F_u$	Specified minimum tensile strength, ksi	$M_e$	Moment at the end of a beam segment, kip-in.
$F_y$	Specified minimum yield stress, ksi	$M_{ei}$	Elastic critical lateral-torsional buckling moment of a curved member subjected to flexure in the plane of curvature, kip-in.
$G$	Shear modulus, ksi	$M_{eo}$	Elastic critical lateral-torsional buckling moment of a curved member subjected to flexure perpendicular to the plane of curvature, kip-in.
$G_c$	Shear modulus of the slab, ksi		

$M_{es}$	Elastic critical lateral-torsional buckling moment of an equivalent straight member subjected to uniform moment with a length equal to $L_{db}$ , kip-in.	$P_{eo}$	Elastic out-of-plane critical buckling load, kips
$M_f$	Moment at an isolated flange, kip-in.	$P_n$	Nominal compressive strength, kips
$M_i$	Moment about the axis of curvature causing in-plane flexure, kip-in.	$P_r$	Required axial strength, kips
$M_{i1}$	First-order in-plane moment, kip-in.	$R$	Centroidal radius of curvature, in.
$M_{ic}$	In-plane closing moment, kip-in.	$R_d$	Bending radius for detailing, in.
$M_{io}$	In-plane opening moment, kip-in.	$R_e$	Equivalent radius for parabolic arches, in.
$M_m$	Moment at the beam midspan, kip-in.	$R_n$	Available strength, kips
$M_n$	Nominal flexural strength, kip-in.	$S$	Section modulus, in. <sup>3</sup>
$M_{ni}$	Nominal in-plane flexural strength, kip-in.	$S_{ei}$	Effective section modulus about the axis of curvature, in. <sup>3</sup>
$M_{nw}$	Nominal flexural strength of the isolated flange, kip-in.	$S_{eo}$	Effective section modulus perpendicular to the axis of curvature, in. <sup>3</sup>
$M_o$	Moment perpendicular to the axis of curvature causing out-of-plane flexure, kip-in.	$S_i$	Section modulus about the axis of curvature, in. <sup>3</sup>
$M_p$	Plastic bending moment, kip-in.	$S_{wc}$	Warping statical moment for the slab, in. <sup>2</sup>
$M_{ri}$	Required in-plane flexural strength, kip-in.	$S_{ws}$	Warping statical moment for the steel beam, in. <sup>2</sup>
$M_{ro}$	Required out-of-plane flexural strength, kip-in.	$V$	Shear force, kips
$M_{rw}$	Required second-order flexural strength of the isolated flange, kip-in.	$V_c$	Available shear strength, kips
$M_{rz}$	Required torsional strength, kip-in.	$V_r$	Required shear strength, kips
$M_x$	Flexural moment about the $x$ -axis, kip-in.	$W_{nc}$	Normalized warping function for the slab, in. <sup>2</sup>
$M_{xc}$	Corrected flexural moment about the $x$ -axis, kip-in.	$W_{ns}$	Normalized warping function for the steel beam, in. <sup>2</sup>
$M_{xm}$	Flexural moment at the midspan of a horizontally curved beam span, kip-in.	$Y_t$	Flange rupture coefficient
$M_{x\theta}$	Flexural moment in a horizontally curved beam span, kip-in.	$Z$	Plastic modulus, in. <sup>3</sup>
$M_{yi}$	In-plane flexural yield moment, kip-in.	$Z_{ei}$	Effective plastic modulus about the axis of curvature, in. <sup>3</sup>
$M_{yo}$	Out-of-plane flexural yield moment, kip-in.	$Z_{eo}$	Effective plastic modulus perpendicular to the axis of curvature, in. <sup>3</sup>
$M_z$	Torsional moment, kip-in.	$Z_f$	Plastic modulus about the strong axis of an isolated flange, in. <sup>3</sup>
$M_{zc}$	Corrected torsional moment, kip-in.	$Z_i$	Plastic modulus about the axis of curvature, in. <sup>3</sup>
$M_{ze}$	Torsional moment at the end of a horizontally curved beam span, kip-in.	$b$	Element width, in.
$M_{z\theta}$	Torsional moment in a horizontally curved beam span, kip-in.	$b_1$	Maximum width including sidewall deformation, in.
$P$	Concentrated load, kips	$b_e$	Effective slab width, in.
$P_c$	Available axial strength, kips	$b_f$	Flange width, in.
$P_{ei}$	Elastic in-plane critical buckling load, kips	$c$	Perpendicular distance from edge to neutral axis of member, in.
		$c_r$	Flexibility characteristic for round HSS
		$d$	Member depth, in.

$d_e$	Distance between flange centroids of the transformed section = $d + (t_e - t_f)/2$	$r_i$	In-plane radius of gyration, in.
$e$	Compression flange distortion, in.	$r_o$	Radius of gyration perpendicular to the axis of curvature, in.
$e_p$	Equivalent eccentricity for horizontally curved beams with midspan concentrated loads, in.	$t$	Element thickness, in.
$e_w$	Equivalent eccentricity for horizontally curved beams with uniformly distributed loads, in.	$t_c$	Slab thickness, in.
$f$	Shape factor	$t_e$	Transformed slab thickness = $t_c/n$ , in.
$f_{fc}$	Distributed radial force per unit length of an isolated flange, kip/in.	$t_f$	Flange thickness, in.
$h$	Clear distance between fillets, in.	$t_w$	Web thickness, in.
$h_o$	Distance between flange centroids, in.	$w$	Linear uniform force per unit length along the span, kip/in.
$k_{ci}$	Circumferential stress factor for in-plane flexure	$w_f$	Radial force per unit length perpendicular to the member axis, kip/in.
$k_{co}$	Circumferential stress factor for out-of-plane flexure	$y$	Distance from neutral axis to the point of interest, perpendicular to the axis of curvature, in.
$k_f$	Reduction factor for flexural properties	$y$	Distance from the top flange centroid to the shear center of the transformed section, in.
$k_i$	Moment of inertia reduction factor	$y_0$	Distance from neutral axis to the outermost fiber, perpendicular to the axis of curvature, in.
$k_s$	Reduction factor for out-of-plane bending of stiffened elements	$z$	Distance along the developed beam length, in.
$k_{si}$	Section modulus reduction factor for in-plane flexure	$\Delta_1$	First-order deflection, in.
$k_{so}$	Section modulus reduction factor for out-of-plane flexure	$\Delta_2$	Second-order deflection, in.
$k_u$	Reduction factor for out-of-plane bending of unstiffened elements	$\alpha$	Strain ratio
$k_{zi}$	Plastic modulus reduction factor for in-plane flexure	$\alpha$	ASD/LRFD force level adjustment factor
$k_{zo}$	Plastic modulus reduction factor for out-of-plane flexure	$\alpha$	Curved member 直 member flexural stress ratio
$l$	Beam length for element out-of-plane bending, in.	$\alpha_i$	Curved member 直 member flexural stress ratio at the inner fiber
$l_w$	Length of weld, in.	$\alpha_o$	Curved member 直 member flexural stress ratio at the outer fiber
$m$	Shear modular ratio = $G/G_c$	$\alpha_t$	Ratio of required torsional moment to plastic torsional strength
$m_f$	Moment per unit length due to the radial load, kip-in.	$\delta_o$	Initial out-of-flatness, in.
$m_n$	Nominal moment per unit length, kip-in.	$\epsilon_{max}$	Maximum flexural strain, in./in.
$m_r$	Required moment per unit length, kip-in.	$\epsilon_y$	Yield strain = $F_y/E$ , in./in.
$m_{zc}$	Torsional moment per unit length, kip-in./in.	$\gamma$	Torsional stiffness parameter
$n$	Modular ratio = $E/E_c$	$\lambda$	Slenderness parameter
$q$	Uniform force per unit length along a curved axis, radial uniform force per unit length along a circularly curved axis, kip/in.	$\lambda_f$	Flange slenderness ratio
$r$	Radius to the point of interest, in.	$\lambda_w$	Web slenderness ratio

$\lambda_{pf}$	Limiting slenderness ratio for the flange of compact member	$\sigma_o$	Flexural stress at the outer extreme fiber of a curved member, ksi
$\lambda_{pw}$	Limiting slenderness ratio for the web of compact member	$\sigma_r$	Residual stress, ksi
$\lambda_{rf}$	Limiting slenderness ratio for flange of noncompact slender member	$\sigma_{rc}$	Compression residual stress, ksi
$\lambda_{rw}$	Limiting slenderness ratio for web of noncompact slender member	$\sigma_{ro}$	Required out-of-plane flexural stress, ksi
$\lambda_e$	Effective slenderness parameter	$\sigma_{rt}$	Tensile residual stress, ksi
$\lambda_{hd}$	Limiting slenderness parameter for highly ductile element	$\sigma_{rw}$	Required second-order warping stress, ksi
$\lambda_p$	Limiting slenderness parameter for compact element	$\sigma_s$	Flexural stress at the extreme fibers of an equivalent straight member, ksi
$\rho$	Ovalization parameter for round HSS	$\sigma_s$	Spring-back stress, ksi
$\rho_w$	Web deformation parameter for square and rectangular HSS	$\sigma_y$	Yield stress, ksi
$\rho_f$	Flange deformation parameter for square and rectangular HSS	$\sigma_z$	Longitudinal flexural stress, ksi
$\sigma$	Radial uniform force per unit area, ksi	$\tau_{ct}$	Available shear stress for torsional loads, ksi
$\sigma_c$	Flexural stress at the extreme fibers of a curved member, ksi	$\tau_{rt}$	Required shear stress due to torsional loads, ksi
$\sigma_{ci}$	Circumferential ovalization stress caused by in-plane flexure, ksi	$\tau_{cv}$	Available shear stress for shear loads, ksi
$\sigma_{co}$	Available out-of-plane flexural stress, ksi	$\tau_{rv}$	Required shear stress due to shear loads, ksi
$\sigma_{co}$	Circumferential stress for out-of-plane flexure, ksi	$\theta$	Subtended angle, rad
$\sigma_{cw}$	Available warping stress, ksi	$\theta_1$	First-order torsional rotation, rad
$\sigma_i$	Flexural stress at the inner extreme fiber of a curved member, ksi	$\theta_2$	Second-order torsional rotation, rad
		$\theta_{2i}$	Inelastic second-order torsional rotation, rad
		$\theta_b$	Subtended angle between braces, rad
		$\theta_b$	Subtended angle between torsional restraints, rad
		$\theta_s$	Span angle, rad
		$\theta_z$	Angle from the end of the segment to the location of interest, rad

# References

AASHTO (2014), *LRFD Bridge Design Specifications*, 7th Ed., American Association of State Highway and Transportation Officials.

AASHTO/NSBA (2008), *S2.1 Steel Bridge Fabrication Guide Specifications*, 2nd Ed., AASHTO/NSBA Steel Bridge Collaboration.

AASHTO/NSBA (2014), *G13.1 Guidelines for Steel Girder Bridge Analysis*, 2nd Ed., AASHTO/NSBA Steel Bridge Collaboration.

Abdul-Baki, A. and Bartel, D. (1969), "Analysis of Helicoidal Girders," *Engineering Journal*, AISC, Vol. 6, No. 3, pp. 84–99.

Adams, P.F. (1966), *Plastic Design in High Strength Steel*, Ph.D. Dissertation, Lehigh University, Bethlehem, PA.

Ahmed, M.Z. and Weisgerber, F.E. (1996), "Torsion Constant for Matrix Analysis of Structures Including Warping Effect," *International Journal of Solids and Structures*, Vol. 33, No. 3, January, pp. 361–374.

AISC (1963), *Steel Gables and Arches*, American Institute of Steel Construction, Chicago, IL.

AISC (2003), "Architecturally Exposed Structural Steel," AESS Supplement, *Modern Steel Construction*, American Institute of Steel Construction, May.

AISC (2016a), *Code of Standard Practice for Steel Buildings and Bridges*, AISC 303-16, June 15, American Institute of Steel Construction, Chicago, IL.

AISC (2016b), *Seismic Provisions for Structural Steel Buildings*, ANSI/AISC 341-16, American Institute of Steel Construction, July 12, Chicago, IL.

AISC (2016c), *Specification for Structural Steel Buildings*, ANSI/AISC 360-16, American Institute of Steel Construction, July 7, Chicago, IL.

AISC (2017), *Steel Construction Manual*, 15th Ed., American Institute of Steel Construction, Chicago, IL.

Alwood, T. (2006), "What Engineers Should Know about Bending Steel," *Modern Steel Construction*, AISC, May.

Arasaratnam, P. (2008), *Effects of Flange Holes on Flexural Behavior of Steel Beams*, Ph.D. Dissertation, McMaster University, Hamilton, Ontario, Canada.

Arnold, P., Adams, P.F. and Lu, L.W. (1968), "Experimental and Analytical Behavior of a Hybrid Frame," *ASCE Proceedings*, American Society of Civil Engineers, Vol. 94, No. ST1, January.

Ashkinadze, K. (2008), "Proposals for Limit States Torsional Strength Design of Wide-Flange Steel Members," *Canadian Journal of Civil Engineering*, Vol. 35, pp. 200–209.

ASME (2015), *Boiler & Pressure Vessel Code*, BPVC-VIII-1, Section VIII, Rules for Construction of Pressure Vessels, Division 1, American Society of Mechanical Engineers, New York, NY.

ASME (2016), *Power Piping-ASME Code for Pressure Piping*, ASME B31.1-2016, American Society of Mechanical Engineers, New York, NY.

ASTM (2007), *Standard Specification for Quenched and Tempered Low-Alloy Structural Steel Plate with 70 ksi Minimum Yield Strength to 4-in. Thick*, ASTM A852/A852M-07, ASTM International, West Conshohocken, PA.

ASTM (2013), *Standard Practice for Safeguarding against Warpage and Distortion During Hot-Dip Galvanizing of Steel Assemblies*, ASTM A384/A384M-07, ASTM International, West Conshohocken, PA.

ASTM (2014), *Standard Practice for Safeguarding against Embrittlement of Hot-Dip Galvanized Structural Steel Products and Procedure for Detecting Embrittlement*, ASTM A143/A143M-07 (2014), ASTM International, West Conshohocken, PA.

ASTM (2016), *Selected ASTM Standards for Structural Steel Fabrication*, ASTM International, West Conshohocken, PA.

Avent, R. and Mukai, D. (1998), *Heat-Straightening Repairs of Damaged Steel Bridges: A Technical Guide and Manual of Practice*, Report FHWA-IF-99-004, Federal Highway Administration, U.S. Department of Transportation, Washington, DC.

Avent, R.R., Mukai, D.J. and Robinson, P.F. (2000), "Effect of Heat Straightening on Material Properties of Steel," *Journal of Materials in Civil Engineering*, ASCE, Vol. 12, No. 3, August, pp. 188–195.

Avent, R.R., Mukai, D.J. and Robinson, P.F. (2001), "Residual Stresses in Heat-Straightened Steel Members," *Journal of Materials in Civil Engineering*, ASCE, Vol. 13, No. 1, January/February, pp. 18–25.

Bala, S.R. and Malik, L. (1983), "Roll Forming to Higher Strain Levels Successful," *Welding and Metal Fabrication*, Vol. 51, No. 2, pp. 100–108.

Baldwin, M.W. (1949), "Macro-Residual Stresses in Metals Resulting from Plastic Deformation," *Cold Working of Metals*, American Society for Metals.

Bangash, M.Y.H. and Bangesh, T. (1999), *Staircases—Structural Analysis and Design*, Balkema, Leiden, The Netherlands.

Barnshaw, R. (2009), "Bending Considerations in Steel Construction," *Modern Steel Construction*, AISC, October, pp. 42–43.

Beedle, L.S. and Tall, L. (1960), "Basic Column Strength," *ASCE Proceedings*, American Society of Civil Engineers, Vol. 86, No. ST7.

Bennetts, I.D., Thomas, I.R. and Grundy, P. (1981), "Torsional Stiffness of Shear Connections," *Proceedings of the Metal Structures Congress*, National Committee on Metal Structures of the Institution of Engineers, Australia, Newcastle, May 11–14, pp. 102–106.

Bergman, V.R. (1956), "Helicoidal Staircases of Reinforced Concrete," *ACI Journal*, American Concrete Institute, Vol. 53, No. 10, pp. 403–412.

Bjorhovde, R. (2006), "Cold Bending of Wide-Flange Shapes for Construction," *Engineering Journal*, AISC, Vol. 43, No. 4, pp. 271–286.

Bjorhovde, R., Engstrom, M.F., Griffis, L.G., Kloiber, L.A. and Malley, J.O. (2001), *Structural Steel Selection Considerations: A Guide for Students, Educators, Designers, and Builders*, ASCE, Reston, Virginia.

Blondeau, R., Boulisset, R., Ramon, J. L., Kaplan, D. and Roesch, L. (1984), "Cold Forming and Welding Behaviors of Heavy Plate Steels for Pressure Vessel Applications," *5th International Conference on Pressure Vessel Technology, Volume 2: Materials and Manufacturing*, ASME, San Francisco, CA, pp. 1,257–1,289.

Boissonnade, N., Muzeau, J.P. and Villette, M. (2002), "Amplification Effects for Lateral Torsional Buckling," *Stability and Ductility of Steel Structures*, Editor: Ivanyi, M. and Kiado, A., pp. 73–80.

Boresi, A.P., Schmidt, R.J. and Sidebottom, O.M. (1993), *Advanced Mechanics of Materials*, 5th Ed., John Wiley & Sons, Inc, Hoboken, NJ.

Boyd, G.M. (1970), *Brittle Fracture in Steel Structures*, Butterworth & Co, London, UK.

Brady, F.J. (1978), *Determination of Minimum Radii for Cold Bending of Square and Rectangular Hollow Structural Sections*, CIDECT Report 11B-78/12, CIDECT.

Bremault, D., Driver, R.G. and Grondin, G.Y. (2008), *Limit States Design Approach for Rolled Wide Flange Beams Subject to Combined Torsion and Flexure*, Structural Engineering Report 279, Department of Civil and Environmental Engineering, University of Alberta, Edmonton, Alberta, Canada.

Brockenbrough, R.L. (1970a), "Theoretical Stresses and Strains from Heat Curving," *Journal of the Structural Division*, ASCE, Vol. 96, No. ST7, July, pp. 1,421–1,445.

Brockenbrough, R.L. (1970b), "Criteria for Heat Curving Steel Beams and Girders," *Journal of the Structural Division*, ASCE, Vol. 96, No. ST10, October, pp. 2,209–2,227.

Cattan, J. (1996), "Statistical Analysis of Charpy V-Notch Toughness for Steel Wide Flange Structural Shapes," *Modern Steel Construction*, AISC, May.

Chajes, A., Britvec, S.J. and Winter, G. (1963), "Effects of Cold-Straining on Structural Sheet Steels," *Journal of the Structural Division*, ASCE, Vol. 89, No. ST2, April, pp. 1–32.

CEN (2009), *Eurocode 3: Design of Steel Structures—Part 2: Steel Bridges*, EN 1993-2, Comité Européen de Normalisation, Brussels, Belgium.

Chiew, S.P., Jin, Y.F. and Lee, C.K. (2016), "Residual Stress Distribution of Roller Bending of Steel Rectangular Structural Hollow Sections," *Journal of Constructional Steel Research*, Vol. 119, pp. 85–97.

CIDECT (1998), *Design Guide for Fabrication, Assembly and Erection of Hollow Section Structures*, Design Guide 7, CIDECT.

Connor, R.J., Urban, M.J. and Kaufmann, E.J. (2008), *Heat-Straightening Repair of Damaged Steel Bridge Girders: Fatigue and Fracture Performance*, NCHRP Report 604, National Cooperative Highway Research Program, Washington, DC.

Cook, R.D. and Young, W.C. (1985), *Advanced Mechanics of Materials*, Macmillan Publishing Company, London, UK.

Cooper, S.E. and Chen, A.C. (1985), *Designing Steel Structures—Methods and Cases*, Prentice-Hall, Upper Saddle River, NJ.

Criste, E. (2009), "Beam Cambering Methods and Costs," *Modern Steel Construction*, AISC, April.

Culver, C.G. and Nasir, G. (1971), "Inelastic Flange Buckling of Plate Girders," *Journal of the Structural Division*, ASCE, Vol. 97, No. 4, April, pp. 1,239–1,257.

Dexter, R.J., Altstadt, S.A. and Gardner, C.A. (2002), *Strength and Ductility of HPS70W Tension Members and Tension Flanges with Holes*, University of Minnesota Civil Engineering Report, Minneapolis, MN.

Ding, Y., Yetsir, M. and Khajehpour, S. (2014), "Predictions of Residual Stresses and Deformations in Pipe Bends Produced Using Cold, Warm and Induction Bending Processes," *Proceedings of the ASME 2014 Pressure Vessel & Piping Conference*, ASME, New York, NY.

Douty, R.T. and McGuire, W. (1965), "High Strength Bolted Moment Connections," *Journal of the Structural Division*, ASCE, Vol. 91, No. ST2, April, pp. 101–128.

Downey, E. (2006), "Specifying Camber," *Modern Steel Construction*, AISC, July.

Dowswell, B. (2010), "Plastic Collapse of Untiffened and Edge-Stiffened Plates," *Proceedings of the Annual Stability Conference*, Structural Stability Research Council, May 12–15, Orlando, FL.

Driver, R.G. and Kennedy, D.J.L. (1989), "Combined Flexure and Torsion of I-Shaped Steel Beams," *Canadian Journal of Civil Engineering*, Vol. 16, pp. 124–139.

ECCS (1976), *Manual on Stability of Steel Structures*, 2nd Ed., European Convention for Constructional Steelwork.

Feldman, B. (2008), "Around the Bend—What You Need to Know about Steel Bending," *Proceedings of the North American Steel Construction Conference*, AISC, April 2–4, Nashville, TN.

FEMA (2000), *State of the Art Report on Base Metals and Fracture*, FEMA-355A, September.

FHWA (2015), *Steel Bridge Design Handbook—Design Example 3: Three-Span Continuous Horizontally Curved Composite Steel I-Girder Bridge*, Publication No. FHWA-HIF-16-002-Vol. 23, Federal Highway Administration, Washington, DC.

Fuller, C.E. and Johnston, W.A. (1919), *Applied Mechanics, Vol. II—Strength of Materials*, John Wiley and Sons, Hoboken, NJ.

Gambhir, M.L. (2004), *Stability Analysis and Design of Structures*, Springer, New York, NY.

Grundy, P., Murray, N.W. and Bennetts, I.D. (1983), "Torsional Rigidity of Standard Beam-to-Column Connections," *Proceedings of the Metal Structures Conference*, National Committee on Metal Structures of the Institution of Engineers, Australia, Brisbane, May 18–20, pp. 164–169.

Heins, C.P. and Firmage, D.A. (1979), *Design of Modern Steel Highway Bridges*, Wiley, Hoboken, NJ.

Heins, C.P. and Kuo, J.T.C. (1972), "Torsional Properties of Composite Girders," *Engineering Journal*, AISC, Vol. 9, No. 2, pp. 79–85.

Huber, A.W. (1958), *Residual Stresses in Wide Flange Beams and Columns*, Fritz Laboratory Report No. 1498, Lehigh University, Bethlehem, PA.

ISO (2009), *Petroleum and Natural Gas Industries—Induction Bends, Fittings and Flanges for Pipeline Transportation Systems—Part 1: Induction Bends*, International Standard 15590-1, 2nd Ed., International Organization for Standardization, Geneva, Switzerland.

Karnovsky, I.A. (2012), *Theory of Arched Structures—Strength, Stability, Vibration*, Springer, New York, NY.

Kaufmann, E.J., Metrovich, B. and Pense, A.W. (2001), *Characterization of Cyclic Inelastic Strain Behavior on Properties of A572 Gr. 50 and A913 Gr. 50 Rolled Sections*, ATLSS Report No. 01-13, Lehigh University, Bethlehem, PA.

Keating, P.B. and Christian, L.C. (2007), "Effects of Bending and Heat on the Ductility and Fracture Toughness of Flange Plate," FHWA/TX-10/0-4624-2, Federal Highway Administration, Washington, DC.

Kellog (1957), *Design of Piping Systems*, 2nd Ed., The M.W. Kellogg Company.

Kennedy, J.B. (1988), *Design Aids—Minimum Bending Radii for Square and Rectangular Hollow Structural Sections Subjected to Cold Bending*, CIDECT Report 11C-88-14-E, CIDECT.

Kennedy, J.B., Seddeik, M. and Brady, F. (1986), "Deformations in Cold-Bent HSS Members," *Engineering Journal*, AISC, Vol. 23, No. 3, pp. 117–123.

Key, P.W. and Hancock, G.J. (1985), *An Experimental Investigation of the Column Behavior of Cold Formed Square Hollow Sections*, Report No. R493, University of Sydney, Sydney, Australia.

Kim, Y.J. and Oh, C.S. (2006), "Closed-Form Plastic Collapse Loads of Pipe Bends under Combined Pressure and In-Plane Bending," *Engineering Fracture Mechanics*, Vol. 73, pp. 1,437–1,454.

King, M. (2005), "Around the Bend—What Detailers Should Know about Bending Steel," *Modern Steel Construction*, AISC, May.

King, C. and Brown, D. (2001), *Design of Curved Steel*, SCI Publication P281, The Steel Construction Institute, Ascot, UK.

Kloiber, L.A. (1989), "Cambering of Steel Beams," *Steel Structures—Proceedings of the Sessions Related to Steel Structures at Structures Congress*, Ed., Iffland, J.S.B., ASCE.

Lange, J. and Grages, H. (2009), "Influence of the Bauschinger Effect on the Deflection Behavior of Cambered Steel and Steel Concrete Composite Beams," *Structural Engineering International*, International Association of Bridge and Structural Engineers.

Lay, M.G. and Ward, R. (1969), "Residual Stresses in Steel Sections," *Steel Construction*, Australian Institute of Steel Construction, Vol. 3, No. 3.

Lebet, J.P. and Hirt, M.A. (2013), *Steel Bridges—Conceptual and Structural Design of Steel and Steel-Composite Bridges*, EPFL Press, Lausanne, Switzerland.

Lindner, J. and Glitsch, T. (2005), "Simplified Design of Crane Girders with Open Cross Sections Subjected to Biaxial Bending and Torsion," *Proceedings of the International Conference on Advances in Steel Structures*, Vol. 1, Edited by Shen, Z.Y., Li, G.Q. and Chan, S.L., pp. 95–104.

Lukey, A.F. and Adams, P.F. (1969), "The Rotational Capacity of Beams under Moment Gradient," *Journal of the Structural Division*, ASCE, Vol. 95, No. ST6, June, pp. 1,173–1,188.

Macgregor, C.W. (1954), "The Significance of Residual Stresses," *Residual Stresses in Metals and Metal Construction*, Ed. Osgood, W.R., Reinhold Publishing Corp.

Mandal, N.R. (1992), "Cold Forming of Welded Steel T-Sections," *Thin-Walled Structures*, Vol 13, pp. 319–335.

Moon, J., Yoon, K.Y., Lee, T.Y. and Lee, H.E. (2009), "Out-of-Plane Buckling of Arches with Varying Curvature," *KSCE Journal of Civil Engineering*, Korean Society of Civil Engineers, Vol. 13, No. 6, November, pp. 441–451.

Moore, W.E. and Mueller, K.M. (2002), "Technical Note: Torsional Analysis of Steel Sections," *Engineering Journal*, AISC, Vol. 39, No. 4, pp. 182–188.

Mourad, H.M. and Younan, M.Y.A. (2001), "Nonlinear Analysis of Pipe Bends Subjected to Out-of-Plane Moment Loading and Internal Pressure," *Journal of Pressure Vessel Technology*, ASME, Vol. 123, May, pp. 253–258.

Mourad, H.M. and Younan, M.Y.A. (2002), "Limit-Load Analysis of Pipe Bends under Out-of-Plane Moment Loading and Internal Pressure," *Transactions of the ASME*, ASME, Vol. 124, February, pp. 32–37.

Nakai, H. and Yoo, C.H. (1988), *Analysis and Design of Curved Steel Bridges*, McGraw-Hill, New York, NY.

Nevling, D., Linzell, D. and Laman, J. (2006), "Examination of Level of Analysis Accuracy for Curved I-Girder Bridges through Comparisons to Field Data," *Journal of Bridge Engineering*, ASCE, Vol. 11, No. 2, March/April, pp. 160–168.

Nie, J., Tang, L. and Cai, C.S. (2009), "Performance of Steel-Concrete Composite Beams Under Combined Bending and Torsion," *Journal of Structural Engineering*, ASCE, Vol. 135, No. 9, September, pp. 1,048–1,057.

Nishida, S., Yoshida, H. and Fukumoto, Y. (1978), "Large Deflection Analysis of Curved Members with Thin Walled Open Cross Section," *Proceedings of the 24th Symposium of Structural Engineering*, February, pp. 77–84.

Nitta, A. and Thurlimann, B. (1960), *Effect of Cold Bending on Column Strength*, Fritz Laboratory Report No. 1744, Lehigh University, Bethlehem, PA.

Papangelis, J.P. and Trahair, N.S. (1987), "Flexural-Torsional Buckling of Arches," *Journal of the Structural Division*, ASCE, Vol. 113, No. 4, April, pp. 889–1,906.

Pi, Y.L. and Bradford, M.A. (2002), "Elastic Flexural-Torsional Buckling of Continuously Restricted Arches," *International Journal of Solids and Structures*, Vol. 39, pp. 2,299–2,322.

Pi, Y.L. and Bradford, M.A. (2004), "In-Plane Strength and Design of Fixed Steel I-Section Arches," *Engineering Structures*, Vol. 26, pp. 291–301.

Pi, Y.L. and Bradford, M.A. (2005), "Out-of-Plane Strength and Design of Fixed Steel I-Section Arches," *Journal of Structural Engineering*, ASCE, Vol. 131, No. 4, April, pp. 560–568.

Pi, Y.L., Bradford, M.A. and Tin-Loi, F. (2007), "Nonlinear Analysis and Buckling of Elastically Supported Circular Shallow Arches," *International Journal of Solids and Structures*, Vol. 44, pp. 2,401–2,405.

Pi, Y.L., Bradford, M.A. and Trahair, N.S. (2000), "Inelastic Analysis and Behavior of Steel I-Beams Curved in Plan," *Journal of Structural Engineering*, ASCE, Vol. 126, No. 7, July, pp. 772–779.

Pi, Y.L., Bradford, M.A. and Uy, B. (2002), "In-Plane Stability of Arches," *International Journal of Solids and Structures*, Vol. 39, pp. 105–125.

Pi, Y.L. and Trahair, N.S. (1994), "Inelastic Bending and Torsion of Steel I-Beams," *Journal of Structural Engineering*, ASCE, Vol. 120, No. 12, December, pp. 3,397–3,417.

Pi, Y.L. and Trahair, N.S. (1998), "Out-of-Plane Inelastic Buckling and Strength of Steel Arches," *Journal of Structural Engineering*, ASCE, Vol. 124, No. 2, February, pp. 174–183.

Pi, Y.L. and Trahair, N.S. (1999), "In-Plane Buckling and Design of Steel Arches," *Journal of Structural Engineering*, ASCE, Vol. 125, No. 11, November, pp. 1,291–1,298.

Pi, Y.L. and Trahair, N.S. (2000), "Inelastic Lateral Buckling Strength and Design of Steel Arches," *Engineering Structures*, Vol. 22, pp. 993–1,005.

Rahrig, P.G. and Krzywicki, J. (2005), Specifying and Detailing for Hot-Dip Galvanizing. *Modern Steel Construction*, AISC, June.

Rettie, N.J. (2015), *Lateral-Torsional Buckling Resistance of Horizontally Curved Steel I-Girders*, Master's Thesis, University of Alberta, Edmonton, Alberta, Canada.

Ricker, D.T. (1989), "Cambering Steel Beams," *Engineering Journal*, AISC, Vol. 26, No. 4.

Ritakallio, P. and Bjork, T. (2014), "Low-Temperature Ductility and Structural Behavior of Cold-Formed Hollow Section Structures-Progress during the Past Two Decades," *Steel Construction*, Vol. 7, No. 2, pp. 107–115.

Riviezzi, G. (1984), "Curving Structural Steel," *Steel Construction*, Australian Institute of Steel Construction, Vol. 18, No. 3, November, pp. 2–12.

Rodabaugh, E.C. (1979), *Interpretive Report on Limit Analysis and Plastic Behavior of Piping Products*, Welding Research Council Bulletin 254, Welding Research Council, Shaker Heights, OH.

Ross, D.A. and Chen, W.F. (1976), *Tests of Fabricated Tubular Columns*, Fritz Laboratory Report No. 477, Lehigh University, Bethlehem, PA.

Rothman, H.B. (1980), "Lake Keowee Cofferdam," *Proceedings of the SSRC*, Structural Stability Research Council.

Save, M.A. and Massonet, C.E. (1972), *Plastic Analysis and Design of Plates, Shells and Disks*, North Holland Publishing Company.

Schlom, R. (1987), "Effect of Bending on Mechanical Properties of Sections," Technical Report, Arbed, Centre de Recherches, Esch-sur-Alzette, Luxembourg.

Schreyer, H.L. and Masur, E.F. (1966), "Buckling of Shallow Arches," *Journal of the Engineering Mechanics Division*, ASCE Proceedings, ASCE, Vol. 92, No. EM4, August, pp. 1–19.

Seaburg, P.A. and Carter, C.J. (1997), *Torsional Analysis of Structural Steel Members*, Design Guide 9, AISC, Chicago, IL.

Seddeik, M.M. (1985), *Deformations of Hollow Structural Sections Subjected to Cold Bending*, Ph.D. Dissertation, University of Windsor, Windsor, Ontario, Canada.

Shank, M.E. (1957), *Control of Steel Construction to Avoid Brittle Failure*, Welding Research Council, New York, NY.

Sharma, M. (2005), *Behavior of Heat Straightened Plates Bent along the Minor Axis*, Master's Thesis, Louisiana State University, Baton Rouge, LA.

Sherman, D.R. (1969), "Residual Stress Measurement in Tubular Members," *Journal of the Structural Division*, ASCE, Vol. 95, No. ST4, April, pp. 635–647.

Sherman, D.R. (1992), "Tubular Members," *Constructional Steel Design—An International Guide*, Elsevier Applied Science.

Sherman, D.R. (1997), "Designing with Structural Tubing," *Modern Steel Construction*, AISC, February, pp. 36–45.

Smith, B. and King, M. (2002), "Bending Square and Rectangular Tubing—Modern Science or Ancient Art?" *The Tube and Pipe Journal*, April/May.

Smith, E.M. (1995), "Cross Stiffeners for Beams in Torsion," *Journal of Structural Engineering*, ASCE, Vol. 121, No. 7, July, pp. 1,119–1,124.

Soares, G.C. (1988), "Design Equation for the Compressive Strength on Unstiffened Plate Elements with Initial Imperfections," *Journal of Constructional Steel Research*, Vol. 9, pp. 287–310.

Spence, J. and Findlay, G.E. (1973), "Limit Loads for Pipe Bends Under In-Plane Bending," *Proceedings of the Second International Conference on Pressure Vessel Technology—Part I, Design and Analysis*, ASME.

Spoorenberg, R.C., Snijder, H.H. and Hoenderkamp, J.C.D. (2011), "Proposed Residual Stress Model for Roller Bent Steel Wide Flange Sections," *Journal of Constructional Steel Research*, Vol. 67, pp. 992–1,000.

Spoorenberg, R.C., Snijder, H.H. and Hoenderkamp, J.C.D. (2012a), "Mechanical Properties of Roller Bent Wide Flange Sections—Part 1: Experimental Investigation," *Journal of Constructional Steel Research*, Vol. 68, pp. 51–62.

Spoorenberg, R.C., Snijder, H.H. and Hoenderkamp, J.C.D. (2012b), "Mechanical Properties of Roller Bent Wide Flange Sections—Part 2: Prediction Model," *Journal of Constructional Steel Research*, Vol. 68, pp. 63–77.

Spoorenberg, R.C., Snijder, H.H., Hoenderkamp, J.C.D. and Beg, D. (2012c), "Design Rules for Out-of-Plane Stability of Roller Bent Steel Arches with FEM," *Journal of Constructional Steel Research*, Vol. 79, pp. 9–21.

Swanson, J.A. (2016), "Strength of Beams in Beam-to-Column Connections with Holes in the Tension Flange," *Engineering Journal*, AISC, Vol. 53, No. 3, pp. 159–172.

Szewczak, R.M., Smith, E.A. and DeWolf, J.T. (1983), "Beams with Torsional Stiffeners," *Journal of Structural Engineering*, ASCE, Vol. 109, No. 7, July, pp. 1,635–1,647.

Tan, E.L. and Uy, B. (2009), "Experimental Study on Curved Composite Beams Subjected to Combined Flexure and Torsion," *Journal of Constructional Steel Research*, Vol. 65, pp. 1,855–1,863.

Tan, E.L. and Uy, B. (2011), "Nonlinear Analysis of Composite Beams Subjected to Combined Flexure and Torsion," *Journal of Constructional Steel Research*, Vol. 67, pp. 790–799.

Taylor, J.S. (2001), *An Engineer's Guide to Fabricating Steel Structures, Volume 1—Fabrication Methods*, Australian Institute of Steel Construction.

Thatcher, W.M. (1967), "Horizontally Curved Steel Girders—Fabrication and Design," *Engineering Journal*, AISC, Vol. 4, No. 3, pp. 107–112.

Timoshenko, S. (1956), *Strength of Materials Part II—Advanced Theory and Problems*, 3rd Ed., D. Van Nostrand Company, New York, NY.

Timoshenko, S.P and Gere, J.M. (1961), *Theory of Elastic Stability*, McGraw-Hill, New York, NY.

Tor, S.S., Stout, R.D., Johnston, B.G. and Ruzek, J.M. (1951), "The Effect of Fabrication Processes on Steels Used in Pressure Vessels," *Welding Journal*, American Welding Society, Vol. 30.

TPA (1998), *Recommended Standards for Induction Bending of Pipe and Tube*, TPA-IBS-98, Tube and Pipe Association International.

Trahair, N.S. and Papangelis, J.P. (1987), "Flexural-Torsional Buckling of Monosymmetric Arches," *Journal of Structural Engineering*, ASCE, Vol. 113, No. 10, October, pp. 2,271–2,288.

Trahair, N.S. and Teh, L.H. (2000), *Second Order Moments in Torsion Members*, Research Report No. R800, Centre for Advanced Structural Engineering, The University of Sydney, Sydney, Australia.

Tung, D.H.H. and Fountain, R.S. (1970), "Approximate Torsional Analysis of Curved Box Girders by the M/R Method," *Engineering Journal*, AISC, Vol. 7, No. 3, pp. 65–74.

Vacharajittiphan, P. and Trahair, N.S. (1974), "Warping and Distortion at I-Section Joints," *Journal of the Structural Division*, ASCE, Vol. 100, No. ST3, March, pp. 547–564.

Vacharajittiphan, P. and Trahair, N.S. (1975), "Flexural-Torsional Buckling of Curved Members," *Journal of the Structural Division*, ASCE, Vol. 101, No. ST6, June, pp. 1,223–1,239.

Vandepitte, D. (1982), "Ultimate Strength of Curved Flanges of I-Beams," *Journal of Constructional Steel Research*, Vol. 2, No. 3, September, pp. 22–28.

Vandepitte, D. (1983), "Ultimate Strength of Curved Flanges in Box Girders," *Instability and Plastic Collapse of Steel Structures*, Editor: Morris, L.J., Granada.

Varma, A.H., and Kowalkowski K.J. (2004), *Effects of Multiple Damage Heat Straightening Repairs on the Structural Properties of Bridge Steels*, MDOT Report RC-1456, Michigan Department of Transportation, Lansing, MI.

Weisenberger, G. (2016), "There's More than One Way to Bend a Beam," *Modern Steel Construction*, AISC, January, pp. 52–55.

Wendt, G. (2010), *Galvanizing Curved Steel*, Presentation at the Kansas City Regional Steel Fabricators Association Biannual Meeting.

White, D. and Coletti, D. (2013), "Building a Better Grid," *Modern Steel Construction*, AISC, September.

White, D.W., Zureick, A.H., Phoawanich, N. and Jung, S.K. (2001), *Development of Unified Equations for Design of Curved and Straight Steel Bridge I Girders*, Georgia Institute of Technology, Atlanta, GA.

Wilson, B.J. and Quereau, J.F. (1928), "A Simple Method of Determining Stress in Curved Flexural Members," *Engineering Experiment Station Circular*, No. 16, January, University of Illinois, Champaign-Urbana, IL.

Yanfei, J., Ping, C.S. and King, L.C. (2015), "Finite Element Simulations of Residual Stresses in Roller Bending Hollow Section Steel Members," *Proceedings of the World Congress on Advances in Civil, Environmental and Materials Research*, Incheon, Korea, August 25–29.

Yoo, C.H., Kang, Y.J. and Davidson, J.S. (1996), "Buckling Analysis of Curved Beams by Finite-Element Discretization," *Journal of Engineering Mechanics*, ASCE, Vol. 122, No. 8, August, pp. 762–770.

Yoo, C.H., Lee, S.C. and Carbine, R.L. (1986), "Experimental and Analytical Study of Horizontally Curved Steel Wide Flange Beams," *Proceedings of the 1986 Annual Technical Session*, Structural Stability Research Council.

Young, W.C. and Budynas, R.G. (2002), *Roark's Formula's for Stress and Strain*, 7th Ed., McGraw-Hill, New York, NY.

Yura, J.A., Galambos, T.V. and Ravinda, K. (1978), "The Bending Resistance of Steel Beams," *Journal of the Structural Division*, ASCE, Vol. 104, No. ST9, pp. 1,255–1,270.

Yura, J.A. and Lu, L.W. (1968), *Ultimate Load Tests on Braced Multi-Story Frames*, Fritz Laboratory Report No. 273.60, Lehigh University, Bethlehem, PA.

Ziemian, R.D. (2010), *Guide to Stability Design Criteria for Metal Structures*, 6th Ed., John Wiley & Sons, Hoboken, NJ.

# Bender/Roller List

## Albina Co., Inc.

[www.albinaco.com](http://www.albinaco.com)  
866.252.4628 (Toll-Free)  
503.692.6010 (Direct)  
12080 SW Myslony St.  
Tualatin, OR 97062

## BendTec, Inc.

[www.bendtec.com](http://www.bendtec.com)  
218.722.0205  
366 Garfield Ave.  
Duluth, MN 55802

## Chicago Metal Rolled Products

[www.cmrp.com](http://www.cmrp.com)  
773.523.5757  
3715 S. Rockwell St.  
Chicago, IL 60632  
816.483.7575  
2193 Manchester Trafficway  
Kansas City, MO 64126

## Greiner Industries, Inc.

[www.greinerindustries.com](http://www.greinerindustries.com)  
800.782.2110  
1650 Steel Way  
Mount Joy, PA 17552

## Hodgson Custom Rolling, Inc.

[www.hcrsteel.com](http://www.hcrsteel.com)  
800.263.2547  
5580 Kalar Road  
Niagara Falls, Ontario  
Canada L2H-3L1

## Hornsby Steel, Inc.

[www.hornsbysteel.net](http://www.hornsbysteel.net)  
205.274.7760  
57 Arena Dr.  
Cleveland, AL 35049

## Kottler Metal Products, Inc.

[www.kottlermetal.com](http://www.kottlermetal.com)  
440.946.7473  
1595 Lost Nation Road  
Willoughby, OH 44094

## Kubes Steel

[www.kubesteel.com](http://www.kubesteel.com)  
905.643.1229  
930 Arvin Ave.  
Stoney Creek, Ontario  
Canada L8E-5Y8

## Max Weiss Company

[www.maxweiss.com](http://www.maxweiss.com)  
414.355.8220  
8625 W. Bradley Road  
Milwaukee, WI 53224

## Paramount Roll & Forming

[www.paramount-roll.com](http://www.paramount-roll.com)  
562.944.6151  
12120 E. Florence Ave.  
Santa Fe Springs, CA 90670

## Shaped Steel, Inc.

[www.shapedsteel.com](http://www.shapedsteel.com)  
866.781.5717  
3000 E. Heartland Drive  
Liberty, MO 64068

## WhiteFab Inc.

[www.whitefab.com](http://www.whitefab.com)  
205.791.2011  
724 Avenue W  
Birmingham, AL 35214



@Seismicisolation



**Smarter. Stronger. Steel.**

American Institute of Steel Construction  
312.670.2400 | [www.aisc.org](http://www.aisc.org)